2015

Dynamic Simulation of Concrete Barriers

Adel Badiee
University of Alabama at Birmingham

DYNAMIC SIMULATION OF CONCRETE BARRIERS

by

ADEL BADIEE

NASIM UDDIN, CHAIR
IAN EDWARD HOSCH
LEE MORADI

A THESIS

Submitted to the graduate faculty of The University of Alabama at Birmingham,
in partial fulfillment of the requirements for the degree of
Master of Science

BIRMINGHAM, ALABAMA

2015

DYNAMIC SIMULATION OF CONCRETE BARRIERS

ADEL BADIEE

CIVIL ENGINEERING

ABSTRACT

The American Association of State Highway and Transportation Officials (AASHTO) Bridge Specifications proposes “Yield Line Theory Analysis” in order to determine the structural capacity of concrete barriers based on their static strength. However, it appears that this method conservatively underestimates the structural capacity of concrete barriers to endure high vehicle impacts. Typically, this deficiency has been compensated for artificial reductions in bridge rail design loads used in the design code. Existing barrier design guidelines - static design methods incorporated into the AASHTO Bridge Specifications - are based upon National Cooperative Highway Research Program (NCHRP) Report 350.

The Manual for Assessing Safety Hardware (MASH) guidelines propose higher impact angles, heavier trucks and higher impact speeds. The impact loads proposed by MASH appeared to be extremely high and were not approved by AASHTO’s T7 Committee on Guardrails and Bridge Rails. Therefore, it seems appropriate to modify the applied load to the barrier by using realistic dynamic impact, not only to meet the AASHTO design requirements but also to achieve a more reliable result.

Barriers are designed to provide the maximum safety on highways, roads, and bridges. Unsymmetrical *New Jersey* - type concrete barriers have been designed to (1) minimize the damage to the vehicle caused by the crash via absorbed energy (2) keep the

vehicle in line and not allow redirection to traffic flow, and (3) in the case of barriers installed on bridges, to not allow the vehicle to fall off the bridge, which would cause significant damage to traffic flow beneath. Hence, barriers not only have to be designed based on their strength capacity, but also need to satisfy all the industry criteria. Current *New Jersey* - type concrete barriers have been designed statically, only taking into consideration their strength capacity. Consequently, there is an opportunity to redesign this barrier using realistic dynamic simulations and analyses, by modeling the barrier and deck overhang from test level 1 through 6, in order to satisfy all criteria.

The objective of this research is to perform analyses using the finite element method based upon the dynamic computer simulation (LS-DYNA) in order to propose five different types of concrete barriers that are different in thickness and geometry to the current *New Jersey* barrier with the aim of developing a more efficient design in terms of production cost and performance. The FEM simulation models are further verified using exiting dynamic field tests. This new proposed design will then be compared to the current *New Jersey* barrier in the interest of finding the best geometry that can provide the maximum safety. This comparison will also present both static design (AASHTO equivalent nominal resistance to transverse load measured at 54.0 kips) and dynamic design of the barrier (based on NCHRP 350 TL-4: NCAC single unit truck, with a velocity of 80 km/h and an angle of crash equal to 15 degrees).

Keywords: NCHRP, MASH, AASHTO, Bridge railing, Yield Line Theory, Report 350, Single Unit Truck, Traffic, Barrier, Deck Overhang, Highway, TL-4, Dynamic, New Jersey

ACKNOWLEDGEMENTS

I greatly appreciate my advisor, Dr. Nasim Uddin, for his help, patience and support, and also for trusting me by giving me an opportunity to prove myself and to develop this project. It has certainly been a rewarding experience.

Moreover, I need to thank Dr. Lee Moradi and Dr. Ian Hosch for all of their time and guidance. I also need to thank Dr. Dean Sicking, Dr. Kevin Schrum, and Ahmed Hattab for their cooperation, expertise, and time.

Of course, I need to give special thanks to my parents and brothers, who are the only reason for me being here, and for all of their love and support.

Last but not least, I thank UAB for giving me the opportunity to continue my education as a Master of Science student, which has allowed me to grow personally and professionally.

Financial support from USDOT Transportation Centers Program: National Center for Transportation System Productivity and Management (NCTSPM)

TABLE OF CONTENTS

Page

TABLE OF FIGURES

Page

1 INTRODUCTION

1.1 History

Traffic barriers are designed to meet four specific criteria (1) minimize the damage to the vehicle by absorbing the impact energy, (2) prevent the vehicle from being redirected back into traffic, and (3) prevent the vehicle from rolling over the barrier, (4) to separate traffic lanes.

Additionally, barriers are designed to prevent vehicle collision with vital structural components. For example, when a vehicle impacts a bridge column directly, the direct impact force could cause irreparable damage to the entire bridge structure and not just the column itself. To this point, it is very important that barriers are designed in a way that would not allow the vehicle to penetrate and directly impact the structure's surface. Hence, the AASHTO requires designers to design barriers based on six different test levels that are divided according to various specification categories, including vehicle weight, geometry, velocity, and impact angle [A13.7.3.1]. The figure below, reproduced from the 2012 Edition of the AASHTO Manual, explains in detail the six different test levels.

Vehicle Characteristics	Small Automobiles		Pickup Truck	Single-Unit Truck	Van Type Tractor-Trailer		Tractor-Tanker Trailer
W (Kips)	1.55	1.8	4.5	18.0	50.0	80.0	80.0
B (ft)	5.5	5.5	6.5	7.5	8.0	8.0	8.0
G (in.)	22	22	27	49	64	73	81
Crash Angle, θ	20°	20°	25°	15°	15°	15°	15°
Test Level	Test Speeds (mph)						
TL-1	30	30	30	N/A	N/A	N/A	N/A
TL-2	45	45	45	N/A	N/A	N/A	N/A
TL-3	60	60	60	N/A	N/A	N/A	N/A
TL-4	60	60	60	50	N/A	N/A	N/A
TL-5	60	60	60	N/A	N/A	50	N/A
TL-6	60	60	60	N/A	N/A	N/A	50

Figure 1: Test Levels Configure ratios. (After AASHTO, A13.7.2-1.)

Here, the symbol "s" is the vehicle weight, B and G are the vehicle's center of gravity measured from the front edge of the vehicle, and θ is the crash angle. As shown in the above-mentioned table, increasing the number of each test level increases the vehicle weight and geometry as well. Each test level has been defined for a specific purpose. For instance, Test Level 4 is used by designers to design barriers for high-speed highways, freeways, expressways, and interstate highways with a mixture of trucks and heavy vehicles [A13.7.2].

Various types of barriers have been designed and developed, each with a different mission and purpose. Concrete barriers are designed for heavy-duty tasks such as fully

absorbing the energy caused by the impact. On the other hand, steel guardrails are designed for light duty tasks. Hence, it is highly recommended to use concrete barriers instead of steel guardrails on bridges with high traffic flow. The *New Jersey* concrete barrier is one of the most common concrete barriers utilized today on bridge structures on highways with high traffic flow. The key objective of this particular concrete barrier is to redirect and keep the vehicle in line so that the vehicle will not be able to redirect the traffic flow or cross the barrier. Therefore, not only does the barrier have to absorb the impact energy during vehicle collision; it also must redirect the vehicle in a controlled manner, and for the above-mentioned purposes, it should satisfy both geometry and strength design.

One of the most recognized types of the barriers is the New Jersey barrier. It has been designed to tolerate AASHTO Test Level 4 design criteria. Figure 2, as seen below, represents the dimensions of the New Jersey barrier

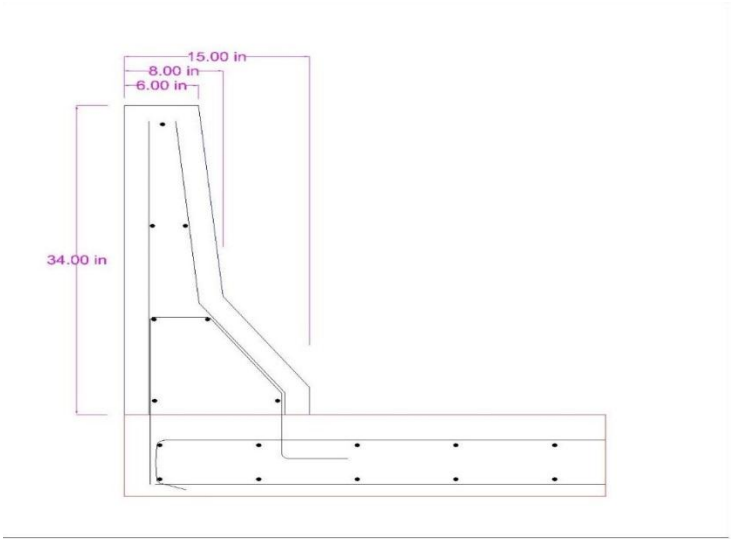

Figure 2: New Jersey barrier – cross section

The strength design of the New Jersey barriers is determined by "Yield Line Theory" (Barker & Puckett, J., 2013). It has been assumed that concrete barriers will break based on certain patterns. The break lines are known as the “Yield Line Failure Pattern”.

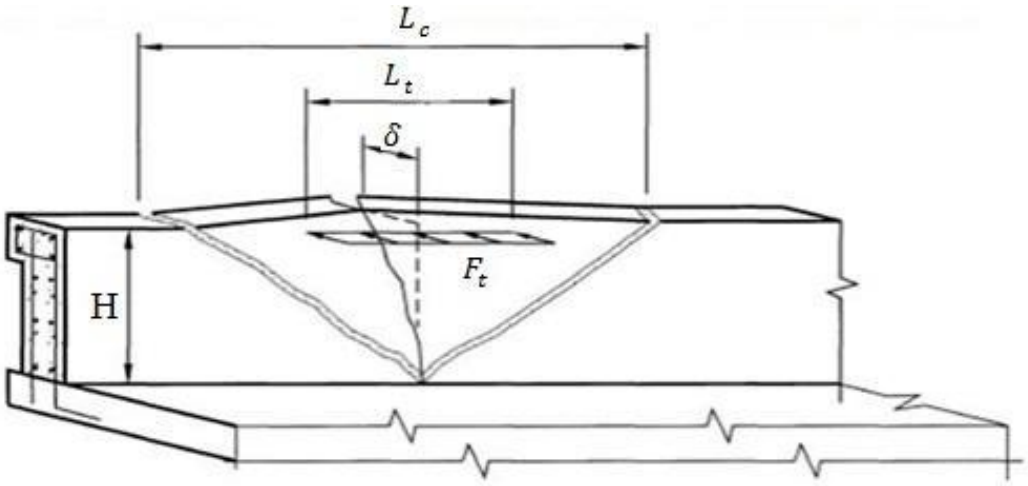

Figure 3: Yield line breaking pattern (After Hirsch, 1978)

In the Figure shown above, $\boldsymbol{L_t}$, is the equivalent of the damage length caused by the vehicle collision, and $\boldsymbol{F_t}$ is the force caused by vehicle collision. In this method, instead of using the exact dynamic load impact caused by the vehicle collision, Hirsch considered $\boldsymbol{F_t}$ as a static load equal to the dynamic load impact.

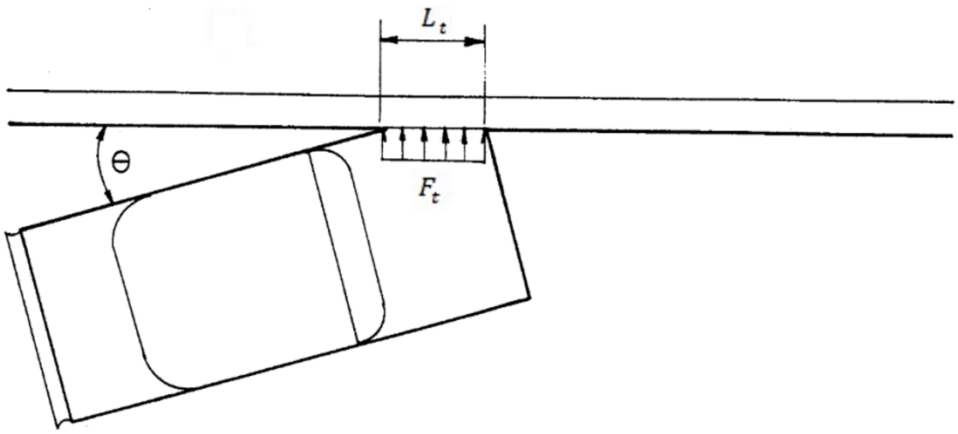

Figure 4: Vehicle crash – top view (After Hirsch, 1978)

1.2 Problem Statement

The yield line method calculates force F_t by considering the external virtual work done by the applied load equal to the internal virtual work done by the resisting moments along the yield lines. The calculated force should be either equal or greater than the real impact force (Hirsch, 1978). Since the yield line theory is determining the strength capacity of the concrete barriers based on a static load design, said theory will not consider the barrier geometry. This method will only require the designers to design the predefined geometry in highways but with different usability. In this case, the vehicle lifting caused by the New Jersey barrier taper and consequent rolling over of the vehicle, has not been considered. Besides, based on a crash test done by Texas A&M University, College Station, for the single unit truck (TL-4) (Sheikh Nauman M., Determination of Minimum Height and Lateral Design Load for Mash Test Level 4 Bridge Rails, 2011), the vehicle rolling over the barrier after impact is obvious.

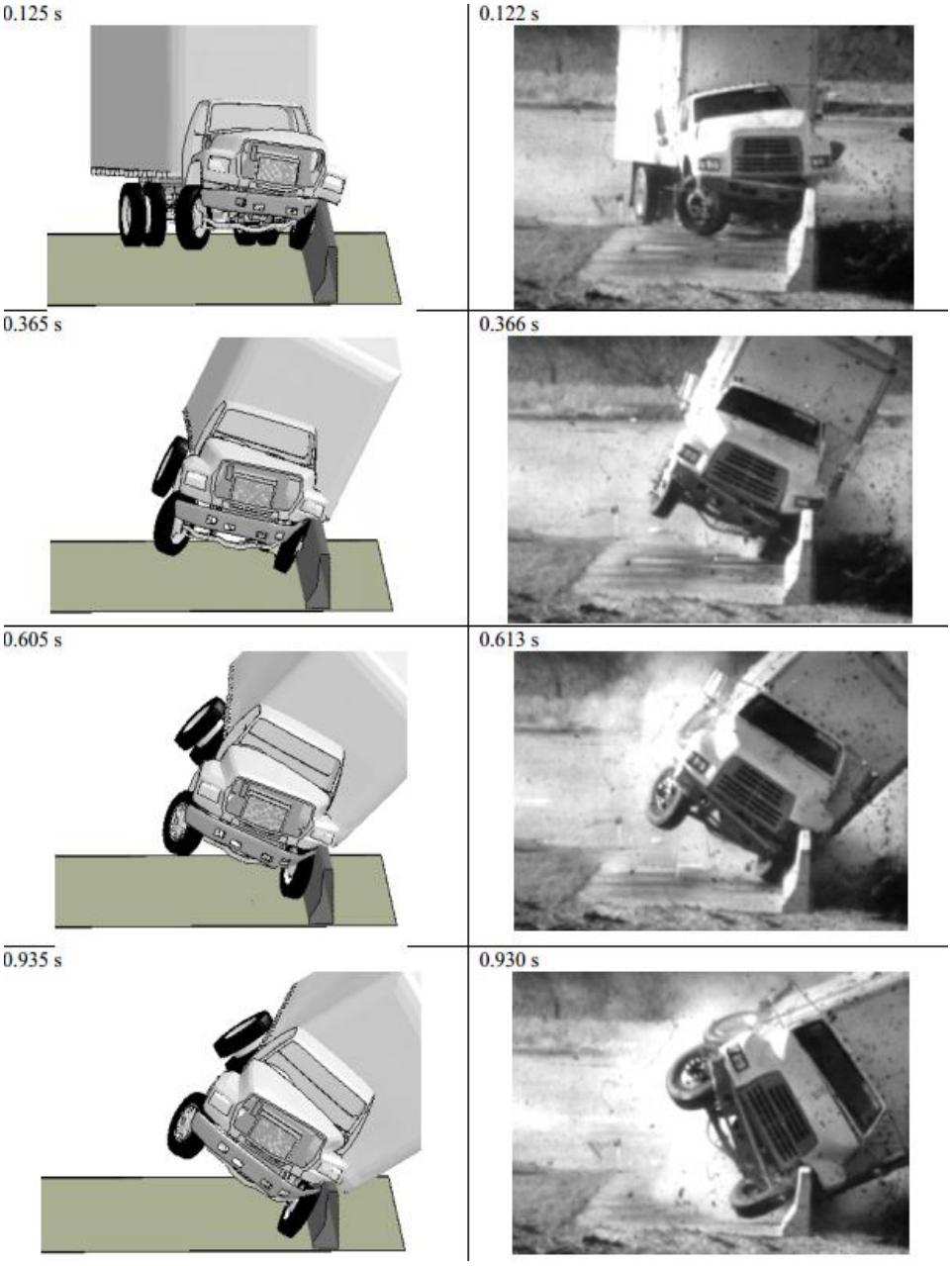

Figure 5: Test Level 4 – Signle Unit Truck (After Sheikh Nauman M., Determination of Minimum Height and Lateral Design Load for Mash Test Level 4 Bridge Rails, 2011)

Additionally, for barriers located on bridge deck overhangs, this method does not consider the energy that is absorbed by the deflection of the deck overhang.

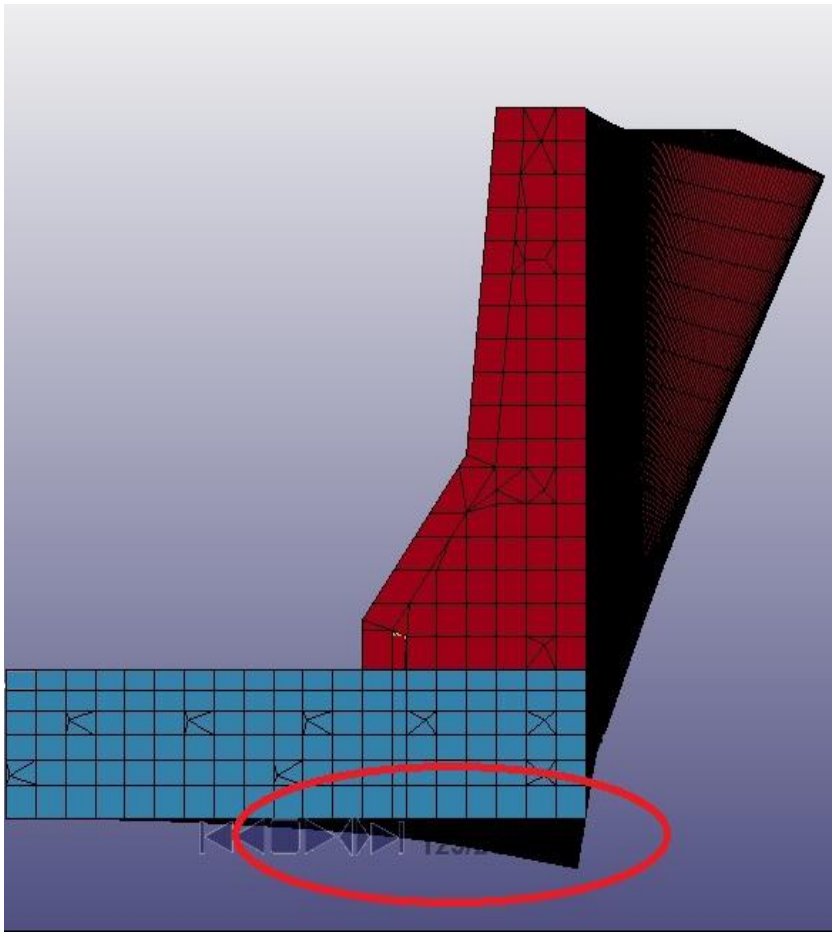

Figure 6: Deck Overhang Deflection

Contrary to popular belief, a thicker concrete block does not necessarily produce a better result in terms of vehicle impact, when compared to a thinner one. All concrete barriers are designed to be able to maximize the energy absorption caused by vehicle impact.

In 2011, Texas Transportation Institute performed a crash test (TL-4) using a MASH single unit truck hitting the single slope concrete barrier as presented in the below figure. (Sheikh, Bligh, & Menges, 2011)

Figure 7: Concrete Barrier Damage after impact – front view (After Sheikh Nauman M., Determination of Minimum Height and Lateral Design Load for Mash Test Level 4 Bridge Rails, 2011)

In the above-mentioned Figure, it is apparent that the barrier did not crack or fail due to vehicle collision and a significant amount of the energy was absorbed by the truck during impact.

1.3 Objective

The objective of this research is to first determine the individual contribution and energy absorption of each component of the New Jersey barrier when located on the bridge deck overhang. After gaining an understanding of each component, by using LS-DYNA finite element software, the research will propose five different types of concrete barriers that vary in terms of thickness and taper slope.

The second objective of this research is to compare all of these newly proposed barrier designs in terms of their overall energy absorption efficiency, and as well, to compare each component to a static load that represents NCAC Single Unit Truck TL-4 utilizing the historical Hirsch theory as a comparison. (AASHTO LRFD bridge design specifications, 2012)

The third objective of this research is to run a simulation to compare the same six barriers according to the energy absorbed by each portion, via LS-DYNA simulation, and using NCAC Single Unit Truck (TL-4) to determine the barrier that absorbs the maximum energy caused by the impact, and as well, the geometry that creates the maximum safety in case of incidental impact. Additionally, this research will compare the safety criteria of each geometry in terms of the propensity for the vehicle to lift up and roll over upon impact, and the damage imposed to each barrier and deck overhang.

While there might be various ways to solve vehicle rolling after impact, such as using taller concrete barriers, or by using steel rails on top of the barriers, the objective of this thesis is to propose use of the 34 inch tall concrete barrier without steel rail installation, thus lowering costs while still maintaining safety standards.

2 LITERATURE REVIEW

In order to provide maximum safety in guardrails, barriers need to be designed based on both strength capacity and geometry. Both of these criteria should be able to provide maximum safety in case of vehicle impact. As mentioned previously, the main purpose of the barrier is to maximize the energy absorption caused by impact based on its strength capacity, while keeping the vehicle in line with the barrier while not letting it redirect to the traffic lane or rolling over.

This chapter presents the history behind the current New Jersey barriers and describes the two current theories for designing concrete barriers located on deck overhangs. By illustrating the problems inherent in these two theories, this research will introduce a new method which is more efficient and economical.

2.1 History of the New Jersey Barriers

The New Jersey barrier is the tapered concrete barrier that is used in many highways medians and sides. Although it is not exactly clear when and where were the concrete median barriers used for the first time, there is evidence that they were used in the 1940s on US-99 in California (NCHRP Synthesis 244, 1997). The first generation of concrete barriers was developed to (1) minimize the number of out-of-control vehicles penetrating the barrier, and (2) to avoid the maintenance costs for the barriers located on high-accident highways with narrow medians (NCHRP Synthesis 244, 1997). These concerns are as valid today as they were 50 years ago.

The first time a concrete barrier was used was in New Jersey in 1955. The height of this barrier was only 18 inches and it was similar to a low vertical wall with a curb on

each side. After a while, several problems were observed, causing the design to change which increased the height to 24 inches. Again on 1959, the height increased to 32 inches and it became the standard New Jersey barrier that is vastly used nowadays. The basic geometry of the New Jersey barrier can be described as one side going upward 2 inches from pavement, then the next 10 inches raises at a 55 degrees angle with respect to the horizontal line, and the remaining has an angle of 84 degrees with respect to the horizontal line (Kozel, 2004).

New Jersey developed such barrier after observing its performance on accidents. The geometry of the barrier was refined as accident data was analyzed. The state did not perform any crash-testing to develop the barrier. Both New Jersey and California continued experimenting in the early 1960s. Subsequently, the state of California installed 132 miles in 1972 and 680 miles in 1988. Today, the New Jersey barrier is accepted and used by almost every state. (Kozel, 2004)

2.2 Yield Line Theory

One of the most common theories to design the concrete barriers that are used nowadays is called “Yield Line Theory”. This theory was introduced by Hirsh in 1978 and then developed for New Jersey barriers by Calloway in 1993 and in 2013 by Barker and Puckett.

In 1978, T. J. Hirsch published “Analytical Evaluation of Texas Bridge Rails to Contain Buses and Trucks”. By analyzing the lateral load capacity of the barriers with uniform thickness, he calculated the strength of the barrier. Further, he calculated the

strength capacity of the guardrail to lateral load, based on the formation of yield line analysis and limit states. Yield line theory assumes a failure pattern of the barrier caused by the vehicle impact (F_t), over the length of a distributed impact force (L_t). Based on this pattern, the external work done by the vehicle should be equal or less than the internal virtual work done by the resisting moment of the barrier along the yield line (Hirsh, 1978).

Figure 8 represented the yield line pattern based on Hirsh theory.

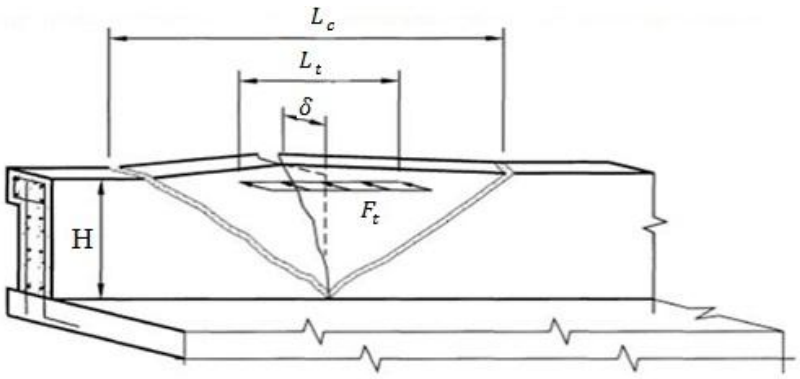

Figure 8: Yield Line Failure Pattern. (After Hirsh, 1978)

In 1993, Benita R Calloway published "Yield Line Analysis of an AASHTO New Jersey Concrete Parapet Wall". In this article, she presented the equation for external virtual work done by an applied load by considering collision force , deformation of the barrier in a horizontal direction (δ), critical length of the barrier (L_c), and the length of the distributed collision force (L_t).

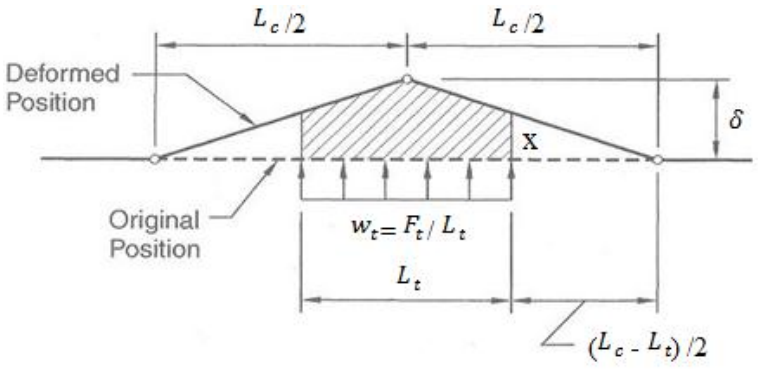

Figure 9: External Virtual Work Done by Vehicle Collision. (After Calloway, 1993)

Calloway states that the hatched area of the above mentioned figure represents the integral of total horizontal deformation.

Hence, the total internal work done by the barrier is equal to the summation of all rotations and moments caused by the barrier displacement. Since it has been assumed that the barrier acts as a rigid wall, all the rotations accrue in yield line paths. By considering this assumption, the rotation of the top part of the barrier can be expressed as,

$$\Theta = \tan \Theta = \frac{2\delta}{L_c} \qquad (5\text{-}1)$$

By dividing the barrier into two segments - the top beam with uniform wall underneath - the top beam developed plastic moment of M_b.

In this case, the horizontal and vertical reinforcement of the barrier develops moment resistance in both the vertical (M_w) and horizontal (M_c) directions of the moments respectively. These two moment capacities (M_α), develop inclined moment capacity along the yield line.

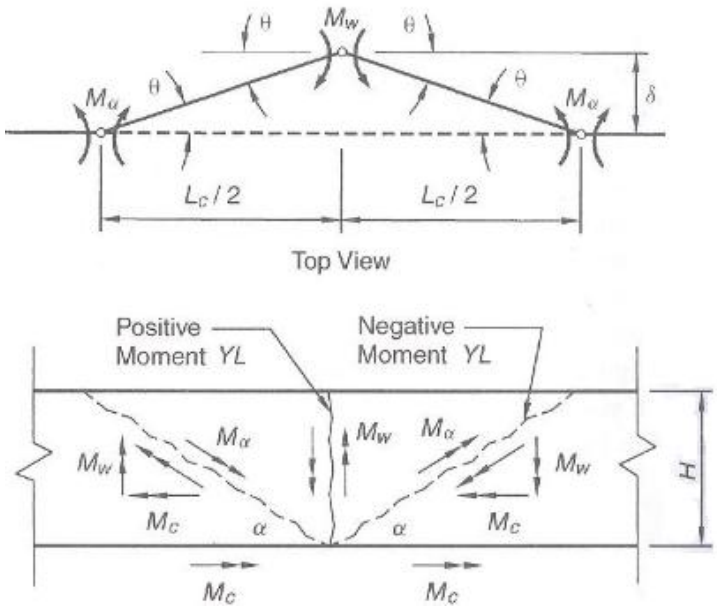

Figure 10: Moment Capacity of the Barrier. (After Calloway, 1993)

Hence, the resistance of the barrier is achieved by adding the virtual work done by moments.

In order to minimize the calculated vehicle impact, the yield line equation should be written based on vehicle impact force and differentiated by respecting the critical length. By setting these results to zero, the critical length of the barrier is achievable. In addition, the vehicle impact force is achievable by substituting the critical length in the yield line equation. The value of the vehicle impact force obtained is indicated as nominal railing resistance of the barrier to transverse loads) (R_w) (Calloway, 1993).

In 2013, Barker and Puckett published "Design of Highway Bridges". They compared both Hirsh and Calloway's theories in terms of critical length and nominal railing resistance to transverse loads, in order to obtain barrier moment capacities. They recommended using Hirsh's equation with the average value for both vertical and

horizontal moment capacities. By using the average value in Hirsh's equation, Calloway determined that the calculated nominal railing resistance to transverse load is 4% less than the actual, which can imply over-designing.

Although the yield line theory is accepted today and used by a variety of structural engineers in order to design concrete barriers, it might have some problems that are listed below:

- This is an old method, proposed almost 40 years ago, and still in use and accepted within the industry.
- In case of barriers located on the deck overhang, this theory did not consider the energy absorbed by deflection of the deck overhang
- The nature of the vehicle impact load is a dynamic load. This method designs the barriers based on a static load with a constant size over time
- Basing barrier construction on a static load, this theory did not consider vehicle roll over and redirection into the traffic lane. For instance, there might be a barrier designed based on this method which is able to resist vehicle impact, but not necessarily safe enough to meet all the criteria of a safe barrier.
- Since the theory is based on static load, it may be over-designed. Therefore, it may be possible to use less concrete in barrier by reducing its thickness.

2.3 Bridge Rail Design Procedure Methods

In 2014, Badiee published "Bridge Rail Design Procedure." By considering the deflection of the deck overhang, this article proposed two different methods for

redesigning the concrete barriers located on deck overhangs: (1) the Work Method, which considered the work done by the deck overhang, and (2) the Energy Method, which considered the energy absorbed by the deck overhang.

2.3.1 Work Method (Modified Yield Line Theory)

This method basically modified the "Yield Line Theory" method by adding the work done by the deck overhang, to this equation which is the base equation for the yield line method:

$$W = W_{yield} \qquad (5\text{-}2)$$

in which:

W = external virtual work done by the applied loads

W_{yield} = internal virtual work done by the resisting moments along the yield lines

By adding the new term which (work done by the deck overhang, W_{yield}), the modified yield line method will be:

$$W - W_d = W_{yield} \qquad (5\text{-}3)$$

Upon calculation, this value was subtracted from the external virtual work done by the applied loads, to obtain the new strength capacity for the barrier (Badiee, 2014).

Following is a brief summary of said method:

First Step: Calculate the Combined Mass Velocity of the vehicle and the barrier which is calculated as:

$$V = \frac{m_1 v_1 \sin\Theta}{m_{1+}m_1} \qquad (5\text{-}4)$$

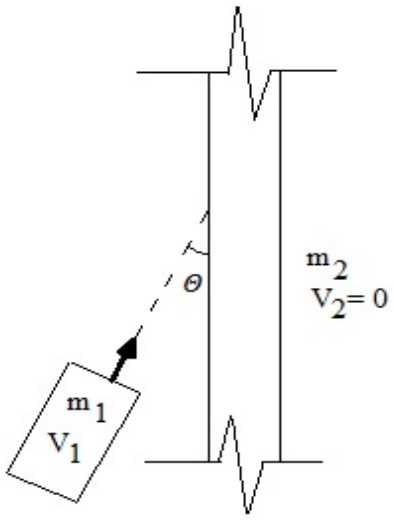

Figure 11: Top View Prior to the Impact (After Badiee, 2014)

Second Step: By having combined velocity, it is possible to obtain Transverse Impact Force (F_t):

$$\begin{cases} m_2 v_2 + \int F_t \, d_t = m_2 \, V \\ \int F_t \, d_t = F_t \, \Delta t \\ v_2 = 0 \end{cases} \quad => \quad F_t = \frac{m_1 m_2 V_1 \sin\Theta}{\Delta t(m_1+m_2)} \qquad (5\text{-}5)$$

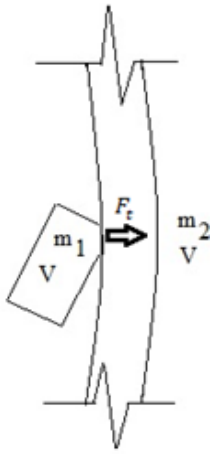

Figure 12: Impact Moment (After Badiee, 2014)

Third Step: By having the moment of inertia of the barrier and deck overhang, and based on the super position method, it is possible to calculate total deflection of the barrier and the deck overhang.

$$\Delta = \Delta_2 + \Delta_1 = \frac{F_t H^3}{3EI_2} + \frac{\left(H+\frac{t}{2}\right)^2 F_t l}{EI_1} \qquad (5\text{-}6)$$

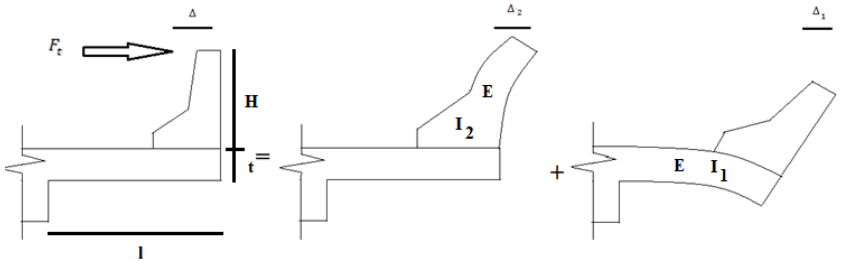

Figure 13: Deflection of the Barrier and the Deck Overhang (After Badiee, 2014) Third Step:

Fourth Step: Calculating the work done by the deflection of the barrier and the deck overhang in the elastic region:

$$W_d = F_t\ (\text{Area}) = \frac{1}{2} F_t^2\ \Delta = \frac{{F_t}^3 H^3}{6EI_2} + \frac{\left(H+\frac{t}{2}\right)^2 {F_t}^3 l}{2EI_1} \quad (5\text{-}7)$$

Fifth Step: As mentioned in "Design of Highway Bridges", based on Yield Line Method, the work done by the barrier (W_{yield}), and the work done by the external virtual load (W) were:

$$W_{yield} = \frac{8M_b\delta}{L_c} + \frac{8M_w\delta}{L_c} + \frac{M_c L_c \delta}{H} \quad (5\text{-}8)$$

$$W = w_t(\text{area}) = F_t \frac{\Delta}{L_c}\left(L_c - \frac{L_t}{2}\right) \quad (5\text{-}9)$$

In which area is:

$$\frac{1}{2}(\delta + X)L_t = \delta \frac{L_t}{L_c}\left(L_c - \frac{L_t}{2}\right) \quad (5\text{-}10)$$

Hence, the modified yield line theory would be equal to:

$$W - W_d - W_{yield} = 0 \quad (5\text{-}11)$$

Hence, the new Transverse Impact (F_t) will be equal to:

$$F_t = -\frac{2(M_c {L_c}^2 + 8HM_w + 8HM_b)}{H\,(L_t - L_c)} \quad (5\text{-}12)$$

Sixth Step: To calculate the critical length of the barrier ($L_{c,}$) that minimized the (F_t), and the new transverse impact force needed to differentiate based on the critical length:

$$\frac{dF_t}{dL_c} = -\frac{2\,M_c {L_c}^2 + 16\,H\,M_w + 16\,H\,M_b}{H\,(L_t - L_c)^2} - \frac{4\,L_c M_c}{H\,(L_t - L_c)} = 0 \quad (5\text{-}13)$$

where the critical length is equal to:

$$\begin{cases} L_{c1} = \dfrac{L_t M_c + \sqrt{M_c(M_c L_t^2 + 8HM_w + 8HM_b)}}{M_c} \\ L_{c2} = \dfrac{L_t M_c - \sqrt{M_c(M_c L_t^2 + 8HM_w + 8HM_b)}}{M_c} \end{cases} \quad L_c = \text{Max}\{L_{c1}, L_{c2}\} = L_{c1} \qquad (5\text{-}14)$$

Seventh Step: Make sure that the calculated transverse impact is less than nominal railing resistance to transverse load (R_w):

$$R_w > F_{t\,(TL)} \qquad (5\text{-}15)$$

2.3.2 Energy Method

Based on this method, all energy absorbed by the (1) deflection of the barrier in elastic and plastic region, (2) deflection of the deck overhang in the elastic region, and (3) vehicle deformation, should be less than the Impact Severity energy:

$$IS \leq (\Delta_1 \text{or } \Delta_2) + \Delta_3 + \Delta_4 \qquad (5\text{-}16)$$

IS = Impact Severity = moving vehicle energy prior to the impact perpendicular to the barrier.

Δ_1 = strain energy absorbed by the barrier in elastic region

Δ_2 = strain energy absorbed by the barrier in the plastic region.

Δ_3 = energy absorption by the vehicle due to its deformation.

Δ_4 = strain energy absorbed by deck overhang in elastic region.

Based on Test Level 4 criteria, impact severity energy for Test Level 4 can be calculated as:

$$IS = E_{\text{Vehicle bf. impact}} = \frac{w_1 v_1^2 \sin\theta^2}{2g_c} \quad (5\text{-}17)$$

Which is equal to:

IS = 100689.4 ft-lbf

At the moment of impact, the velocity of the barrier and the vehicle is the same and by considering the barrier length equal to vehicle length (27.6 ft), this velocity is equal to:

$$\mathbf{V} = \frac{\mathbf{m_1 v_1 \sin\theta}}{\mathbf{m_1 + m_2}} = 8.68 \text{ mph} = 12.73 \text{ ft/sec} \quad (5\text{-}18)$$

In which M_1 and M_2 are the mass of the vehicle and barrier respectively.

The next step was to calculate the strain energy of the barrier in elastic and plastic region and the strain energy absorbed by the vehicle (which was considered as 56% of vehicle initial kinetic energy).

- Strain energy absorbed by the barrier in elastic region:

$$\Delta_1 = \frac{w_2 V^2}{2g_c} = 22237.9 \text{ ft-lbf} \quad (5\text{-}19)$$

Or 22% of perpendicular vector of impact energy (IS = 100689.4 ft-lbf)

- Strain energy absorbed by the barrier (If Section Reach PLASTIC Region):

- $\Delta_2 = W_{\text{yield line}} = \frac{8M_b\delta}{L_c} + \frac{8M_w\delta}{L_c} + \frac{M_cL_c\delta}{H} = 45\delta$ ft-lbf (5-20)

In which δ is the maximum horizontal displacement of the barrier

- Strain energy absorbed by the vehicle

$$\Delta_{3-2} = E_{\text{Vehicle,AFTER impact}} = \frac{w_1V^2}{2g_c} = 45296.09 \text{ ft-lbf} \quad (5\text{-}21)$$

Hence, the strain energy absorbed by the deck overhang in elastic region was:

$$\Delta_4 = IS - (\Delta_1 + \Delta_3) = 33142.86 \text{ ft-lbf} \quad (5\text{-}22)$$

which was 32% of the total impact energy

Although the modified yield line theory and the new energy method allowed for significant progress being made in the designing of the barriers located on deck overhangs, it also had some problems listed below:

- All assumptions of work method are based on Yield Line Theory, which is an old method.
- The nature of the vehicle impact load is a dynamic load. The work method designs the barriers based on a static load which has a constant size over time.
- Since both methods are based on static load and mathematical formulas, they did not consider vehicle roll-over and redirection to the traffic lane.

- Using the Energy Method, the mass of the barrier calculated was based on the length of the truck. This assumption seems inaccurate.
- Since the Work Method proposed was based on a static load, it did not consider the work done by the deformation of the vehicle.

Although Yield Line Theory is the preferred method by designers in different states, and even though Modified Yield Line Theory made significant progress by considering work done by the deck overhang, the proposed approach in this research aims to address the drawbacks and shortcomings of the aforementioned theories by providing a better and more reliable method that considers all aspects of the vehicle impact such as:

- Barrier and deck overhang damage due to vehicle sliding
- Amount of energy that will absorb by truck's deformation
- Safety criteria such as vehicle lift up and vehicle roll over

The next chapter will discussed the new method that is being proposed.

3 PROPOSED NEW METHOD

Reviewing previous design methodologies for constructing barriers located on deck overhangs has aided this research in proposing a new method, using the LS-DYNA simulation in order to obtain a more efficient result which is not only closer to reality but also considers all aspects of impact design. To clarify that both of the said methods might be inaccurate, this research ran both static simulation and dynamic simulation to compare them with the previous methods. By having the static load results, it is possible to study the energy absorption of each component in the system and compare it with the dynamic simulation results. This comparison can provide a better understanding about the role of the vehicle in the system which was neglected by the previous design methodologies.

Moreover, this research proposes five different geometries in order to:

- Produce a more economical barrier by reducing the amount of material used while still maintaining the capacity to resist the impact force
- Reduce the risk of vehicle lift up and roll over that is observed in the current New Jersey barriers

3.1 Static Simulation

This section ran the static simulation with all assumptions mentioned in Chapter 3, in order to compare it with the previous methods.

It is obvious that when a 54 kips load is imposed upon a barrier, the system is going to have two different moments applied to the barrier and the deck overhang. Figure 14 represents these two moments.

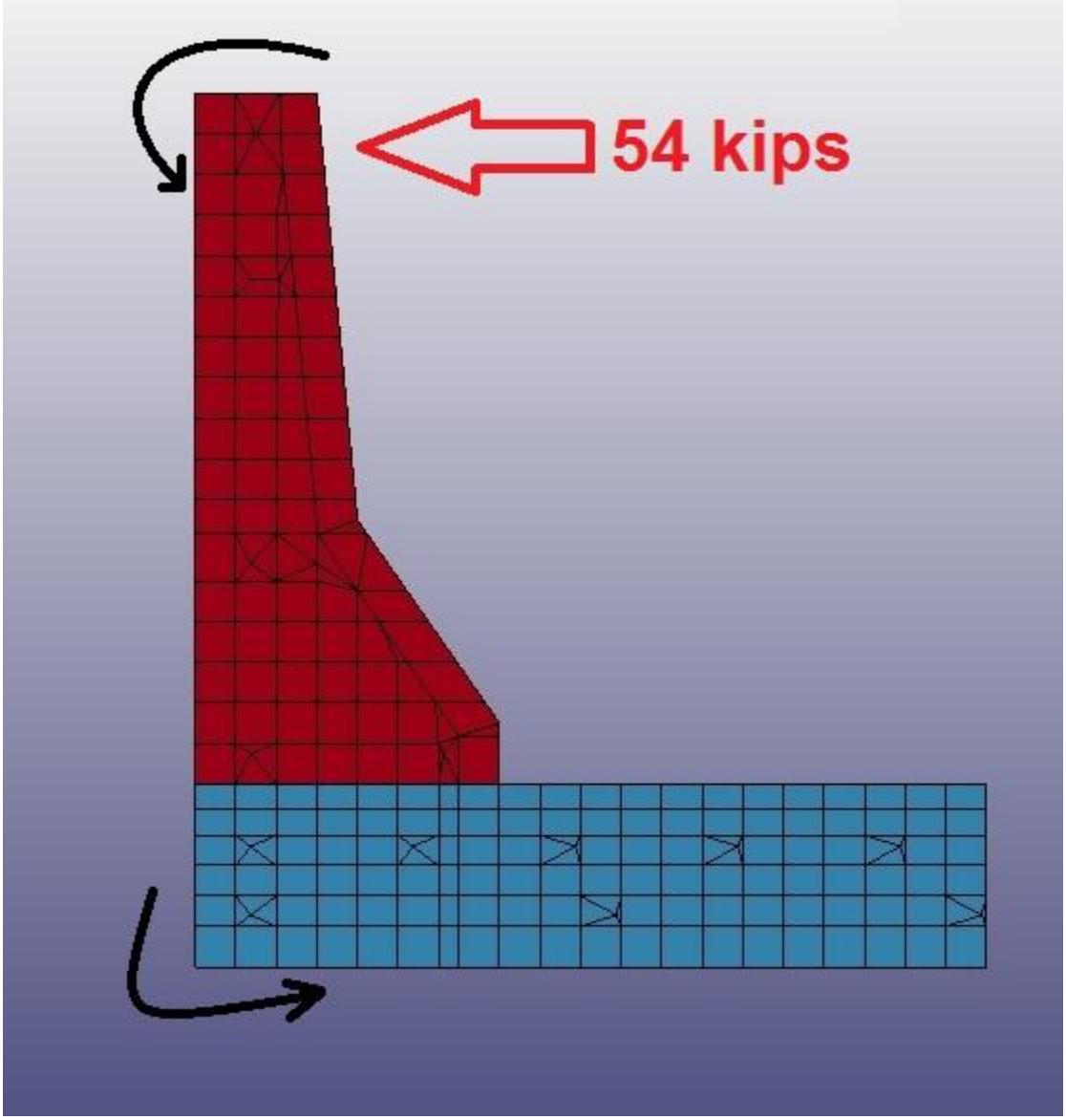

Figure 14: Moments by barrier and deck overhang

The top arrow represents the moment imposed upon the barrier and the bottom arrow represents the moment imposed upon the deck overhang. These moments cause the

tension and compression on the front and back face of the barrier. On the other hand, some of the energy caused by the 54 kips force was tolerated by the deflection of the deck overhang. The moment imposed upon this portion caused the top and bottom of the deck overhang to respond to tension and compression respectively.

Based on all of the said assumptions in Chapter 3, the energy absorbed by each portion was:

Absorbed energy by the barrier = 2.08e5 n-mm = 45.62% of total energy

Absorbed energy by the deck overhang = 2.00e5 n-mm = 43.87% of total energy

Absorbed energy by the reinforcement bars = 4.79e4 n-mm = 10.51% of total energy

Total energy = 4.559e5 n-mm

Figure 15 to Figure 17 showed the energy absorbed by each portion.

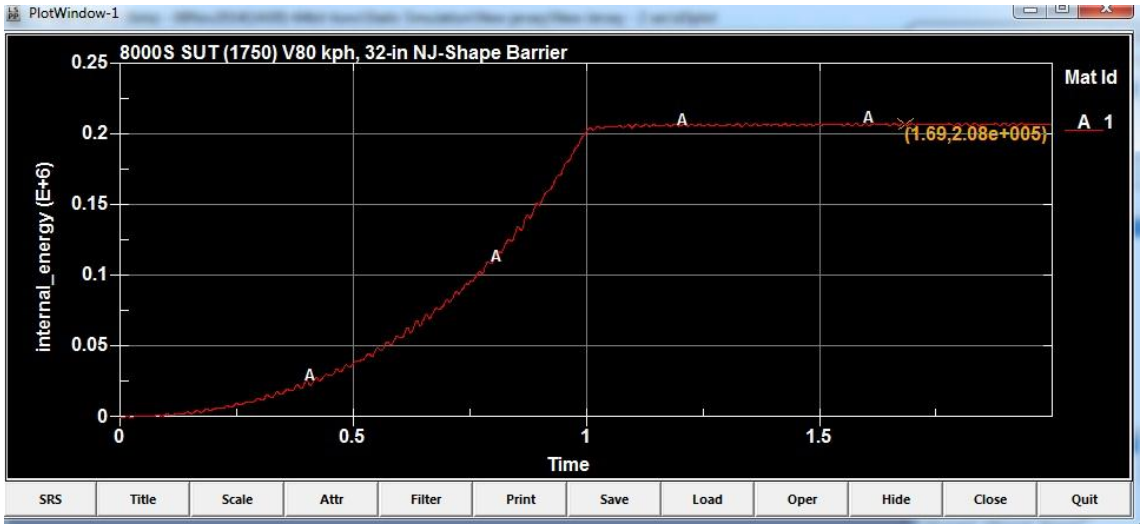

Figure 15: Energy absorbed by the barrier – Static load

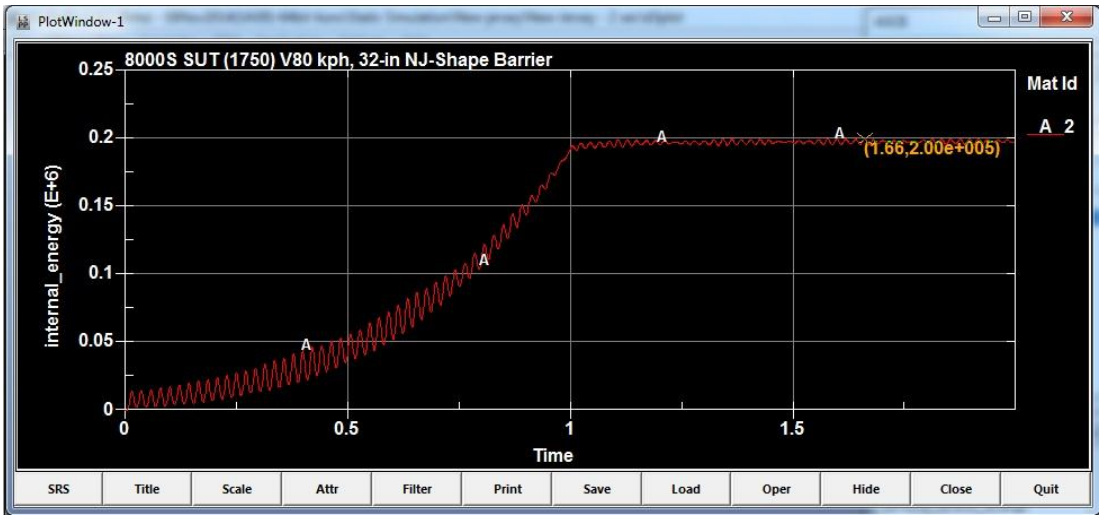

Figure 16: Energy absorbed by the deck overhang – Static load

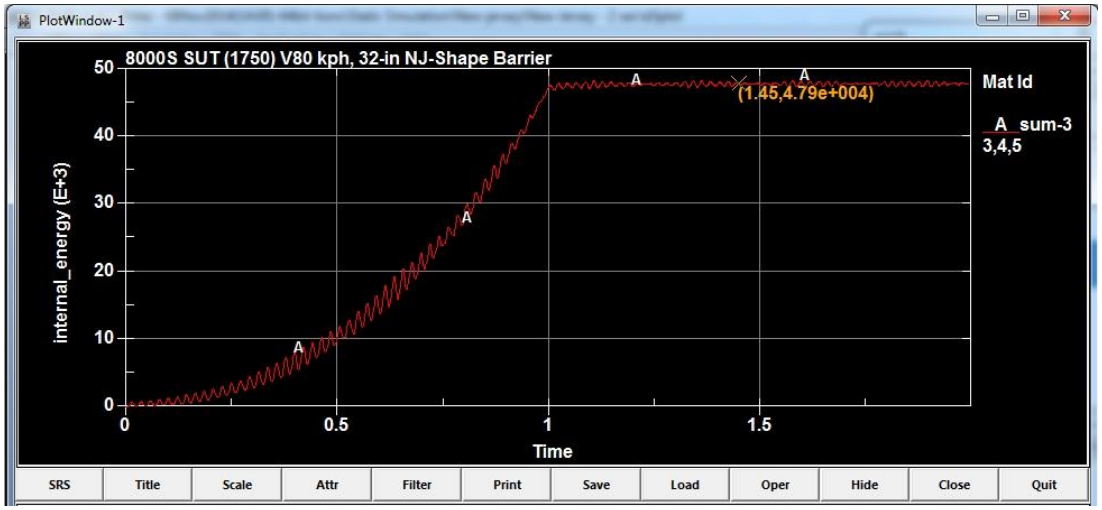

Figure 17: Energy absorbed by the reinforcement bars – Static load

As it has been calculated, if one considers half of the reinforcement bars energy absorbed by the reinforcement bars in the deck overhang, all the deck overhang has the energy absorption of close to 50% of the total energy. Compared to the Yield Line Method, this amount of energy was totally neglected, and Yield Line Method considered

all of the energy absorbed by the barrier, which is not realistic. Hence, there might be a chance to design a thinner barrier.

On the other hand, although the energy method mentioned before considered the energy absorbed by the deck overhang, it was based on Yield Line Method, which calculated the total energy absorbed by the deck overhang as 32% of the total energy. However, it was something closer to 50% of the total energy. This difference might be (1) caused by the length of the deck overhang and the barrier used to calculate their mass, which was based on the length of the vehicle and (2) neglecting vehicle sliding.

Hence, this simulation shows that both of the aforementioned methods have their problems and numerical differences in assumptions and results.

3.2 Dynamic Simulation

As mentioned before, since the static load simulation is not realistic and simply based on an assumption aimed at simplifying Test Level 4, the new method is needed to include and develop dynamic load, which is more realistic and makes the model reliable for future applications and research. Hence, for this research, Ford Single Unit Truck from NCAC finite element models was considered (Finite Element Model Archive, 2008). By calculating the internal energy absorbed by all portions after the second impact of the truck, it is possible to compare whether the assumptions in the previous methods are correct.

Based on the results that this research obtained from the finite element model, the energies absorbed by each portion after second impact (at 0.62 seconds) are:

Absorbed energy by the truck = 1.36e8 n-mm = 11.90% of total energy

Absorbed energy by the barrier = 2.58e8 n-mm = 22.57% of total energy

Absorbed energy by the deck Overhang= 5.99e8 n-mm = 52.41% of total energy

Absorbed energy by the reinforcement bars = 1.50e8 n-mm = 13.12% of total energy

Total energy = 1.14e9 n-mm

Figure 18 to Figure 21 showed the energy absorbed by each portion.

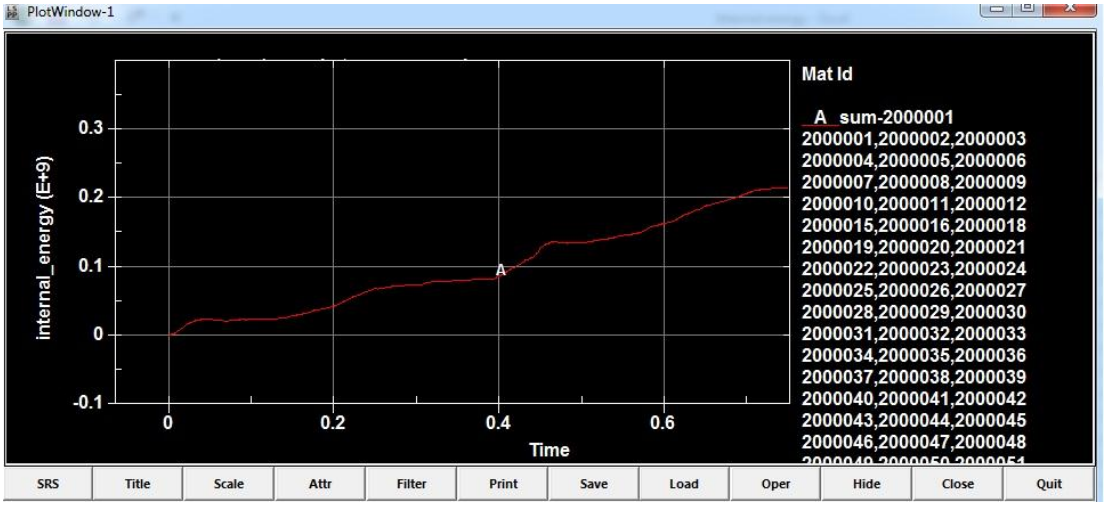

Figure 18: Energy absorbed by the truck - Dynamic Impact

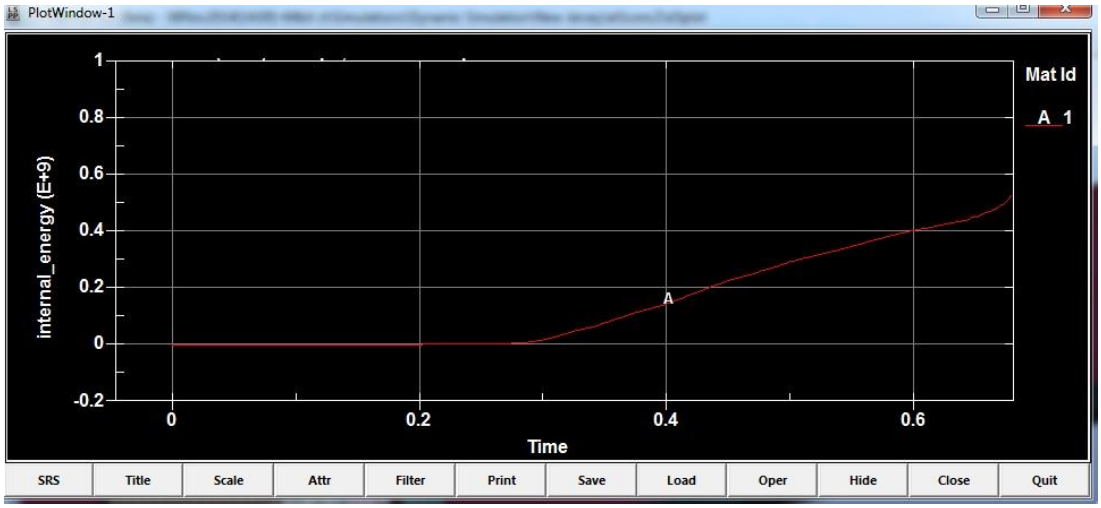

Figure 19: Energy absorbed by the barrier - Dynamic Impact

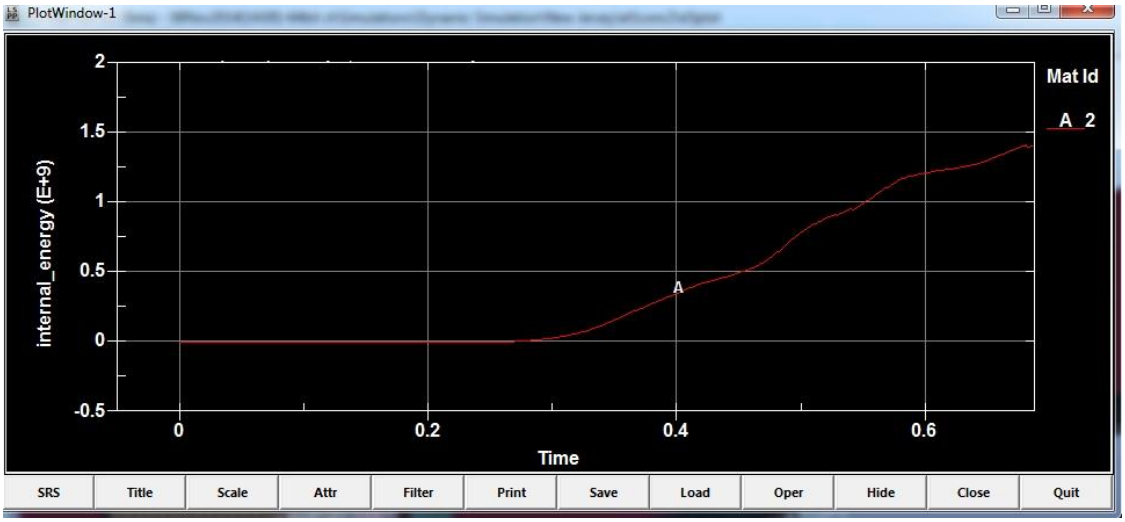

Figure 20: Energy absorbed by the deck overhang - Dynamic Impact

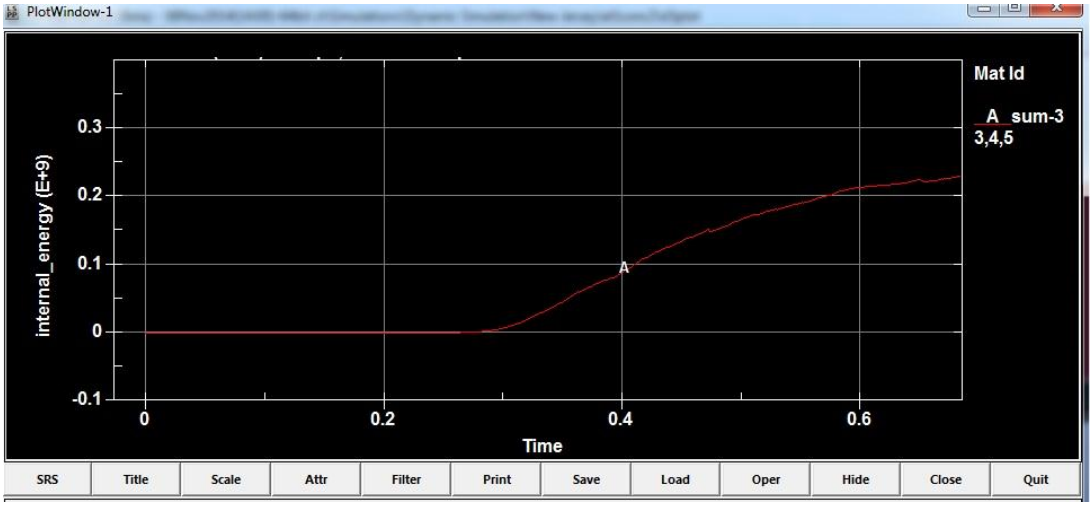

Figure 21: Energy absorbed by the reinforcement bars - Dynamic Impact

First and foremost, the energy quantity absorbed by dynamic impact is higher than the energy absorbed in static load. The total energy absorbed based on static load is almost 4% of the total energy absorbed in dynamic load, because in dynamic simulation a vehicle is moving with certain kinetic energy to the barrier, while in static load, only a transformed static load is applied to the barrier. The barrier in dynamic impact had damage to some of its elements because it absorbed a lot of energy

Moreover, the energy absorption's percentage for all portions in dynamic simulation match closely with the static load, the only difference being the absence of a vehicle in static load. The vehicle's energy absorption's percentage added to the barrier.

Figure 22 showed the percentage of energy absorbed by each portion, in static and dynamic load.

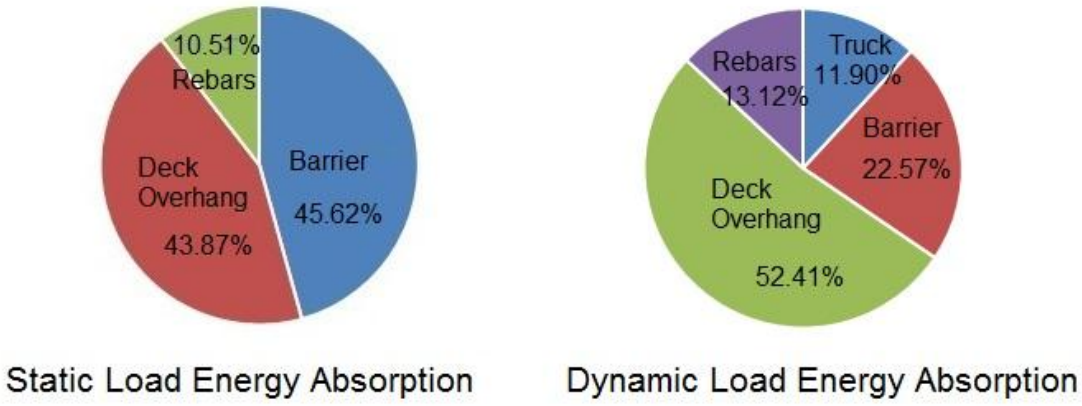

Figure 22: Dynamic Load vs. Static Load - Internal Energy Absorption

With the use of dynamic impact simulation, we can surmise that more than 50% percent of the vehicle impact is absorbed by the deck overhang, a factor completely neglected in Yield Line Method. Although the Energy Method considered the deflection of the deck overhang, it was still a static assumption and therefore, not reliable. In addition, the energy absorbed by the Energy Method - calculated at 32% - is less than 52% of the energy calculated using dynamic impact simulation. As mentioned earlier, this difference might be based on the length of the barrier – also considered as length of the truck - and consequently, might not be realistic. There is a vehicle in the dynamic model simulation, which is totally neglected by the said two methods,

This truck can absorb almost 12% of the energy caused by its deformation. Moreover, the said two methods designed the barrier based on certain criteria and calculations. The safety of the road parallel to the barrier and underneath traffic layers are completely neglected. In the previous three chapters, the research showed that vehicle

roll-over is a major concern and there may be better geometries in order to avoid this occurrence.

3.3 Geometries

This research seeks to analyze and determine an appropriate redesign with the best geometry of the concrete barrier located in the bridge deck overhang. In order to reach this goal, an ideal geometry should be able to (1) minimize vehicle damage and keep the vehicle in line with the guardrail by not letting it roll over the barrier or falling off the bridge or redirected to the traffic lane, (2) maximize the energy absorption caused by the vehicle collision by barrier breakage while still being able to provide maximum safety, and (3) not to let the bridge experience any damage caused by deck overhang deflection.

All of the aforementioned tasks need a lot of experiment and simulation. This research provided five different geometries (with the exception of the New-Jersey type concrete barrier located on deck overhang), and by comparing all of these geometries - in terms of energy absorption by each portion, deflection, and deformation - it is possible to decide which geometry is best for future research. All of the proposed barriers have the same amount of reinforcement bar equal to New Jersey type concrete barriers. The height considered for all geometries as 34 inches like the current New Jersey geometry.

3.3.1 New-Jersey Barrier

New Jersey barrier is the most widely utilized barrier today, especially on high traffic highways. They are most often used to separate traffic lanes and/or at the sides of highways to keep vehicles in line with traffic lanes in case of incidental impact. Based on

this research, the problem with this barrier is that (1) the internal energy that will be absorbed by this geometry is not efficient, (2) based on "Determination of Minimum Height and Lateral Design Load for MASH Test Level 4 Bridge Rails" (after Sheikh, Nauman M, 2011), the slope on the bottom segment of the barrier will cause the single unit truck to lift up and roll over the barrier. The New Jersey barrier cross-section is referenced in Figure 23

Figure 23: Vehicle Lifting Up (After Mohan, Marzougui, & Kan, 2003)

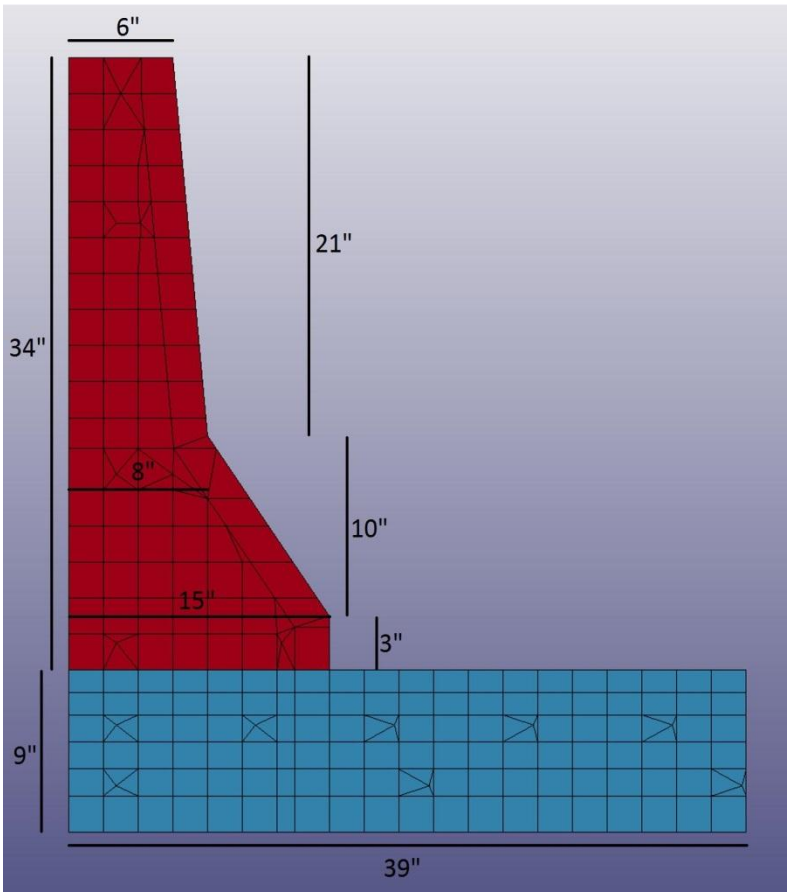

Figure 24: New Jersey Barrier Cross-Section

3.3.2 Modified New Jersey Barrier

This geometry is being presented to study the behavior change of the barrier by modifying its taper slope and thickness. Modifying thickness helps the barrier to break during impact and absorb more energy which results in less damage to the vehicle. Moreover, increasing taper slope helps the vehicle to lift up less which results in less rolling over and redirecting of the vehicle into the traffic lane. In addition, less concrete is needed to pour this barrier geometry. Figure 25 depicts the cross section of the modified New Jersey barrier.

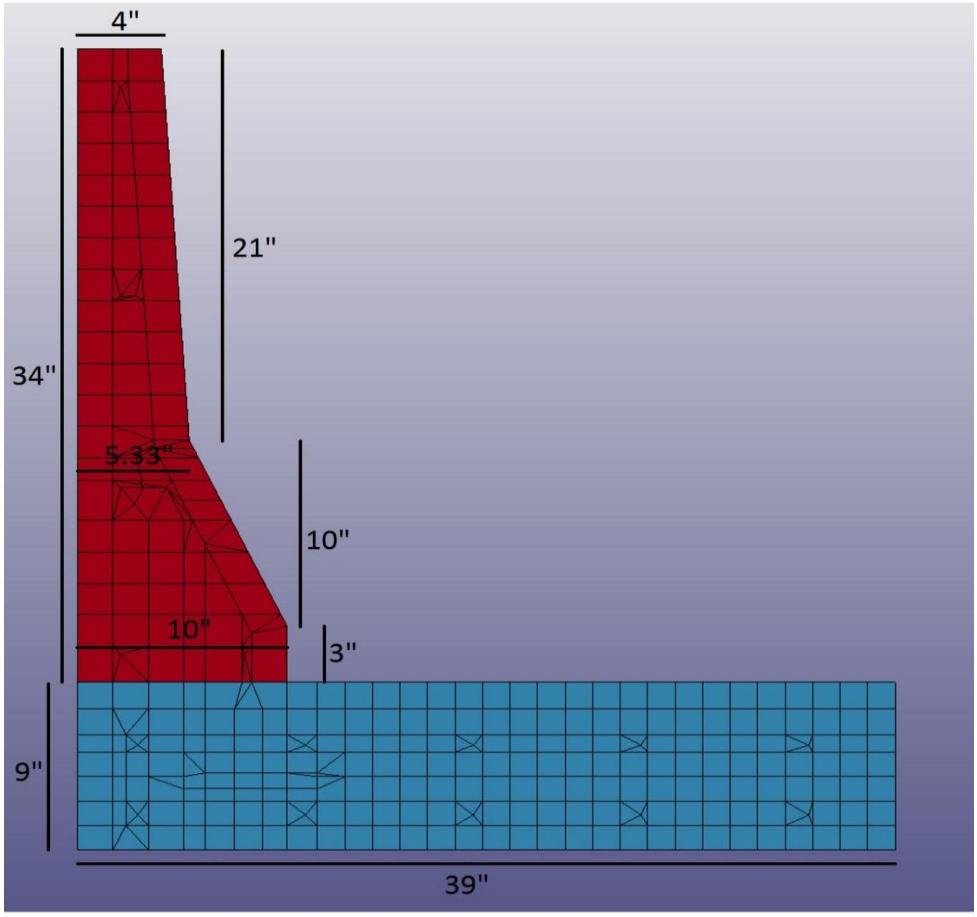

Figure 25: Modified New Jersey Barrier Cross Section

3.3.3 Rectangular - 8 Inch Thickness Barrier

Although this example causes more damage to the truck, the purpose of presenting this geometry is to eliminate the slope of the two segments in New Jersey barriers, in order to minimize vehicle rolling over and redirection into the traffic lane.

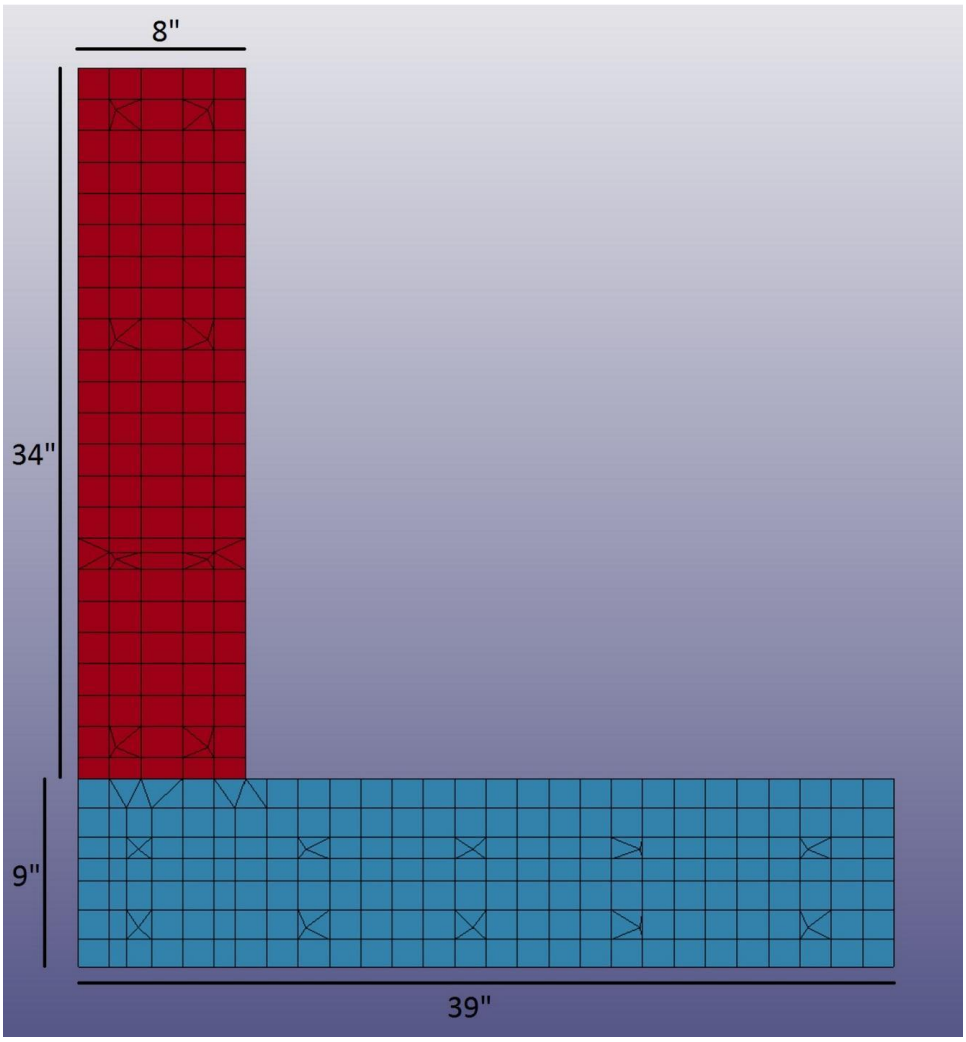

Figure 26: Rectangular – 8 inch Thick Barrier

3.3.4 Rectangular - 6 Inch Thickness Barrier

This barrier is similar to the aforementioned rectangular – 8 inch barrier, but by reducing the thickness by 2 inches, it would use less concrete and be more economical to produce.

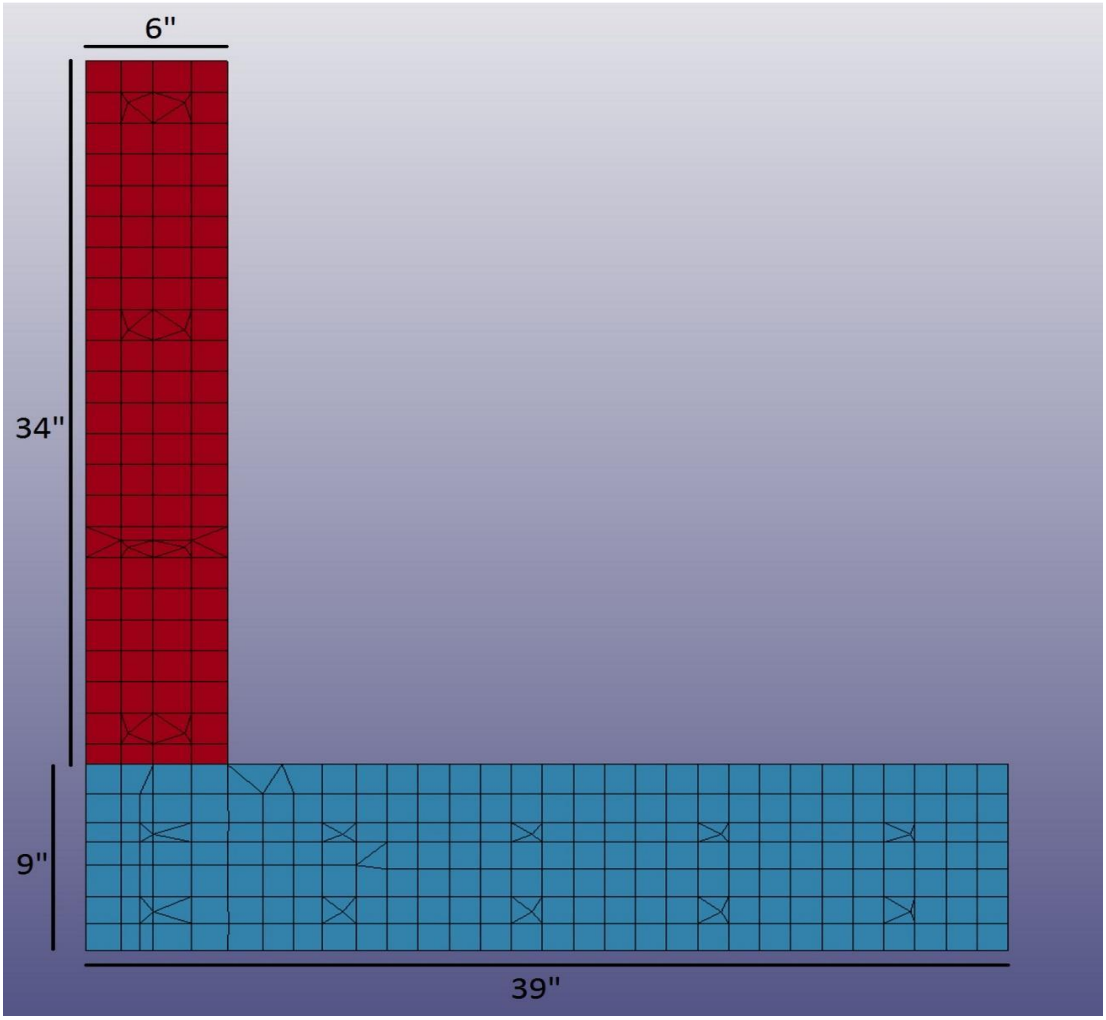

Figure 27: Rectangular – 6 inch Thick Barrier

3.3.5 Modified Single Slope Barrier

Single slope barriers are typically used in the middle of intersections for separating highway traffic flow. Their dimensions are often a thickness of 8 inches at the top and 24 inches at the bottom with an overall height of 42 inches. This research presents a modified single-slope barrier that is asymmetric and located on the bridge deck overhang. It has a thickness of 4 inches at the top and 10 inches at the bottom, and is 34 inches tall.

The purpose of presenting this geometry is to have a uniform slope in order to avoid a vehicle lifting up and rolling over, while still using the same height as New Jersey barrier to reduce the pouring costs for concrete.

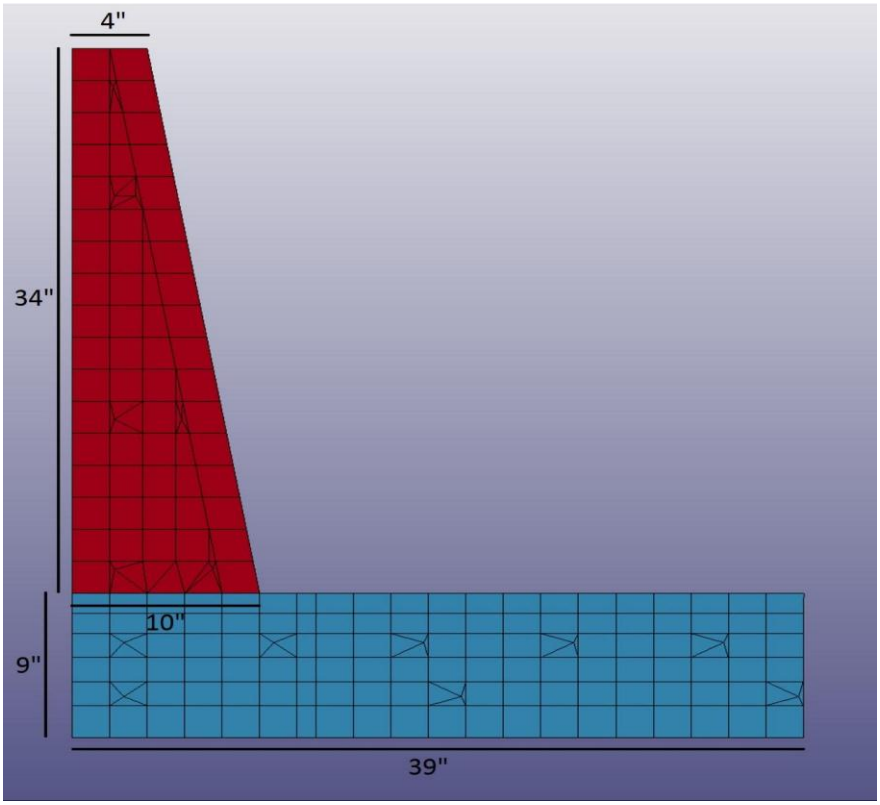

Figure 28: Modified Single Slope Barrier

3.3.6 Inverted Modified Single Slope Barrier

The functionality of this barrier type is the same as for rectangular barriers, but since it has different thicknesses along its height, in case of higher impacts to the bottom portion of the barrier, it performs more efficiently, while still at a height of 34 inches.

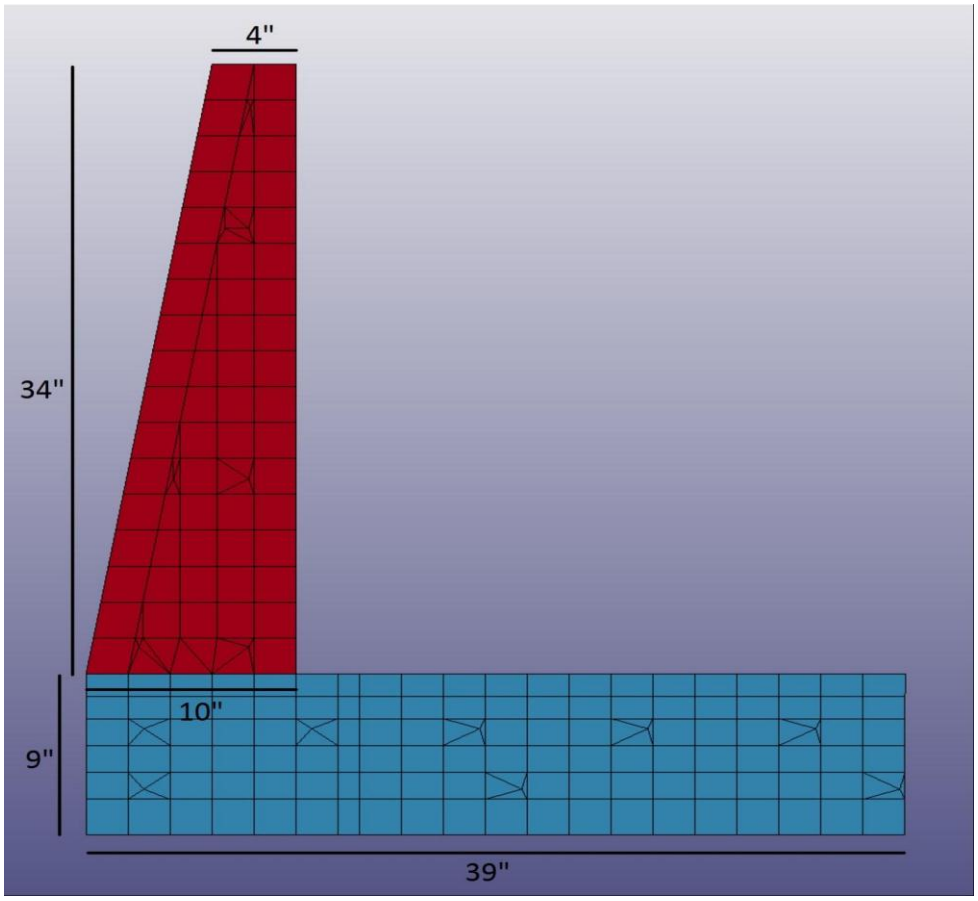

Figure 29: Inverted Modified Single Slope Barrier

4 FINITE ELEMENT MODEL SPECIFICATIONS

The research simulated the New Jersey barrier in depth using LS-DYNA, in an effort to determine which core components of the barrier could be improved. According to these findings, this research proposed the said five geometries. This chapter describes in detail all the assumptions and selections that were considered in order to generate and run the simulation.

4.1 Assumptions

4.1.1 Deck Overhang Dimensions

Concrete barriers are located between bridge traffic lanes to separate them, and on bridge sides in order to prevent vehicles falling off the bridge. Concrete barriers on bridge sides are located on deck overhangs that are 9 inches thick and 39 inches in length from the middle of the bridge girder or column (Barker & Puckett, J., 2013).

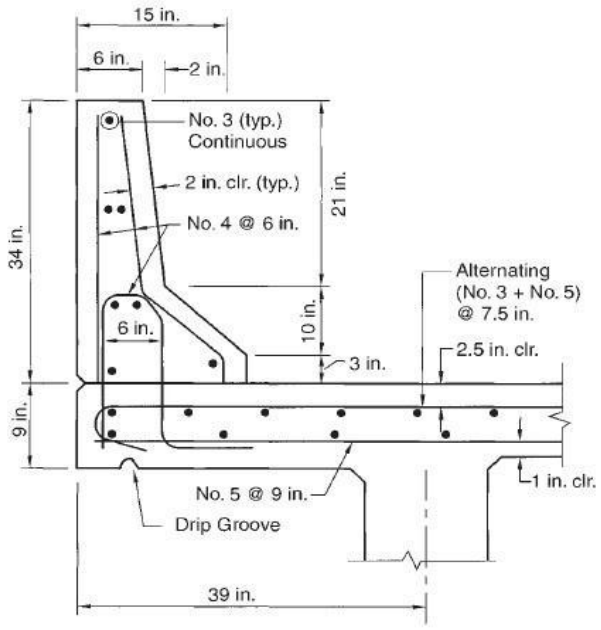

Figure 30: Barrier and deck overhang cross-section (After Baker & Puckett, 2013)

This research considered the length of deck overhangs to be 39 inches.

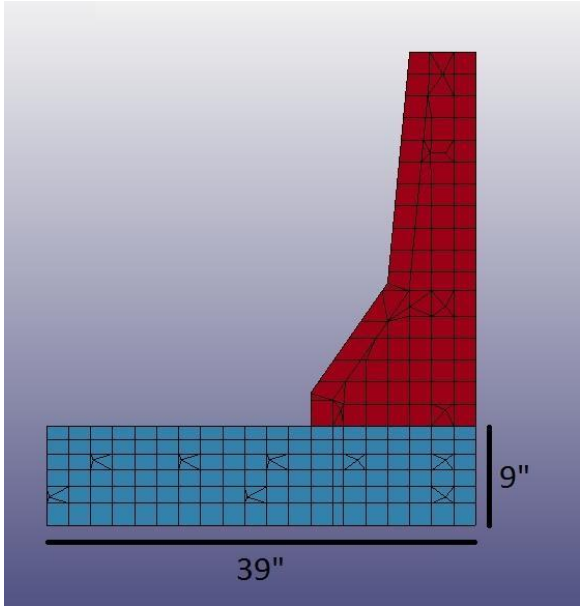

Figure 31: Deck Overhang Length

4.1.2 Bridge Pad

To simplify the finite element model, this research used a rigid body pad that represents the bridge surface. Figure 32 shows the dimensions of this pad.

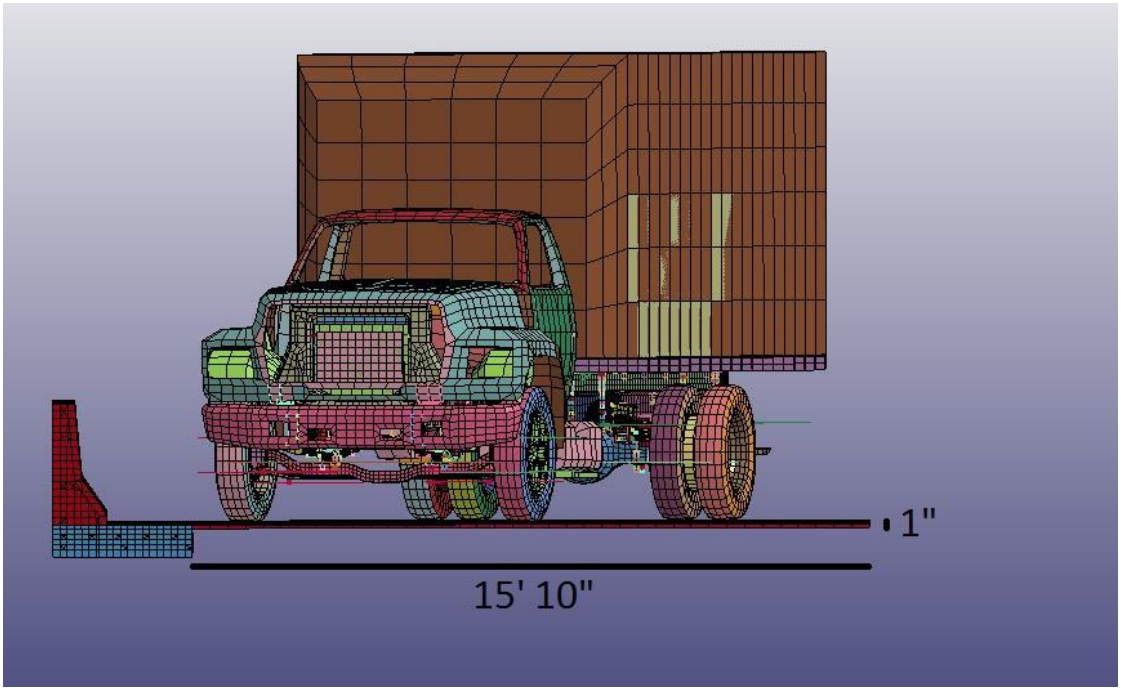

Figure 32: Rigid Pad Dimension

4.1.3 Barrier and Deck Overhang Length

In 2008, the National Crash Analysis Center (NCAC) of George Washington University, under a contract with the FHWA and NHTSA of the US DOT, developed a TL-4 model using Ford Single Unit Truck for the LS-DYNA simulations. This finite element model used a barrier length of 120 feet. This research used the same length for the simulation (Finite Element Model Archive, 2008).

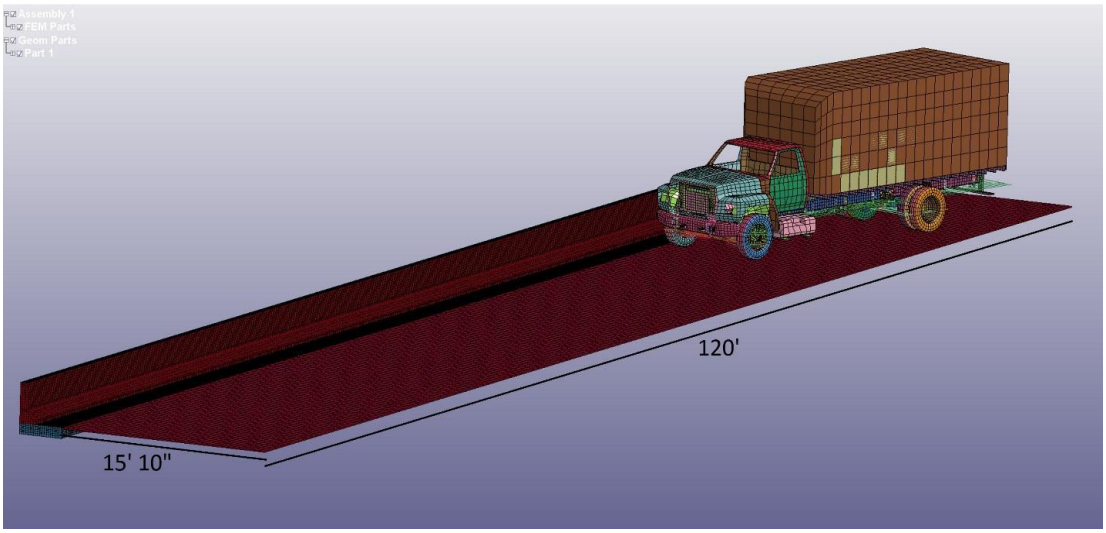

Figure 33: Deck Overhang Length

4.1.4 Single Unit Truck Specifications

Based on AASHTO, Test Level four means that a single unit truck hits the guardrail at 50 mph (80 kmph), and at an angle of 15 degrees. In 1993 The National Cooperative Highway Research Program (NCHRP) published a report - "Recommended Procedures for the Safety Performance Evaluation of Highway Features" - that indicated that the weight for the single unit truck in Test Level 4 should be considered as 8000 kg (Ross, Sicking, Zimmer, & Michie, 1993). As mentioned in Chapter 3.2.3, NCAC made the Ford truck based on NCHRP report 350 that has 35,353 elements. This research used an F800 truck in order to simulate the behavior with different proposed barriers. The distance between barrier and truck for all barriers was considered to be 3 feet.

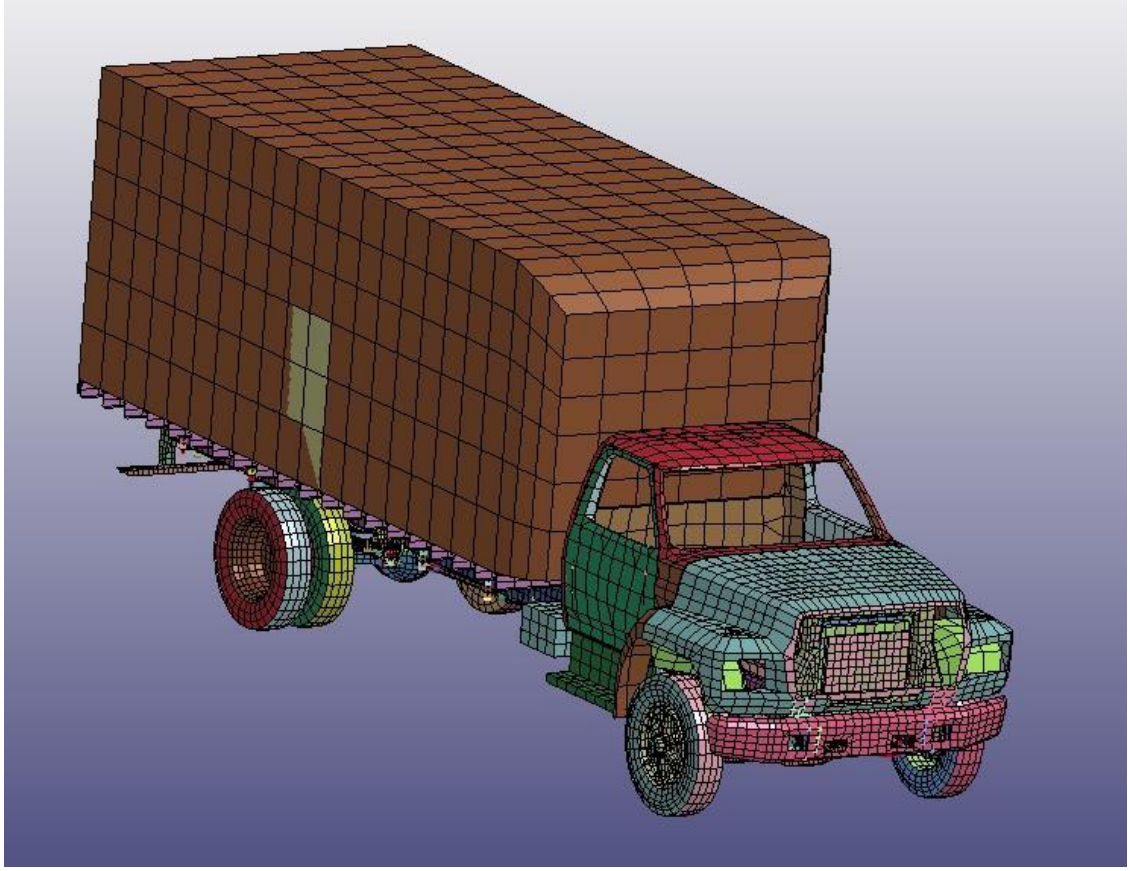

Figure 34: F800 Single Unit Truck (Finite Element Model Archive, 2008)

4.1.5 Static Load Specifications

AASHTO requires the designers to design the barriers for high-speed highways, freeways, expressways, and interstate highways with a traffic mixture of trucks and heavy vehicles based on Test Level 4. Based on the impact simulation, the height of the distributed load should be 13 inches and starts from the top of the barrier. The equivalent static load that represents Test Level 4 is a distributed 54 kips load with the length of 3.5 feet (Barker & Puckett, J., 2013).

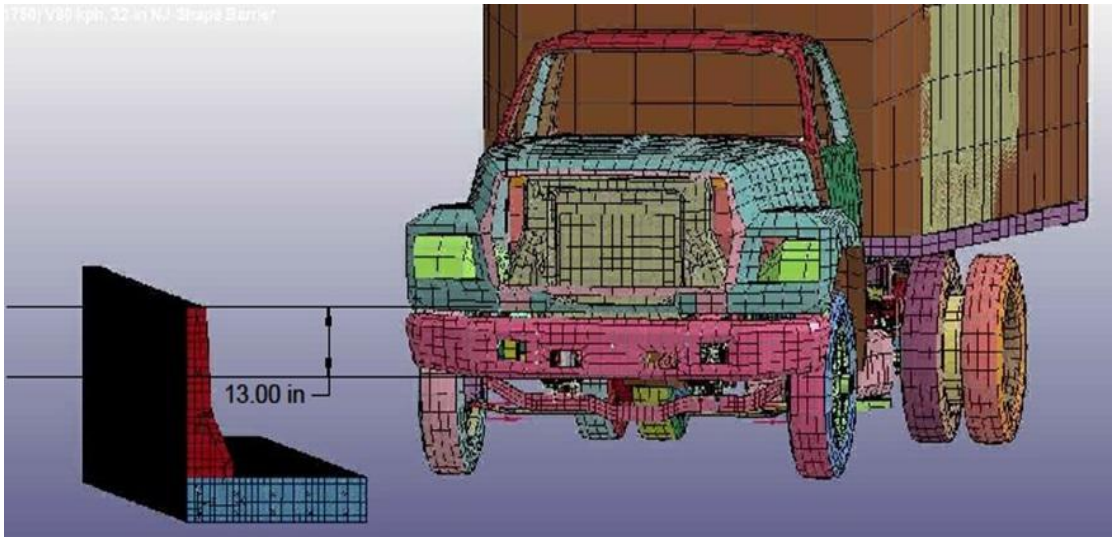

Figure 35: Distributed Static Load Height

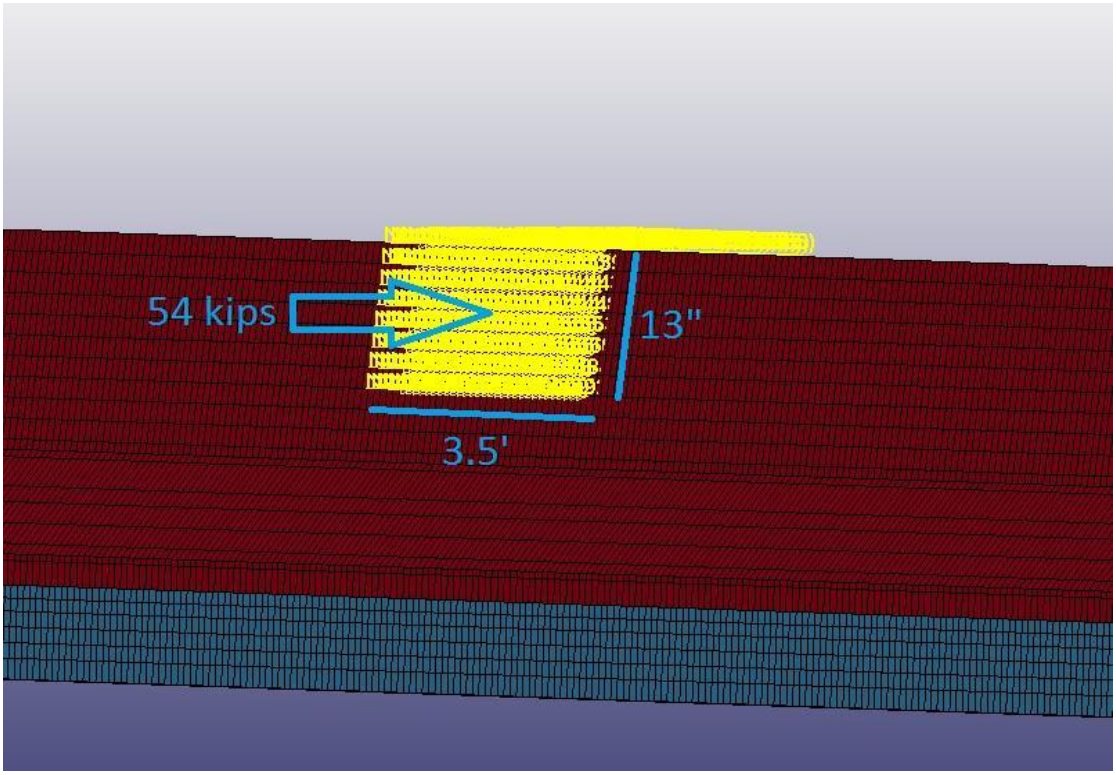

Figure 36: Length and Height of Static Load

4.1.6 Contact Definition Between the Truck and the Barrier

Bala and Dale published "General Guidelines for Crash Analysis in LS-DYNA" that indicates that the best contact to simulate crash analysis in LS-DYNA is "Automatic Single Surface". It further mentioned that for contact surfaces with sharp corners, SOFT should be equal to 2 (Bala & Day). Figure 37 shows the specifications of this contact between the truck and the barrier.

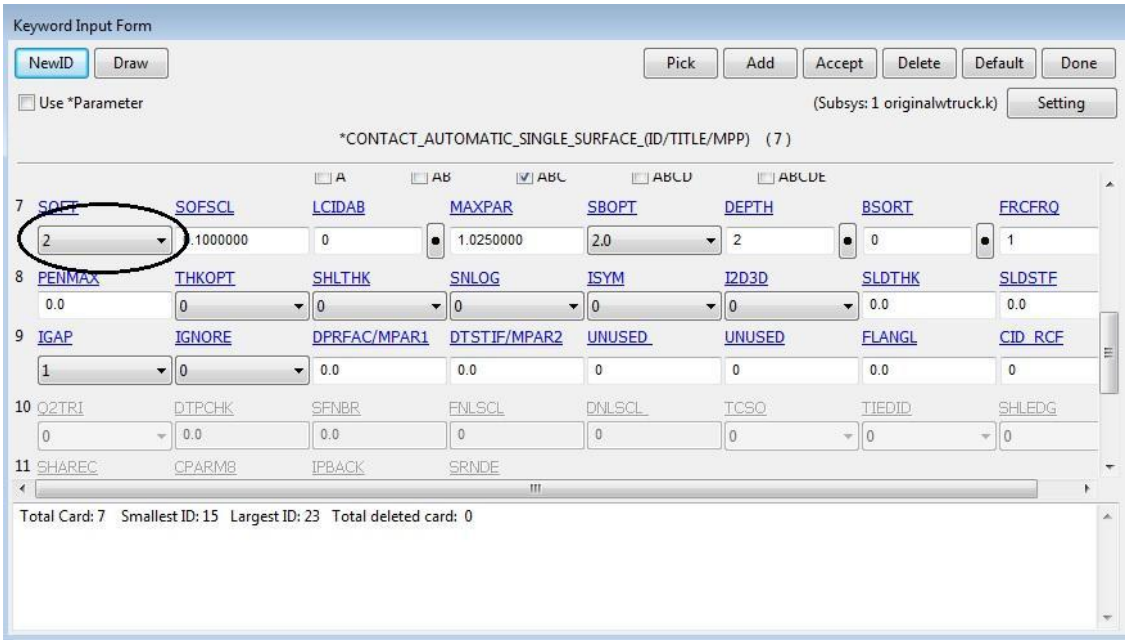

Figure 37: Automatic Single Surface specifications (LS-DYNA)

3.2.7 Hourglass Effect

The Hourglass Effect is a spurious deformation in finite element meshes without absorbing or releasing any energy. Normally, hourglass effects in crash analysis should be less than 10% of the total energy (Bala & Day). In LS-DYNA, there is a card that can

control hourglass effects. This research utilized the hourglass card that defined the single unit truck model for NCAC.

4.1.7 Boundary Condition Assumptions

This research considered both ends of the barrier and deck overhang as fixed supports.

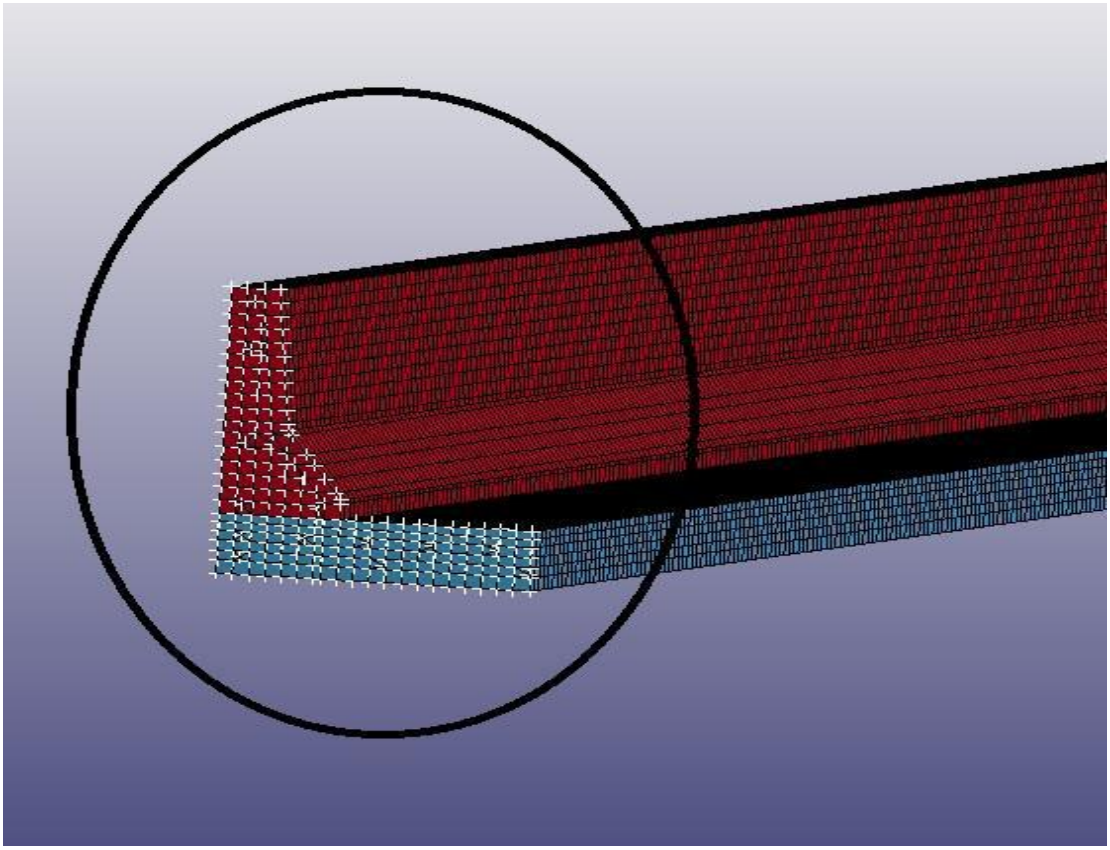

Figure 38: Fixed Supports (Both ends)

This research additionally considered the deck overhang as a cantilever; hence, the side of the deck overhang located on the column is considered as fixed support.

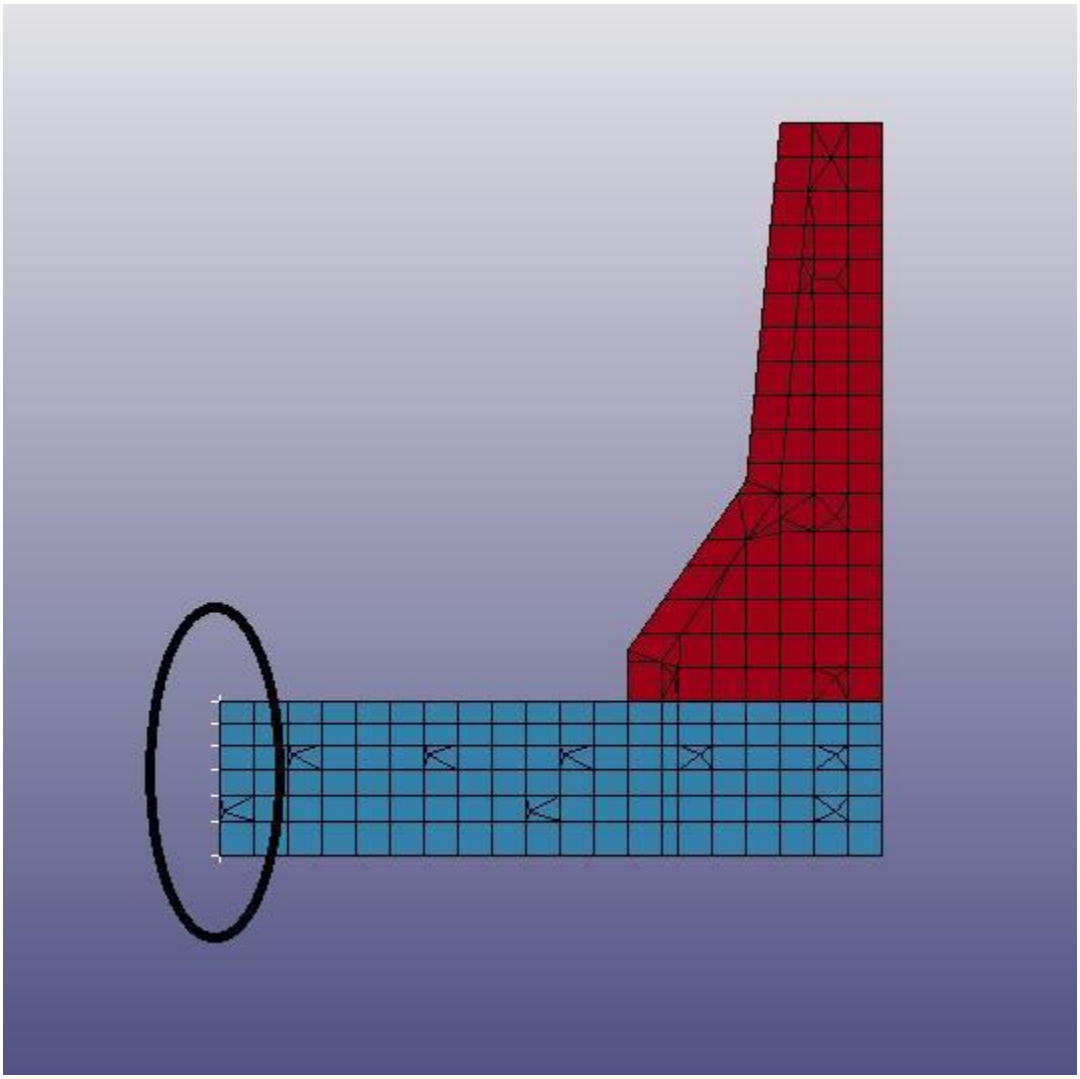

Figure 39: Fixed Support (deck overhang)

In dynamic simulation, the rigid pad under the vehicle is also considered as fixed support.

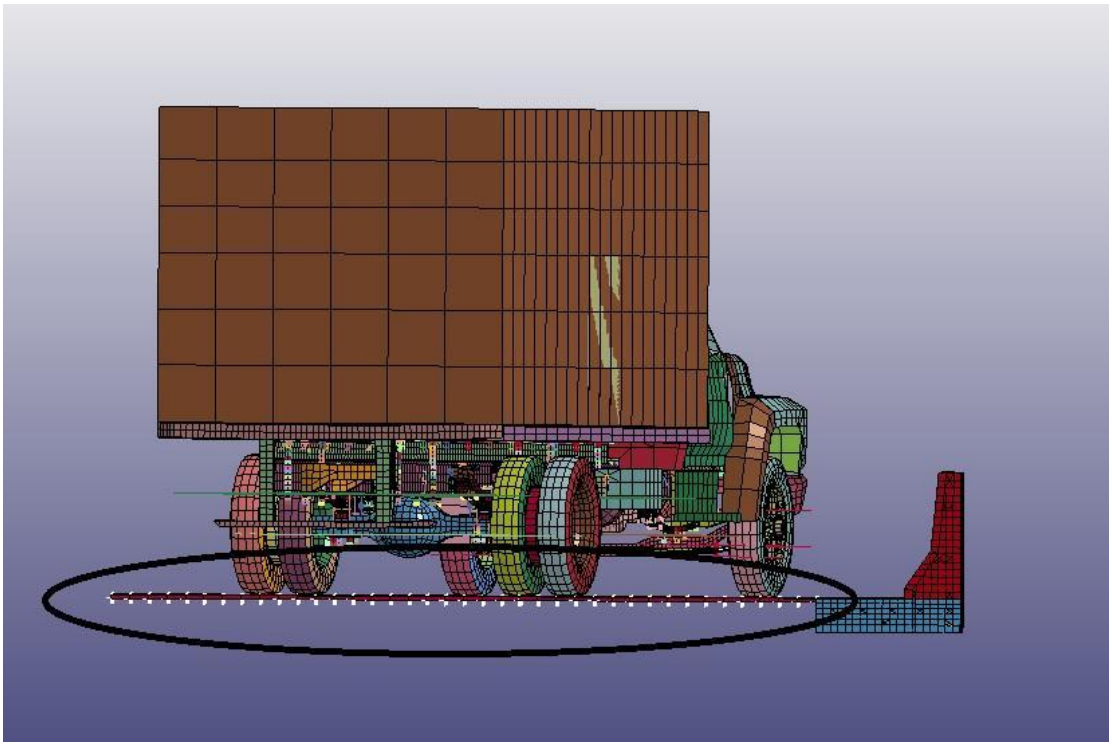

Figure 40: Fixed Support (Rigid pad)

4.1.8 Load Curves

In LS-DYNA, for each static load, the user must define a load curve. In this research for the dynamic simulation, one load curve is defined as representing gravity. For the static simulation, two load curve are defined. The first load curve represents gravity and the second one represents the 54 kips static load.

Figure 41: Gravity Load Curve

Figure 42: Static Load Curve

The research considered the termination time for static load equal to 2 seconds.

4.1.9 Mesh Size

To simulate the New Jersey concrete barrier, the National Crash Analysis Center (NCAC) used a mesh size with the average dimension of 3.2 inches and a maximum dimension of 3.78 inches.

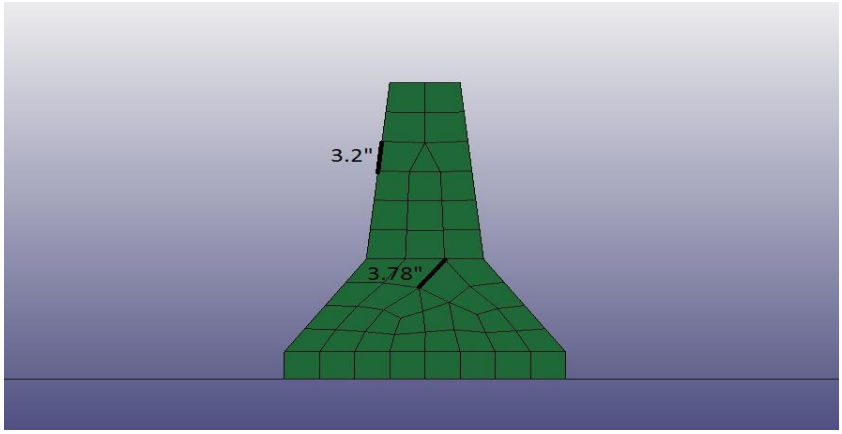

Figure 43: Average and Maximum Mesh Dimension of the New Jersey Concrete Barrier (Finite Element Model Archive, 2008)

To be on the safe side, this research considered the average mesh dimension for all proposed concrete barriers at 2.0 inches, and with a maximum mesh dimension of 2.44 inches.

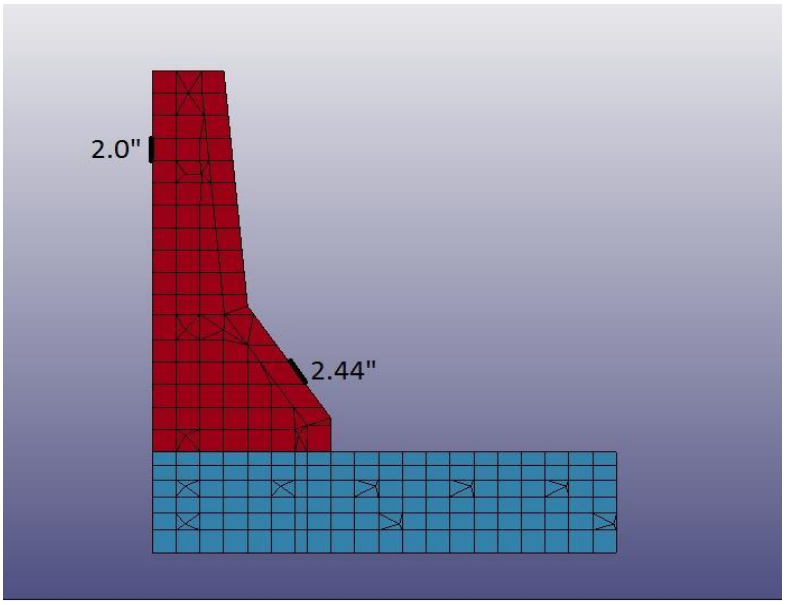

Figure 44: Average and Maximum mesh dimension of the New Jersey concrete barrier with deck overhang.

4.2 Materials

4.2.1 Concrete

In 2007 Murray, Abu-Odeh, and Bligh published "Evaluation of LS-DYNA Concrete Material Model 159". Their research simulated different concrete structures such as concrete beam, Texas T4 bridge rail, and safety-shaped barrier. Since their research paper tested these concrete structures in reality and got an acceptable result, *this research paper* used Murray et al.'s assumption for concrete properties to simulate the proposed concrete barriers and deck overhang. Figure 45 and Figure 46 show the properties for concrete material 159 in LS-DYNA.

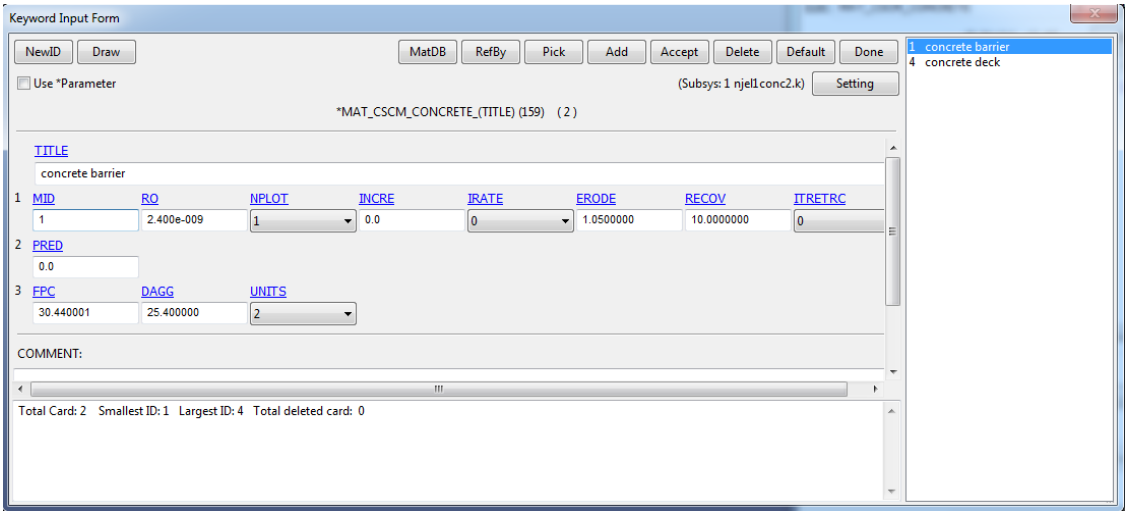

Figure 45: Concrete Material 159 for Barrier

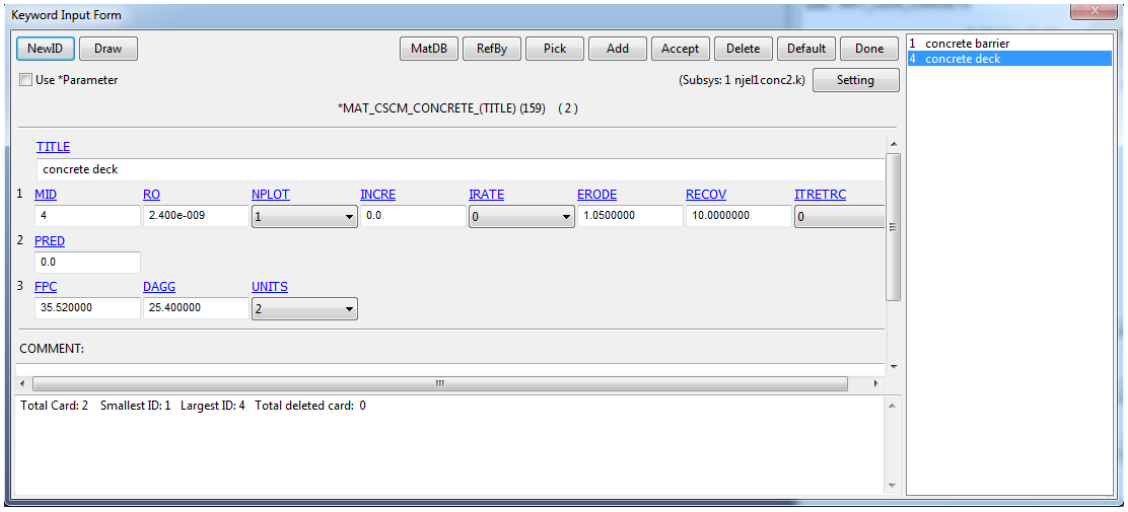

Figure 46: Concrete Material 159 for deck overhang

ACI 318-11 provided a formula to calculate normal weight concrete module of rupture. This formula is: $f_r = 7.5\sqrt{f'_c}$ in which both f'_c and f_r are based on psi. Hence, module of rupture for the concrete:

- Used in barrier: : $7.5\sqrt{4415}\ (psi)$ or 498.34 (psi) = 3.44 Mpa
- Used in deck overhang: $7.5\sqrt{5152}\ (psi)$ or 538.33 (psi) = 3.71 Mpa

In 2011 Pajak published "the Influence of the Strain Rate on the Strength of Concrete Taking Into Account the Experimental Techniques". He mentioned that In order to reflect the dynamic loading in the analysis for concrete, modulus of elasticity and compressive strength of the concrete must be multiplied by the DIF factor (PAJAK, 2011). As a result, based on the below mentioned figure, Dynamic Increase Factor (DIF) for the impact is between 1.2 – 1.05. To be conservative, for comparison between the geometries in tension and compression, DIF considered as 1.05. Hence, for the dynamic comparison, new f'_c and f_r would be:

- New f'_c = 1.05 x 30.44 MPa = 31.96 MPa Barrier
- New f'_c = 1.05 x 35.52 MPa = 37.30 MPa Deck Overhang

- New f_r = 1.05 x 3.44 MPa = 3.61 MPa Barrier
- New f_r = 1.05 x 3.71 MPa = 3.90 MPa Deck Overhang

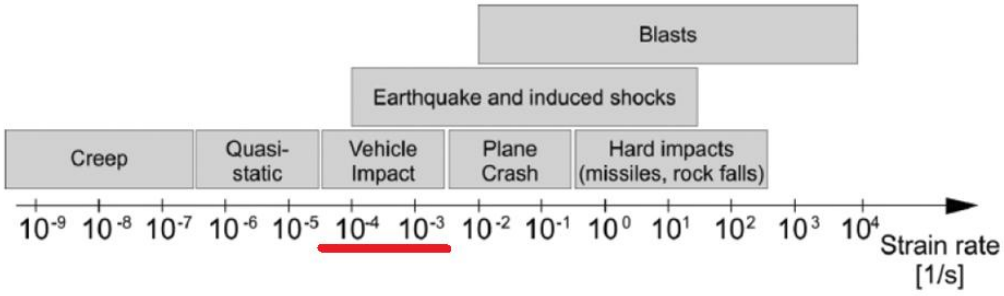

Figure 47: Dynamic Increase Factor Domain for Vehicle Impact (After Pajak, 2011)

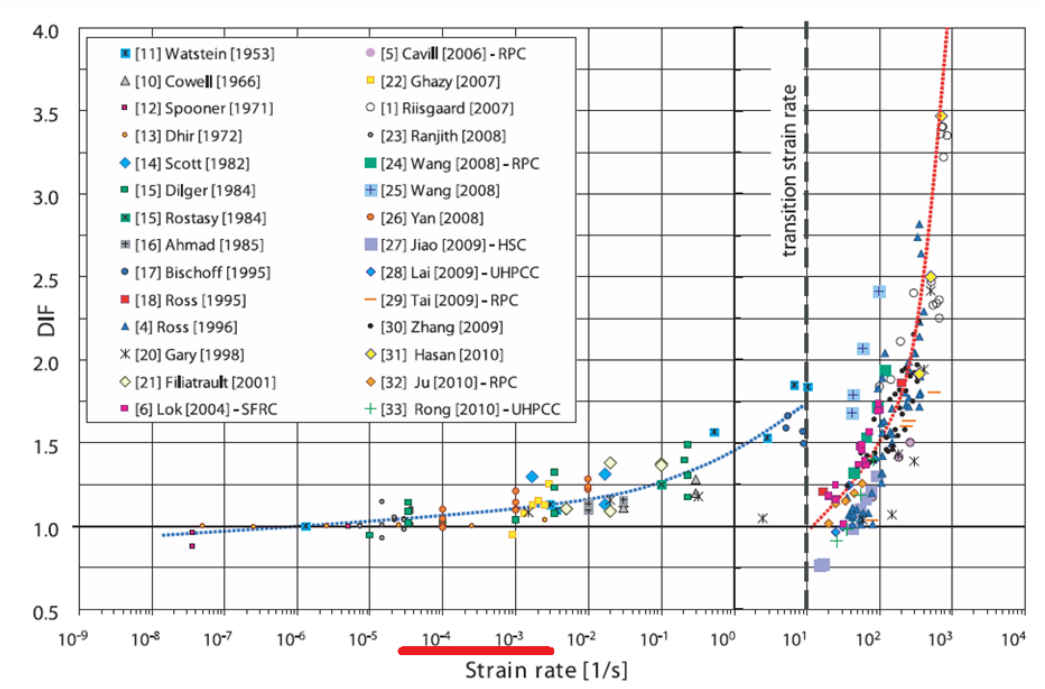

Figure 48: Dynamic Increase Factor (Compressive Strength of Concrete)

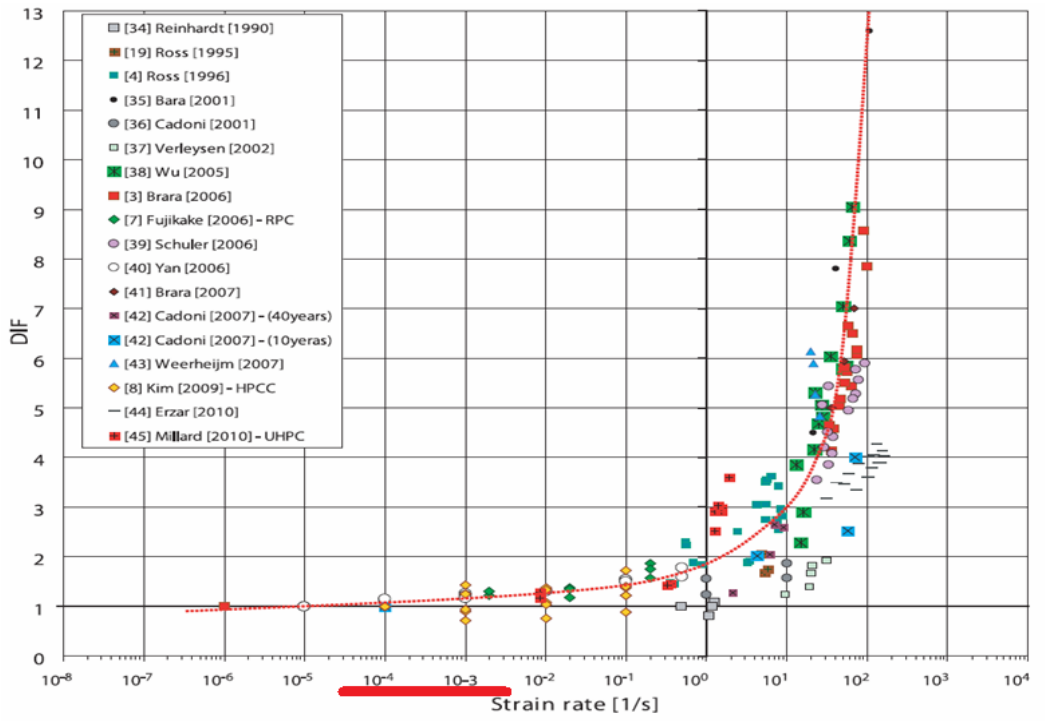

Figure 49: Dynamic Increase Factor (Tensile Strength of Concrete)

Elements erode when damage exceeds 99% and the maximum principal strain exceeds ERODE-1.0 (LS-DYNA Keyword User's Manual, 2007). The recommendation is to specify erosion from 5% to 10% of the maximum principal strain (Abu-Odeh, Bligh, & Yvonne, 2007).

Therefore, this research considered ERODE for concrete material that is equal to 5%. Based on the "General Guidelines for Crash Analysis in LS-DYNA", solid section considered for concrete with a element formulation of 1 that is suitable for crash simulations (Bala & Day).

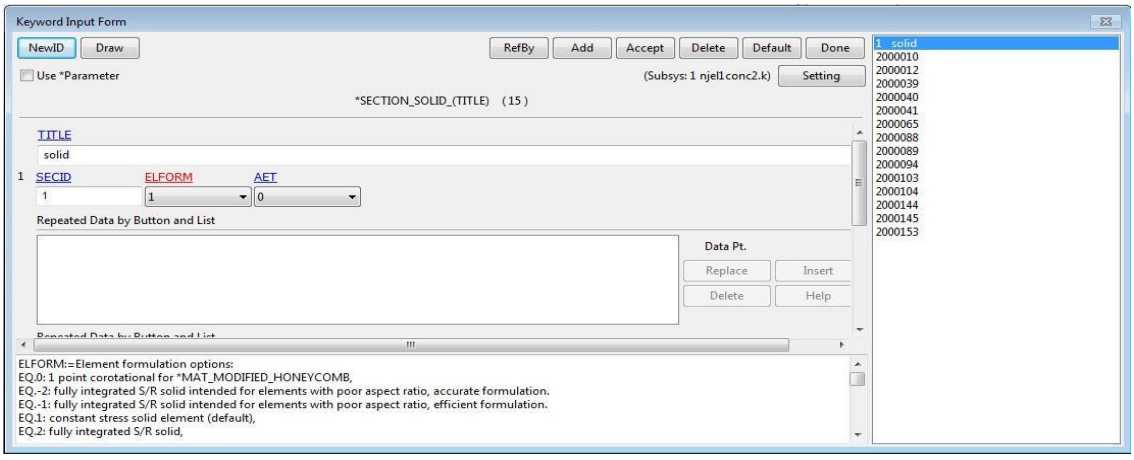

Figure 50: Solid Section Specifications

4.2.2 Reinforcement bar

AASHTO considers reinforcement bar as a perfectly-plastic material.

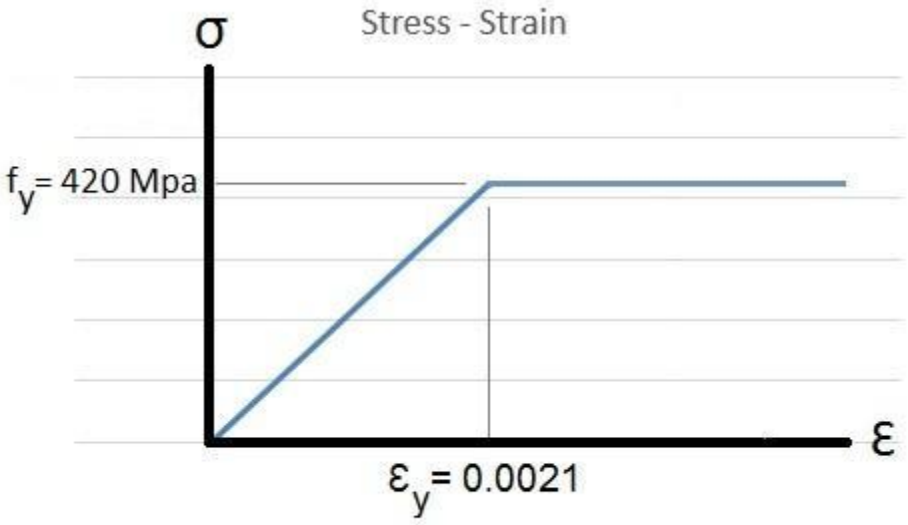

Figure 51: Perfectly-Plastic Stress-Strain Graph

Represented here is the real behavior of reinforcement bar grade 60 ksi/400 Mpa. As is shown in the graph below, yield stress for this type of reinforcement bar is close to 75 ksi. Alternatively, ultimate stress is close to 113 ksi.

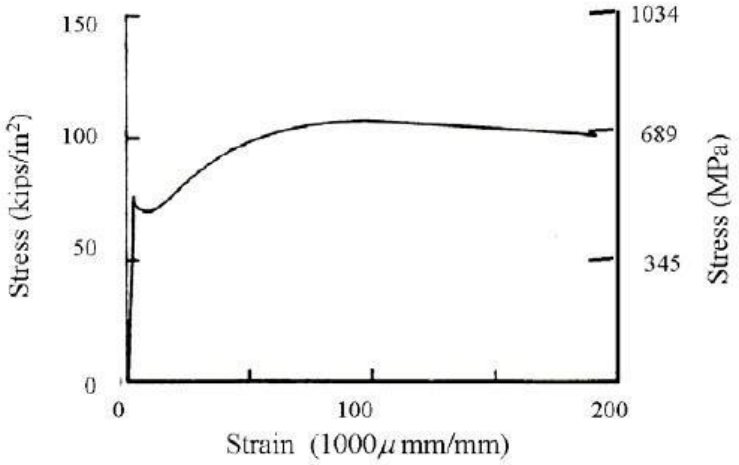

Figure 52: Stress-Strain Graph for reinforcement bar grade 60/400 (After Murray & Odeh, Evaluation of LS-DYNA concrete material model 159, 2007)

As depicted in the Figure above, in reality, the reinforcement bar grade 60 can tolerate up to 15 ksi a higher yield than originally considered in AASHTO. This comparison shows AASHTO is conservative on this subject. This research considered yield stress of the reinforcement bar as 60 ksi, but instead of using the perfectly plastic graph to represent the reinforcement bar, it used the semi-plastic graph in LS-DYNA. This assumption is somewhat conservative when designing reinforced concrete, but not as conservative as AASHTO's assumption.

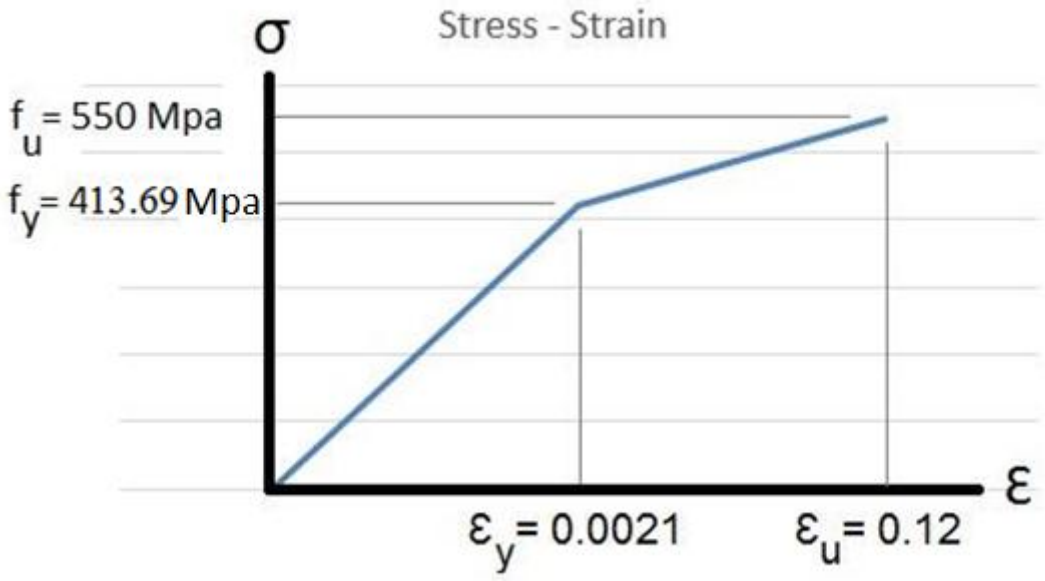

Figure 53: Semi-Plastic Stress-Strain Graph (After Caltrans Seismic Design Criteria Version 1.7, 2013)

In order to define reinforcement bar in LS-DYNA, the research uses plastic kinematic material.

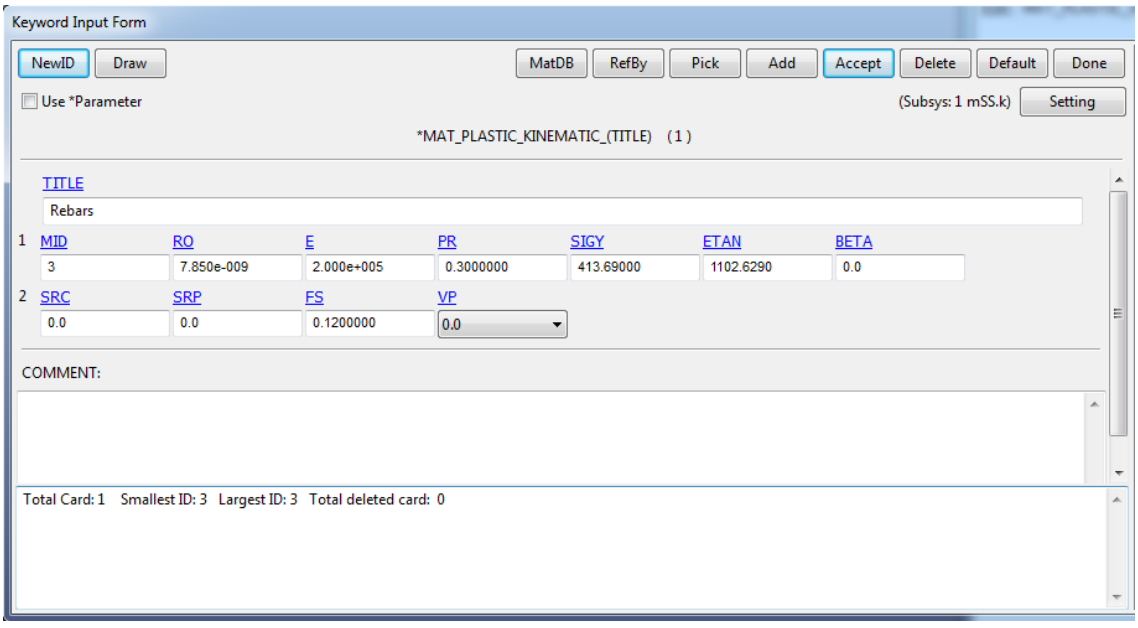

Figure 54: Kinematic Material Specifications

In the above-mentioned Figure, RO refers to “Mass Density”, E is “Young Modulus”, PR refers to “Poisson’s Ratio”, ETAN is the stress-strain tangent.

As the LS-DYNA manual explained, element formulation Number 3 considers the member as a truss. This means the element will not be able to tolerate moment forces. Since the amount of moment force reinforcement bar can handle is small, this research neglected that and considered reinforcement bar as a truss member.

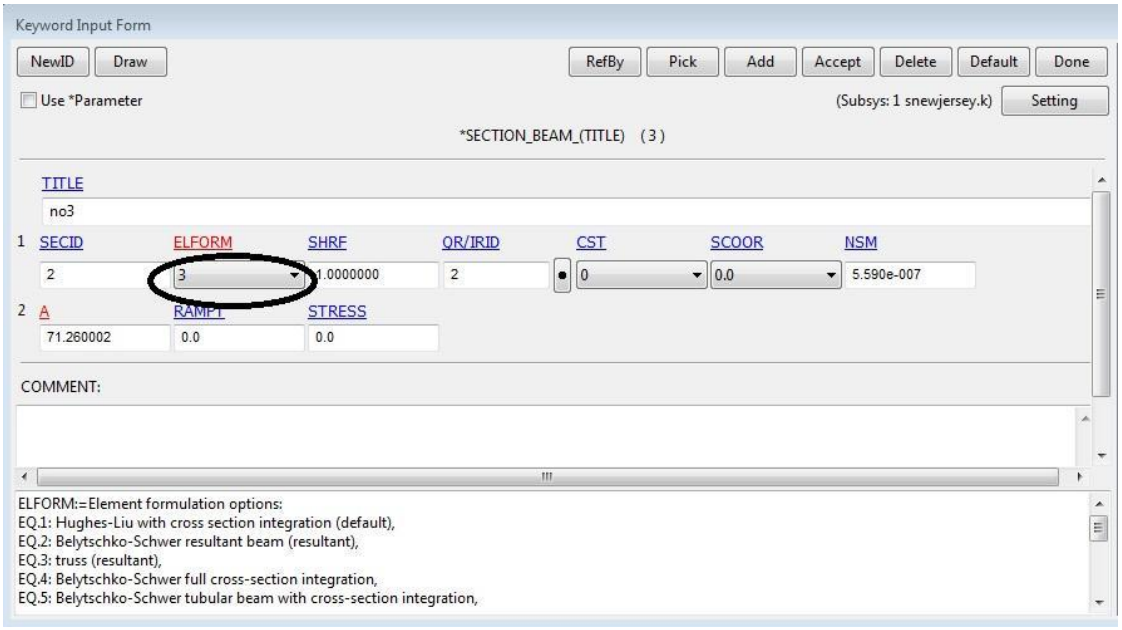

Figure 55: Reinforcement bar Element Formulations

5 FINITE ELEMENT MODEL VERIFICATION

Before running a finite element model or any simulation, research needs to be certain that the model, with all assumptions, is acceptable enough to give the best results that is closest to reality. Hence, this chapter reviews Chapter 9 of "Evaluation of LS-DYNA Concrete Material 159" to make sure that all assumptions are correct and reliable.

In May 2009, Texas A&M University, with Texas Transportation Institute's cooperation, performed a test in reality by imposing a static load of 156 kN (35.1 kips) on a Florida safety-shape barrier with a New Jersey profile. The load capacity calculated for this geometry using "Yield Line Analysis" method was 185 kN (41.6 kips). As mentioned in this paper, the apparent difference between these two numbers was due to the distance of last stirrup from the end of the parapet, which was considered as 50.8mm (2 inches) in calculation, but in reality, was 125 mm (6 inches). Since this model was fairly close to finite element models on this research, the author found it the best candidate to verify research's assumptions.

5.1 Real Test Assumptions

As showed in the figure, the load was applied by using a hydraulic cylinder with an inline load cell. This hydraulic cylinder was attach to a fabricated steel frame that was bolted to the concrete deck. At the parapet side, a wide flange steel, stiffened with welded gussets, was clamped to the face of the parapet in order to distribute the applied load over a distance of 1219 mm (4 ft). Since the parapet had taper on the cylinder side, a tapered wood block was installed between the parapet and the wide flange steel. This system was

located at the top edge of the parapet, and the hydraulic cylinder applied the load to the middle of the steel beam. Displacement of the parapet was measured using a string pot.

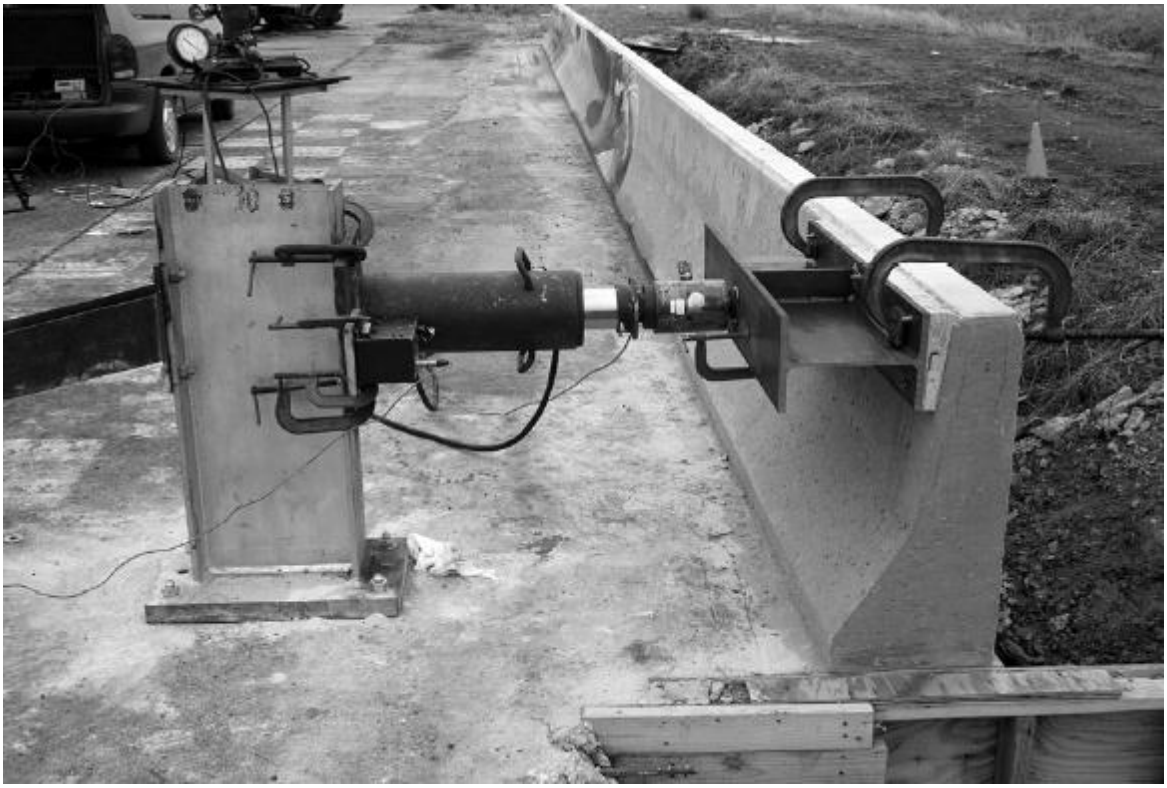

Figure 56: Static Load Test Setup for Safety-Shaped Barrier (After Abu-Odeh, Bligh, & Yvonne, 2007)

Figure 57 represented the Force-Displacement diagram measured by string pot.

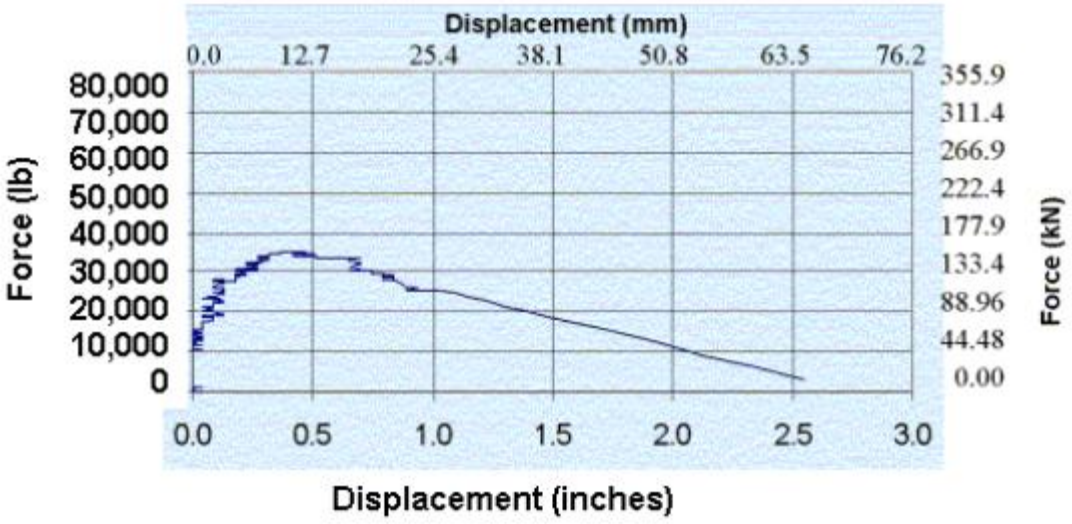

Figure 57: Load Displacement Graph for Safety-Shaped Barrier (After Abu-Odeh, Bligh, & Yvonne, 2007)

5.2 Finite Element Model Assumptions

5.2.1 Assumptions

A modeling approach similar to that used for the Texas T4 bridge rail was followed for the New Jersey safety-shape rail system. In accordance with this research's assumptions, the concrete barrier and bridge deck were modeled using solid elements. All reinforcement bar inside the barrier and bridge deck were considered as beam elements. Element formulation type 1 or Hughes-Liu were used for all steel reinforcements. Element formulation type 1 or under integrated type were used for all concrete materials. The steel reinforcement was buried into the surrounding concrete using the *CONSTRAINED_LAGRANGE_IN_SOLID feature card in LS-DYNA.

Figure 58 shows the cross section area of the barrier located on deck overhang.

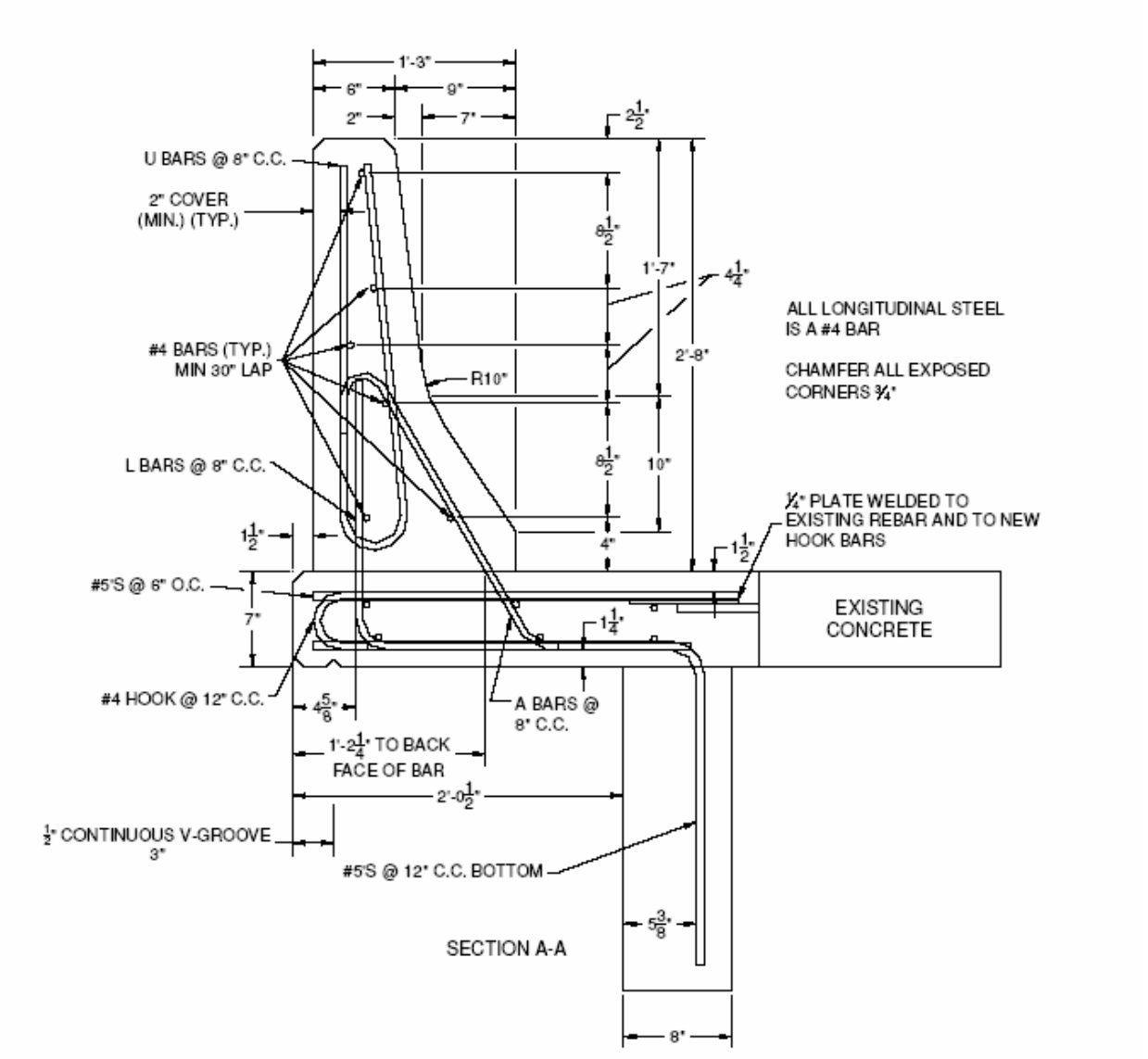

Figure 58: Cross-section of the Florida safety-shaped barrier with New Jersey profile (After Abu-Odeh, Bligh, & Yvonne, 2007)

To model the impactor, a simple surrogate impactor was defined to model the hydraulic impactor. The duration of the simulation was 0.15 sec, which is a fraction of the actual test.

Figure 59 represents the cross-section of the concrete and reinforcement bars located in the barrier and deck overhang.

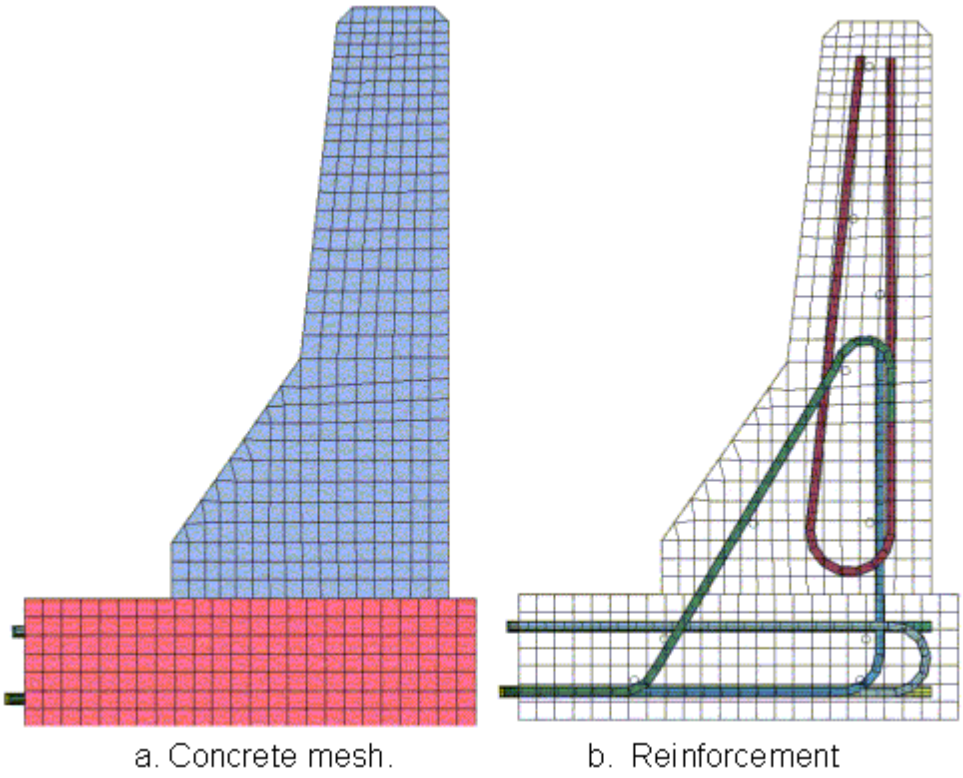

Figure 59: Concrete Mesh and Reinforcement (After Abu-Odeh, Bligh, & Yvonne, 2007)

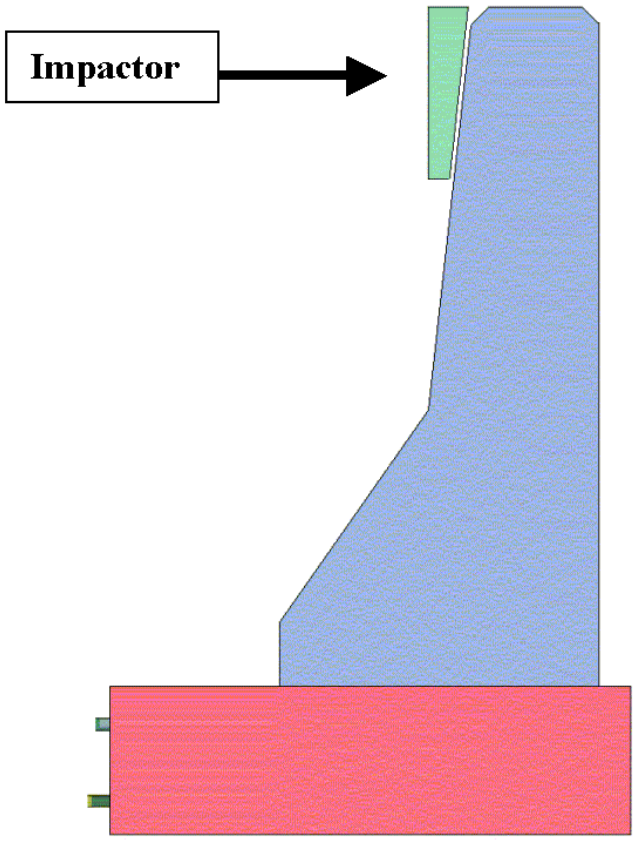

Figure 60: Model of quasi-static load test setup (After Abu-Odeh, Bligh, & Yvonne, 2007)

All calculation was performed with erosion occurred at 99% and maximum principal strain of 5% (ERODE = 1.05). A joint exists between the barrier and deck overhang is much weaker than the one in solid concrete. Hence, this joint interface was adjusted from *CONTACT_TIED_NODES_TO_SURFACE to *CONTACT_NODES_TO_SURFACE, to allow separation in tension.

The timber is modeled as elastic, using material model 1 with a modulus of 247 MPa (35,824 lbf/inch2).

Rate effect was turned off in the concrete model. Turning off this option allowed quasi-static simulations to run at a higher rate than the quasi-static test. As the research mentioned, turning off this option is typical and necessary.

The applied displacement increased from 0 to 38.1 mm (0 to 1.5 inches) over 150 msec.

5.2.2 Results

Damage fringed at about 70 msec with the displacement of 16 mm (0.63 inches). Three regions of high damage were noted. First, barrier damage initiated from the front at mid-level to the back at deck-level. As well, a large inclined shear crack extended from mid-level upward to the top of the barrier. Finally, concentrated damage also occurred, where the bottom edge of the timber contacted the barrier. Close examination of the computed results indicated that the timber does not maintain continuous contact with the barrier. This fact caused the stress concentration in the concrete at the bottom point of the timber.

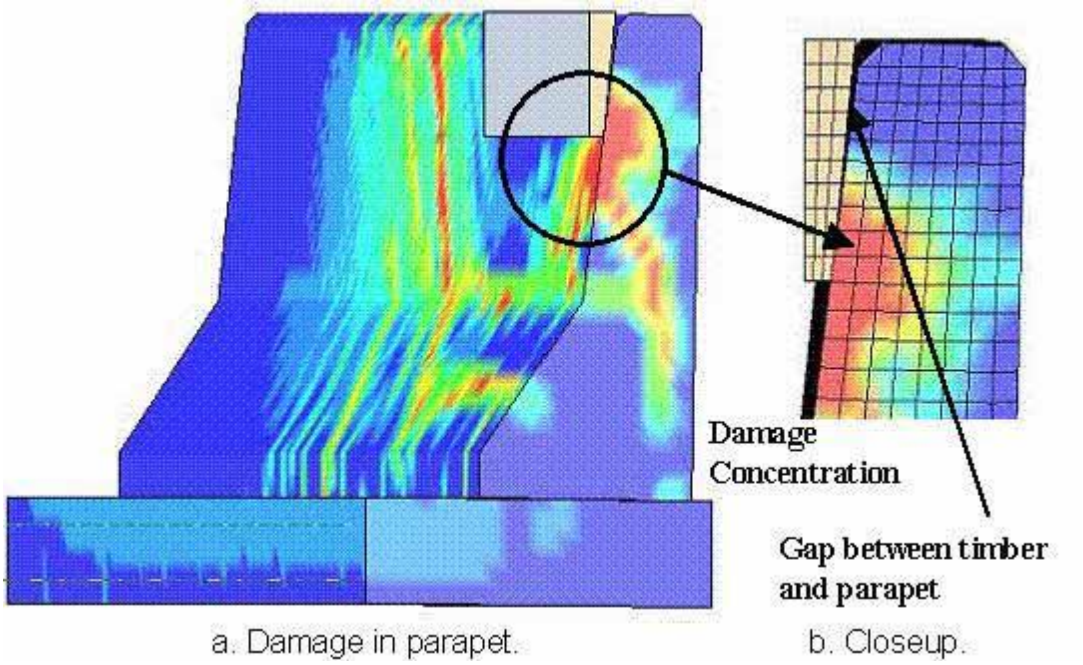

Figure 61: Gap between timber wood and barrier's concrete (After Abu-Odeh, Bligh, & Yvonne, 2007)

Since this concentration is not realistic, and the developer thought that contact was uniform over the timber's surface, a second test was performed in which the timber was modeled as a plastic, deformable and damageable material using wood material 143. Figure 62 exhibited damage fringes at 16.5 mm (0.65 inches) and 38.1 mm (1.5 inches) of lateral deflection. Switching the timber model from elastic to elastoplastic caused the stress to spread along the timber instead of concentrated at the bottom of the timber. The peak force attained in the calculation is 282 kN (63.4 kips), which is 81% more than the realistic load measured during the test.

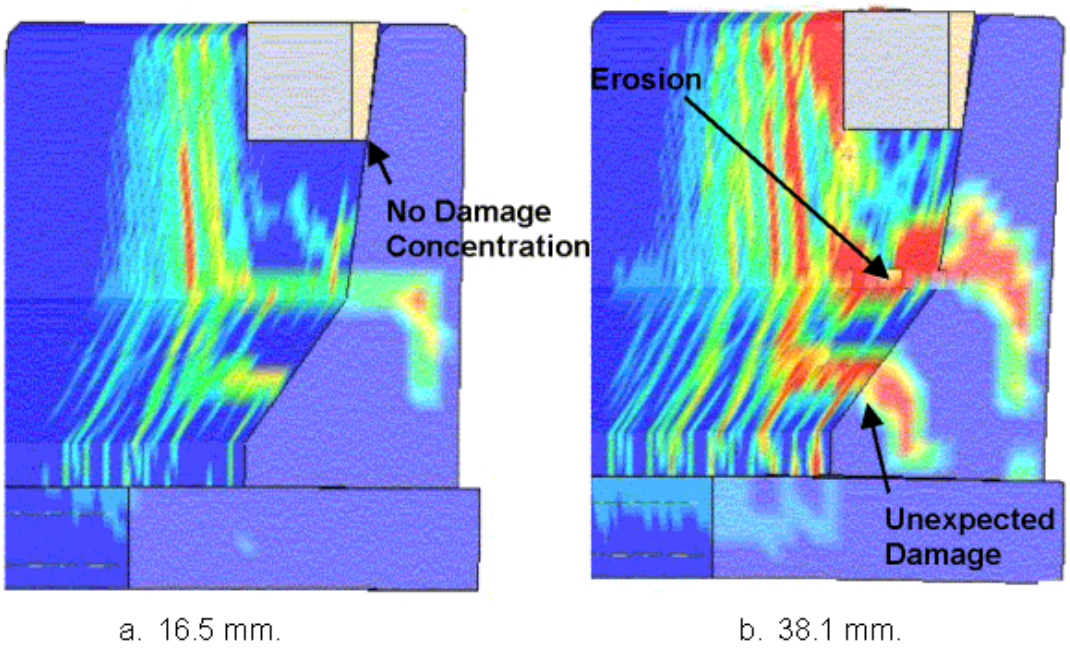

Figure 62: Damage concentration with the wood timber realistically modeled as an elastoplastic damaging material (After Abu-Odeh, Bligh, & Yvonne, 2007)

Since the number obtained for stress was 81% more than the realistic test, another two tests were performed in order to retain contact between the spreader beam and parapet, and to reduce the computed peak force. Hence, a single rigid element, that represented the hydraulic ram, was added to the model. A contact surface of *CONTACT_NODES_TO_SURFACE was defined for the model in order to separate the ram element from the spreader beam elements in order to allow for separation without penetration.

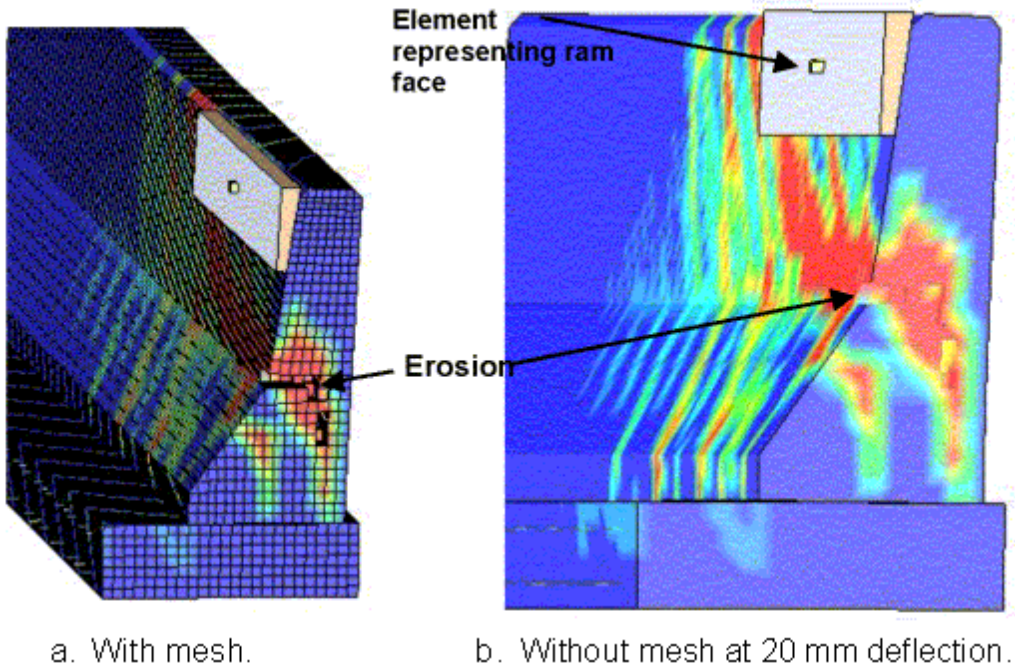

Figure 63: Realistic damage and erosion pattern (ERODE = 1.05) (After Abu-Odeh, Bligh, & Yvonne, 2007)

The peak force attained in this calculation was 185 kN (41.6 kips) at 31 mm (1.2 inches) deflection, which was still 17% higher than the realistic force.

Figure 64 and Figure 65 represented the damage fringes at 10 and 20 mm respectively, by considering ERODE equal to 1.0.

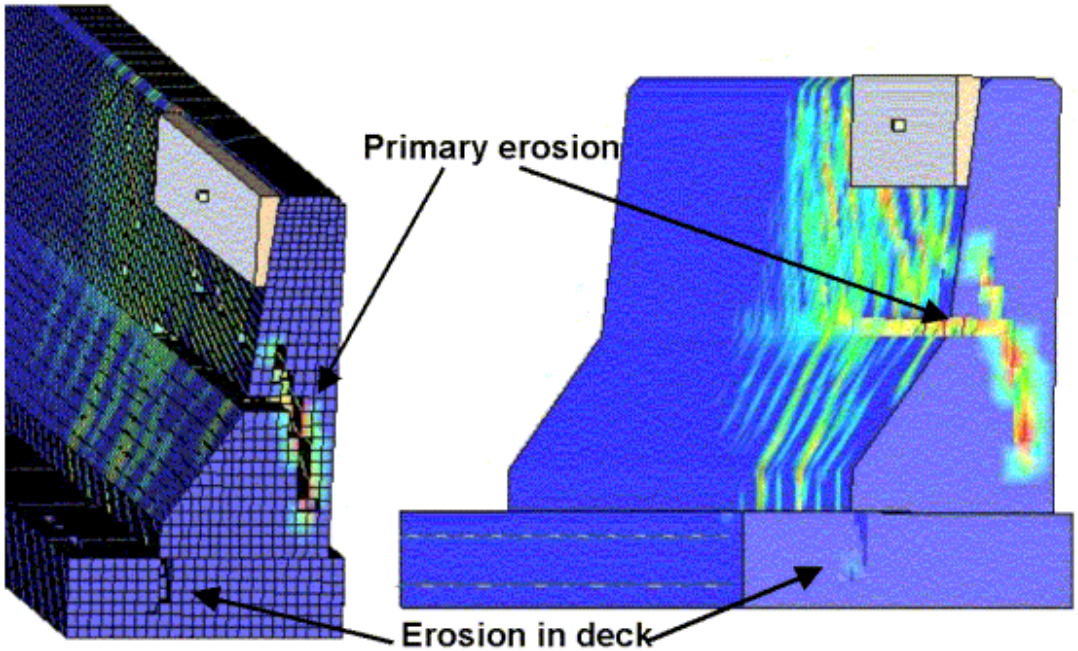

Figure 64: Primary deflection at 10 mm deflection (ERODE = 1.0) (After Abu-Odeh, Bligh, & Yvonne, 2007)

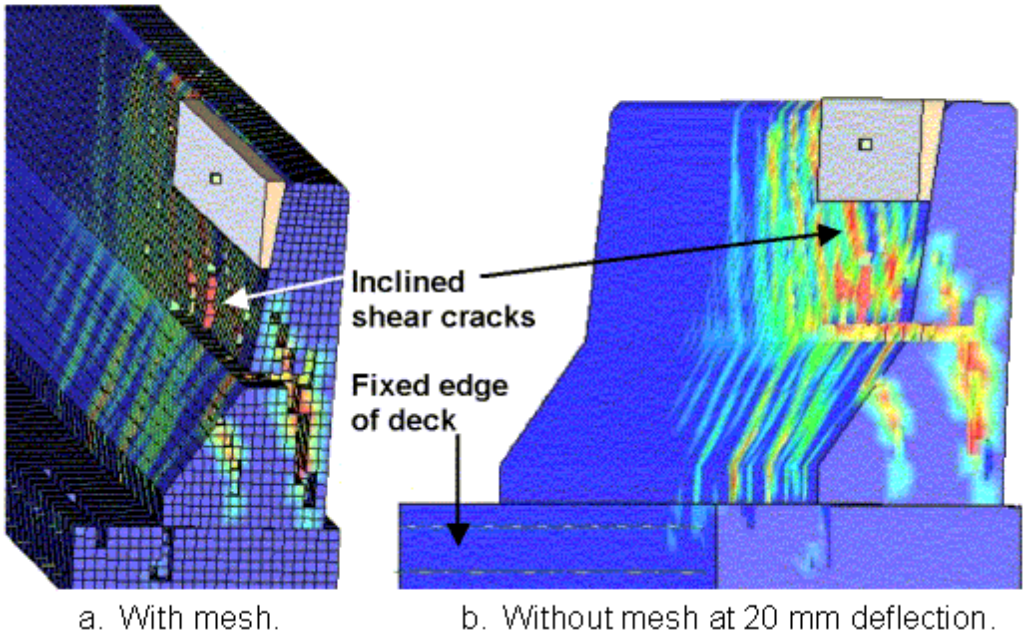

Figure 65: Primary deflection at 20 mm deflection (ERODE = 1.0) (After Abu-Odeh, Bligh, & Yvonne, 2007)

The peak force was measured at approximately 10 mm of deflection. The final measurement before loss of strength was approximately 20 mm of deflection. With this assumption, the damage and erosion pattern is more similar to reality. The peak force attained in this calculation was 181 kN (40.1 kips) at 31 mm (1.2 inches). This number is within 16% of the measured value. Figure 66 shows the calculated force-deflection graph for this assumption.

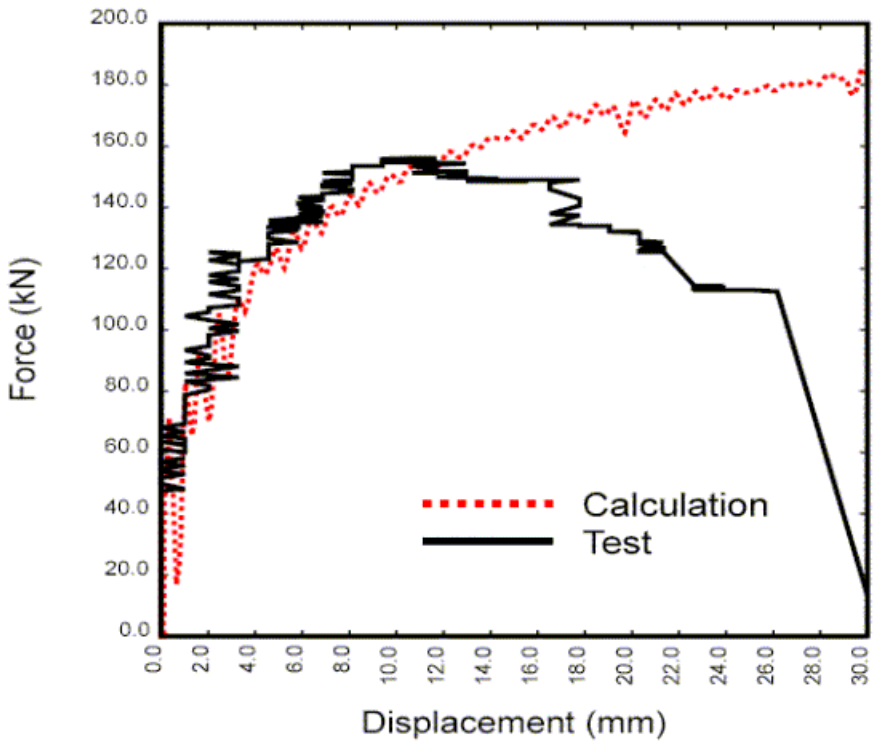

Figure 66: The calculated force-deflection with the measured curve for the first 12 mm of deflection (After Abu-Odeh, Bligh, & Yvonne, 2007)

The peak force continues to increase after 12 mm, and with more ductile behavior than what was measured.

For the last simulation, instead of using the timber wood and hydraulic element, the developer directly applied a 156 kN (35.1 kips) distributed load over a 40 msec period. The load remained at 35.1 kips until 50 msec was reached. Then, the timber, steel and hydraulic ram were completely removed from the finite element model. Two simulations were conducted with different erosion values. Figure 67 represents the computed damage using a distributed load. As shown in the figure, the damage is similar to the model which had the timber remaining in contact with parapet.

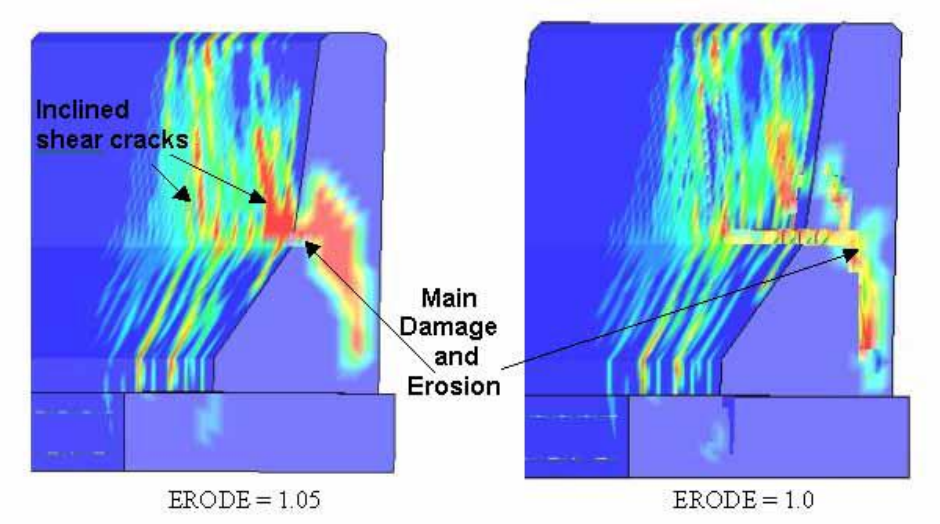

Figure 67: Computed damage using distributed load (After Abu-Odeh, Bligh, & Yvonne, 2007)

Figure 68 represents the computed force-displacement unloads when distributed load are applied.

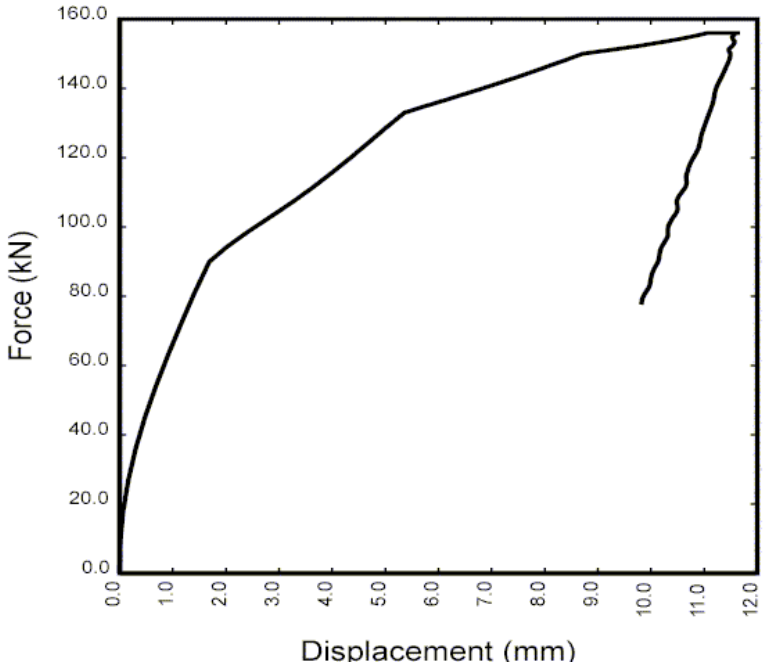

Figure 68: Force-displacement for distributed load (ERODE = 1.05) (After Abu-Odeh, Bligh, & Yvonne, 2007)

Barrier deflection of between 11 mm (0.43 inches) and 12 mm (0.5 inches) was calculated at the center of the loading region when the applied load was 156 kN (35.1 kips). This result is in agreement with the measured displacement resulting from the "real" test, but once the applied load began to drop upon reaching 50 msec, the barrier displacement began to decrease, which is not realistic.

All in all, since AASHTO required the designers to use a 3.5 ft distributed load in order to design the barrier, based on Test Level 4, this research assumed the 54 kips load as a distributed load imposed upon the barrier. As stated in this chapter, each assumption had its own pros and cons. Since this chapter showed that considering a distributed load can give us reliable results similar to reality, this research, therefore, utilized 54 kips of static load - representing Test Level 4 - as a distributed load imposed upon the barrier. On the other hand, this chapter also showed that barrier models simulated in LS-DYNA have almost the same results in terms of cracking and the maximum force imposed upon them. Hence, by considering these assumptions, the results obtained from static load testing can be considered reliable, and acceptable, allowing for a small degree of tolerance.

6 STATIC LOAD SIMULATION

This chapter compares all of the proposed barrier geometries by simulating them in LS-DYNA using a static load value that represents Test Level 4. As mentioned before, this load is a 54 kip distributed load, 13 inches in height and 3.5 ft. in width. The result of this study shows deflection of the barrier and deck overhang, maximum stress in the concrete block, and internal energy absorbed by the barrier, deck overhang and reinforcement bars.

As has been shown in Figure 69 and Figure 70, maximum stress and deflection, as reflected by compression and tension measurements, was in the middle of the barrier because the static load was located exactly in the middle. Since the entire barrier absorbed the same force in the same location, this assumption was correct for all other presented barriers. Hence, to measure the maximum displacement and stress of the barrier and deck overhang, the middle of the geometry was considered.

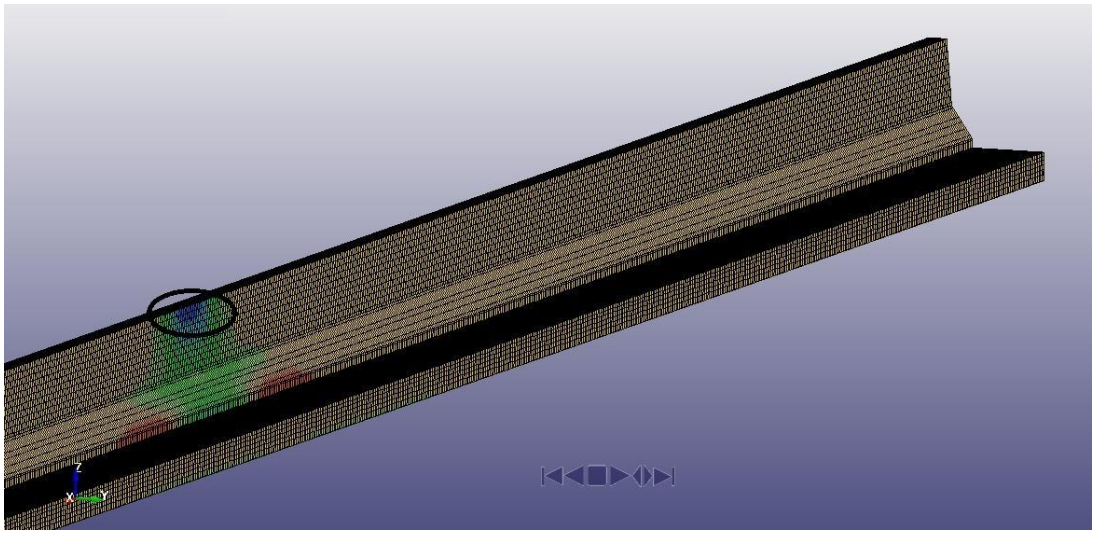

Figure 69: Maximum Stress in Face of Barrier – 3D model

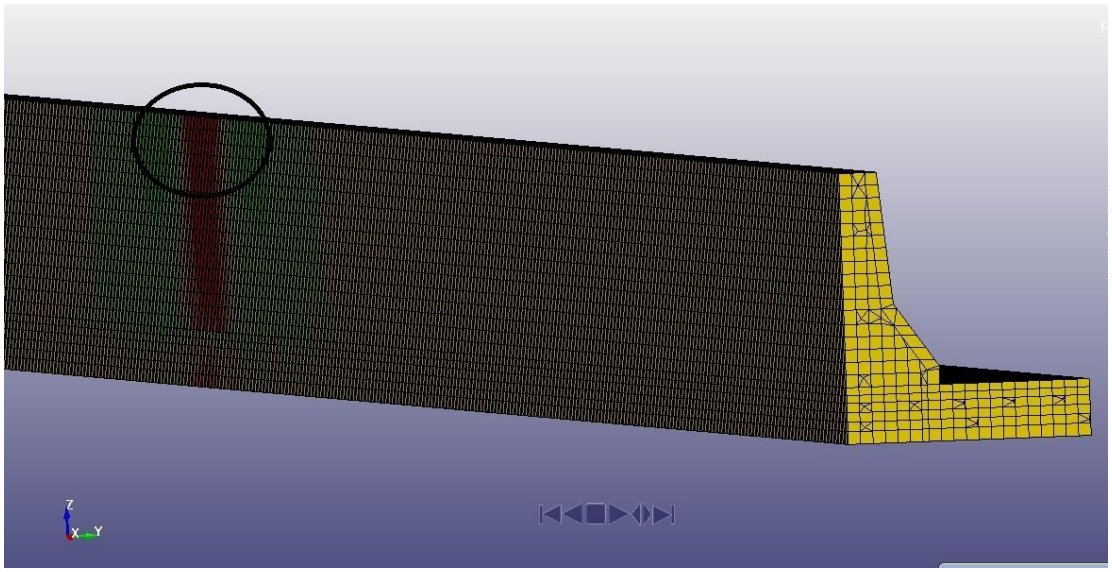

Figure 70: Maximum stress in back of Barrier – 3D model

6.1 Maximum Stress

6.1.1 New-Jersey Barrier

6.1.1.1 Maximum Stress in the Barrier

6.1.1.1.1 Compression Side

Figure 71 depicts the printed stress graph for the middle top element of the barrier on its compression side, the element with maximum compressive stress. As shown in the graph, the maximum stress in the barrier is 5.21 Mpa.

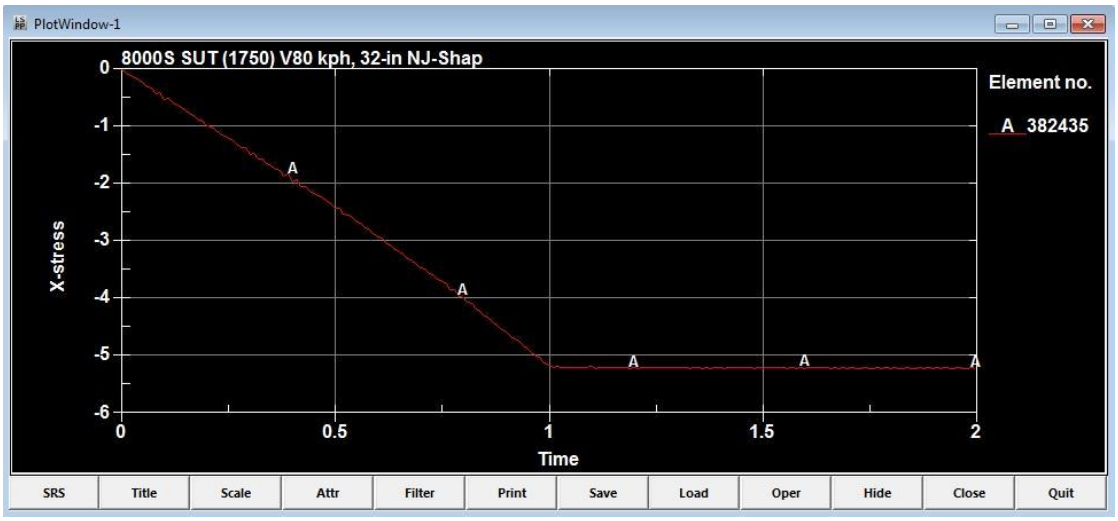

Figure 71: Time-stress graph of New Jersey concrete barrier element in compression side with maximum stress

6.1.1.1.2 Tension Side

Figure 72 shows the printed stress graph for the middle top element of the barrier in tension side. That is the element with maximum tensile stress. Typically, maximum tensile stress of the concrete is equal to 10% of its maximum compressive stress. As indicated in the graph, the maximum tensile stress of the concrete in the barrier is 2.42 Mpa.

Figure 72: Time-stress graph of New Jersey concrete barrier element in tension side with maximum stress

6.1.1.2 Maximum Stress in Deck Overhang

As shown in Figure 73 and Figure 74, maximum stress in the compression and tension side was in the middle of the deck overhang because the static load is located exactly in the middle of the barrier. As explained in Chapter 2, the concrete used for deck overhang has the compressive strength of 35.52 Mpa.

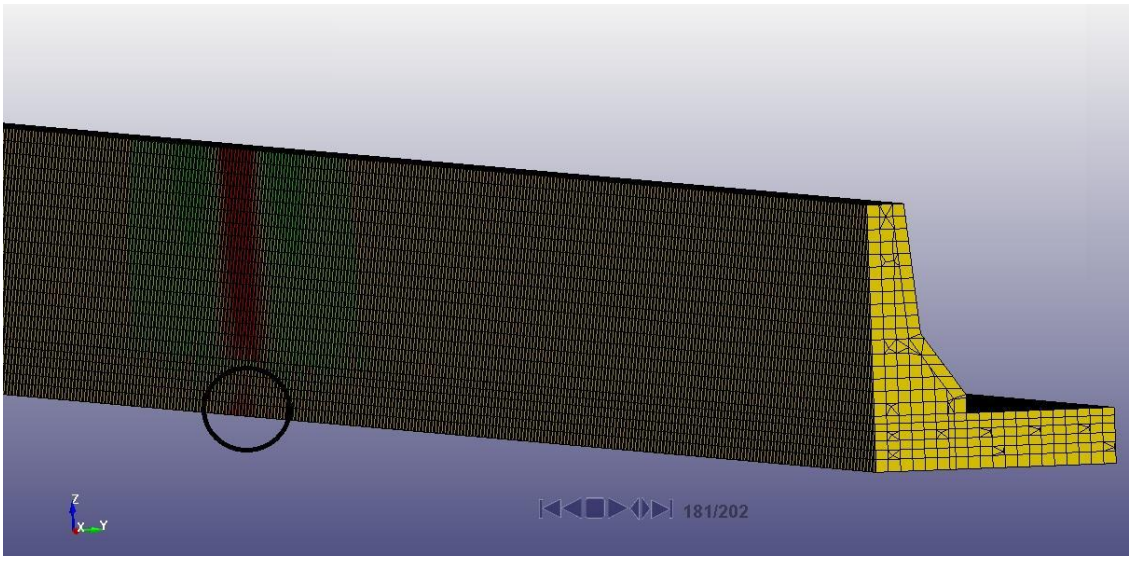

Figure 73 Maximum Stress in the back of deck overhang related to New Jersey barrier - 3D model

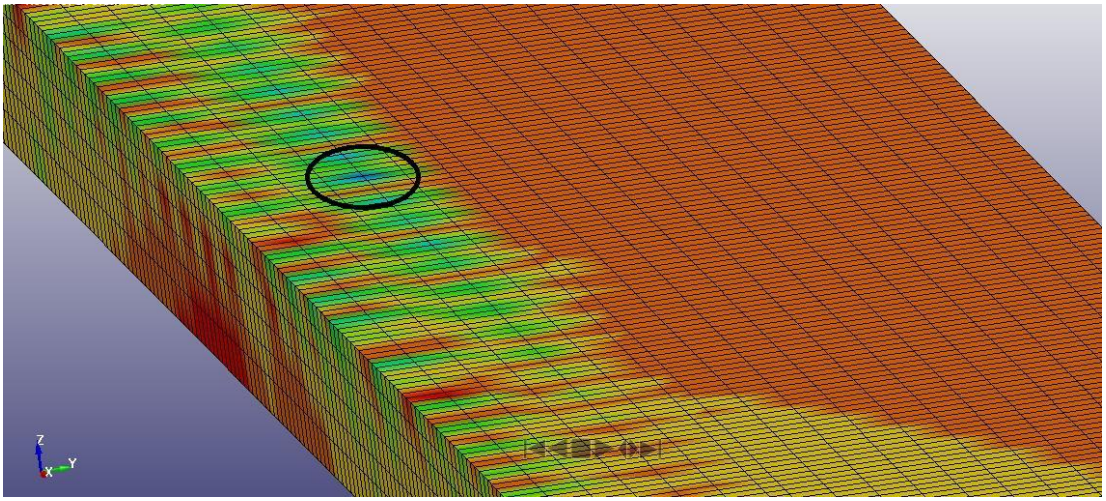

Figure 74: Maximum stress in face of deck overhang related to New Jersey barrier – 3D model

6.1.1.2.1 Compression Side

Figure 75 shows the printed stress graph for the middle top element of the deck overhang in compression side. That is the element with maximum compressive stress. As shown in the graph, the maximum stress in the barrier is 4.02 Mpa.

Figure 75: Time-stress graph of New Jersey concrete deck overhang element in compression side with maximum stress

6.1.1.2.2 Tension Side

As seen in Figure 76 the maximum stress imposed to the deck overhang in tension side was 1.15 Mpa.

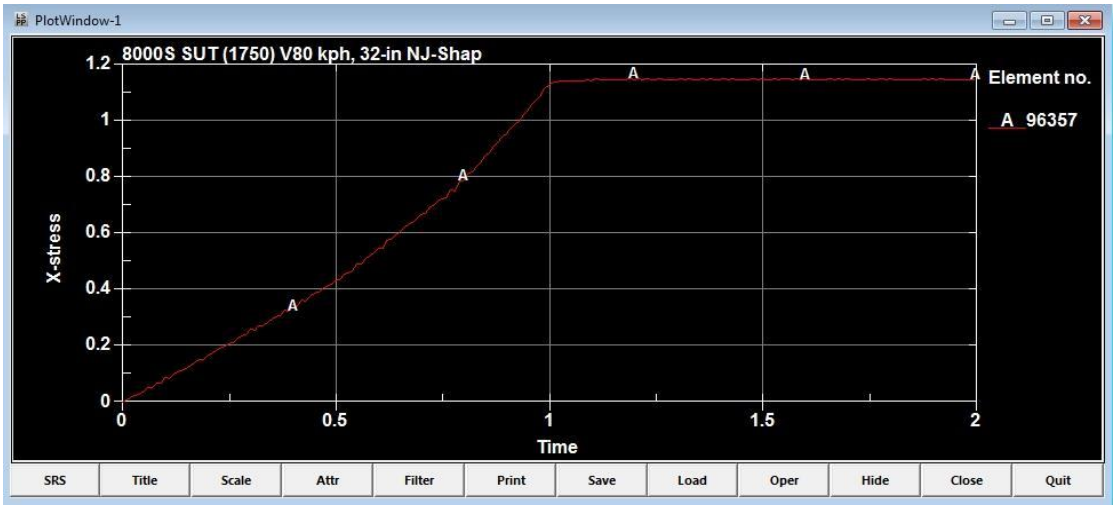

Figure 76: Time-stress graph of New Jersey concrete deck overhang element in tension side with maximum stress

6.1.1.3 Maximum Stress in Reinforcement bars

As seen in Figure 30, all longitudinal reinforcement bars are #3 vertical reinforcement bars, and hairpin dowels are #4. Figure 77 represents the location of maximum stress in reinforcement bar. As mentioned before, since the static load is located in the middle of the barrier, the maximum tension and compressive stress appeared in the middle hairpin dowels, at the face and back of the barrier.

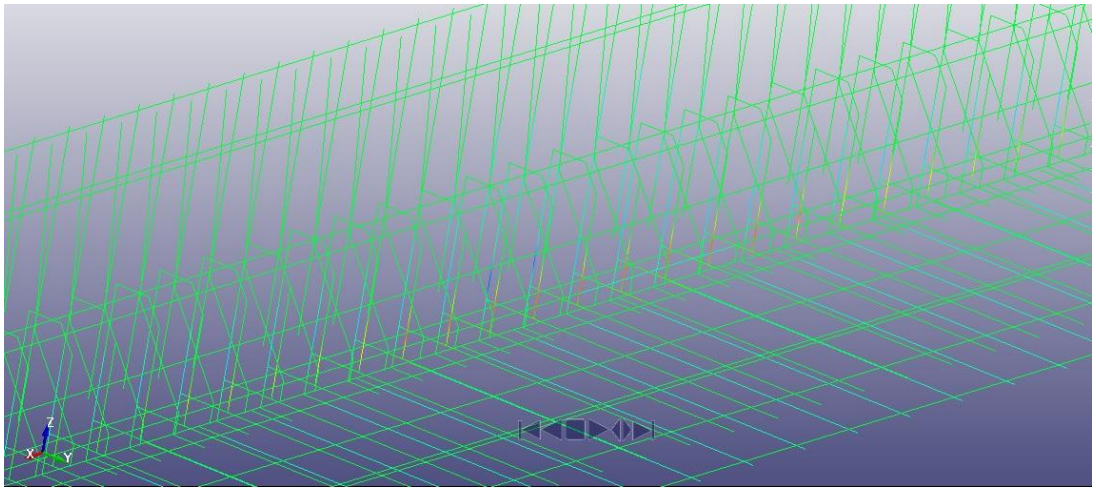

Figure 77: Maximum stress in tension and compression sides of reinforcement bars located in New Jersey barrier – 3D model

6.1.1.3.1 Tension Side

The maximum axial force in tension side for hairpin dowels is 4.29e4 N. By dividing the cross-section area to this value, the maximum stress in tension side after 1 sec was:

4.29e4 N / 129 mm^2 = 332.56 MPa = 48.23 ksi

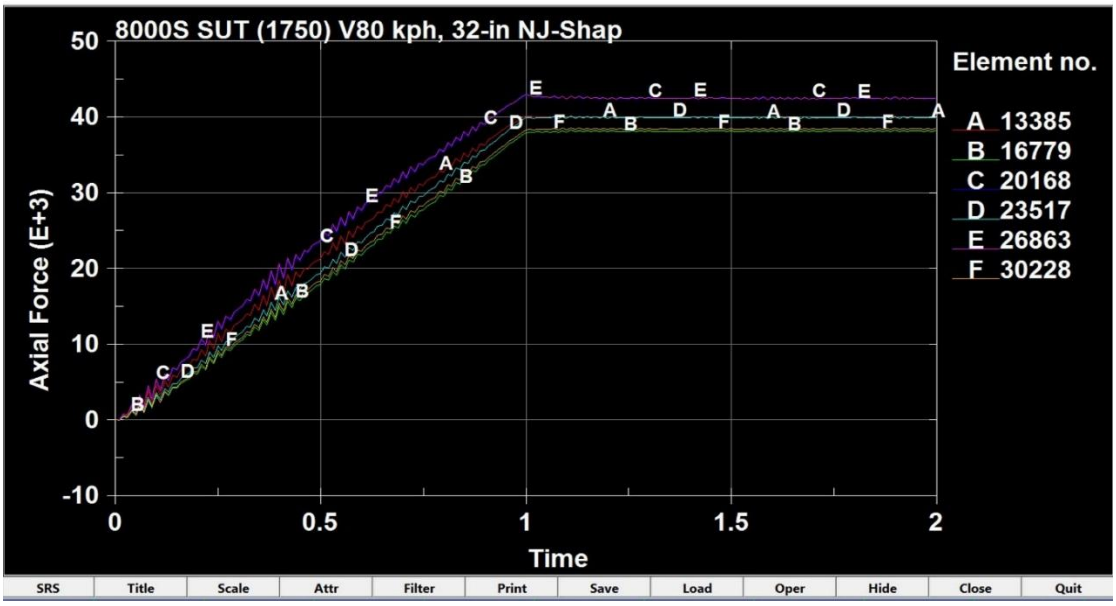

Figure 78: Time-Axial Force Graph of New Jersey barrier hairpin dowel reinforcement bar element in tension side with maximum stress

6.1.1.3.2 Compression Side

The maximum stress of the hairpin dowel reinforcement bar in compression side was 3.08e4 N. Hence, the maximum stress in compression side for the reinforcement bar after 1 sec was:

3.08e4 N / 129 mm^2 = 238.7 MPa = 34.62 ksi

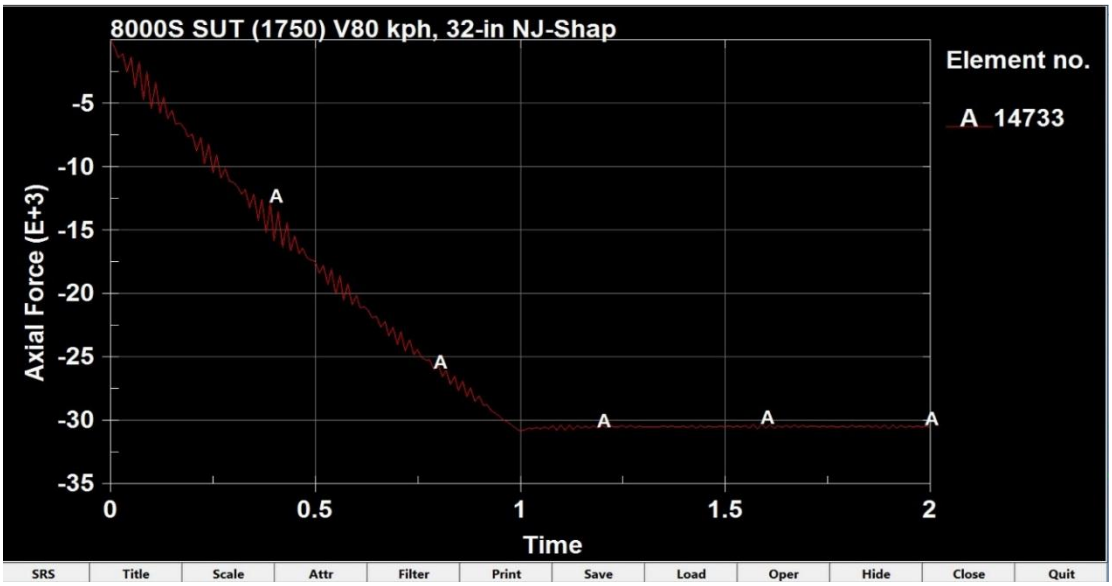

Figure 79: Time-Axial Force Graph of New Jersey barrier hairpin dowel reinforcement bar element in compression side with maximum stress

6.1.2 Modified New Jersey Barrier

6.1.2.1 Maximum Stress in the Barrier

6.1.2.1.1 Compression Side

Figure 80 shows the printed stress graph for the middle top element of the barrier in compression side, the element with maximum compressive stress. As is shown on the graph, the maximum stress in the barrier is 9.59 Mpa, far less than the compressive strength of the barrier concrete, assessed at 30.44 Mpa.

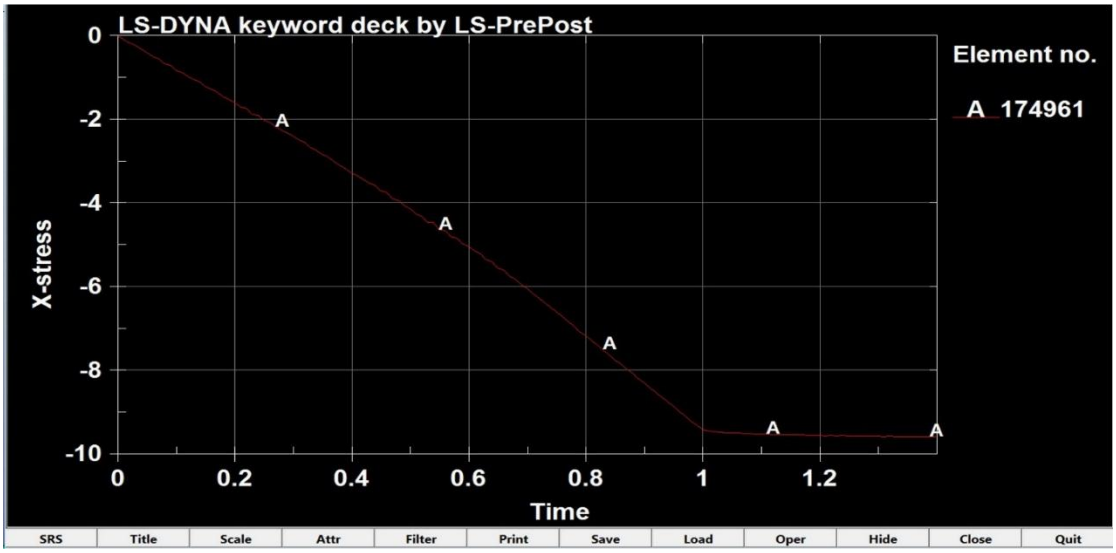

Figure 80: Time-stress graph of modified New Jersey concrete barrier element in compression side with maximum stress

6.1.2.1.2 Tension side

Figure 81 shows the printed stress graph for the middle top element of the barrier in tension side, the element with maximum tensile stress. As is indicated on the graph, the maximum tensile stress of the concrete in the barrier is 2.37 Mpa.

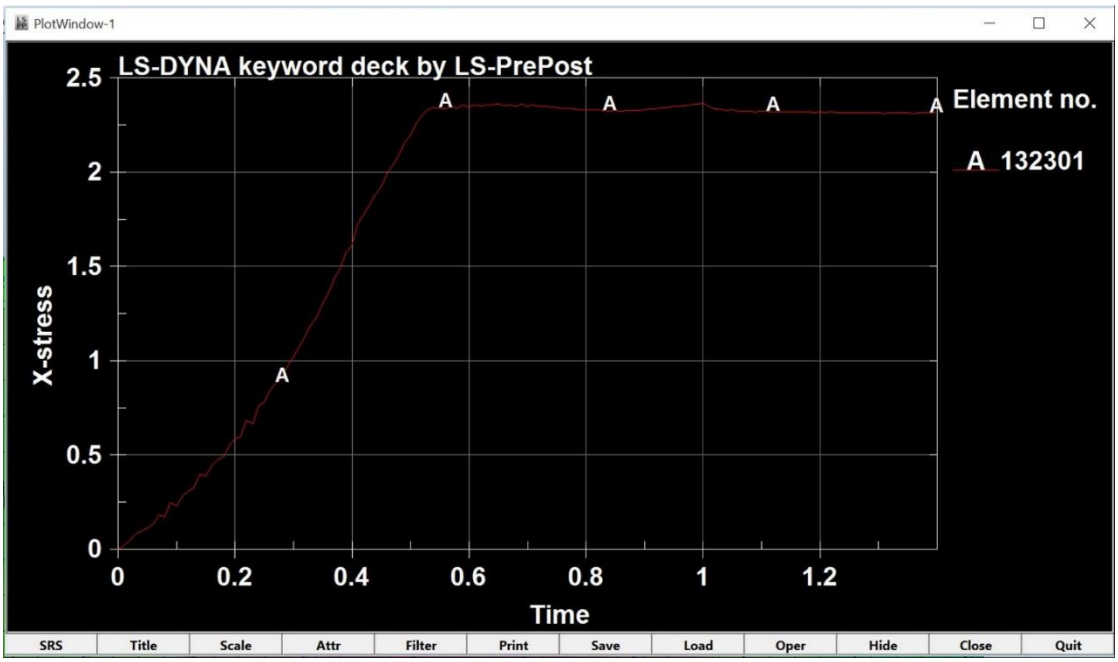

Figure 81: Time-stress graph of modified New Jersey concrete barrier element in tension side with maximum stress

6.1.2.2 Maximum stress in deck overhang:

As has been shown in Figure 82 and Figure 83, maximum stress in the compression and tension sides was in the middle of the deck overhang because the static load is located exactly in the middle of the barrier. As explained in Chapter 2, the concrete used for the deck overhang has a compressive strength of 35.52 Mpa.

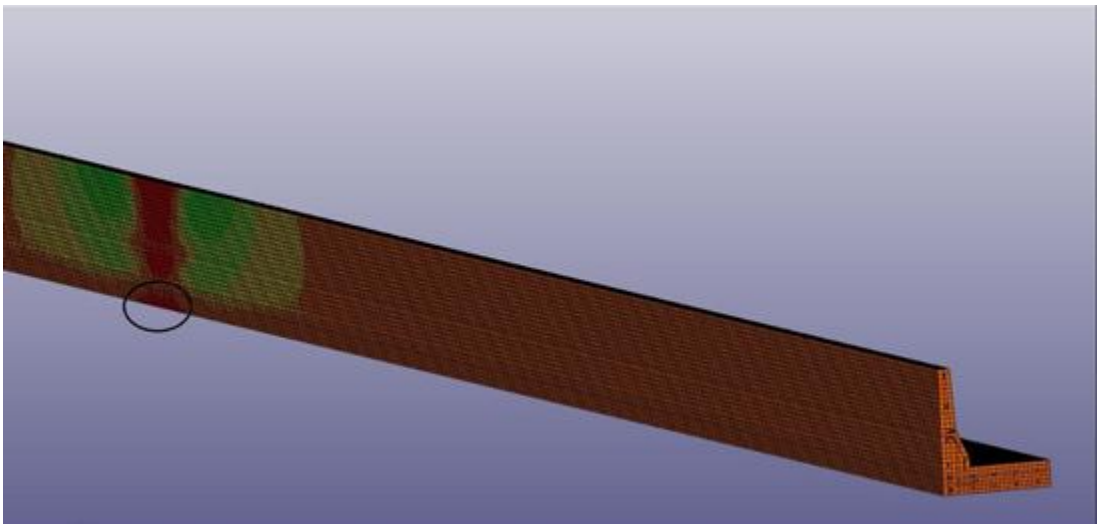

Figure 82: Maximum stress in back of deck overhang related to modified New Jersey barrier – 3D model

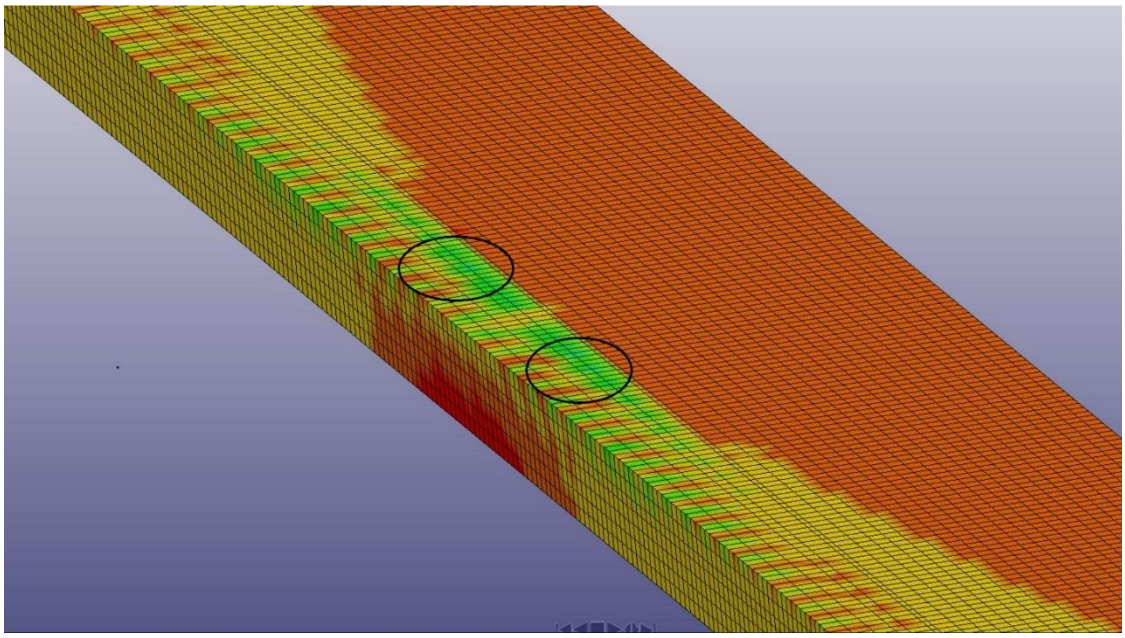

Figure 83: Maximum stress in face of deck overhang related to modified New Jersey barrier – 3D model

6.1.2.2.1 Compression side

Figure 84 shows the printed stress graph for the middle top element of the deck overhang in compression side, the element with maximum compressive stress. As has been shown on the graph, the maximum stress in the barrier is 6.07 Mpa.

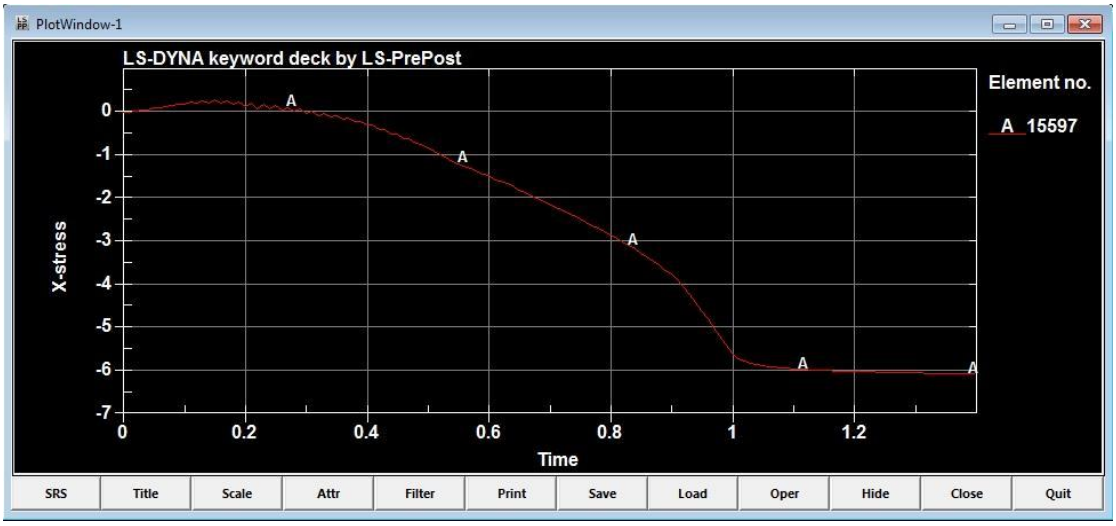

Figure 84: Time-stress graph of modified New Jersey concrete deck overhang element in compression side with maximum stress

6.1.2.2.2 Tension side

As seen in Figure 85 the maximum stress imposed to the deck overhang in tension side was 2.11 Mpa.

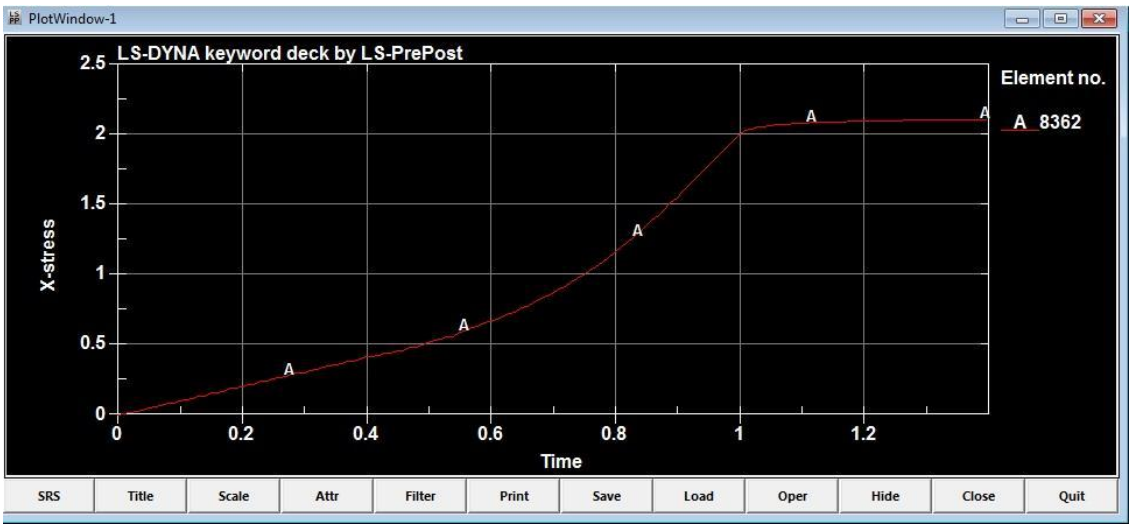

Figure 85: Time-stress graph of modified New Jersey concrete deck overhang element in tension side with maximum stress

6.1.2.3 Maximum stress in reinforcement bars

As mentioned before, the modified New Jersey barrier used the same amount and number of reinforcement bar in its cross-section, #4 hairpin dowel and stirrups, and #3 longitudinal reinforcement bars. Since we have the static load in the middle of the barrier, the maximum tension and compressive stress appears in the middle hairpin dowels, at the face and back of the barrier.

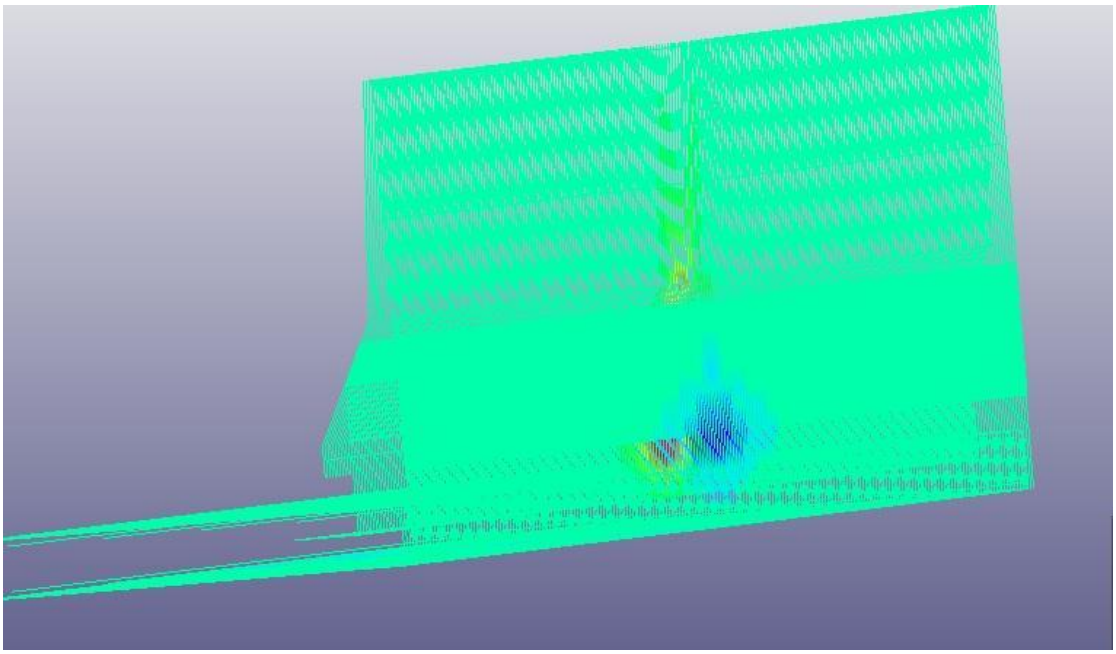

Figure 86: Maximum stress in tension and compression sides of reinforcement bars located in modified New Jersey barrier – 3D model

6.1.2.3.1 Tension Side

The maximum axial force in tension side for hairpin dowels is 5.36e4 N. By dividing the cross-section area to this number, the maximum stress in tension side after 1 sec was:

5.36e4 N / 129 mm^2 = 415.50 MPa = 60.26 ksi

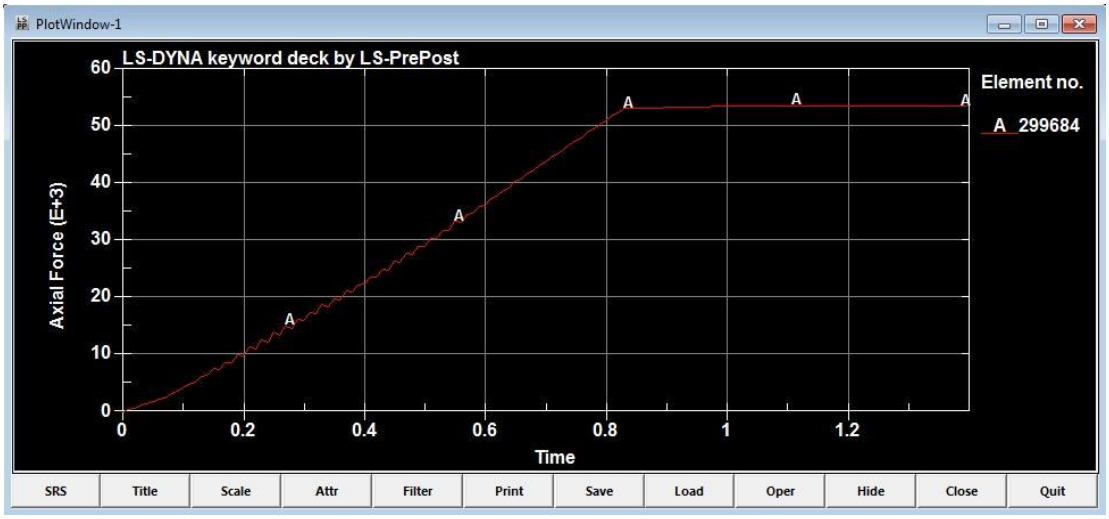

Figure 87: Time-axial force graph of modified New Jersey barrier hairpin dowel reinforcement bar elements in tension side with maximum stress

6.1.2.3.2 Compression side

The maximum stress of the hairpin dowel reinforcement bar in compression side was 2.65e4 N. Hence, the maximum stress in compression side for the reinforcement bar after 1 sec was:

2.65e4 N / 129 mm^2 = 205.43 MPa = 29.80 ksi

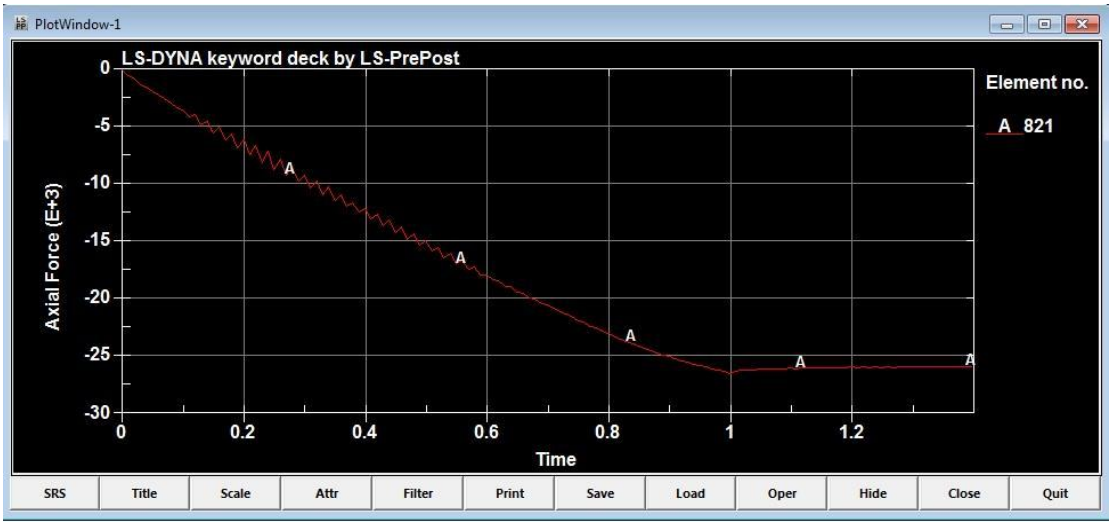

Figure 88: Time-axial force graph of modified New Jersey barrier hairpin dowel reinforcement bar elements in compression side with maximum stress

6.1.3 Rectangular – 8 inch Barrier

6.1.3.1 Maximum stress in the Barrier

6.1.3.1.1 Compression side

Figure 89 shows the printed stress graph for the middle top element of the barrier in compression side, the element with maximum compressive stress. As shown in the graph, the maximum stress in the barrier is 7.62 Mpa.

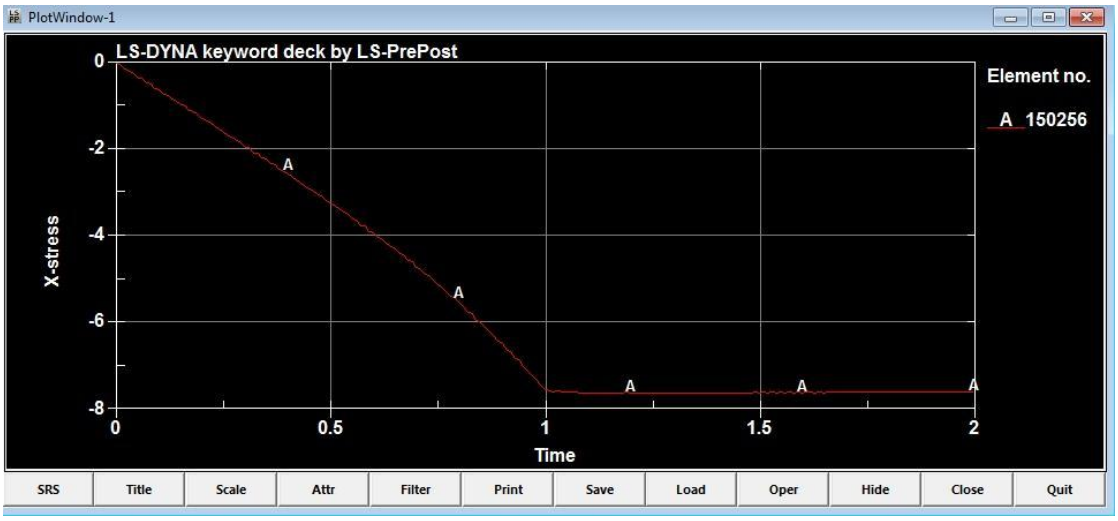

Figure 89: Time-stress graph of rectangular – 8 inch concrete barrier element in compression side with maximum stress

6.1.3.1.2 Tension side

Figure 90 shows the printed stress graph for the middle top element of the barrier in tension side, the element with maximum tensile stress. As indicated in the graph, the maximum tensile stress of the concrete in the barrier is 2.45 Mpa.

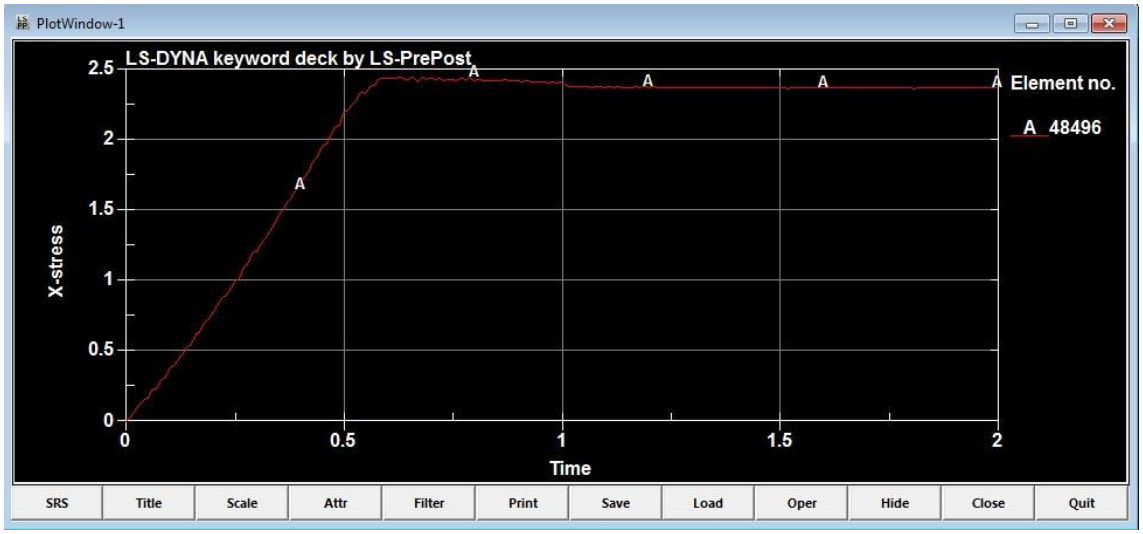

Figure 90: Time-stress graph of rectangular – 8 inch concrete barrier element in tension side with maximum stress

6.1.3.2 Maximum stress in deck overhang:

As it had been shown in Figure 91 and Figure 92, maximum stress in the compression and tension sides was in the middle of the deck overhang because the static load is located exactly in the middle of the Barrier. As explained in Chapter 2, the concrete used for the deck overhang has the compressive strength of 35.52 Mpa.

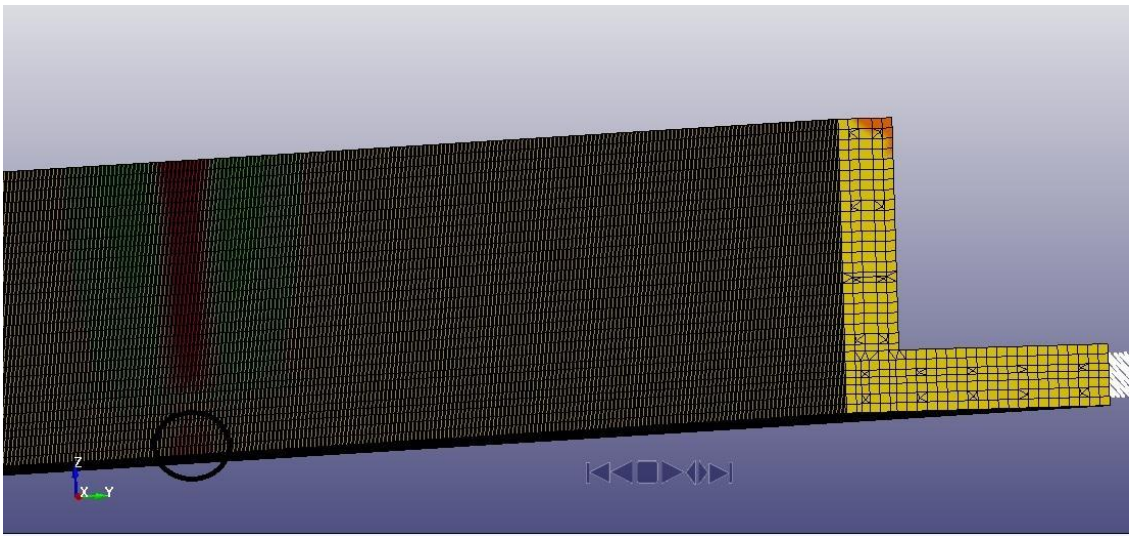

Figure 91: Maximum Stress in back of deck overhang related to rectangular – 8 inch concrete barrier – 3D model

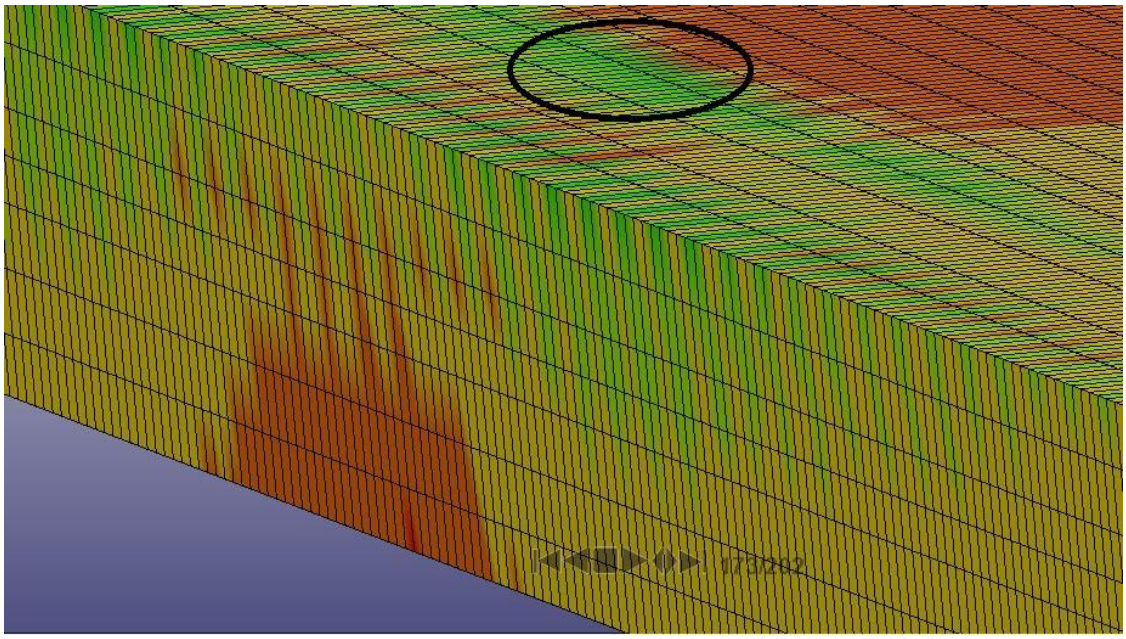

Figure 92: Maximum stress in face of deck overhang related to rectangular – 8 inch concrete barrier – 3D model

6.1.3.2.1 Compression side

Figure 93 shows the printed stress graph for the middle top element of the deck overhang in compression side, the element with maximum compressive stress. As shown on the graph, the maximum stress in the barrier is 4.45 Mpa.

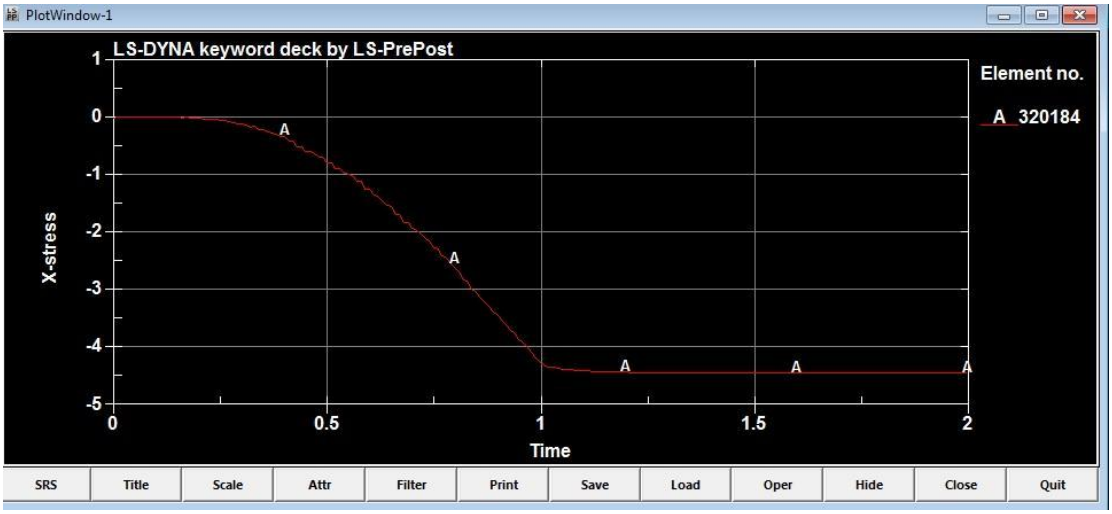

Figure 93: Time-Stress Graph of Rectangular – 8 inch concrete deck overhang element in compression side with maximum stress

6.1.3.2.2 Tension side

As seen in Figure 94 the maximum stress imposed to the deck overhang in tension side was 1.22 Mpa.

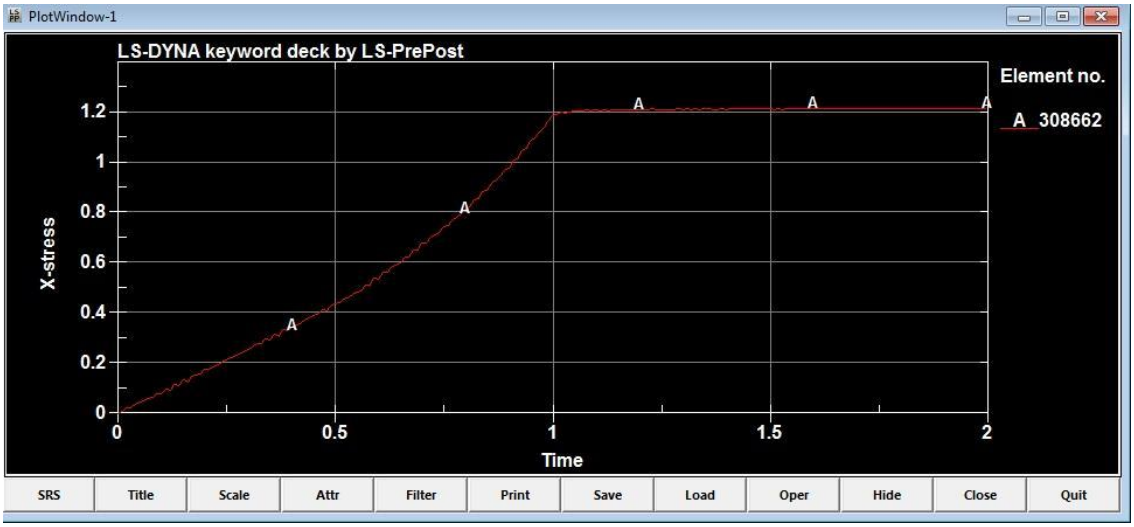

Figure 94: Time-stress graph of rectangular – 8 inch concrete deck overhang element in tension side with maximum stress

6.1.3.3 Maximum stress in reinforcement bars

As mentioned before, the rectangular – 8 inch concrete barrier used the same amount and number of reinforcement bar in its cross section, #4 hairpin dowel and stirrups, and #3 longitudinal reinforcement bars. Since we have the static load in the middle of the barrier, the maximum tension and compressive stress appeared in the middle hairpin dowels, at face and back of the barrier.

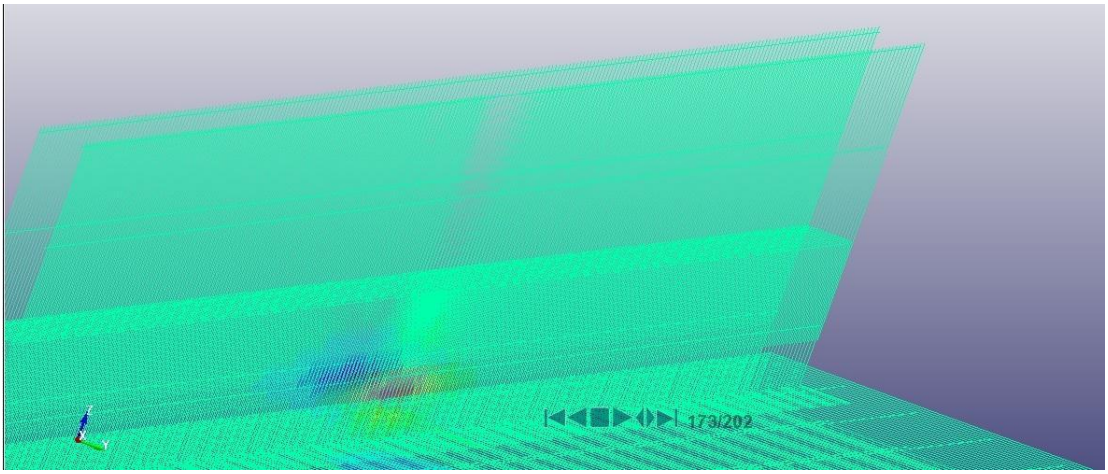

Figure 95: Maximum stress in tension and compression sides of reinforcement bars located in rectangular – 8 inch Barrier – 3D model

6.1.3.3.1 Tension side

The maximum axial force in tension side for hairpin dowels is 4.00e4 N. By dividing the cross-section area into this number, the maximum stress in tension side after 1 sec was:

4.00e4 N / 129 mm^2 = 310.08 MPa = 44.97 ksi

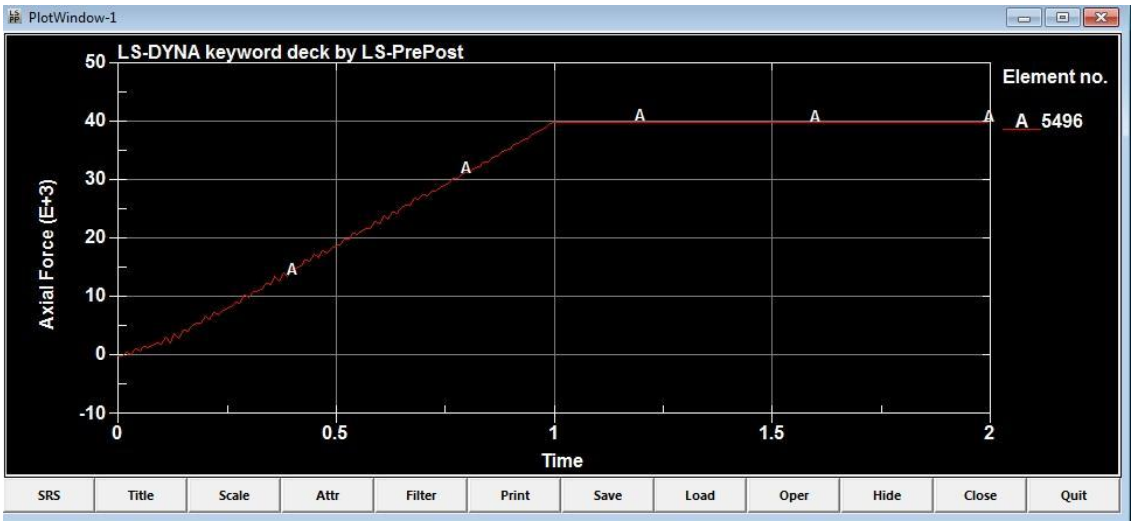

Figure 96: Time-axial force graph of rectangular – 8 inch barrier hairpin dowel reinforcement bar element in tension side with maximum stress

6.1.3.3.2 Compression side

The maximum stress of the hairpin dowel reinforcement bar in compression side was 2.12e4 N. Hence, the maximum stress in compression side for the reinforcement bar after 1 sec was:

2.12e4 N / 129 mm^2 = 164.3a MPa = 23.84 ksi

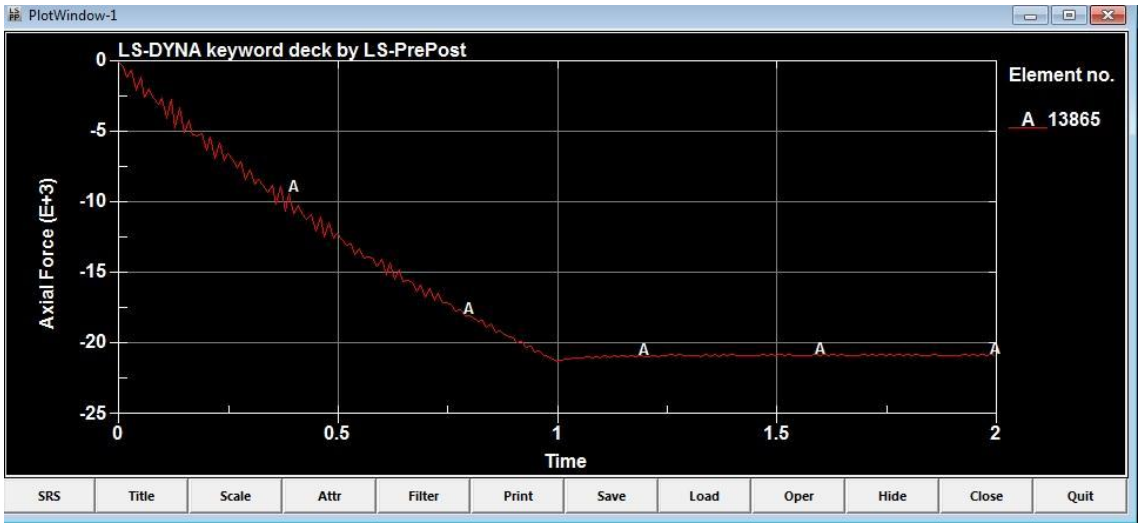

Figure 97: Time-axial force graph of rectangular – 8 inch barrier hairpin dowel reinforcement bar elements in compression side with maximum stress

6.1.4 Rectangular – 6 inch Barrier

6.1.4.1 Maximum stress in the Barrier

6.1.4.1.1 Compression side

Figure 98 shows the printed stress graph for the middle top element of the barrier in compression side, the element with maximum compressive stress. As shown in the graph, the maximum stress in the barrier is 15.2 Mpa.

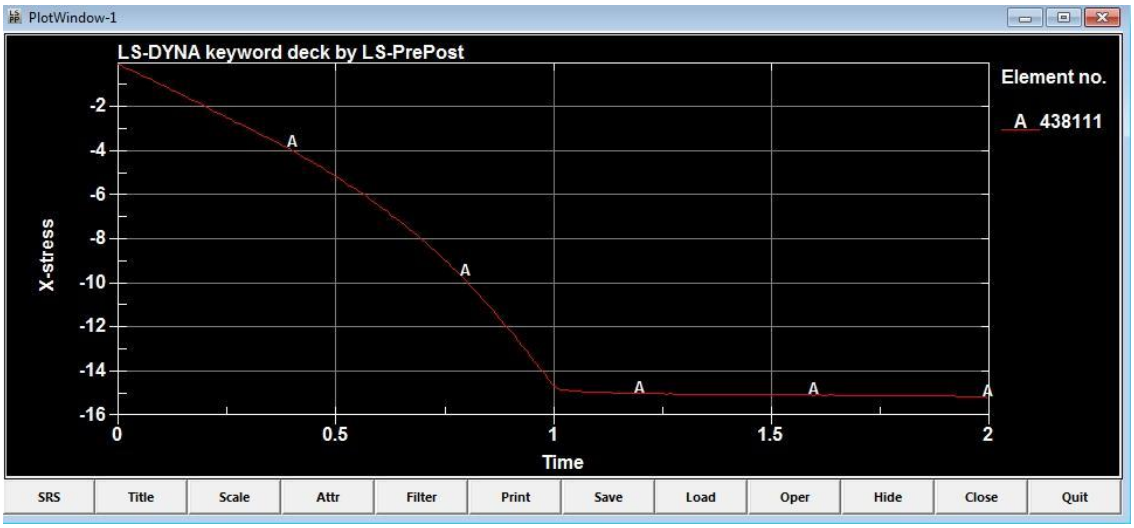

Figure 98: Time-stress graph of rectangular – 6 inch concrete barrier element in compression side with maximum stress

6.1.4.1.2 Tension Side

Figure 99 shows the printed stress graph for the middle top element of the barrier in tension side, the element with maximum tensile stress. As indicated on the graph, the maximum tensile stress of the concrete in the barrier is 2.45 Mpa.

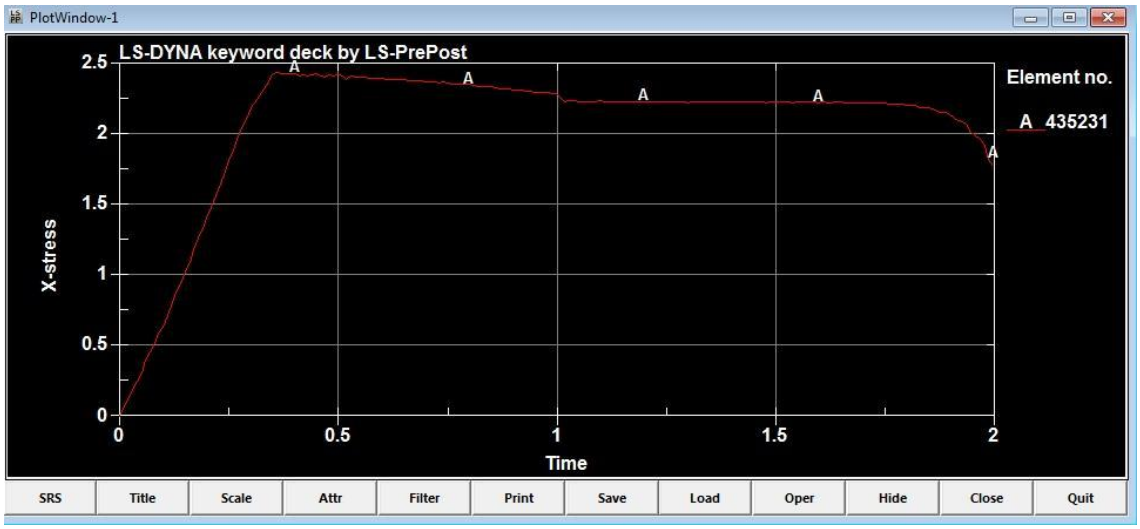

Figure 99: Time-stress graph of rectangular – 6 inch concrete barrier element in tension side with maximum stress

6.1.4.2 Maximum Stress in Deck Overhang:

As previously shown in Figure 100 and Figure 101, the maximum stress in compression and tension side was in the middle of the deck overhang because the static load is located exactly in the middle of the barrier. As explained in Chapter 2, the concrete used for deck overhang has the compressive strength of 35.52 Mpa.

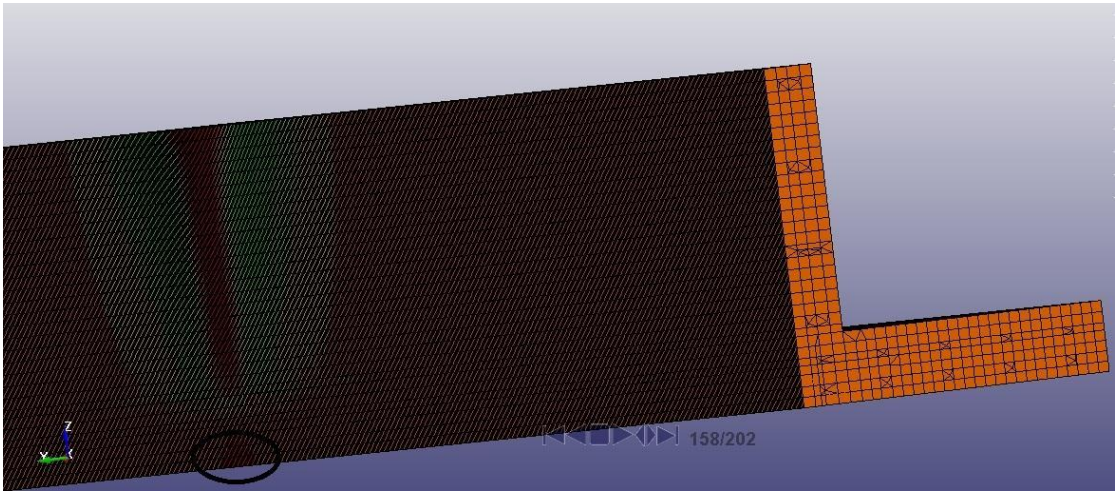

Figure 100: Maximum Stress in back of deck overhang related to rectangular – 6 inch concrete barrier – 3D model

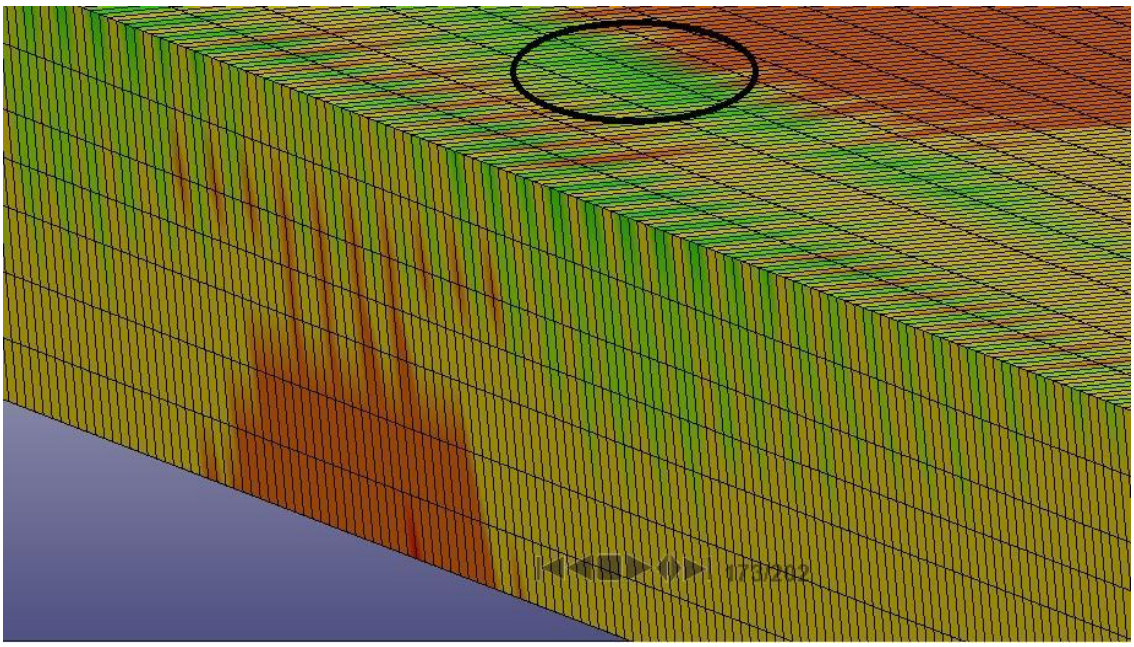

Figure 101: Maximum stress in face of deck overhang related to rectangular – 6 inch concrete barrier – 3D model

6.1.4.2.1 Compression side

Figure 102 shows the printed stress graph for the middle top element of the deck overhang in compression side, the element with maximum compressive stress. As shown in the graph, the maximum stress in the barrier is 4.76 Mpa.

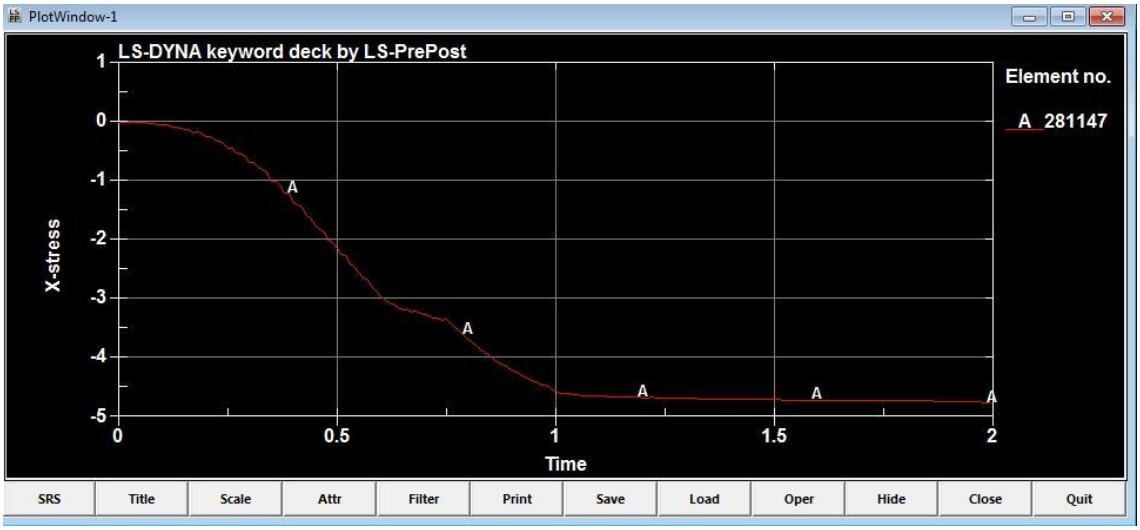

Figure 102: Time-stress graph of rectangular – 6 inch concrete deck overhang element in compression side with maximum stress

6.1.4.2.2 Tension side

As seen in Figure 103 the maximum stress imposed to the deck overhang in tension side was 1.88 Mpa.

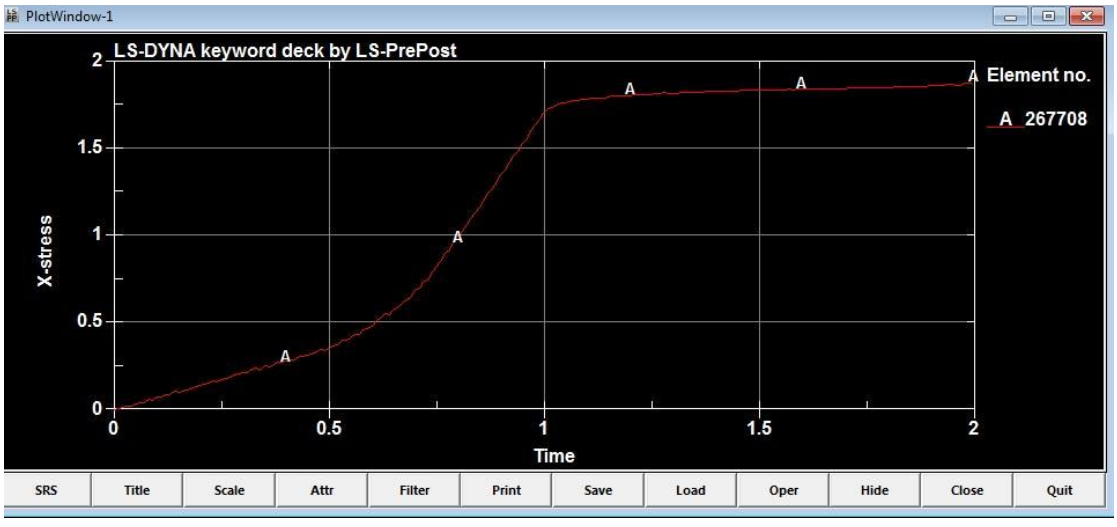

Figure 103: Time-stress graph of rectangular – 6 inch concrete deck overhang element in tension side with maximum stress

6.1.4.3 Maximum Stress in Reinforcement bars

As mentioned before, the rectangular – 6 inch concrete barrier used the same amount and number of reinforcement bar in its cross section, #4 hairpin dowel and stirrups, and #3 longitudinal reinforcement bars. Since we have the static load in the middle of the barrier, the maximum tension and compressive stress appeared in the middle hairpin dowels, at face and back of the barrier.

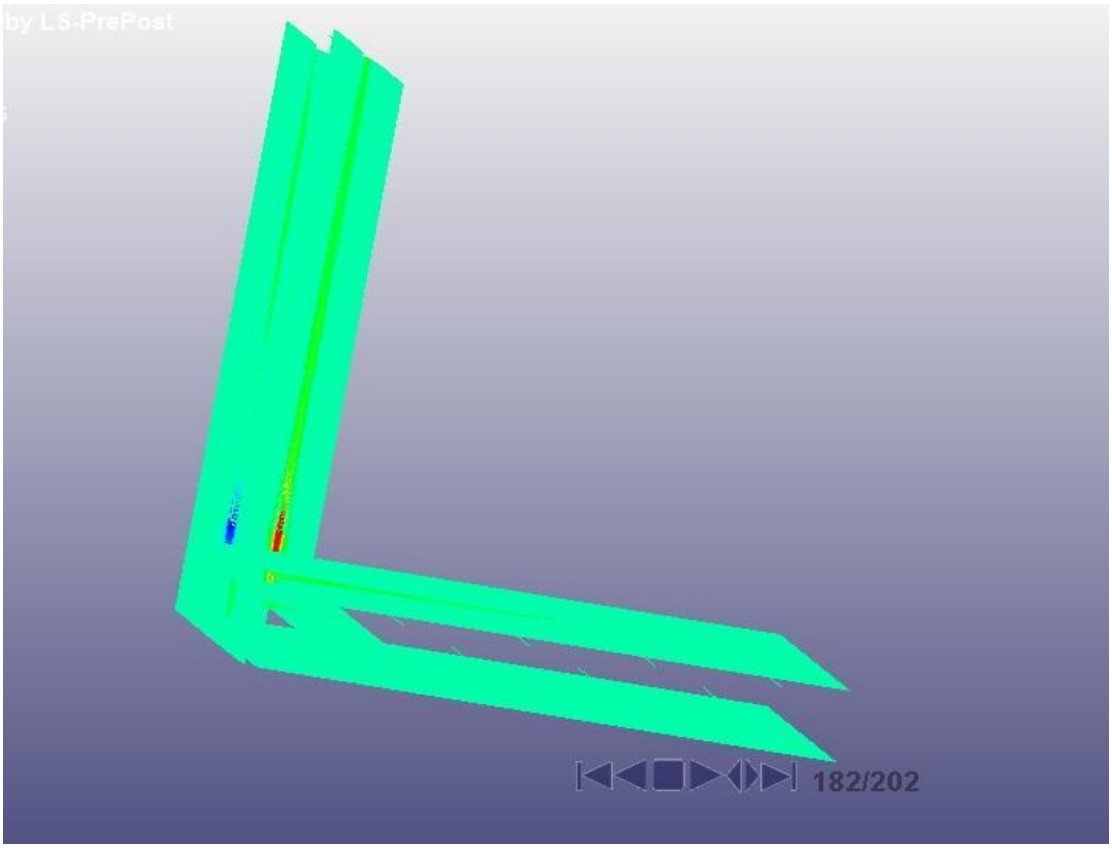

Figure 104: Maximum stress in tension and compression sides of reinforcement bar located in rectangular– 6 inch barrier – 3D model

6.1.4.3.1 Tension Side

The maximum axial force in tension side for hairpin dowels is 5.34e4 N. By dividing cross-section area into this number, the maximum stress in tension side after 1 sec was:

5.34e4 N / 129 mm^2 = 413.95 MPa = 60.04 ksi

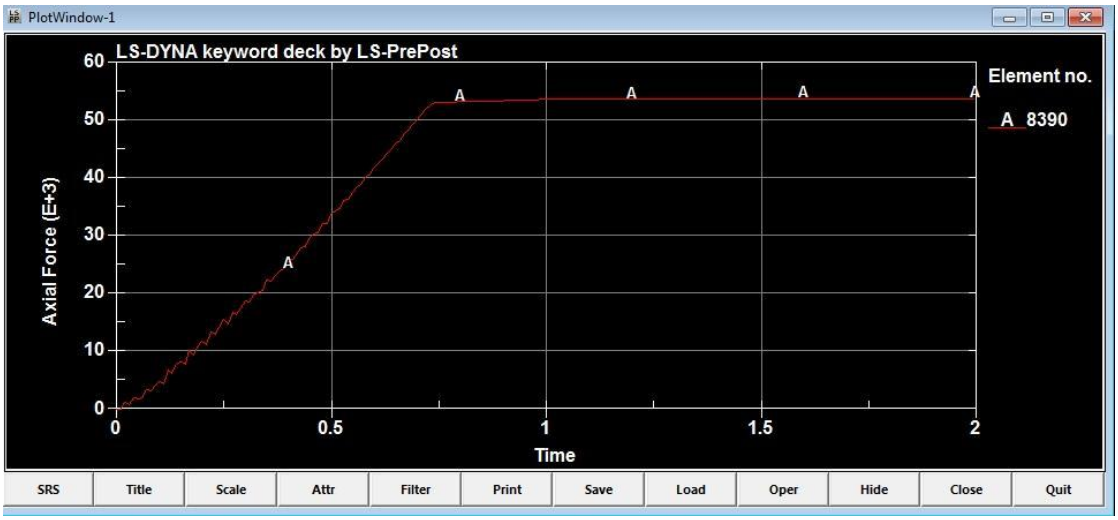

Figure 105: time-axial force graph of rectangular – 6 inch barrier hairpin dowel reinforcement bar elements in tension side with maximum stress

6.1.4.3.2 Compression Side

The maximum stress of the hairpin dowel reinforcement bar in compression side was 3.40e4 N. Hence, the maximum stress in compression side for the reinforcement bar after 1 sec was:

3.40e4 N / 129 mm^2 = 263.57 MPa = 38.23 ksi

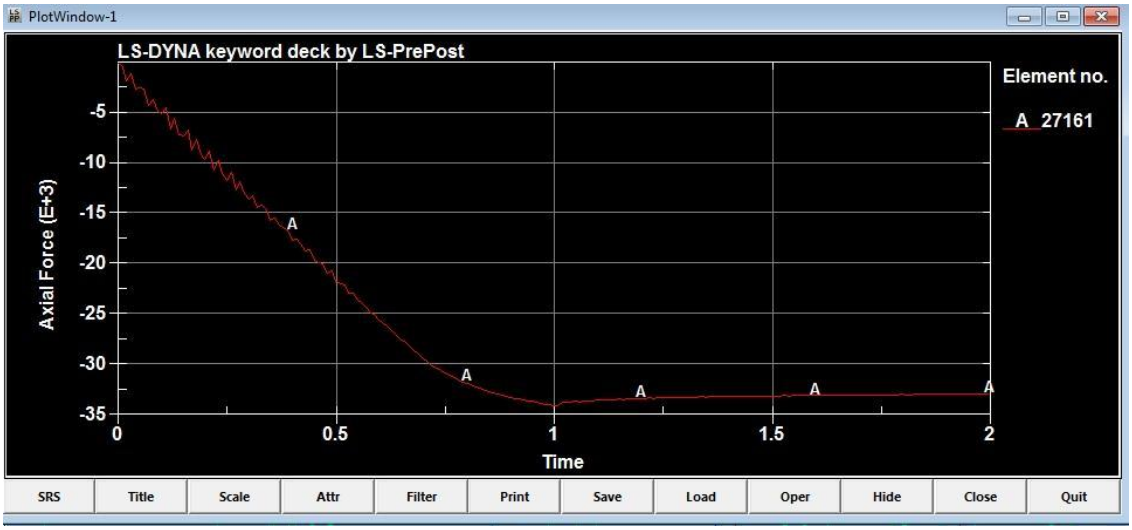

Figure 106: time-axial force graph of rectangular – 6 inch barrier hairpin dowel reinforcement bar elements in compression side with maximum stress

6.1.5 Modified Single-Slope Barrier

6.1.5.1 Maximum Stress in the Barrier

As seen in Figure 107, the maximum stress in compression side of the barrier moved down in location coming almost to the center of the barrier.

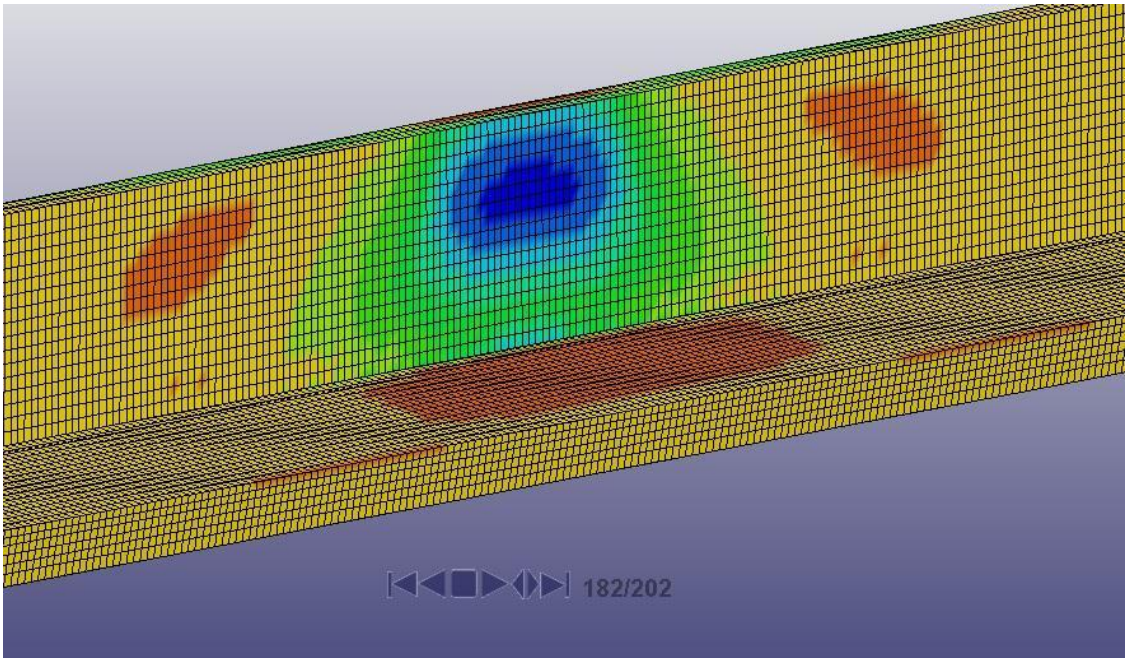

Figure 107: Maximum stress in face of modified single-slope barrier – 3D model

6.1.5.1.1 Compression Side

Figure 108 shows the printed stress graph for the middle top element of the barrier in compression side, the element with maximum compressive stress. As shown on the graph, the maximum stress in the barrier is 6.74 Mpa.

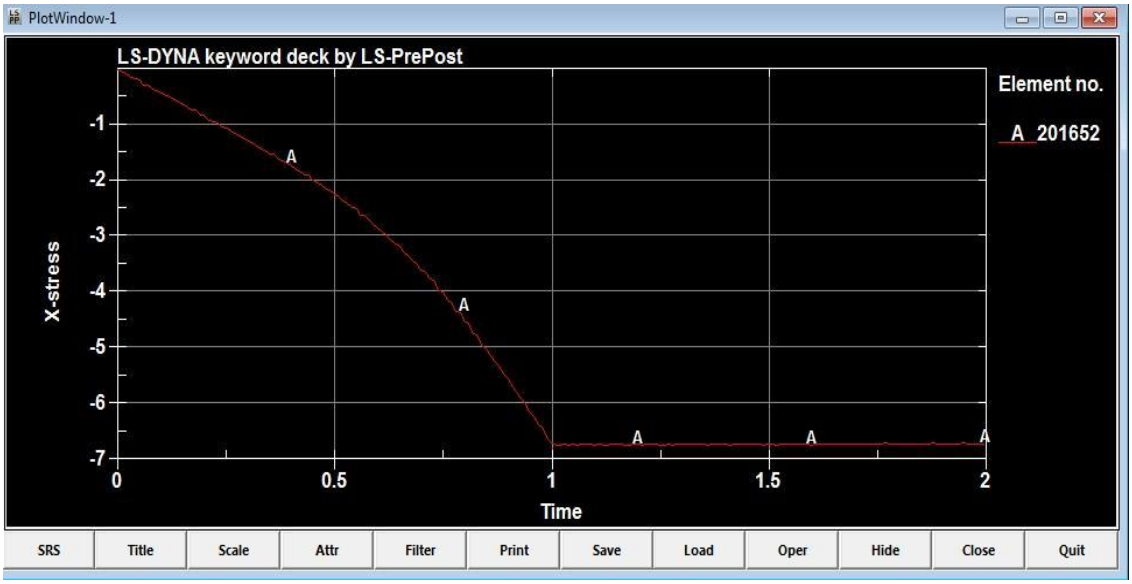

Figure 108: Time-stress graph of modified single-slope concrete barrier element in compression side with maximum stress

Compared with New Jersey barrier, the compressive stress in this geometry increased, because a thinner concrete layer was used with linear gradient thickness among the height causing extra stress in compression side of the barrier.

6.1.5.1.2 Tension Side

Figure 109 shows the printed stress graph for the middle top element of the barrier in tension side, the element with maximum tensile stress. As indicated on the graph, the maximum tensile stress of the concrete in the barrier is 2.36 Mpa.

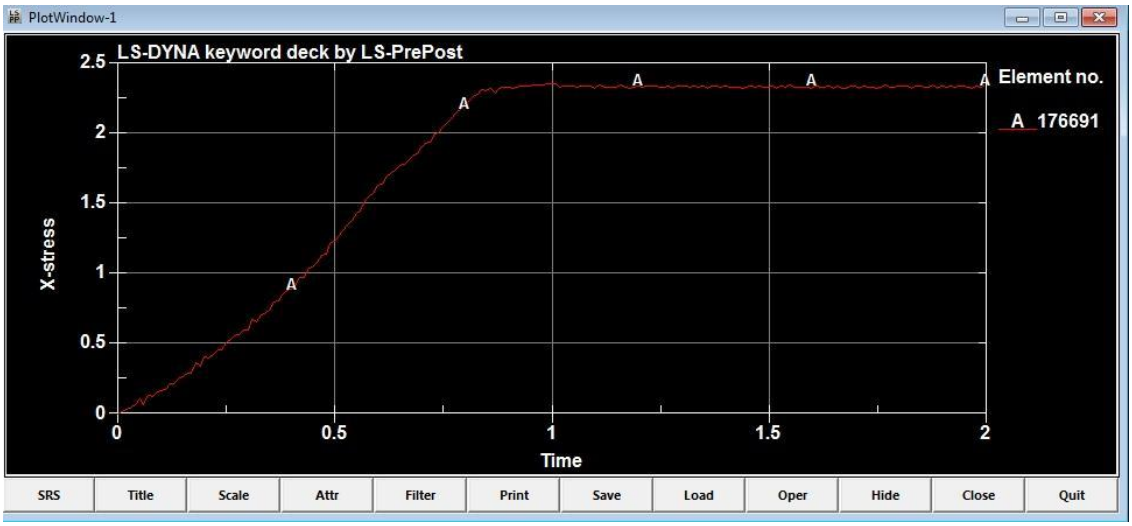

Figure 109: Time-stress graph of modified single-slope concrete barrier element in tension side with maximum stress

6.1.5.2 Maximum Stress in Deck Overhang:

As shown in Figure 110 and Figure 111, maximum stress in the compression and tension sides was in the middle of the deck overhang because the static load is located exactly in the middle of the barrier. As explained in Chapter 2, the concrete used for the deck overhang has the compressive strength of 35.52 Mpa.

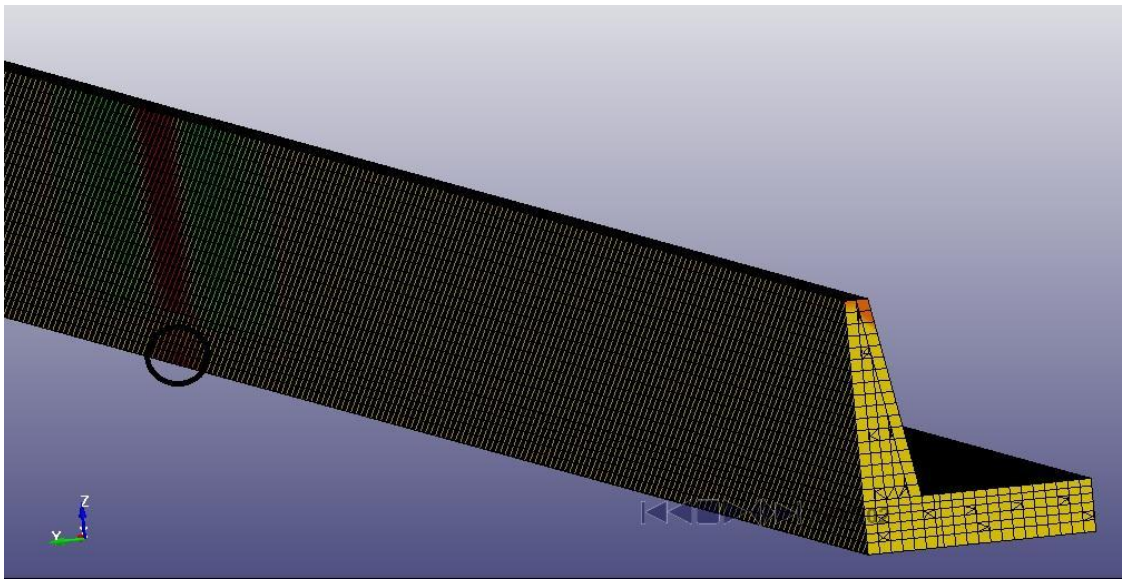

Figure 110: Maximum stress in back of deck overhang related to modified single-slope concrete barrier – 3D model

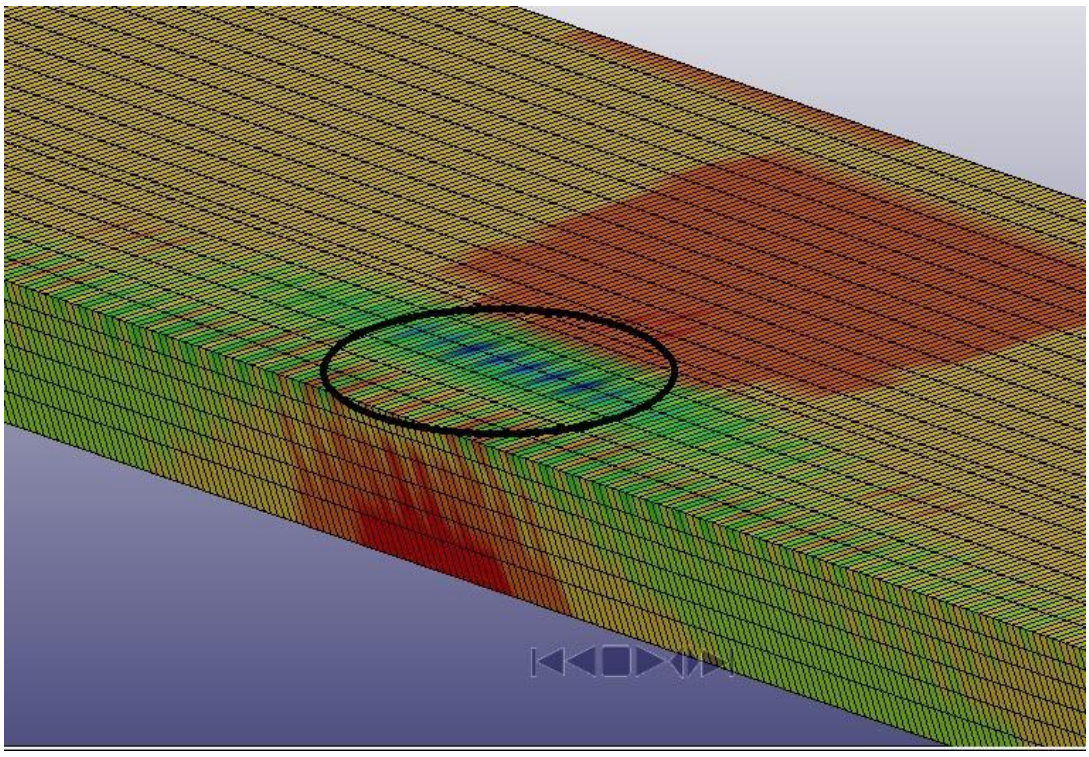

Figure 111: Maximum stress in face of deck overhang related to modified single-slope concrete barrier – 3D model

6.1.5.2.1 Compression Side

Figure 112 shows the printed stress graph for the middle top element of the deck overhang in compression side, the element with maximum compressive stress. As shown on the graph, the maximum stress in the barrier is 4.39 Mpa.

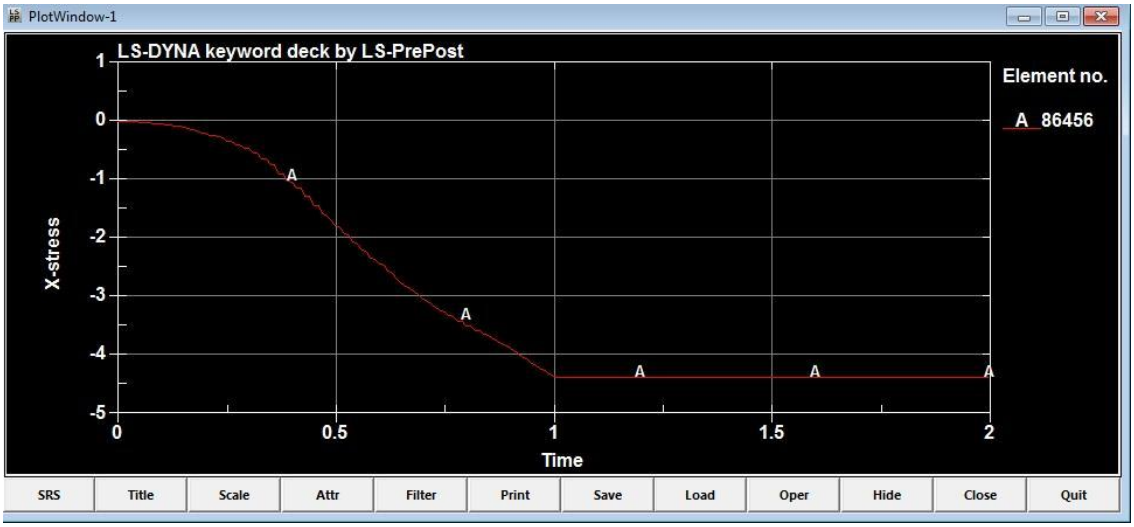

Figure 112: Time-stress graph of modified single-slope concrete barrier deck overhang element in compression side with maximum stress

6.1.5.2.2 Tension Side:

As seen in Figure 113 the maximum stress imposed to the deck overhang in tension side was 1.71 Mpa.

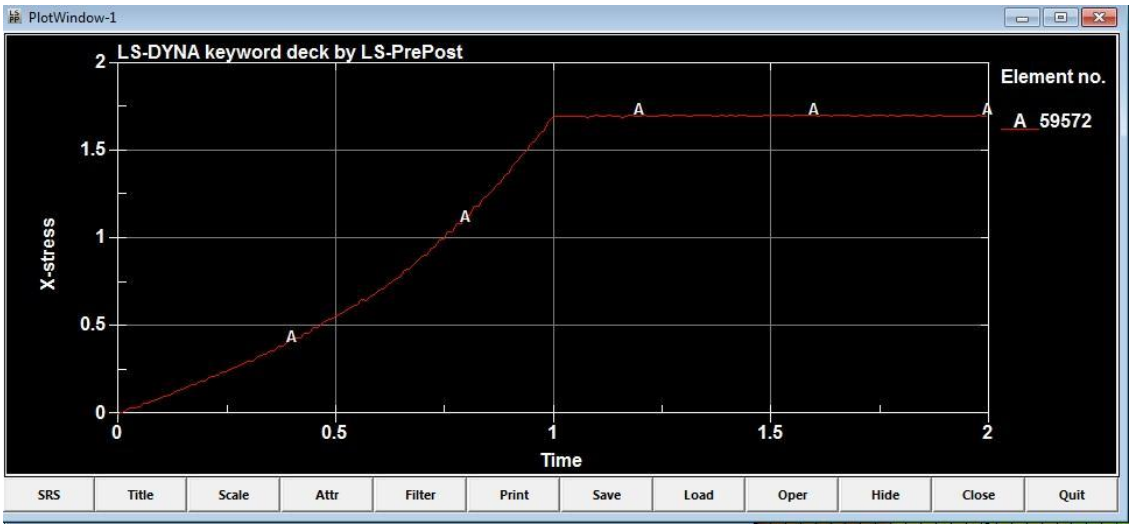

Figure 113: Time-stress graph of modified single-slope concrete barrier deck overhang element in tension side with maximum stress

6.1.5.3 Maximum stress in reinforcement bars

As previously mentioned, the rectangular – 6 inch concrete barrier used the same amount and number of reinforcement bar in its cross section, #4 hairpin dowel and stirrups, and #3 longitudinal reinforcement bars. Since the static load is located in the middle of the barrier, the maximum tension and compressive stress appeared in the middle hairpin dowels, at face and back of the barrier.

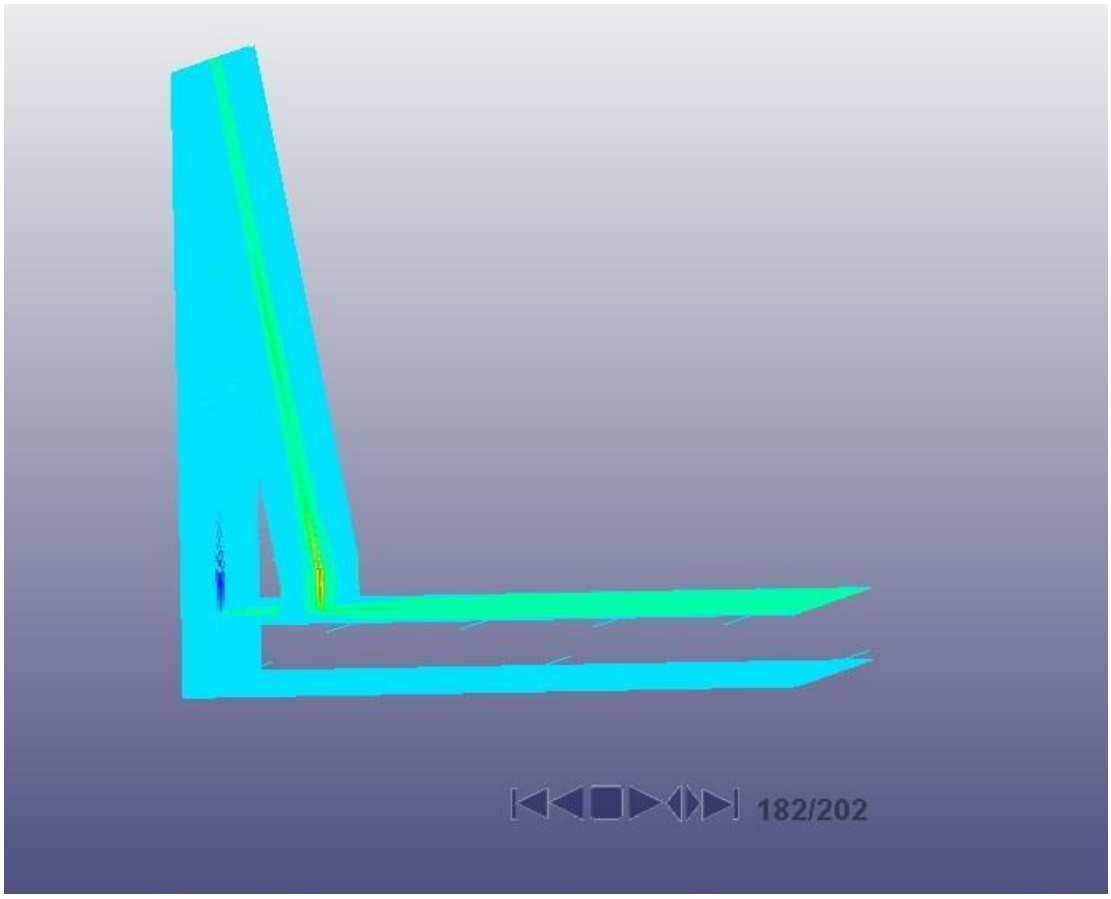

Figure 114: Maximum stress in tension and compression sides of reinforcement bars located in modified single-slope concrete barrier – 3D model

6.1.5.3.1 Tension side

The maximum axial force in tension side for hairpin dowels is 4.63e4 N. By dividing cross-section area into this number, the maximum stress in tension side after 1 sec was:

4.63e4 N / 129 mm^2 = 358.91 MPa = 52.06 ksi

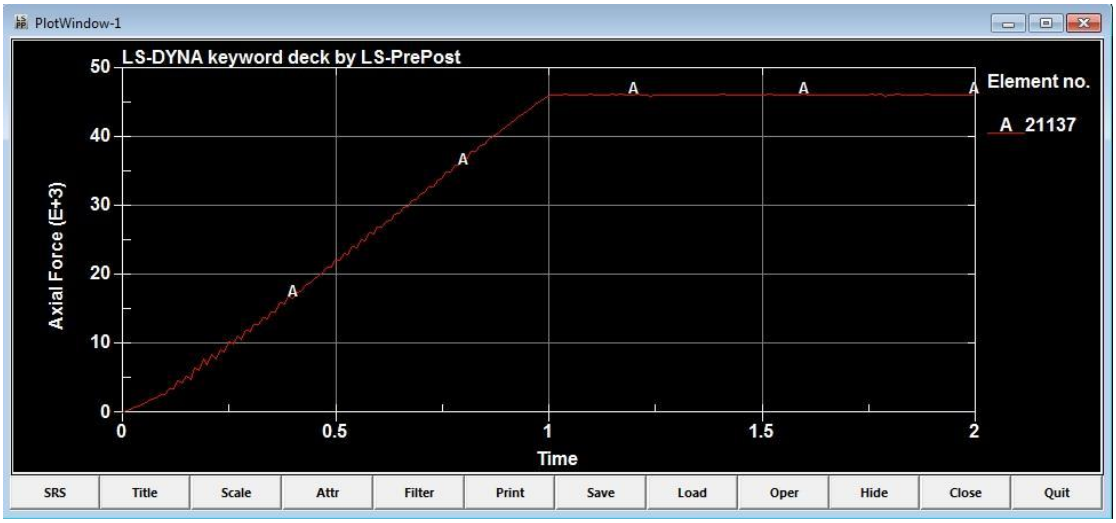

Figure 115: Time-axial force graph of modified single-slope concrete barrier hairpin dowel reinforcement bar element in tension side with maximum stress

6.1.5.3.2 Compression side

The maximum stress of the hairpin dowel reinforcement bar in compression side was 1.98e4 N. Hence, the maximum stress in compression side for the reinforcement bar after 1 sec was:

1.98e4 N / 129 mm^2 = 153.49 MPa = 22.26 ksi

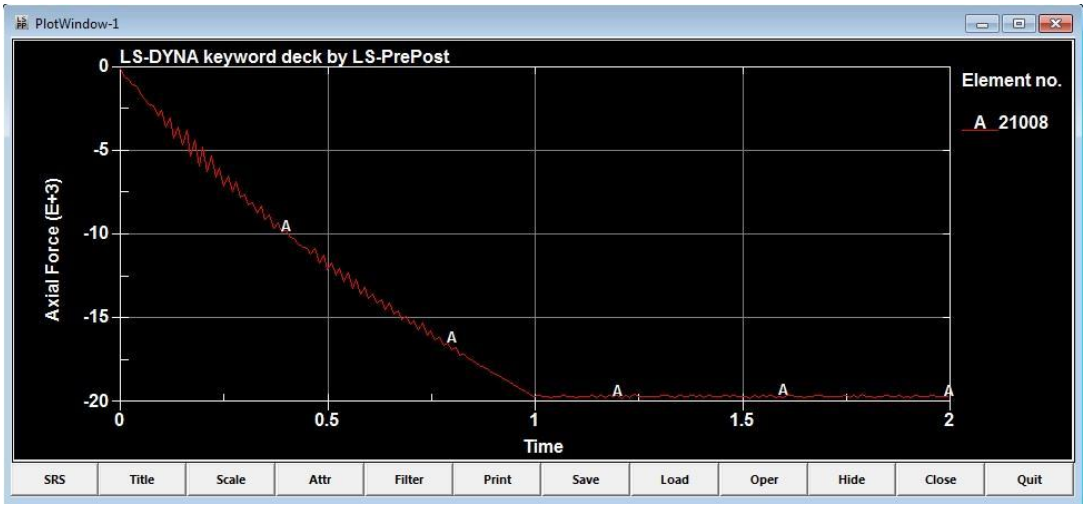

Figure 116: Time-axial force graph of modified single-slope concrete barrier hairpin dowel reinforcement bar element in compression side with maximum stress

6.1.6 Inverted Modified Single-Slope Barrier

6.1.6.1 Maximum Stress in the Barrier

As seen in Figure 117, the location for the maximum stress in compression side of the barrier lowered, relocating almost to the center of the barrier. The elements in compression side in this barrier had less stress than all other barriers.

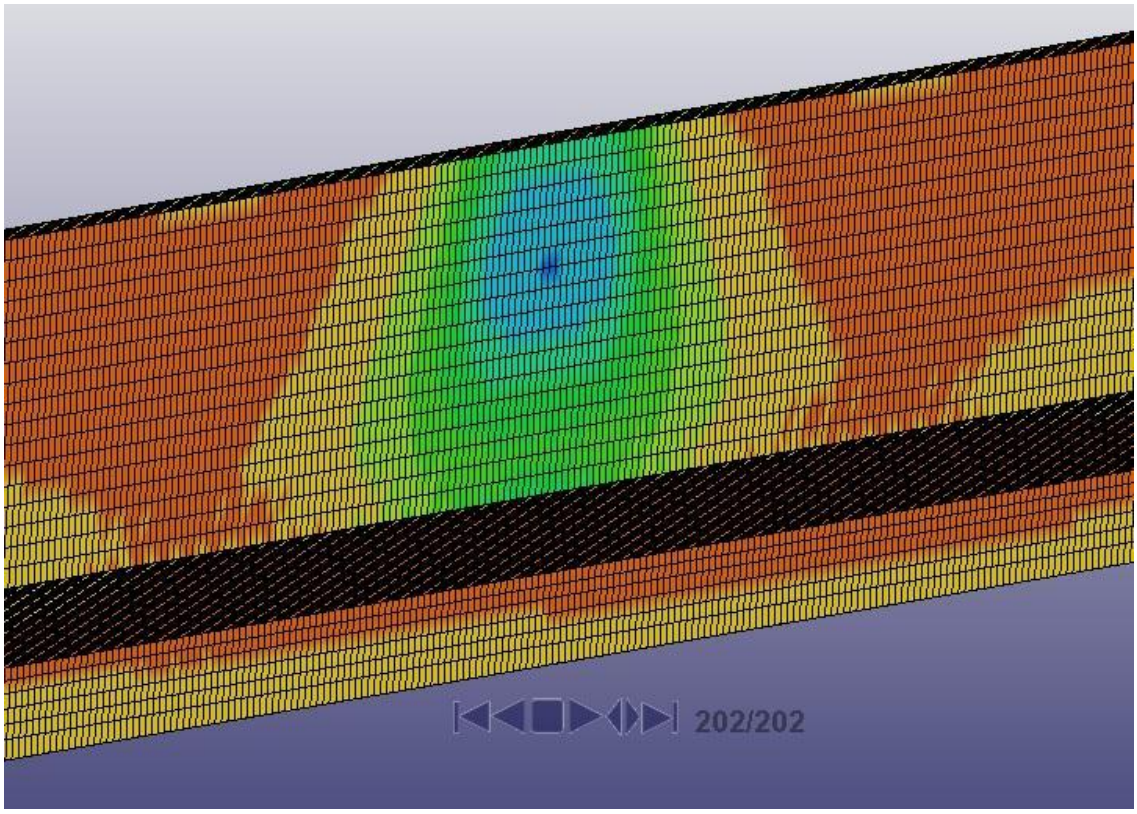

Figure 117: Maximum stress in face of inverted modified single-slope barrier – 3D model

6.1.6.1.1 Compression Side

Figure 118, shows the printed stress graph for the middle top element of the barrier in compression side, the element with maximum compressive stress. As shown on the graph, the maximum stress in the barrier is 6.51 Mpa.

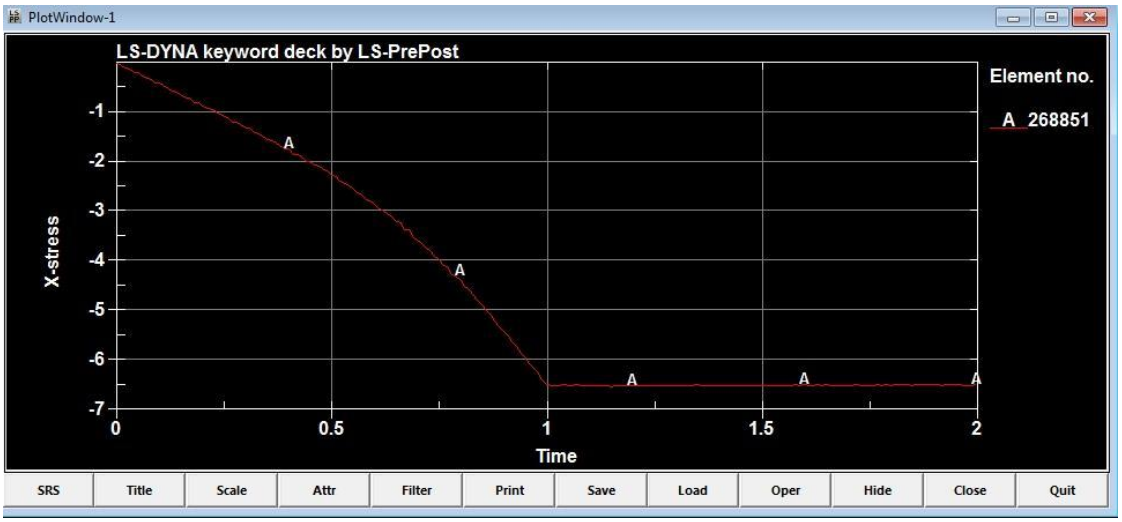

Figure 118: Time-stress graph of inverted modified single-slope concrete barrier element in compression side with maximum stress

Compared to New Jersey barrier, the compressive strength of this geometry increased because thinner concrete layers were used with linear gradient thickness among the height causing extra stress in compression side of the barrier.

6.1.6.1.2 Tension Side

Figure 119 shows the printed stress graph for the middle top element of the barrier in tension side, the element with maximum tensile stress. As indicated on the graph, the maximum tensile stress of the concrete in the barrier is 2.30 Mpa,

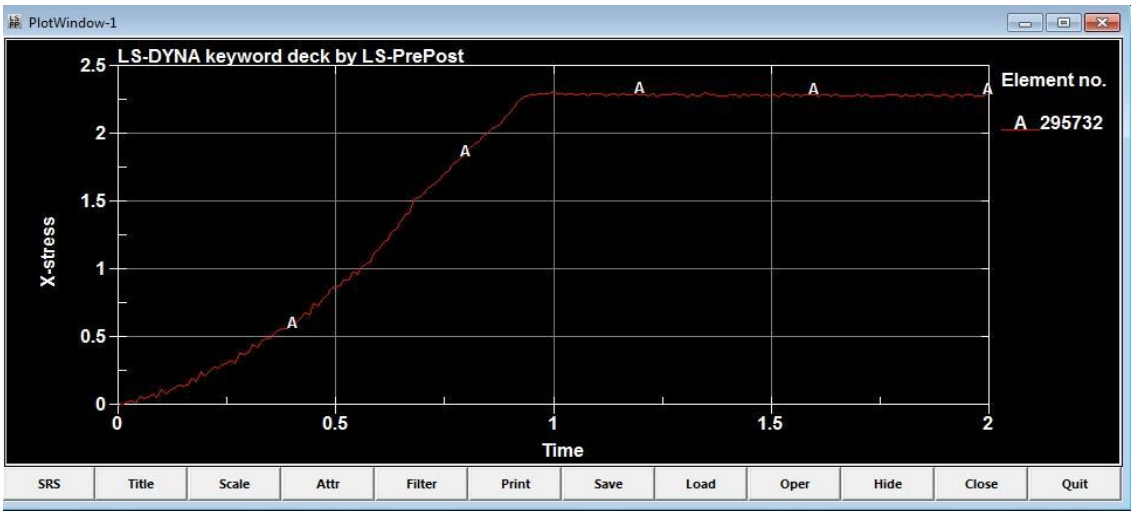

Figure 119: Time-stress graph of inverted modified single-slope concrete barrier element in tension side with maximum stress

6.1.6.2 Maximum Stress in Deck Overhang:

As shown in Figure 120 and Figure 121, maximum stress in the compression and tension sides was in the middle of the deck overhang because the static load is located exactly in the middle of the barrier. As explained in Chapter 2, the concrete used for the deck overhang has the compressive strength of 35.52 Mpa.

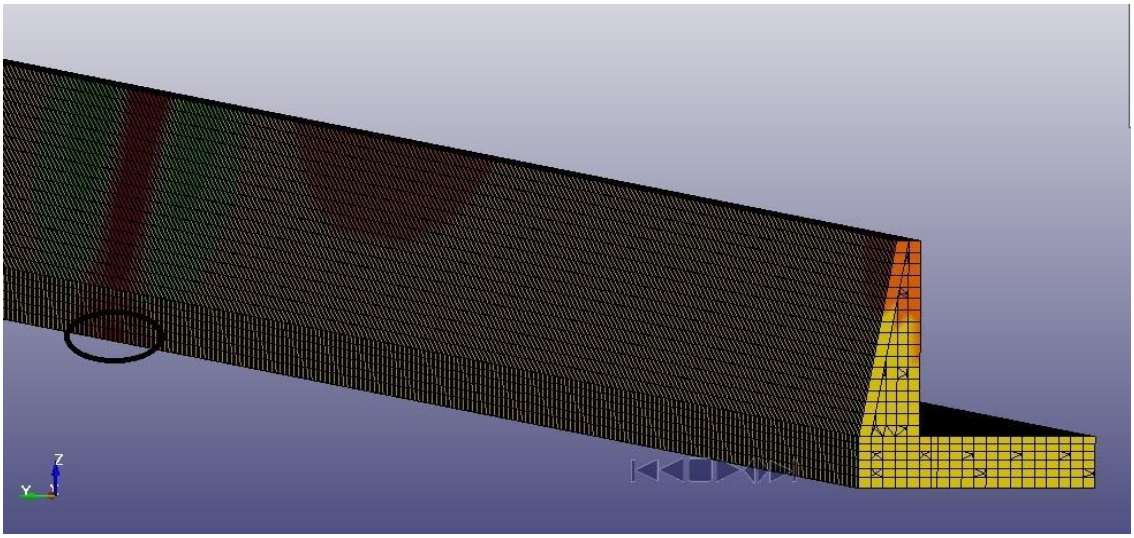

Figure 120: Maximum stress in back of deck overhang related to inverted modified single-slope concrete barrier – 3D model

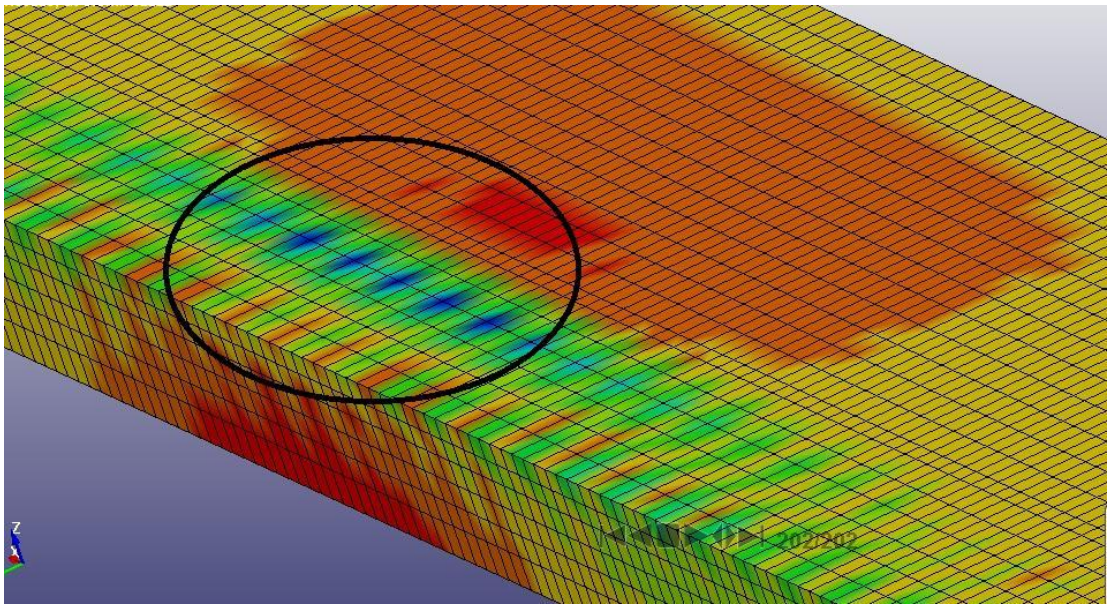

Figure 121: Maximum stress in face of deck overhang related to inverted modified single-slope concrete barrier – 3D model

6.1.6.2.1 Compression Side

Figure 122 shows the printed stress graph for the middle top element of the deck overhang in compression side, the element with maximum compressive stress. As shown on the graph, the maximum stress in the barrier is 4.25 Mpa.

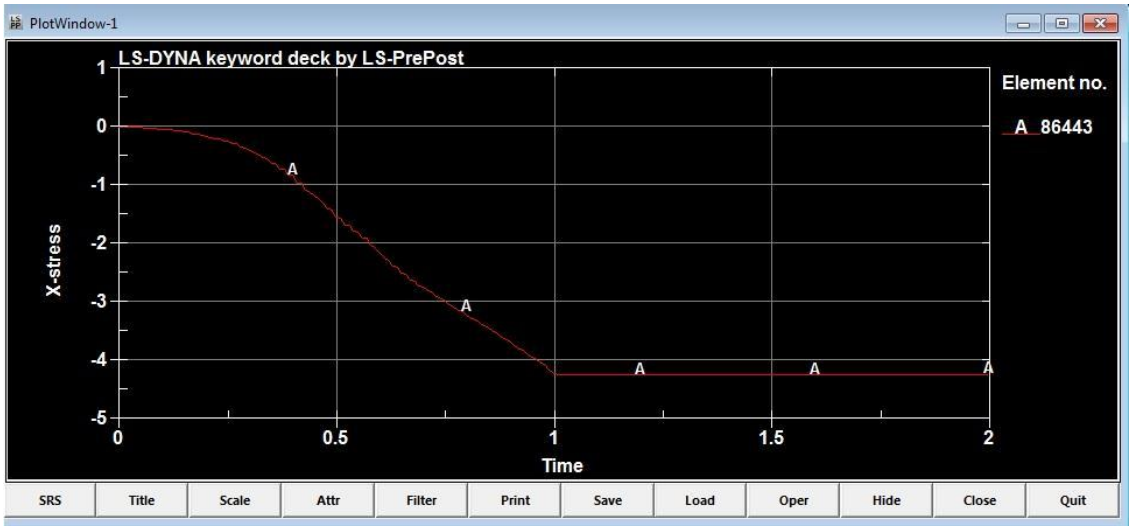

Figure 122: Time-stress graph of inverted modified single-slope concrete barrier deck overhang element in compression side with maximum stress

6.1.6.2.2 Tension Side

As seen in Figure 123, the maximum stress imposed to the deck overhang in tension side was 1.55 Mpa.

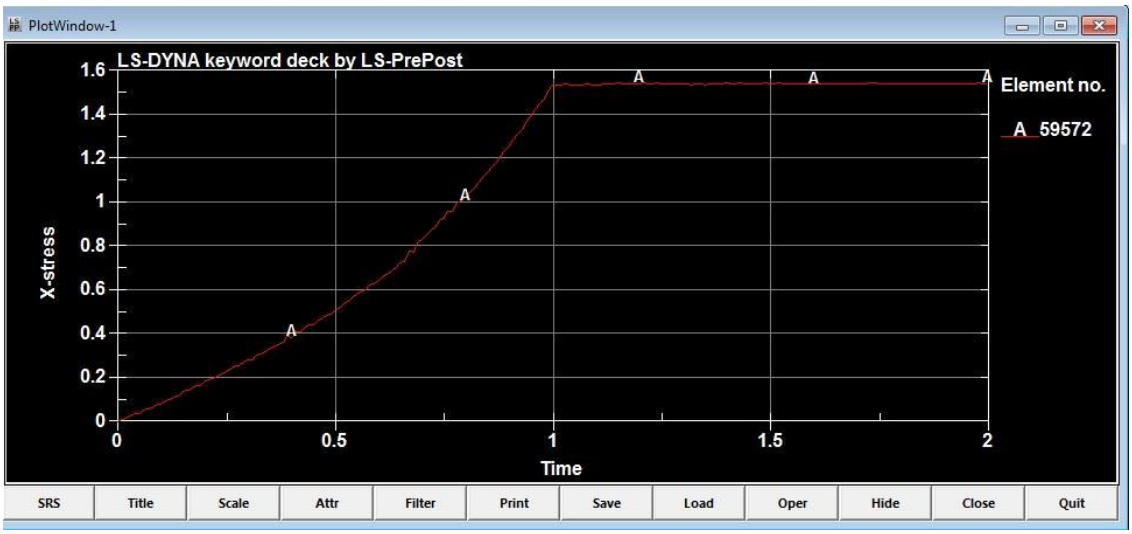

Figure 123: Time-stress graph of inverted modified single-slope concrete barrier deck overhang element in tension side with maximum stress

6.1.6.3 Maximum Stress in Reinforcement bars

As mentioned before, the inverted modified single-slope concrete barrier used the same amount and number of reinforcement bar in its cross section, #4 hairpin dowel and stirrups, and #3 longitudinal reinforcement bars. Since the static load is located in the middle of the barrier, the maximum tension and compressive stress appeared in the middle hairpin dowels, at face and back of the barrier.

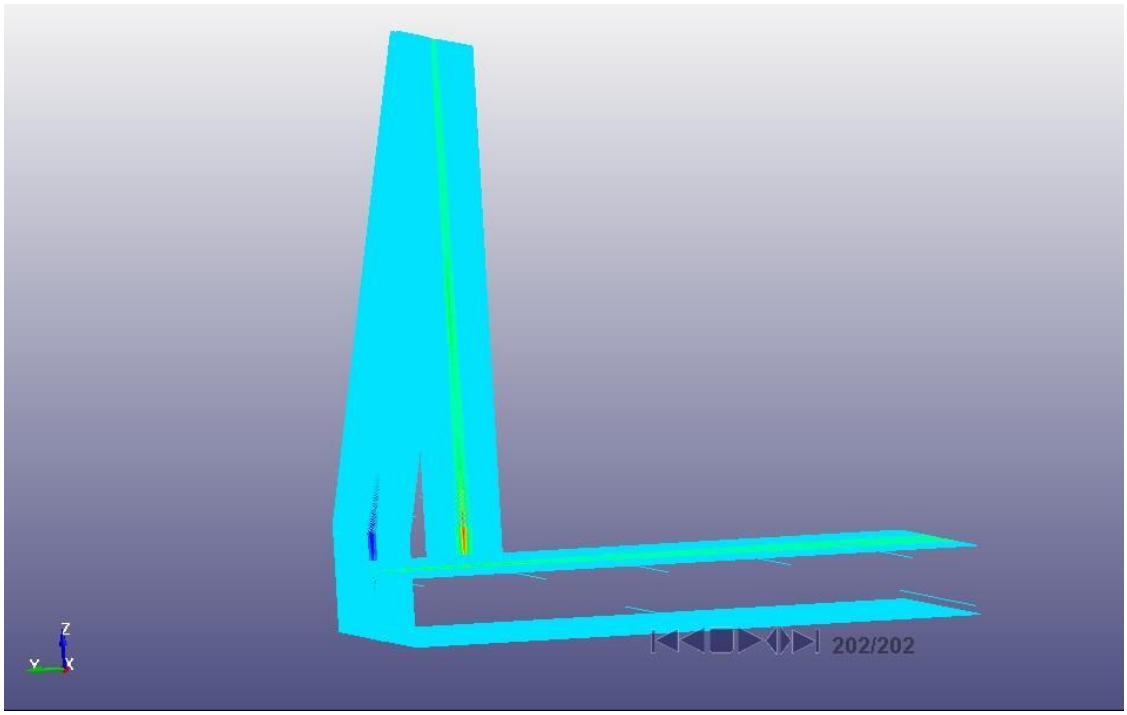

Figure 124: Maximum stress in tension and compression sides of reinforcement bars located in inverted modified single-slope concrete barrier – 3D model

6.1.6.3.1 Tension Side

The maximum axial force in tension side for hairpin dowels was 4.61e4 N. By dividing cross-section area into this number, the maximum stress in tension side after 1 sec was:

4.61e4 N / 129 mm^2 = 357.36 MPa = 51.83 ksi

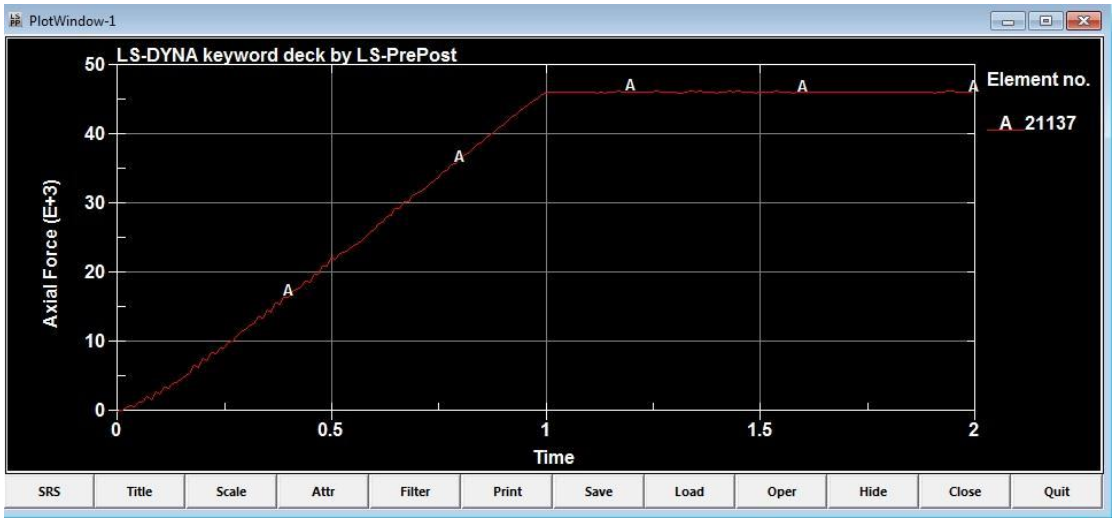

Figure 125: Time-axial force graph of inverted modified single-slope concrete barrier hairpin dowel reinforcement bar element in compression side with maximum stress

6.1.6.3.2 Compression Side

The maximum stress of the hairpin dowel reinforcement bar in compression side was 1.95e4 N. Hence, the maximum stress in compression side for the reinforcement bar after 1 sec was:

1.95e4 N / 129 mm^2 = 151.16 MPa = 21.92 ksi

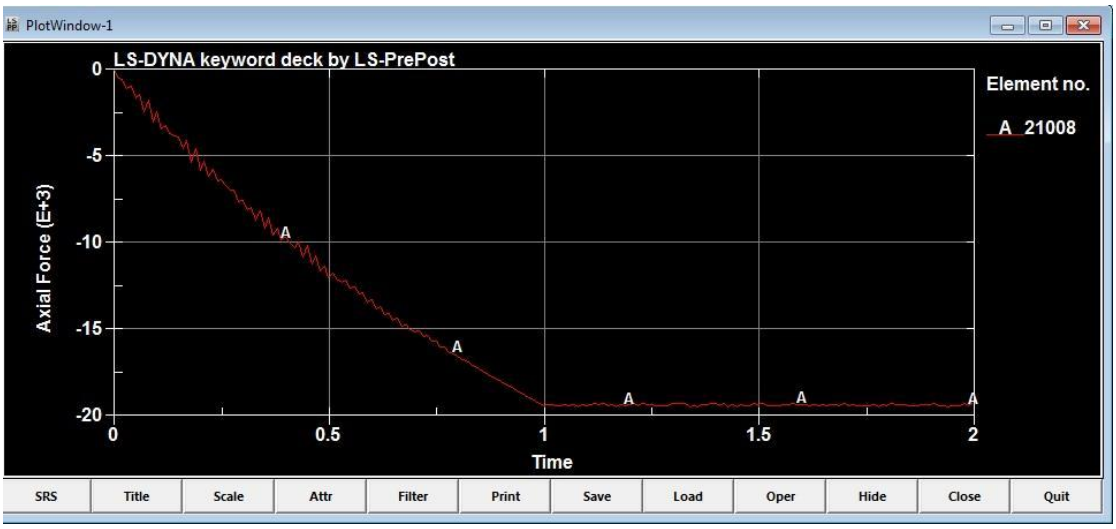

Figure 126: Time-Axial Force Graph of inverted modified single-slope concrete Barrier hairpin dowel reinforcement bar element in compression side with maximum stress

6.1.7 Comparison between the Barrier Geometries – Maximum Stress

Graph 127 to 132 compared the maximum stress in compression and tension side of the concrete, and reinforcement bars in all of the above mentioned barriers.

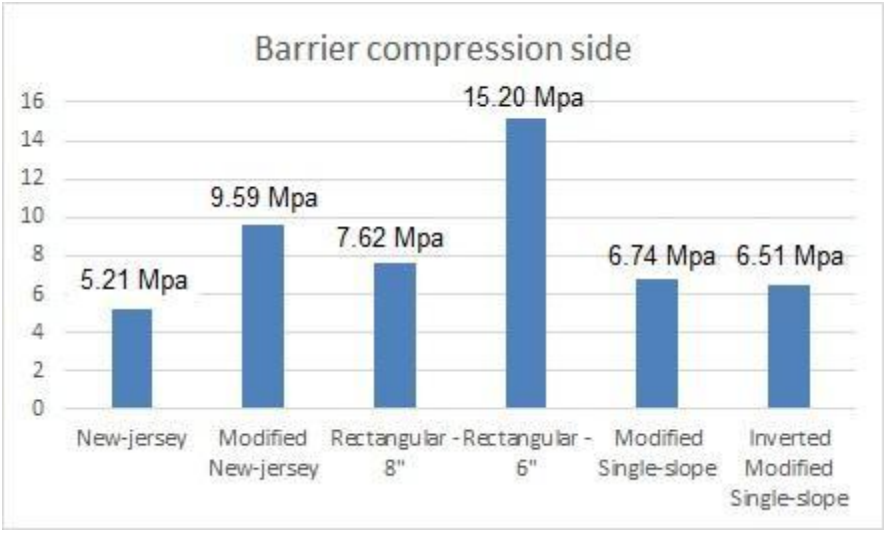

Figure 127: Barrier concrete Block on compression side

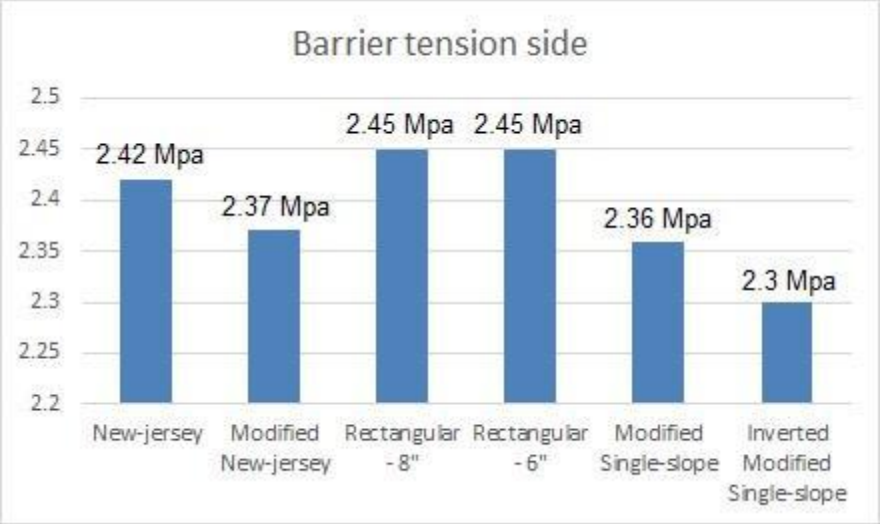

Figure 128: Barrier Concrete Block on tension side

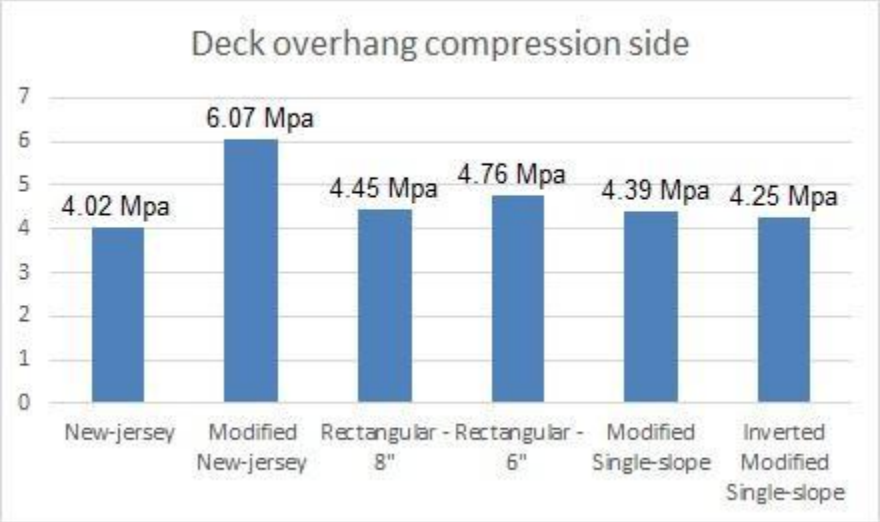

Figure 129: Deck Overhang Concrete Block in compression side

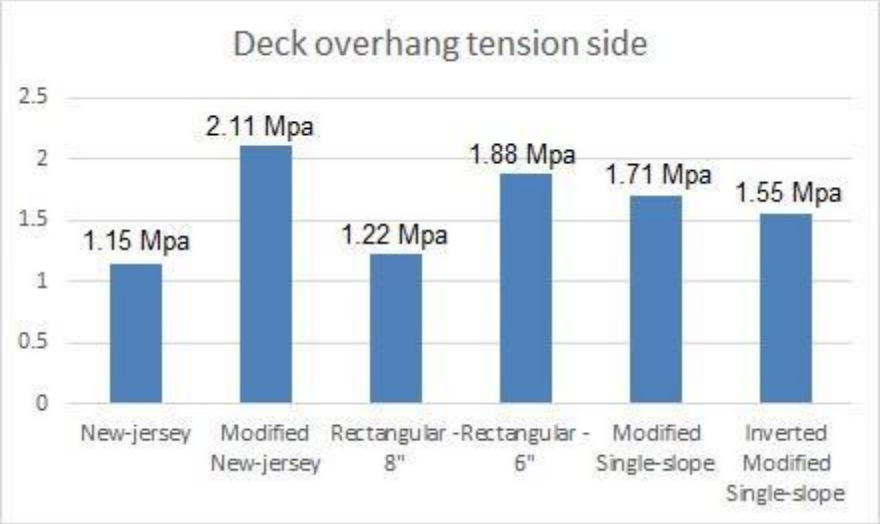

Figure 130: Deck Overhang Concrete Block on Tension Side

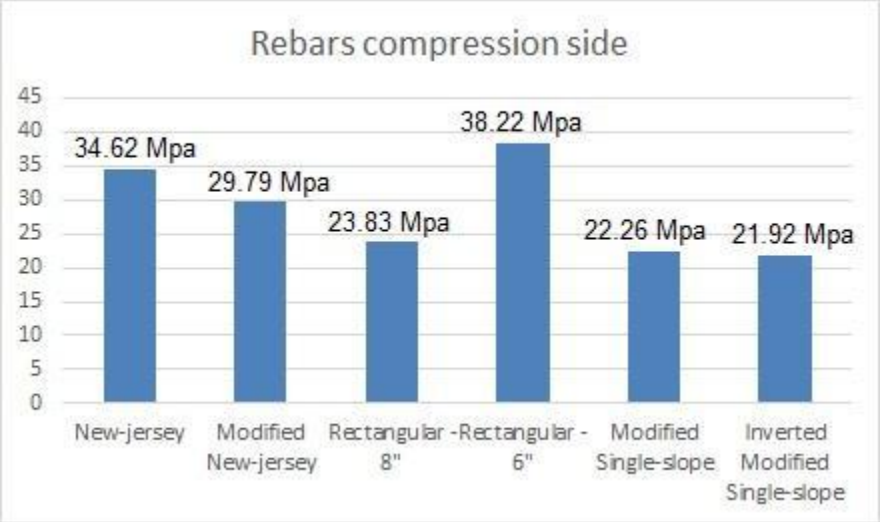

Figure 131: Reinforcement bars On Compression Side

Figure 132: Reinforcement bars on Tension Side

As seen on the previous graphs, based on TL-4 static load, all barriers stayed on the safe side without any cracks appearing. Only in modified New Jersey and rectangular– 6 inch geometries, the reinforcement bars reached yield point but did not reach the plasticity limit. This comparison shows that there might be a chance to reduce barrier thickness in order to optimize the geometry with less pour costs; however, it cannot acknowledge the safety of the proposed barriers.

6.2 Maximum Deflection

As mentioned before, maximum stress and maximum deflection of the barriers and deck overhangs were in the middle of the length of the barrier. This was due to the applied load, representing TL-4, being located in the middle of the barrier.

6.2.1 New Jersey Barrier

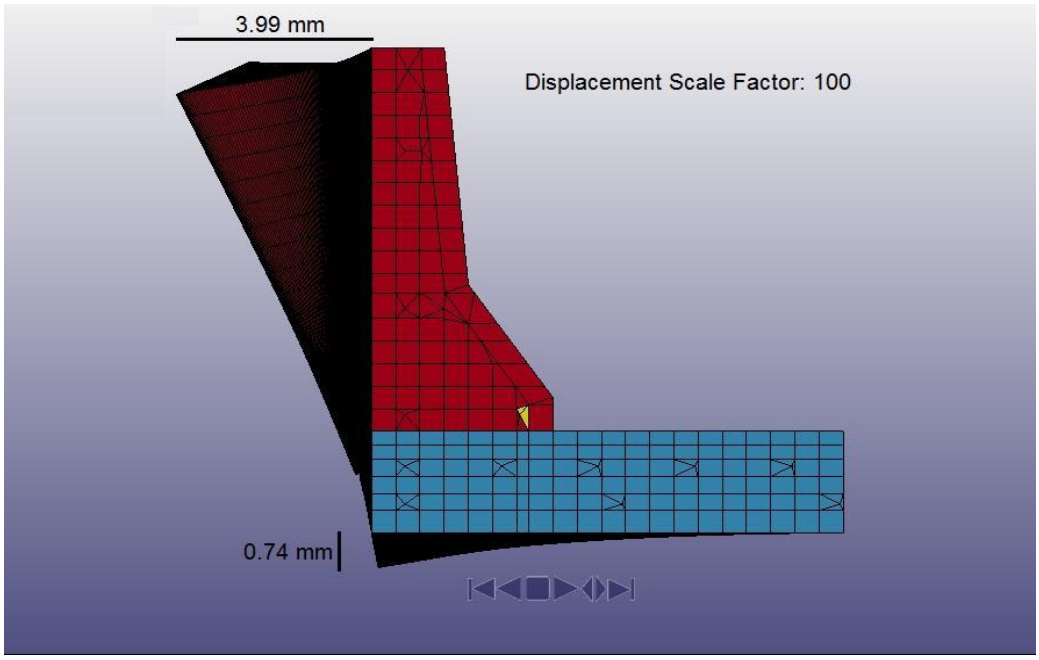

Figure 133: Maximum Deflection of Barrier and Deck Overhang – New Jersey

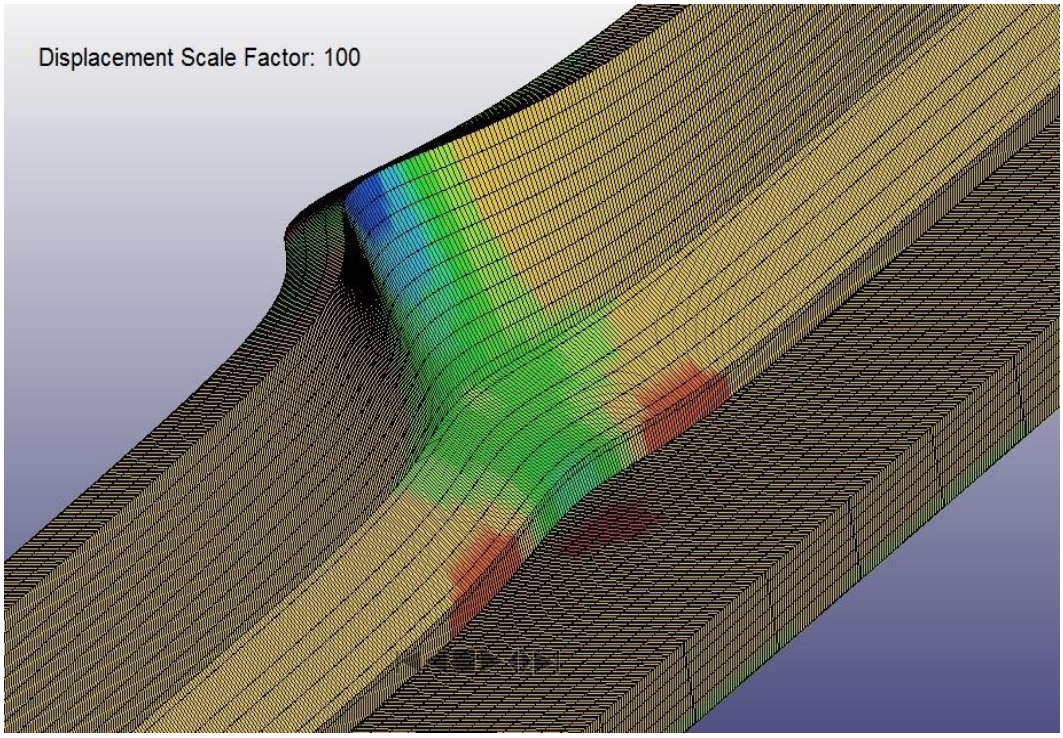

Figure 134: Maximum Deflection of Barrier and Deck Overhang – 3D model – New Jersey

6.2.1.1 Maximum Deflection in Barrier

As seen in Figure 135, the maximum deflection in the Barrier was 3.99 mm or 0.16 inches.

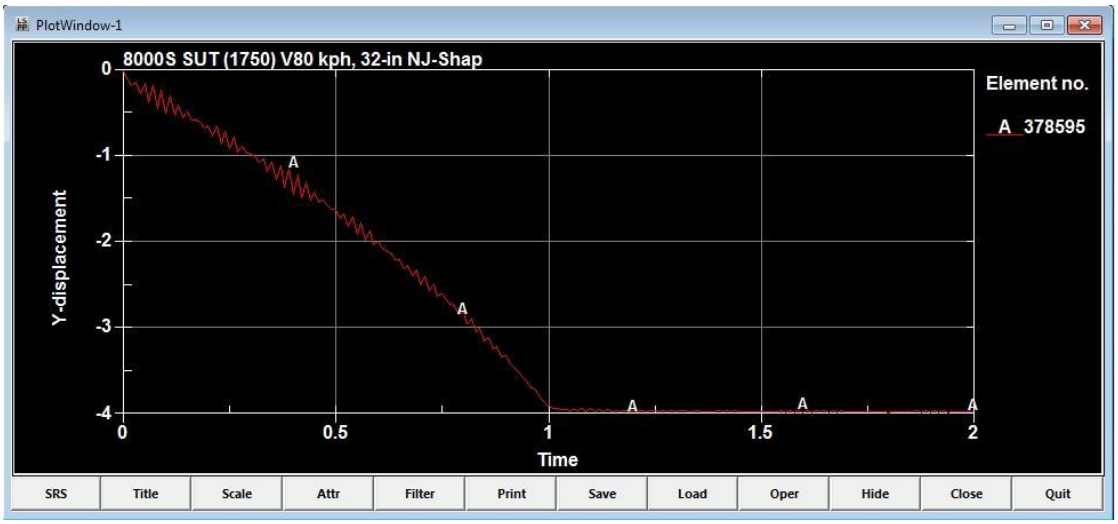

Figure 135: Maximum Deflection of the New Jersey Barrier

6.2.1.2 Maximum Deflection in Deck Overhang

As seen in Figure 136, the maximum deflection in the deck overhang was 0.74 mm or 0.03 inches.

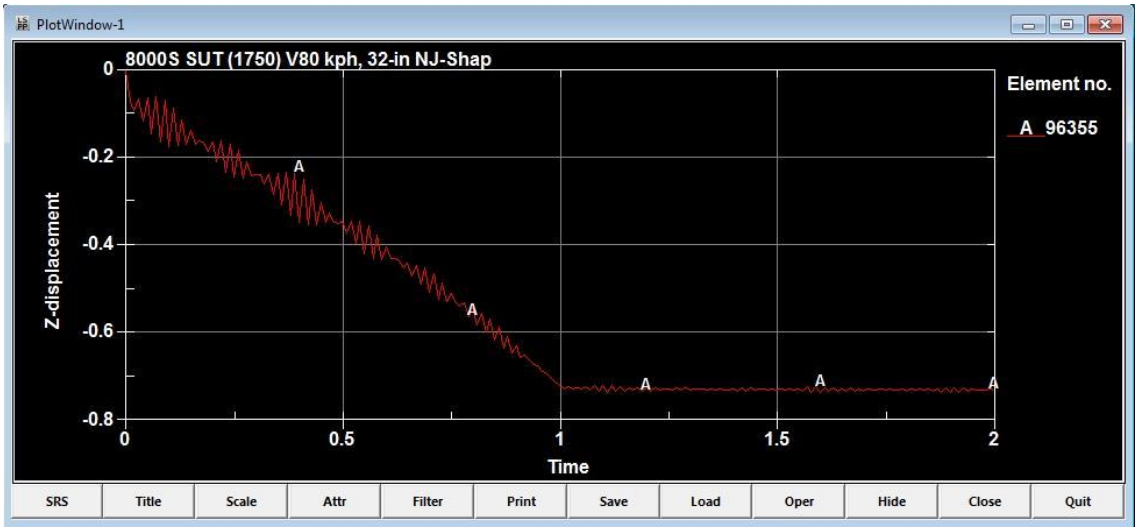

Figure 136: Maximum Deflection of the Deck Overhang – New Jersey Barrier

6.2.2 Modified New-Jersey Barrier

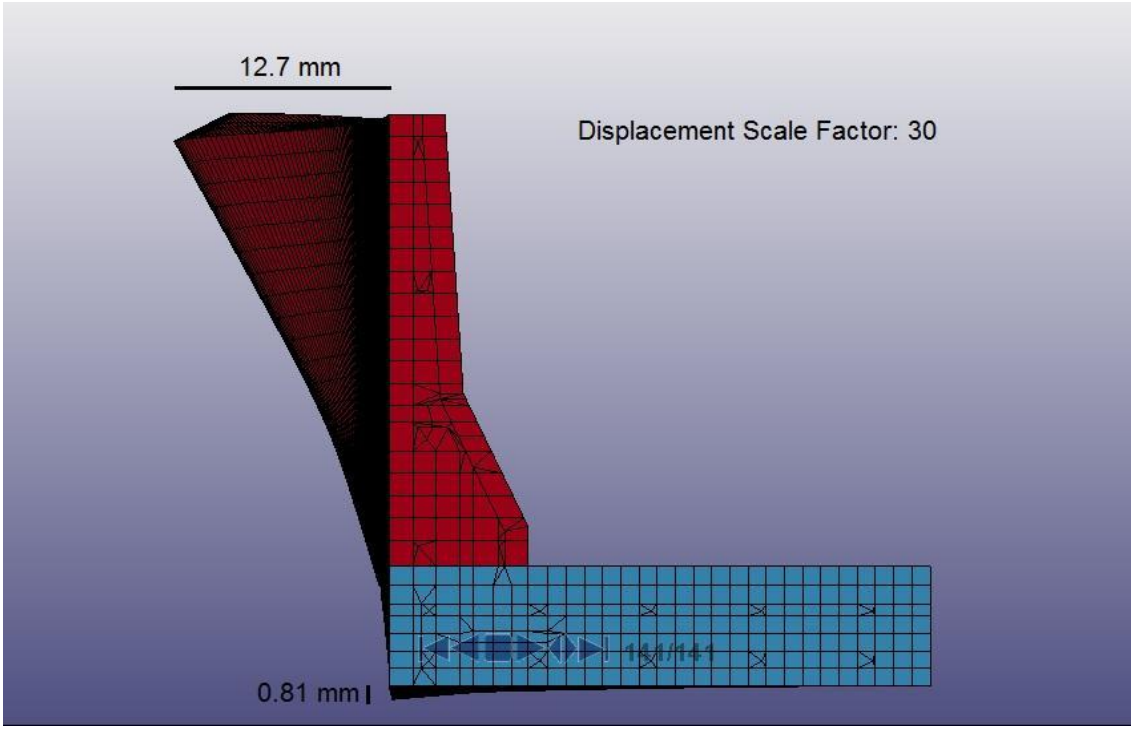

Figure 137: Maximum deflection of Barrier and deck overhang – Modified New-Jersey

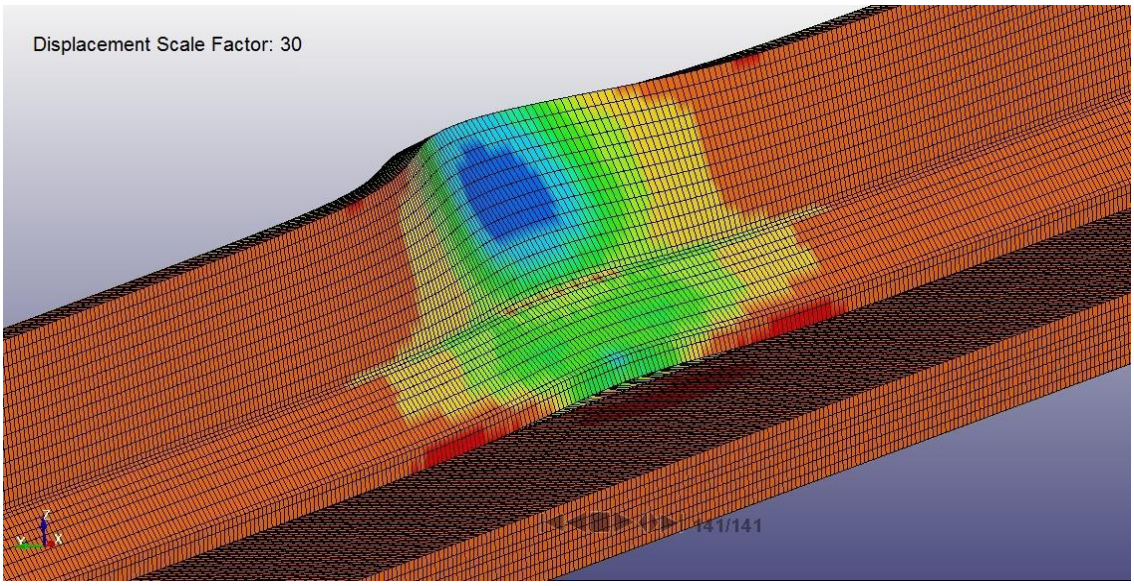

Figure 138: Maximum deflection of Barrier and deck overhang –3D model – modified New-Jersey

6.2.2.1 Maximum Deflection in Barrier

As seen in Figure 139, the maximum deflection in the barrier was 12.7 mm or 0.5 inches.

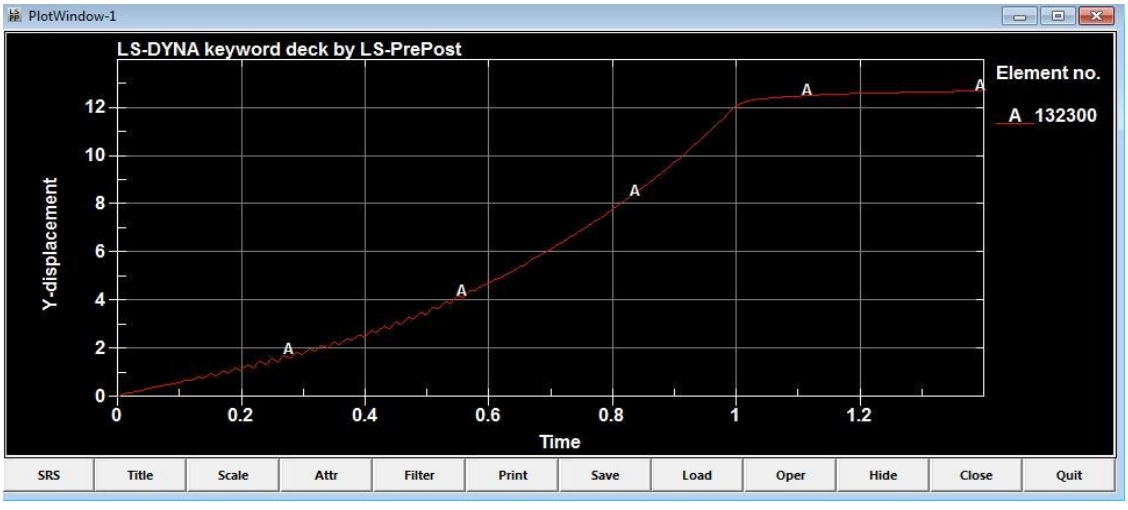

Figure 139: Maximum deflection of the Barrier – Modified New-Jersey

6.2.2.2 Maximum Deflection in Deck Overhang

As seen in Figure 140 maximum deflection in the deck overhang was 0.81 mm or 0.03 inches.

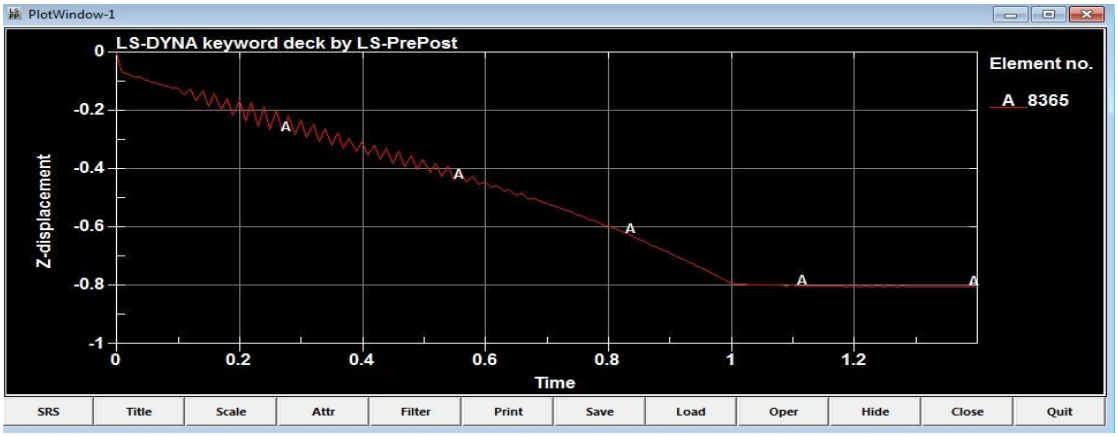

Figure 140: Maximum deflection of the deck overhang – Modified New Jersey

6.2.3 Rectangular – 8 inch Barrier

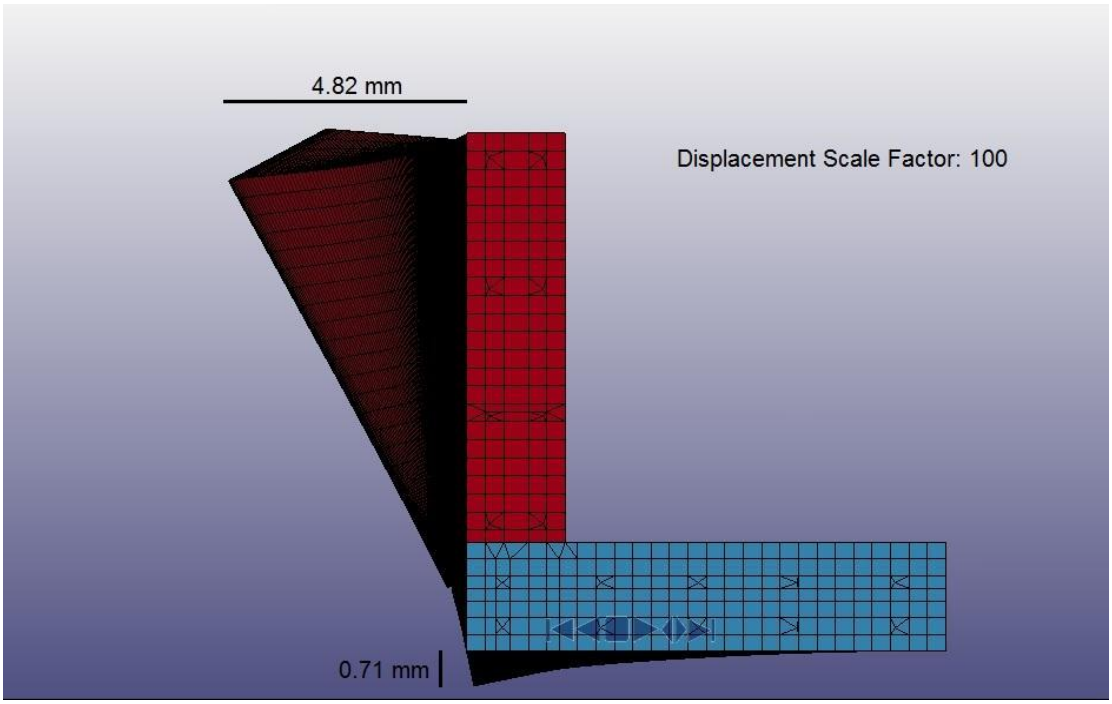

Figure 141: Maximum Deflection of Barrier and Deck Overhang – Rectangular 8 inch

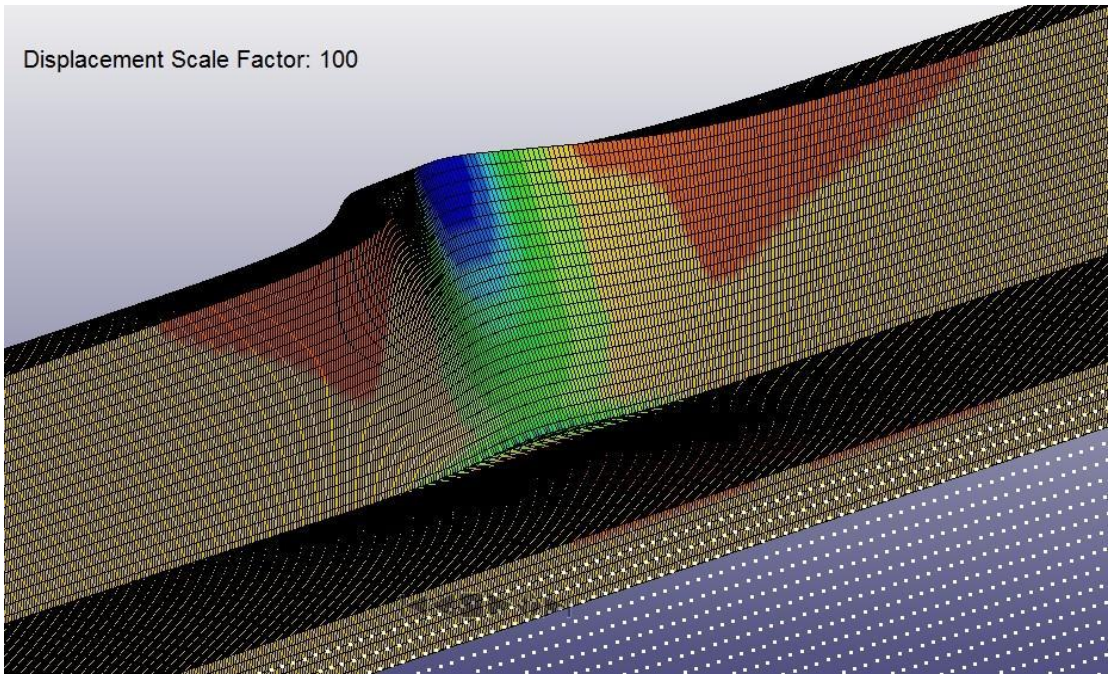

Figure 142: Maximum Deflection of Barrier and Deck overhang 3D model - Rectangular 8 inch

6.2.3.1 Maximum Deflection in Barrier

As seen in Figure 143 maximum deflection in the Barrier was 4.82 mm or inches.

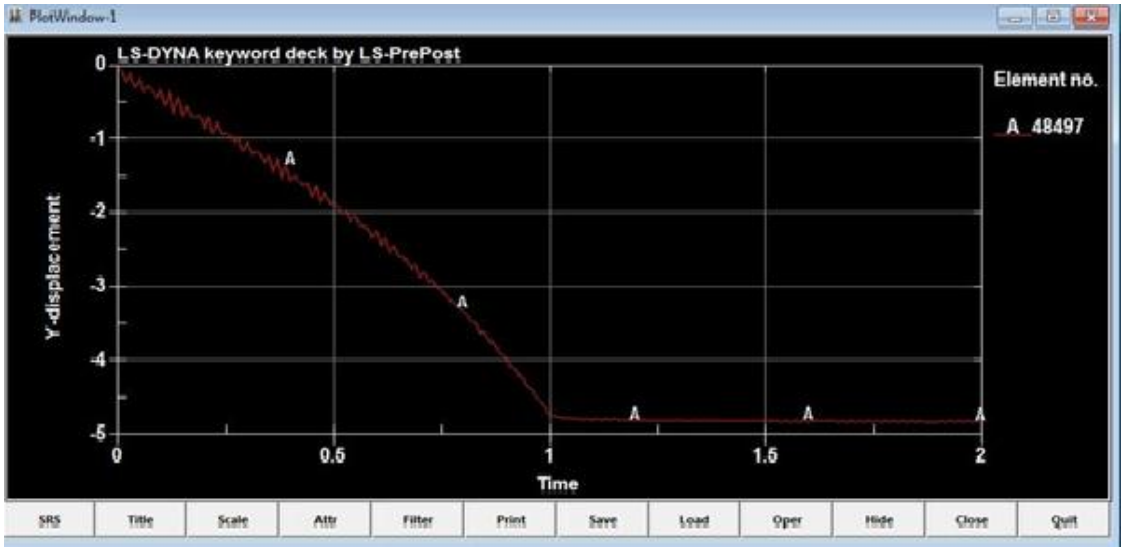

Figure 143: Maximum Deflection of the Barrier – Rectangular 8 inch

6.2.3.2 Maximum Deflection in Deck Overhang

As seen below in Figure, the maximum deflection in the deck overhang was 0.71 mm or 0.03 inches.

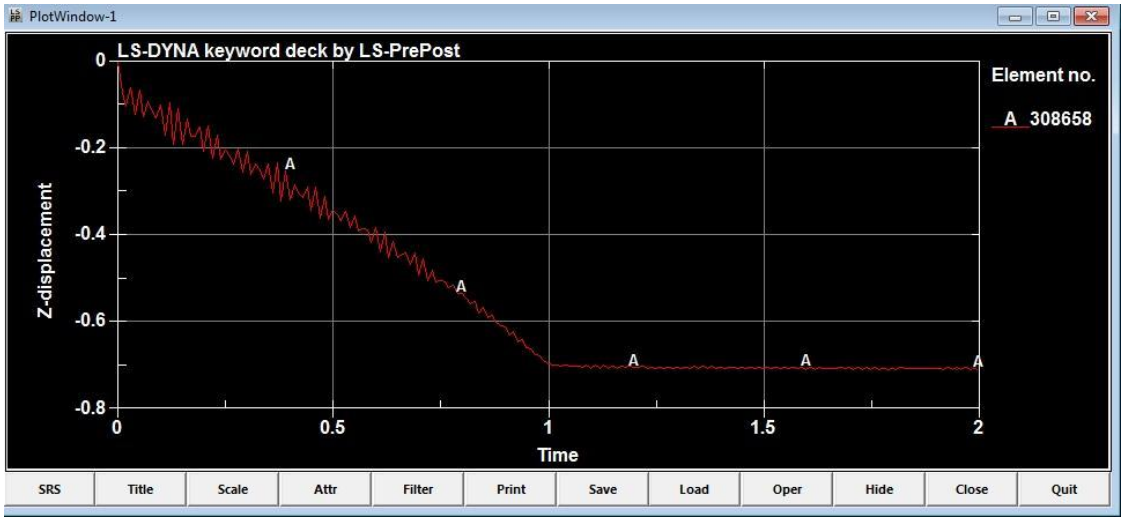

Figure 144: Maximum Deflection of the Deck Overhang – Rectangular 8 inch

6.2.4 Rectangular – 6 inch Barrier

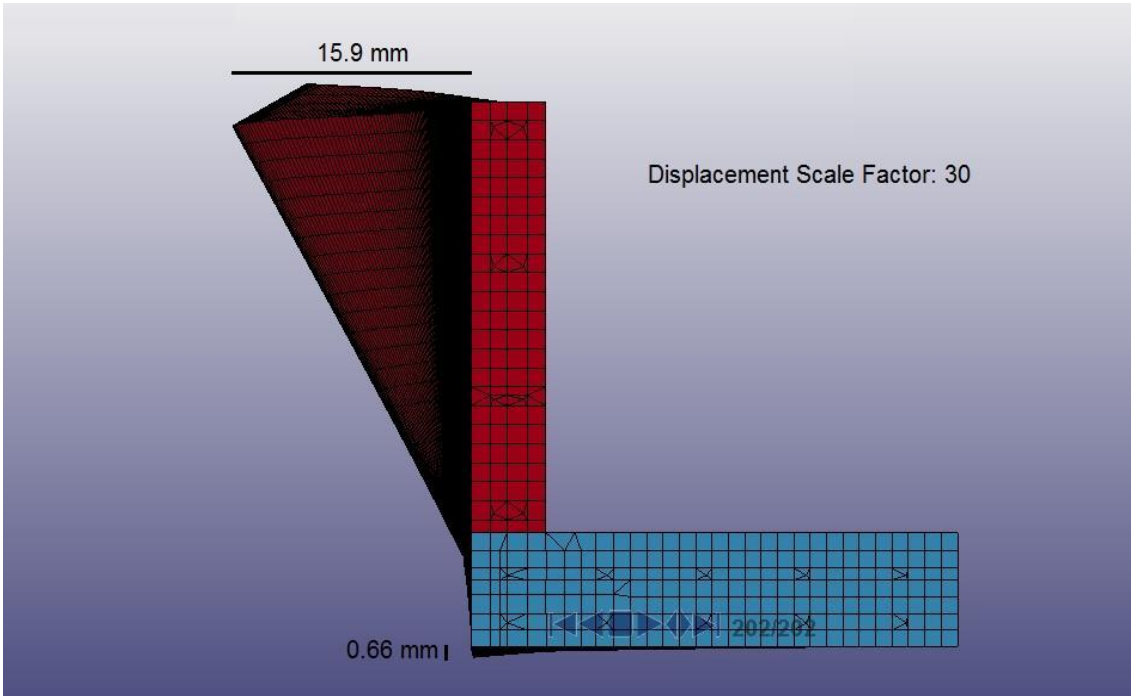

Figure 145: Maximum Deflection of Barrier and Deck Overhang – Rectangular 6 inch

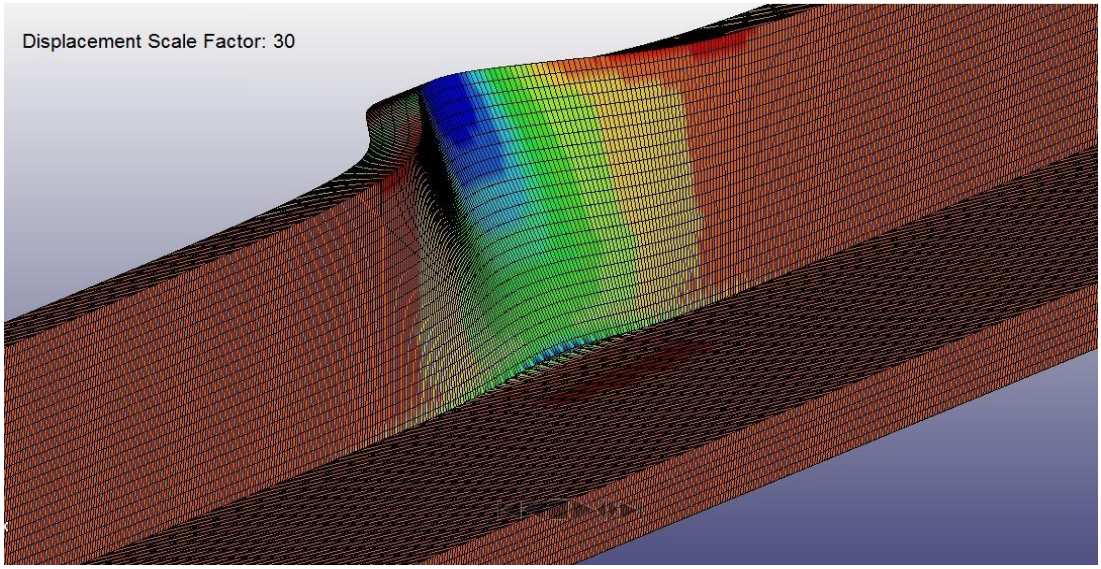

Figure 146: Maximum Deflection of Barrier and Deck Overhang – 3D model – Rectangular 6 inch

6.2.4.1 Maximum Deflection in Barrier

As seen in Figure 147 maximum deflection in the barrier was 15.9 mm or 0.63 inches.

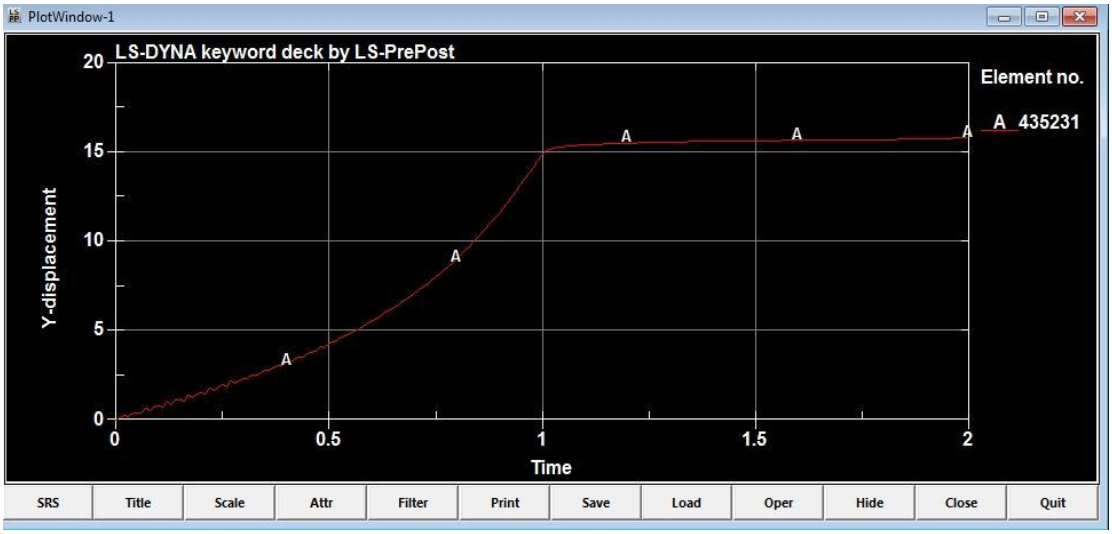

Figure 147: Maximum Deflection of the Barrier – Rectangular 6 inch

6.2.4.2 Maximum Deflection in Deck Overhang

As seen in Figure 148, maximum deflection in the deck overhang was 0.66 mm or 0.03 inches.

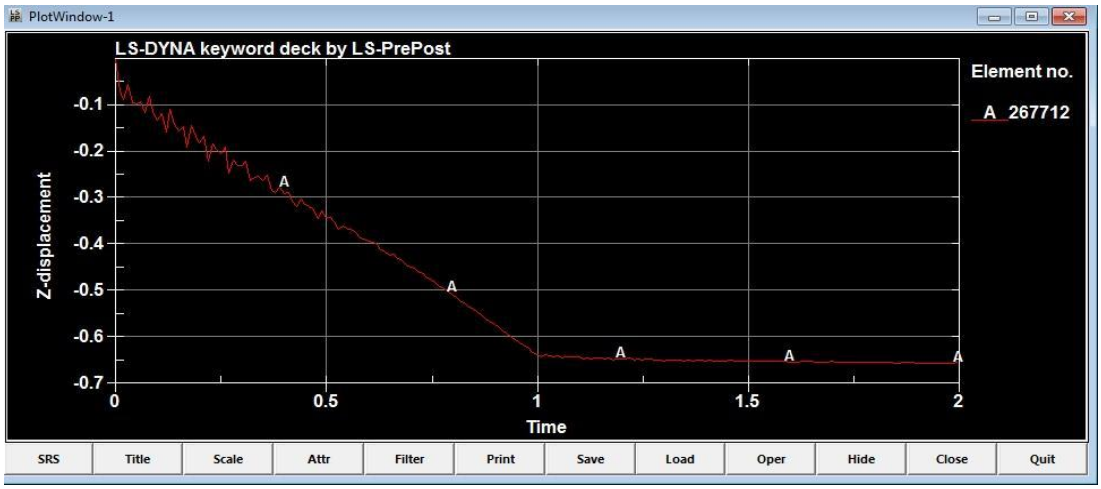

Figure 148: Maximum Deflection of the Deck Overhang – Rectangular 6 inch

6.2.5 Modified Single-Slope Barrier

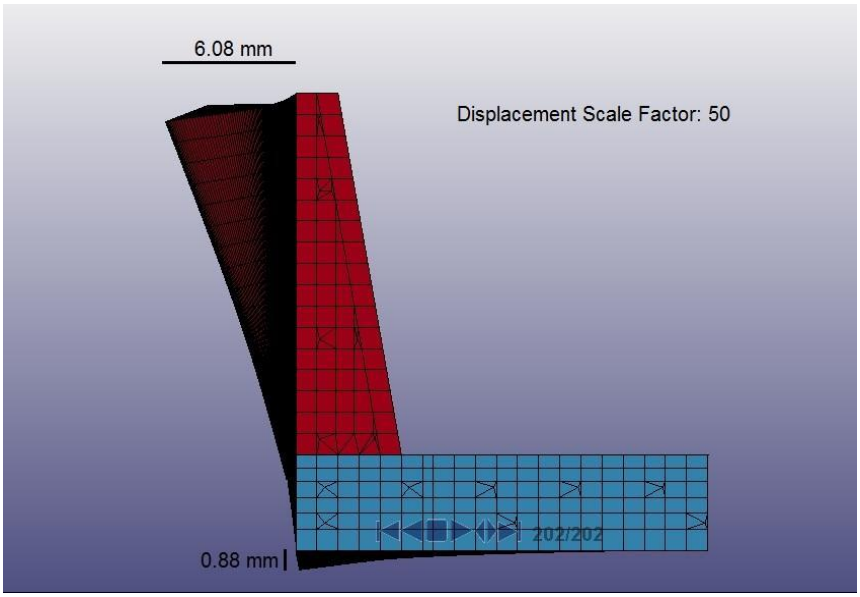

Figure 149: Maximum Deflection of Barrier and Deck Overhang – Modified Single-Slope

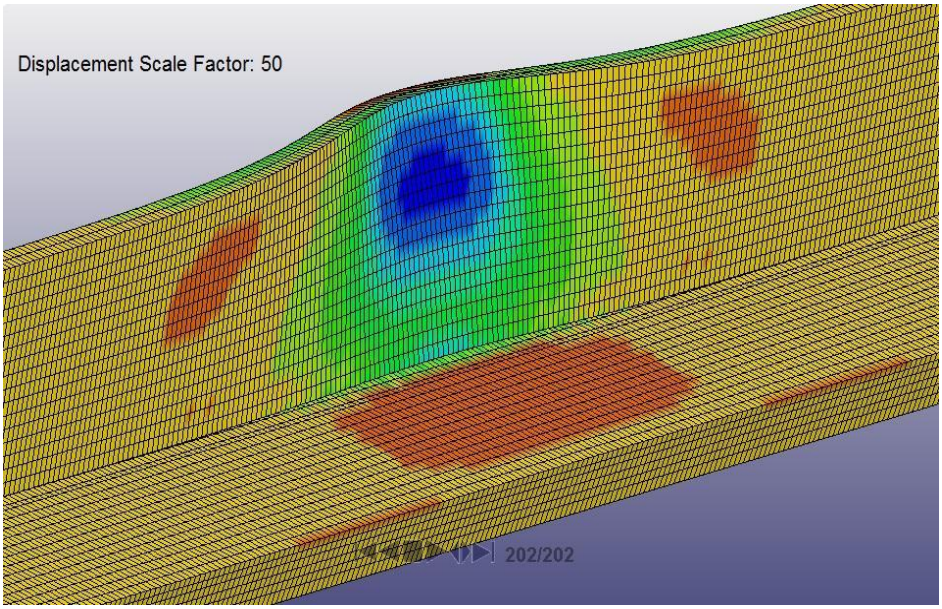

Figure 150: Maximum Deflection of Barrier and Deck Overhang – 3D model – Modified Single-Slope

6.2.5.1 Maximum Deflection in Barrier

As shown in Figure 151, the maximum deflection in the barrier was 6.08 mm or 0.24 inches

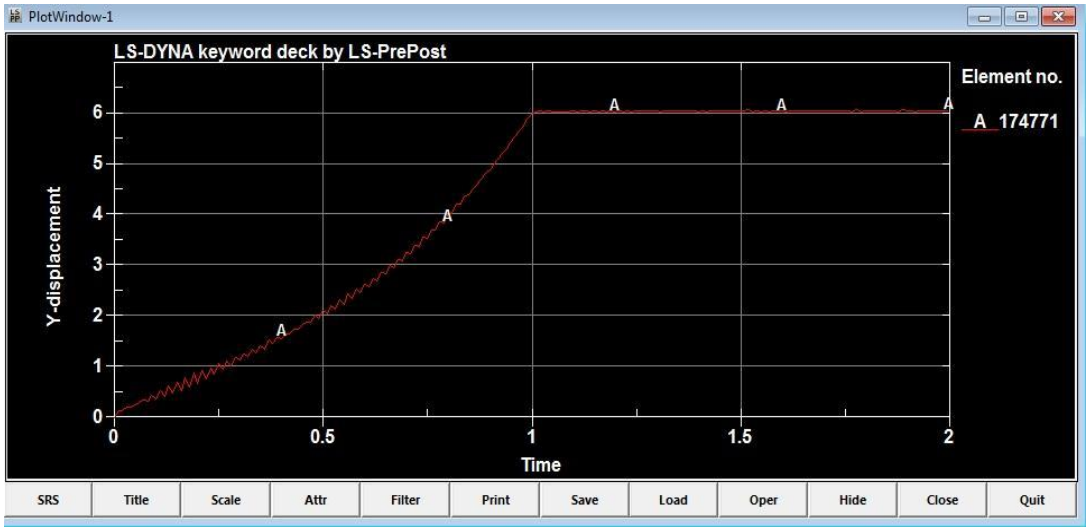

Figure 151: Maximum Deflection of the Barrier – Modified Single-Slope

6.2.5.2 Maximum Deflection in Deck Overhang

As shown in Figure 152, the maximum deflection in the deck overhang was 0.88 mm or 0.03 inches.

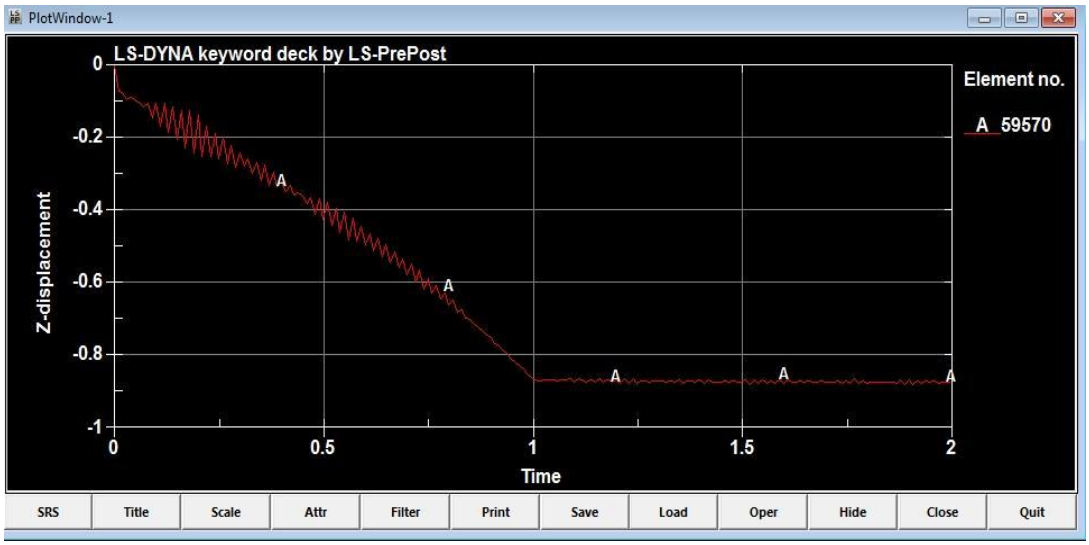

Figure 152: Maximum Deflection of the Deck Overhang – Modified Single-Slope

6.2.6 Inverted Modified Single-Slope Barrier

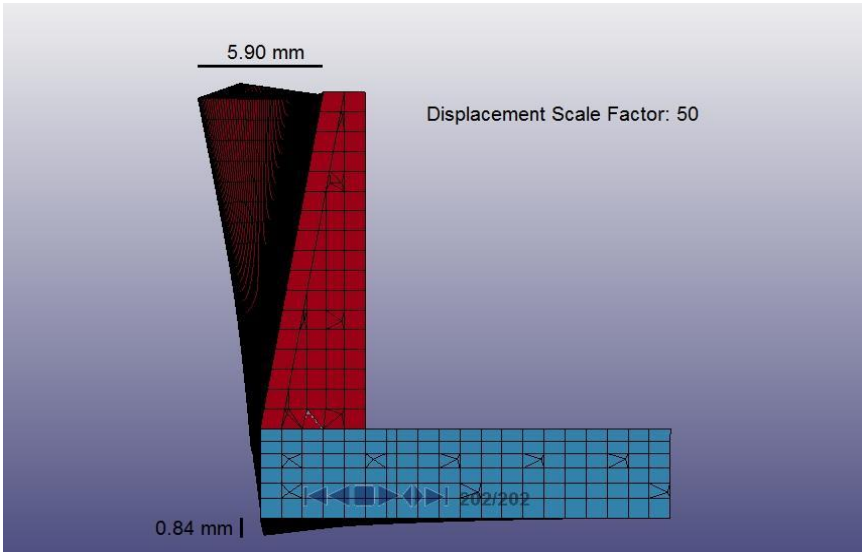

Figure 153: Maximum Deflection of Barrier and Deck Overhang – Inverted Modified Single-Slope

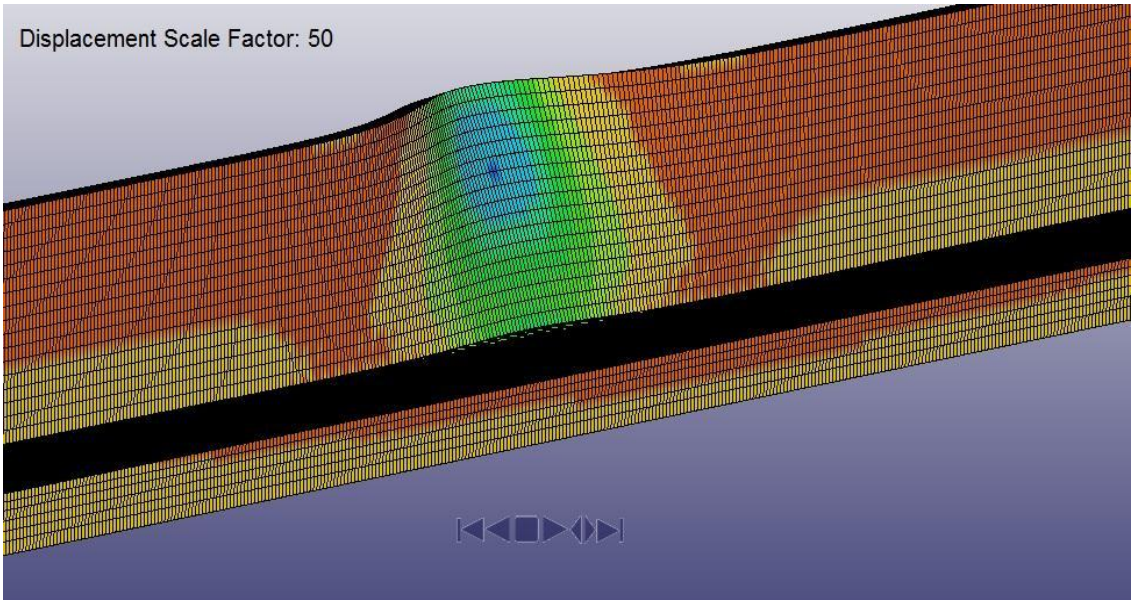

Figure 154: Maximum Deflection of Barrier and Deck Overhang 3D model – Inverted Modified Single-Slope

6.2.6.1 Maximum Deflection in Barrier

As seen in Figure 155, maximum deflection in the Barrier was 5.90 mm or 0.23 inches

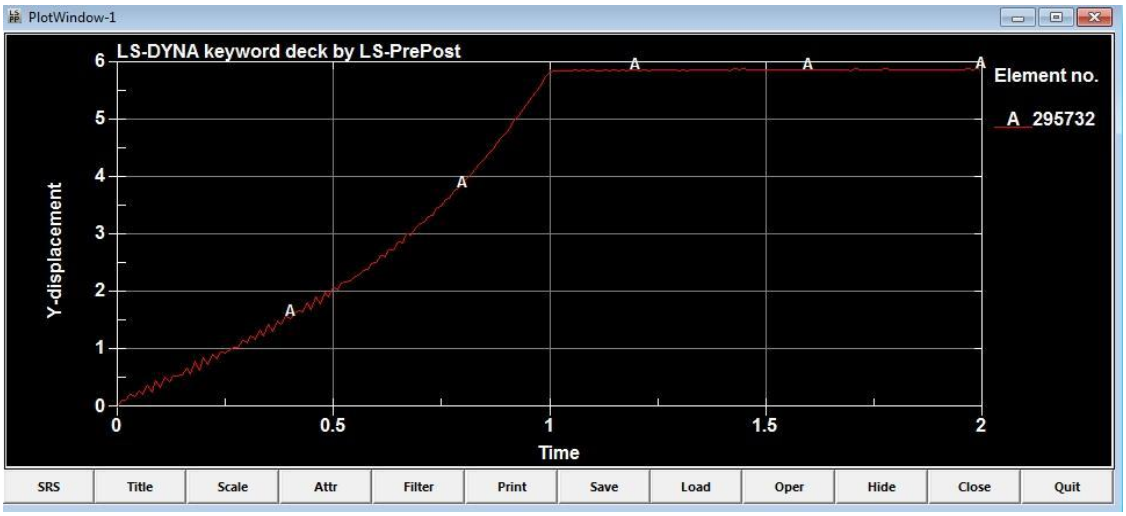

Figure 155: Maximum deflection of the Barrier – Inverted Modified Single-Slope

6.2.6.2 Maximum Deflection in Deck Overhang

As displayed in Figure 156, the maximum deflection of the deck overhang was 0.84 mm or 0.03 inches.

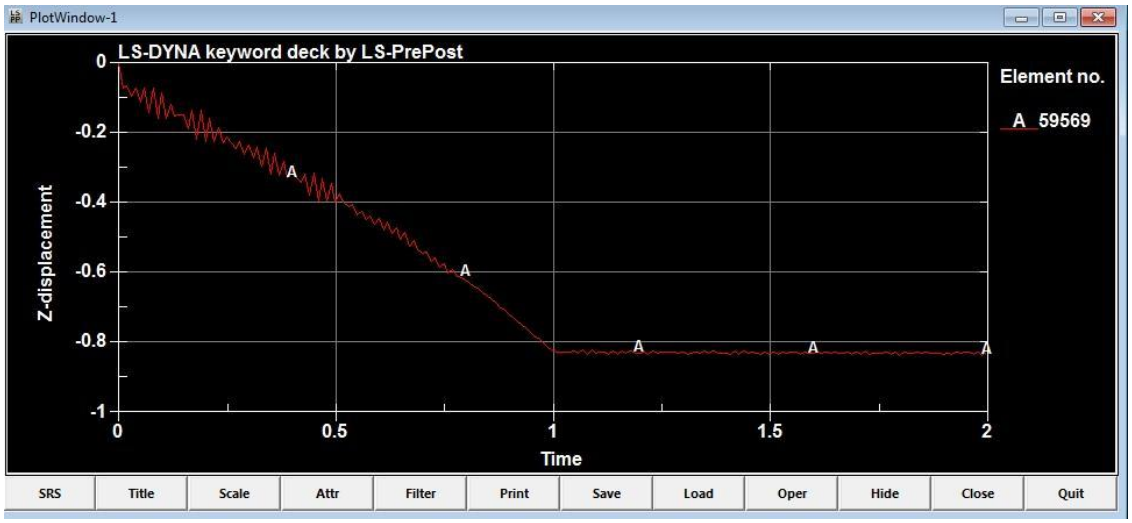

Figure 156: Maximum Deflection of the Deck Overhang – Inverted Modified Single-Slope

6.2.7 Comparison Between the Barrier Geometries – Maximum Deflection

Figures 157 and 158 display a graphical representation of the maximum deflection between the barriers and deck overhang in all six proposed geometries.

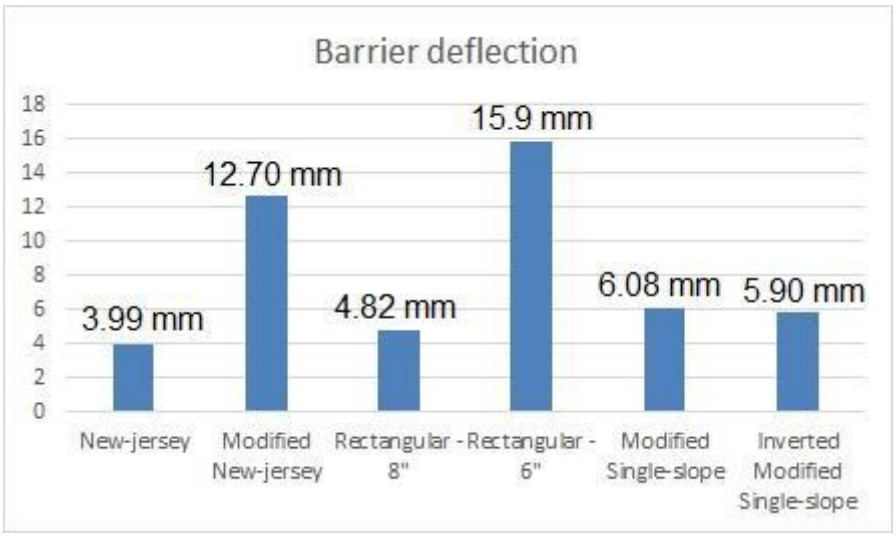

Figure 157: Maximum Deflections in Barriers

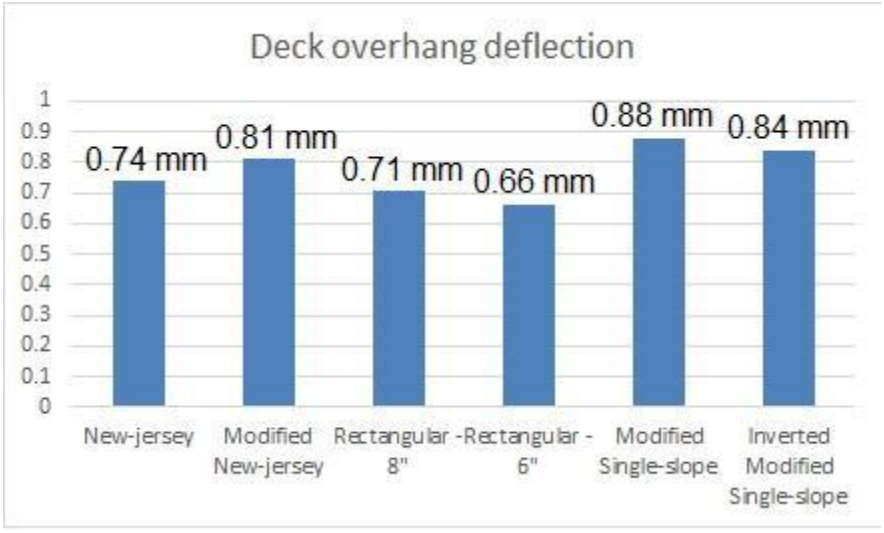

Figure 158: Maximum Deflections in Deck Overhangs

As displayed above, the maximum deflection appeared in the rectangular – 6 inch geometry due to the shape's minimum thickness when compared with all other geometries. While the minimum deflection happened in the New Jersey geometry, that does appear as a logical test result as it has the maximum thickness among all other geometries.

7 DYNAMIC LOAD SIMULATION

This chapter compares all of the proposed barrier geometries by simulating them in LS-DYNA using single unit truck that represents Test Level 4. As mentioned earlier, the truck was a Ford provided by "National Crash Analysis Center (NCAC)" in 2008. Based on AASHTO's test level specifications, the angle impact between the barrier and the side of the truck is 15 degrees, and the truck moves at a speed of 50 mph (80 kmph). This comparison not only shows the maximum deflection and stress in the barrier and deck overhang, but also the deformation of the truck and the roll-over after impact.

This chapter also compared the internal energy absorbed by each portion and compared them with each other. As mentioned in Chapter 1, the results of this comparison are fairly close to the reality test. Hence, it is possible to determine the best candidate from this comparison.

To obtain useful and usable results from all simulations, the truck's exact location had to be consistent for all simulations before barrier impact. Figure 159 represented the exact location of the truck before impacting the barriers.

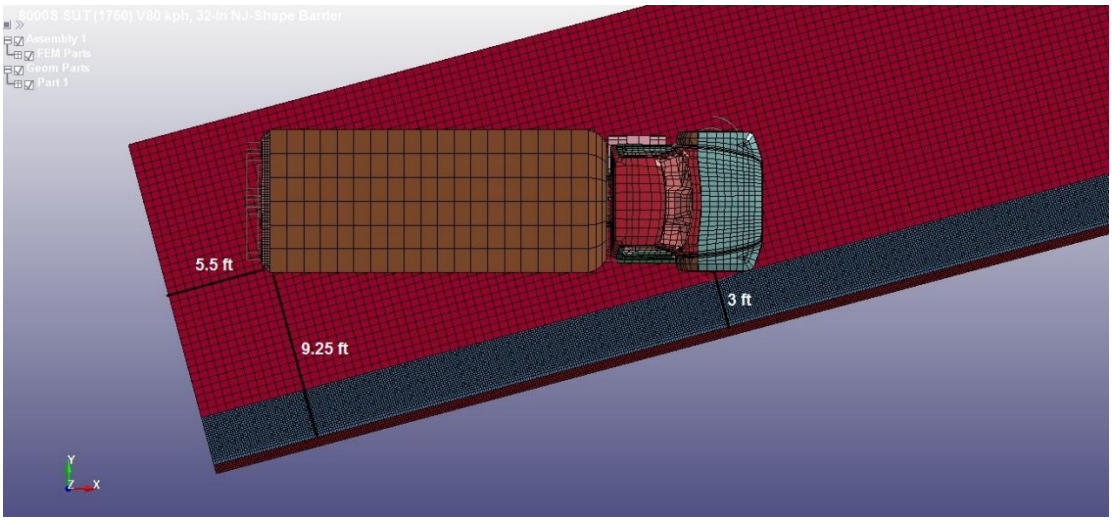

Figure 159: Truck's location – Top View

The research measured the maximum amount of stress, deflection, and energy absorption in the concrete block resulting from the first and second impact of the crash. Figure 160 and 161 indicated the point of first impact and second impact clearly. The moment of impact for different geometries might be different. This can happen because the geometry of the barrier varies in thickness which may cause the truck to impact at different times.

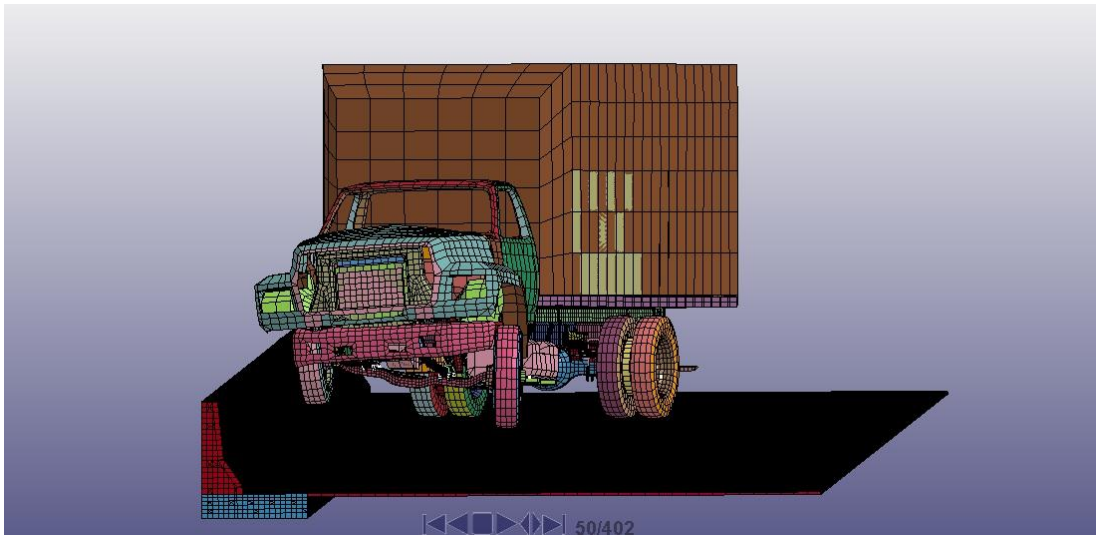

Figure 160: First impact – front of the truck

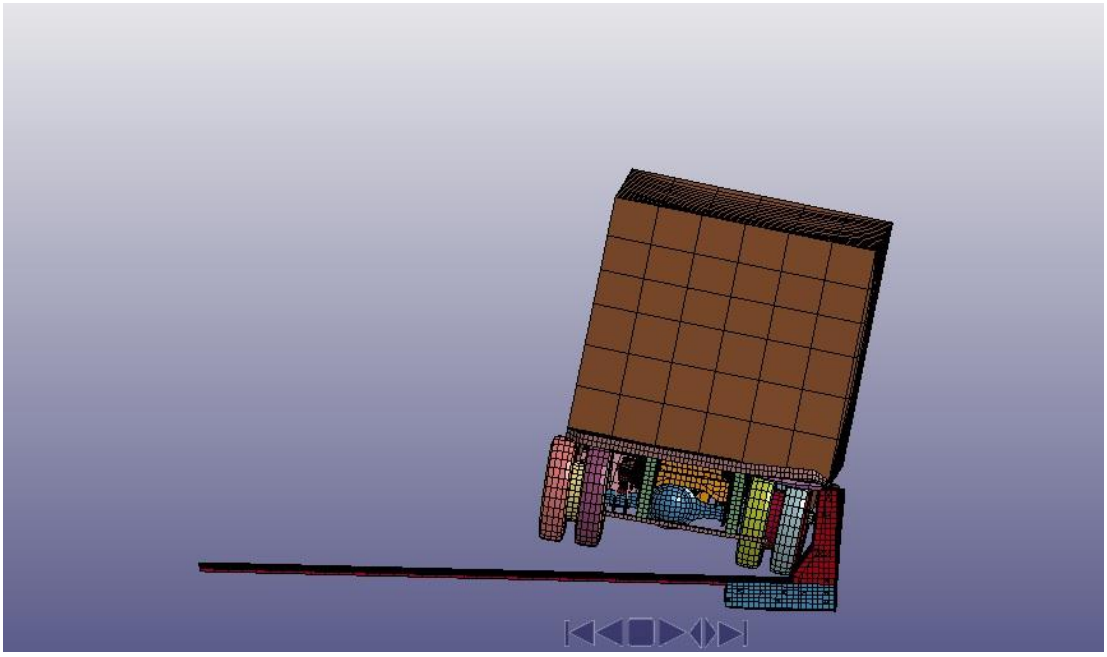

Figure 161: Second impact – back of the truck

7.1 First impact

7.1.1 Maximum Stress

Maximum stress in dynamic simulation is different compared with static simulation. Since the truck has some sharp edges, by impacting the barrier it might penetrate the concrete causing damage to the barrier. In addition, the nature of dynamic load is different than static load. Hence, this research does not look for the stress in all single concrete elements that might be damaged by the truck's sharp edges. This research is seeking the point of maximum stress where maximum deflection occurred. The maximum deflection happened at the first and second impact of the truck as has been shown previously.

7.1.1.1 New Jersey barrier

Figure 162 represents the truck before it starts to hit the barrier.

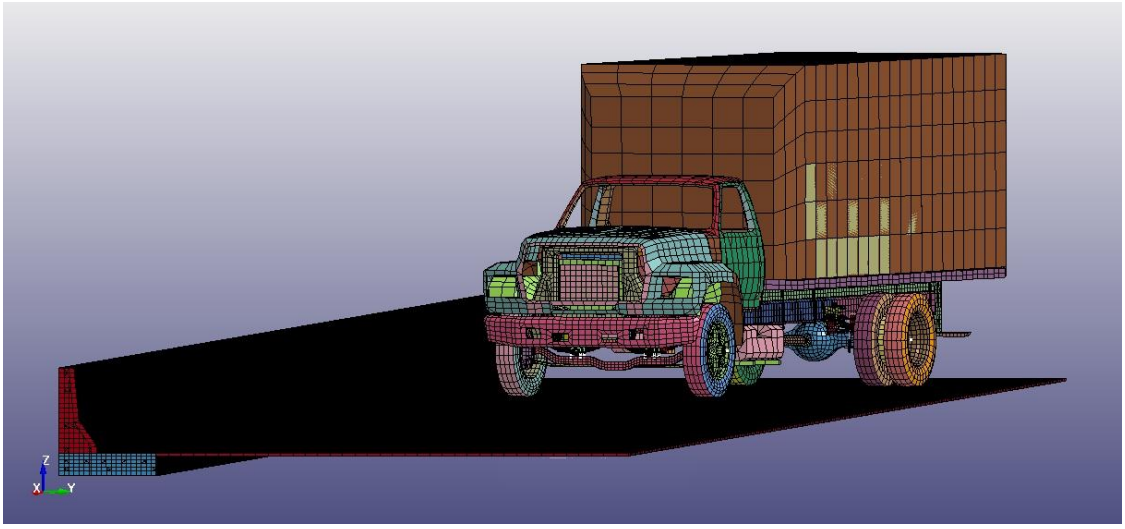

Figure 162: New Jersey Geometry Model with NCAC single unit truck

7.1.1.1.1 Maximum Stress in the Barrier

7.1.1.1.1.1 Compression Side

Maximum stress in compression side of the barrier, caused by front bumper of the truck, has been shown in the Figure 163, Maximum compression at first impact of the barrier was 20.72 Mpa.

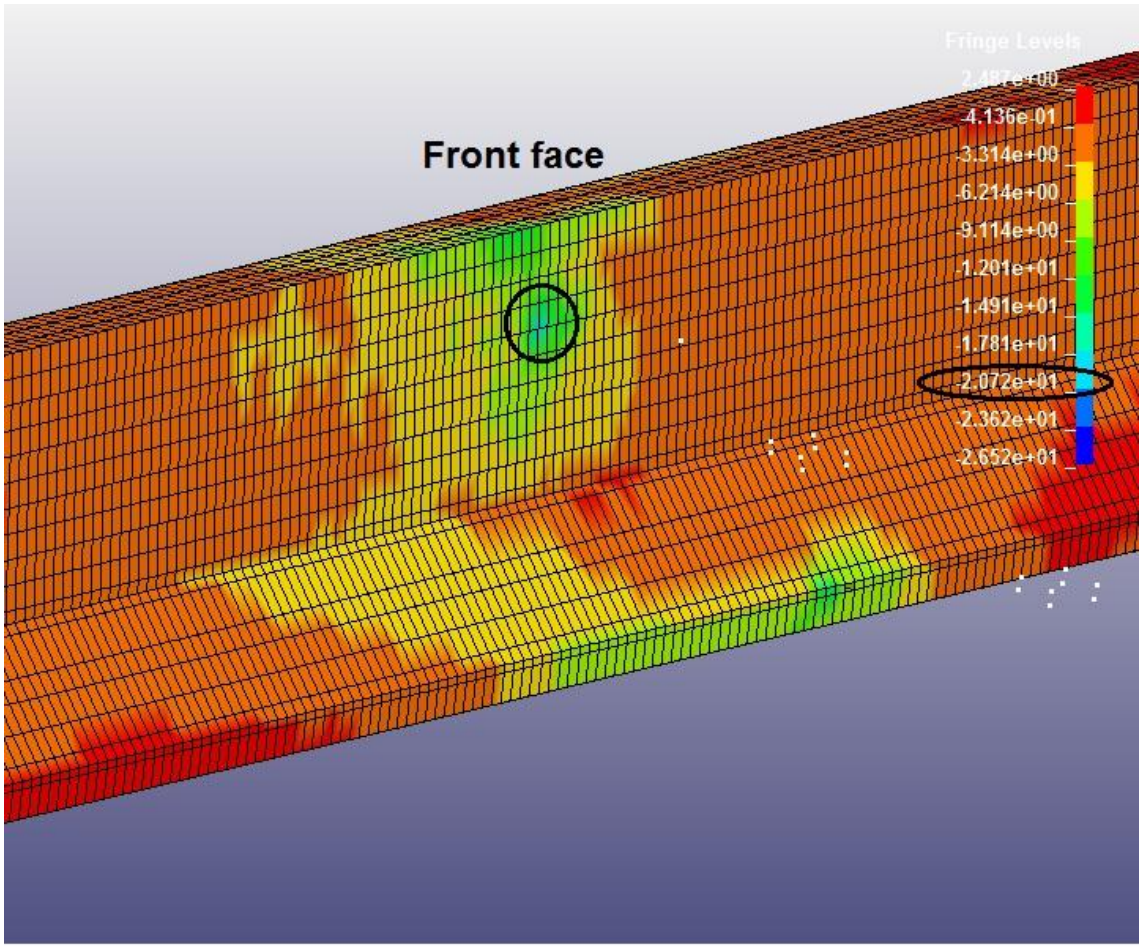

Figure 163: First impact compression effects on New Jersery barrier – 3d model – front face

7.1.1.1.1.2 Tension side

The maximum stress in tension side of the barrier is illustrated in Figure 164, the maximum tensile stress at the moment of first impact was 2.8 Mpa.

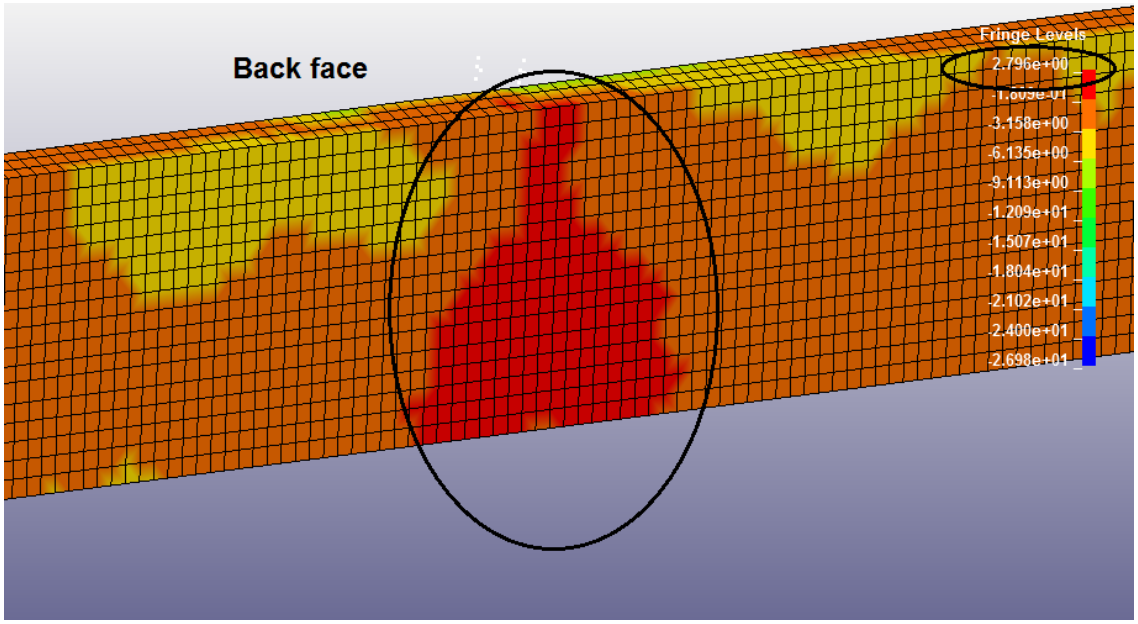

Figure 164: First impact tension effect on New Jersey barrier – 3d model – back face

7.1.1.1.2 Maximum stress in the deck overhang

7.1.1.1.2.1 Compression side

Maximum stress in compression side of the deck overhang is shown in Figure 165, Maximum compression at first impact at the barrier was 9.31 Mpa.

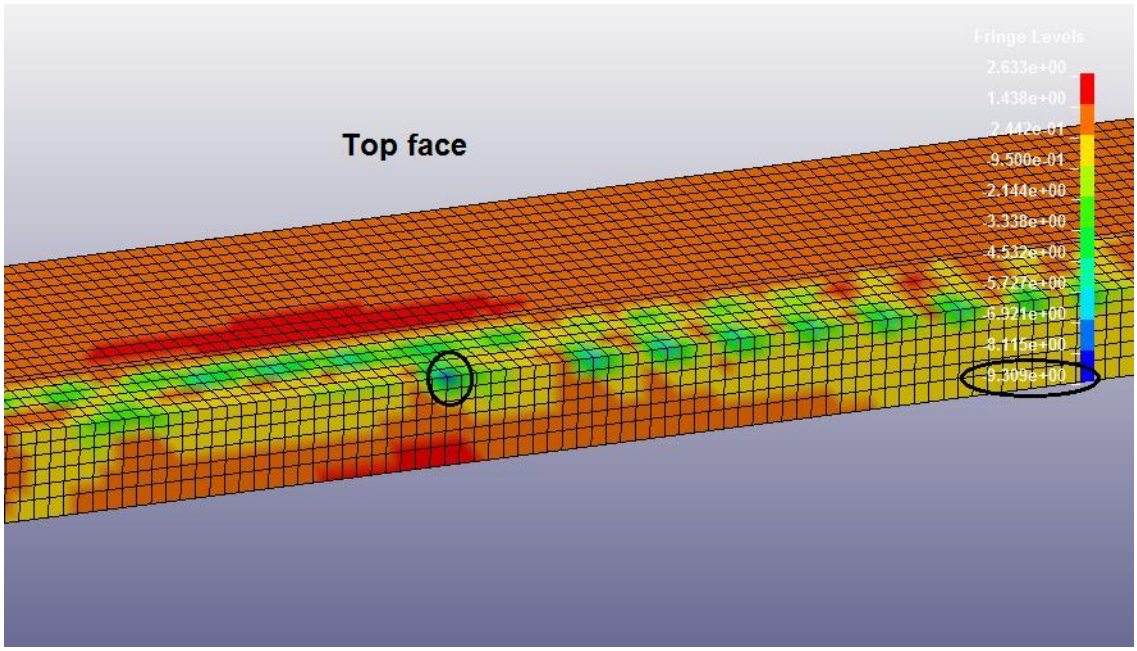

Figure 165: New Jersey barrier first impact in compression side of the deck overhang – top face

7.1.1.1.2.2 Tension Side

The maximum stress in tension side of the deck overhang is illustrated in Figure 166. The maximum tensile stress at the moment of first impact was 2.63 Mpa.

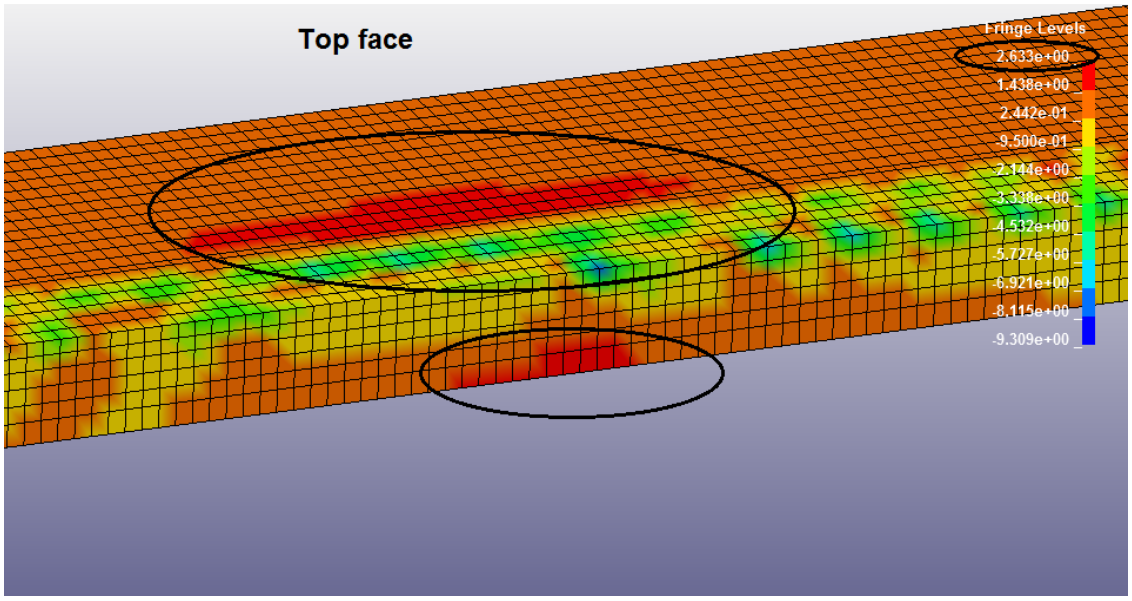

Figure 166: New Jersey barrier first impact in tension side of the deck overhang – bottom face

7.1.1.1.3 Maximum Stress in Reinforcement bars

7.1.1.1.3.1 Tension side

As seen in Figure 167, maximum tensile reinforcement bars are #4 vertical reinforcement bars. Reinforcement bars are front hairpin dowels that connect the barrier to the deck overhang. Hence, the tensile stress is:

4.93e4 N / 129 mm^2 = 382.17 MPa = 55.43ksi

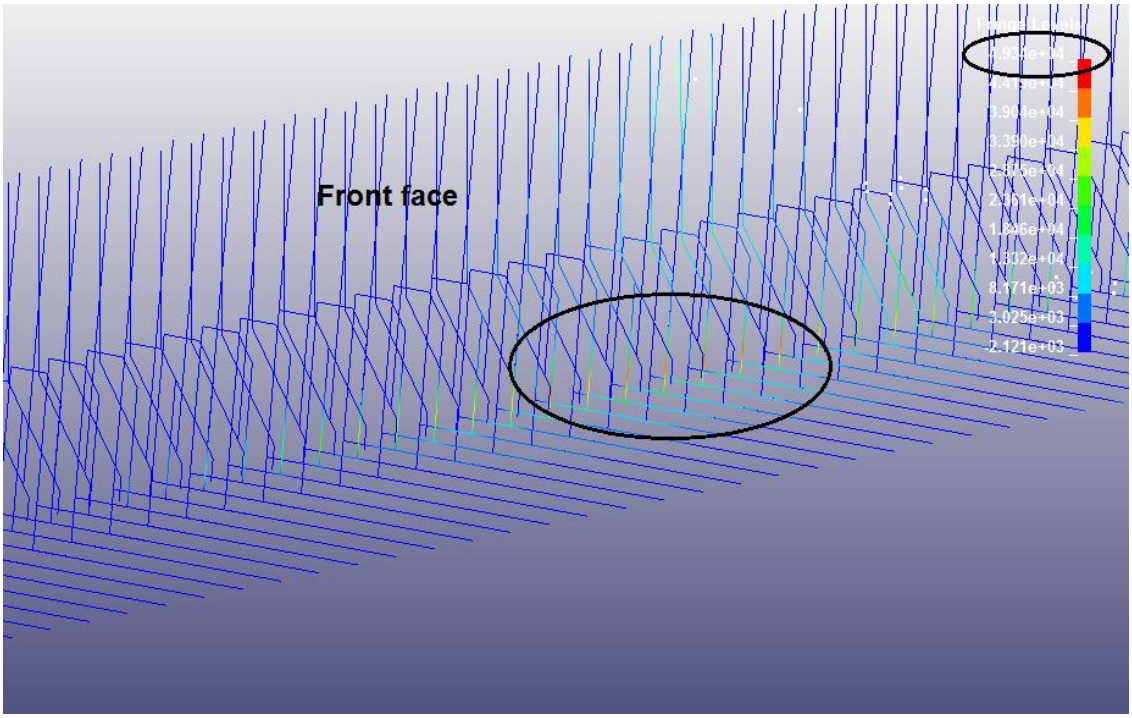

Figure 167: Axial force of the reinforcement bar in tension side at the moment of first impact – New Jersey barrier – front face

7.1.1.1.3.2 Compression side

As seen in Figure 168, maximum compression reinforcement bars are #3 horizontal reinforcement bars at the bottom face of the barrier. Hence, the compressive stress is:

3.67e3 N / 71 mm^2 = 51.69 MPa = 7.50ksi

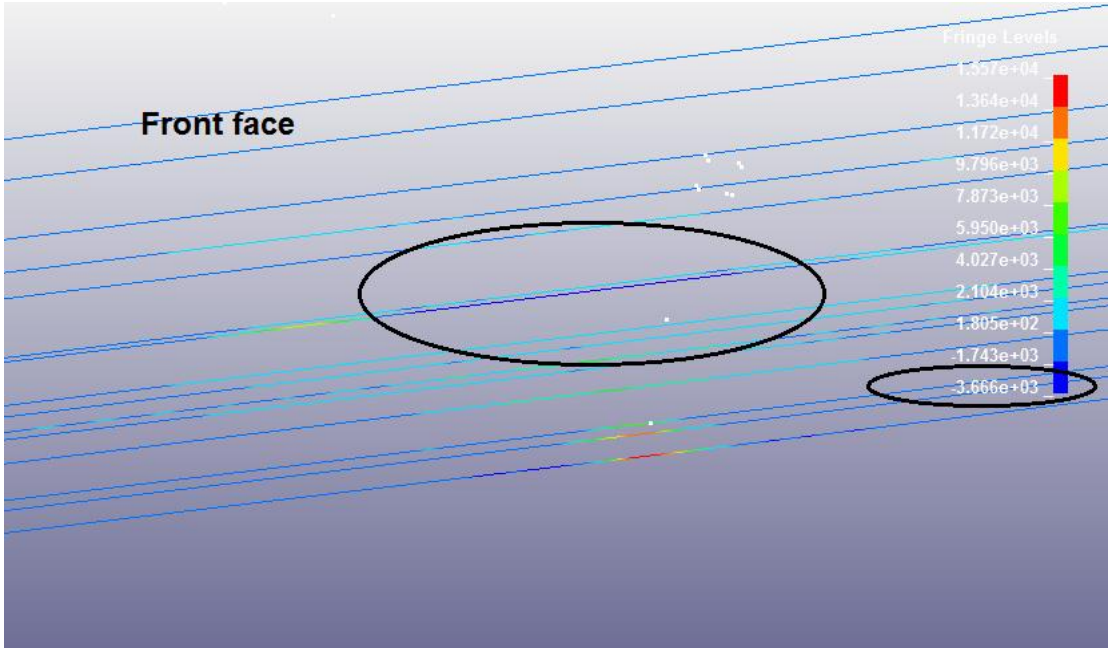

Figure 168: Axial force of the reinforcement bar in compression side at the moment of first impact – New Jersey barrier – front face

7.1.1.2 Modified New-Jersey Barrier

Figure 169 represents the truck before it starts to hit the barrier.

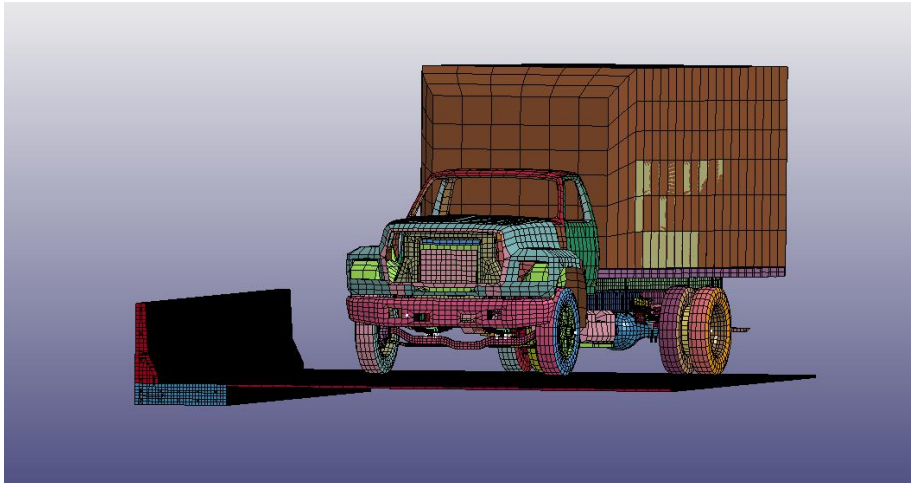

Figure 169: Modified New Jersey geometry model with NCAC single unit truck

7.1.1.2.1 Maximum Stress in the Barrier

7.1.1.2.1.1 Compression Side

Figure 170 shows the maximum stress in compression side of the barrier caused by front bumper of the truck. Maximum compression at first impact at the barrier was 20.22 Mpa.

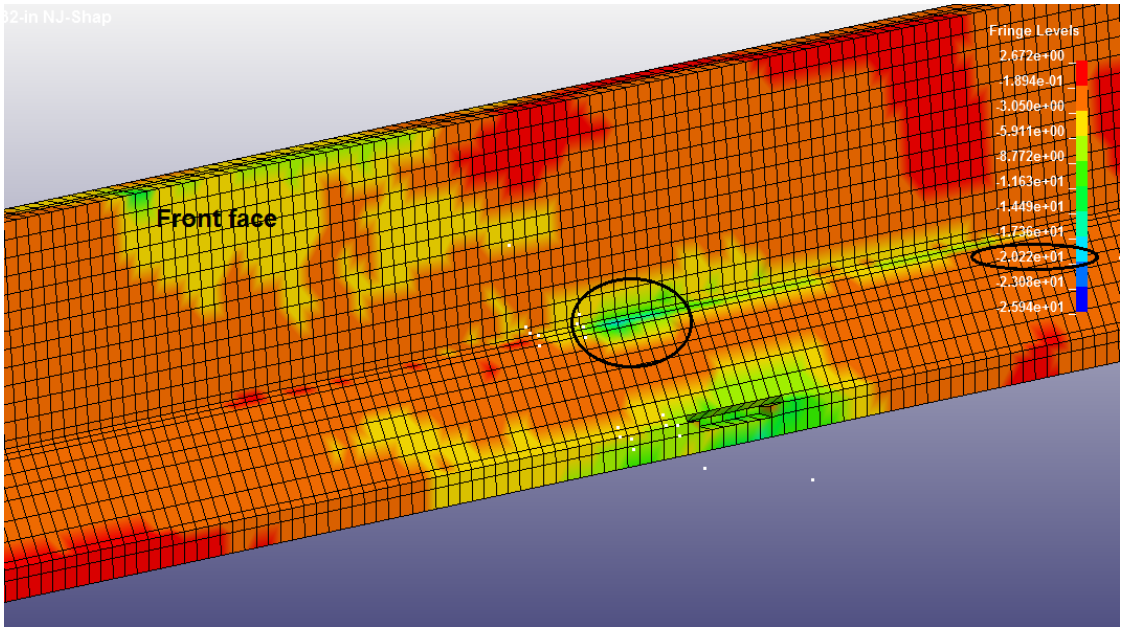

Figure 170: First impact compression effects on modified New Jersey barrier – 3d model – front face

7.1.1.2.1.2 Tension side

The maximum stress in tension side of the barrier is illustrated in Figure 171. The maximum tensile stress at the moment of first impact was 2.67Mpa.

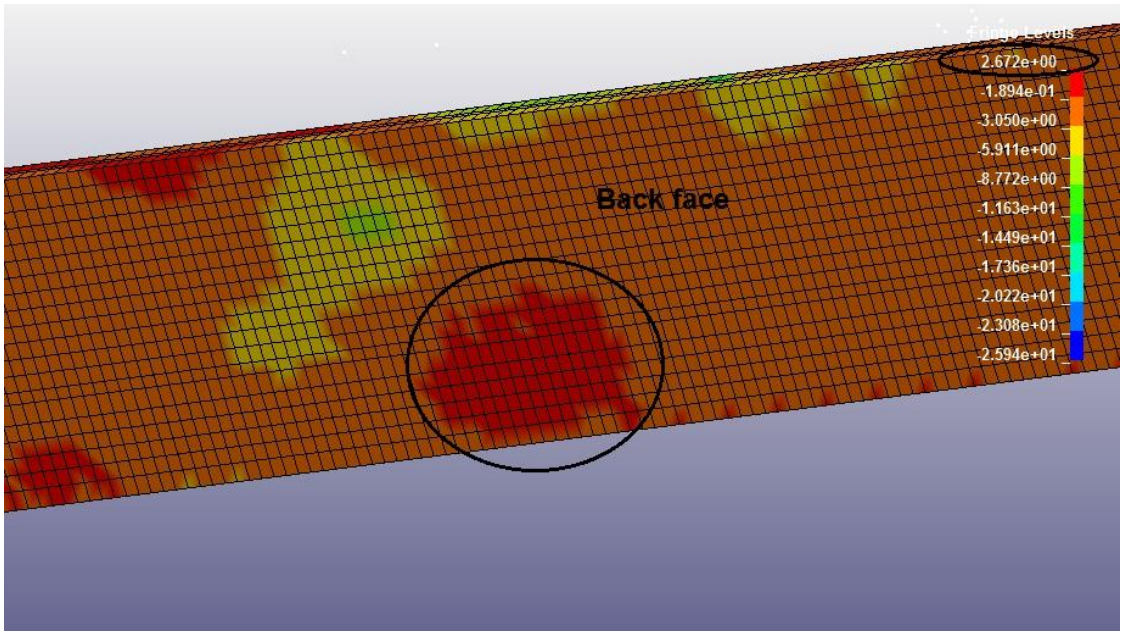

Figure 171: First impact tension effect on modified New Jersey barrier – 3d model – back face

7.1.1.2.2 Maximum stress in the deck overhang

7.1.1.2.2.1 Compression Side

Maximum stress in compression side of the deck overhang is illustrated in Figure 172 Maximum compression at first impact at the barrier was 5.30 Mpa.

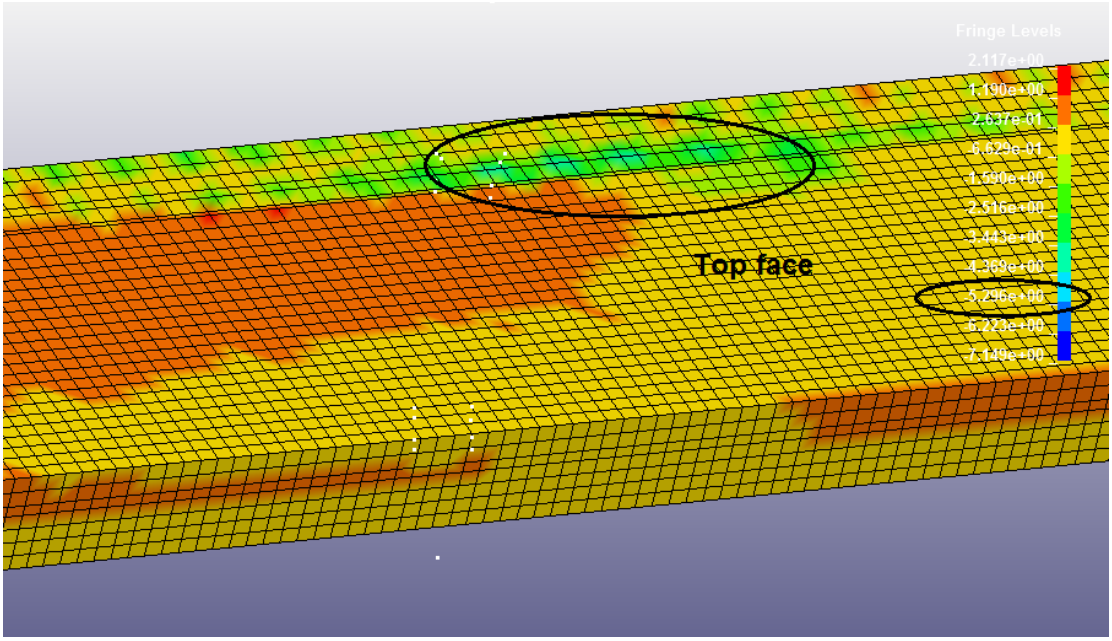

Figure 172: Modified New Jersey barrier first impact in compression side of the deck overhang – top face

7.1.1.2.2.2 Tension Side

The maximum stress in tension side of the deck overhang is illustrated in Figure 173. The maximum tensile stress at the moment of first impact was 2.12 Mpa.

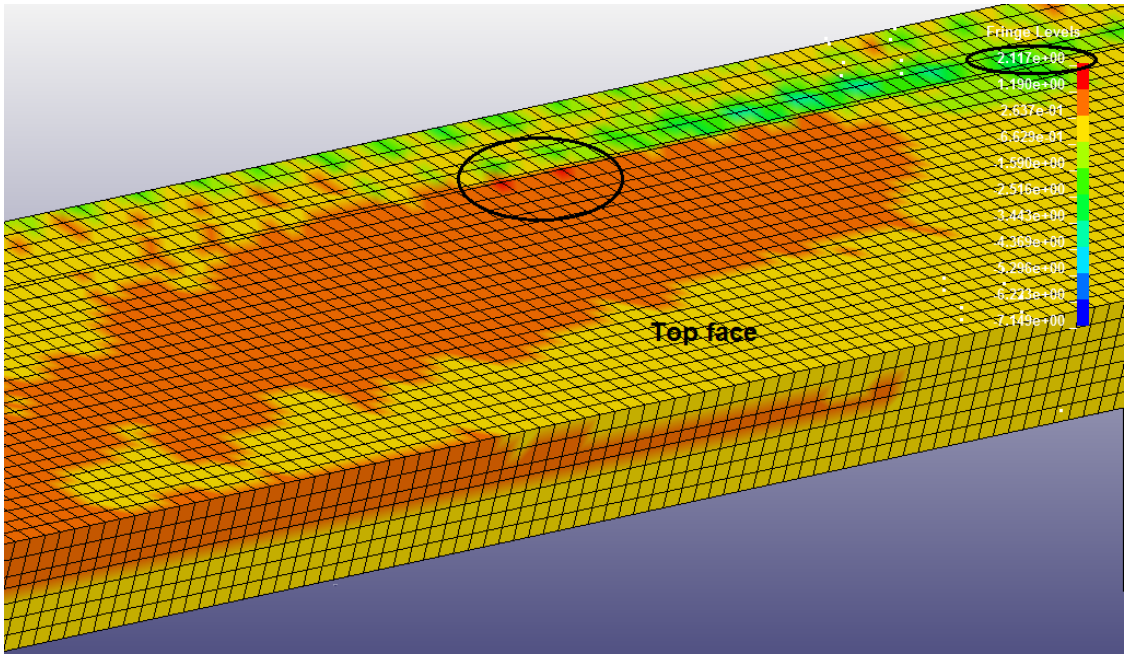

Figure 173: Modified New Jersey barrier - first impact in tension side of the deck overhang – top face

7.1.1.2.3 Maximum Stress in Reinforcement bars

7.1.1.2.3.1 Tension Side

As seen in Figure 174, the maximum tensile stress on reinforcement bars are on the #4 vertical reinforcement bars, located in the middle of the barrier and at the front face. Hence, the tensile stress is:

4.34e4 N / 129 mm^2 = 336.43 MPa = 48.80ksi

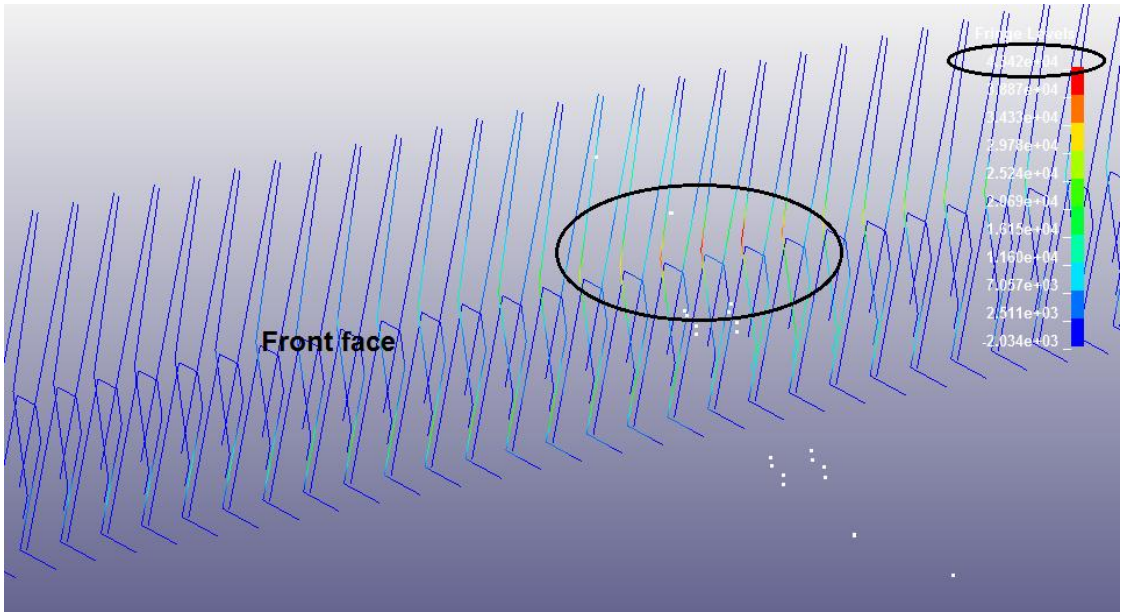

Figure 174: Axial force of the reinforcement bar in tension side at the moment of first impact – Modified New Jersey barrier – front face

7.1.1.2.3.2 Compression Side

As seen in Figure 175, maximum compression on reinforcement bars is on the #3 horizontal reinforcement bars at the bottom and top face of the barrier. Hence, the compressive stress is:

2.52e3 N / 71 mm^2 = 35.49 MPa = 5.15 ksi

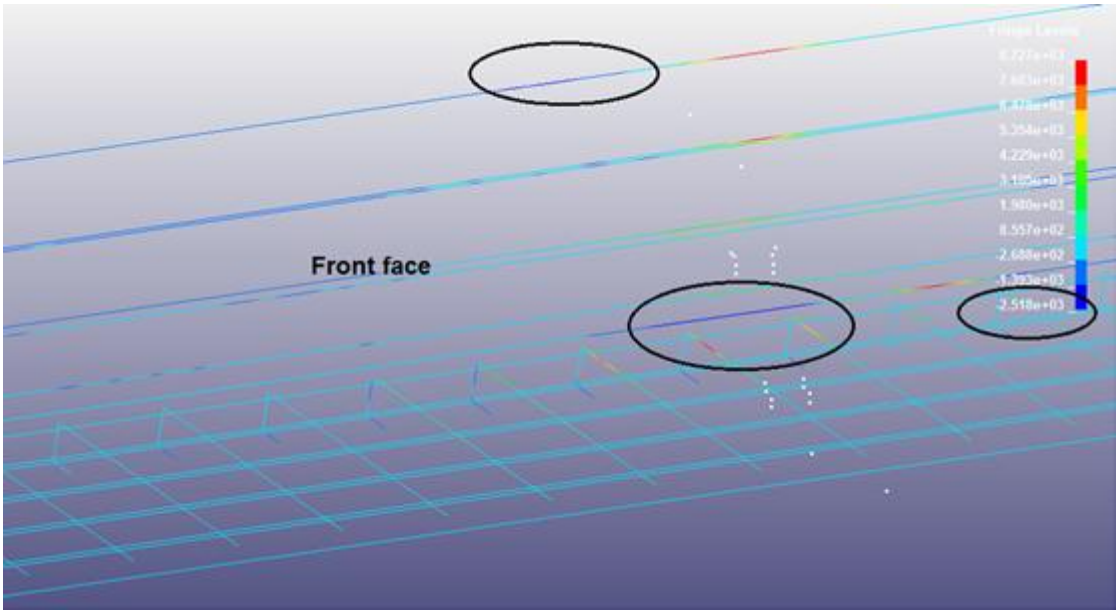

Figure 175: Axial force of the reinforcement bar in compression side at the moment of first impact – Modified New Jersey barrier – front face

7.1.1.3 Rectangular – 8 Inch Barrier

Figure 176 represents the truck before it starts to hit the barrier.

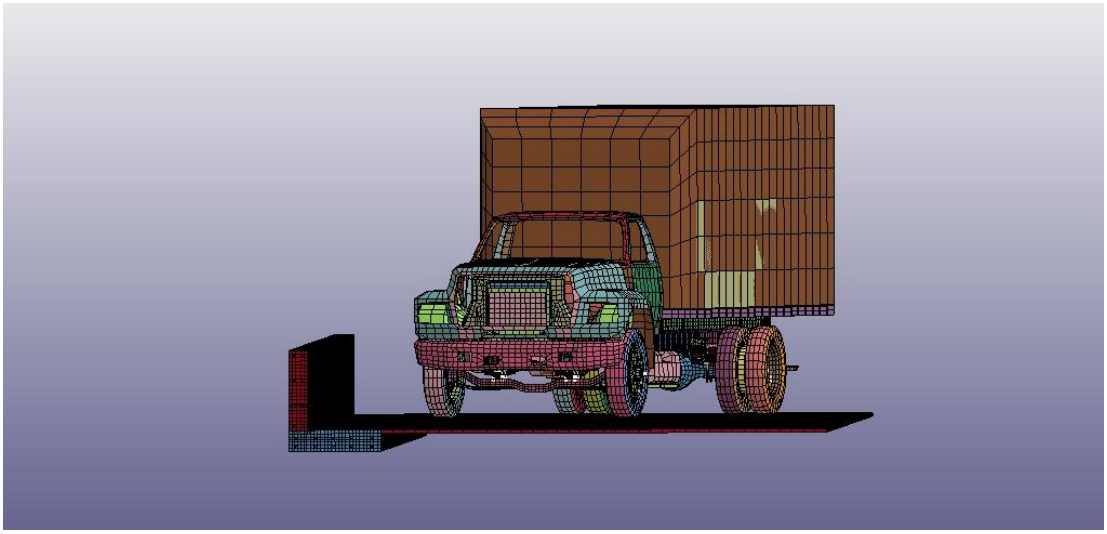

Figure 176: Rectangular – 8 inch geometry model with NCAC single unit truck

7.1.1.3.1 Maximum Stress in the Barrier

7.1.1.3.1.1 Compression Side

Maximum stress in compression side of the barrier, caused by front bumper of the truck, is shown in Figure 177, maximum compression at first impact at the barrier was 31.05 Mpa.

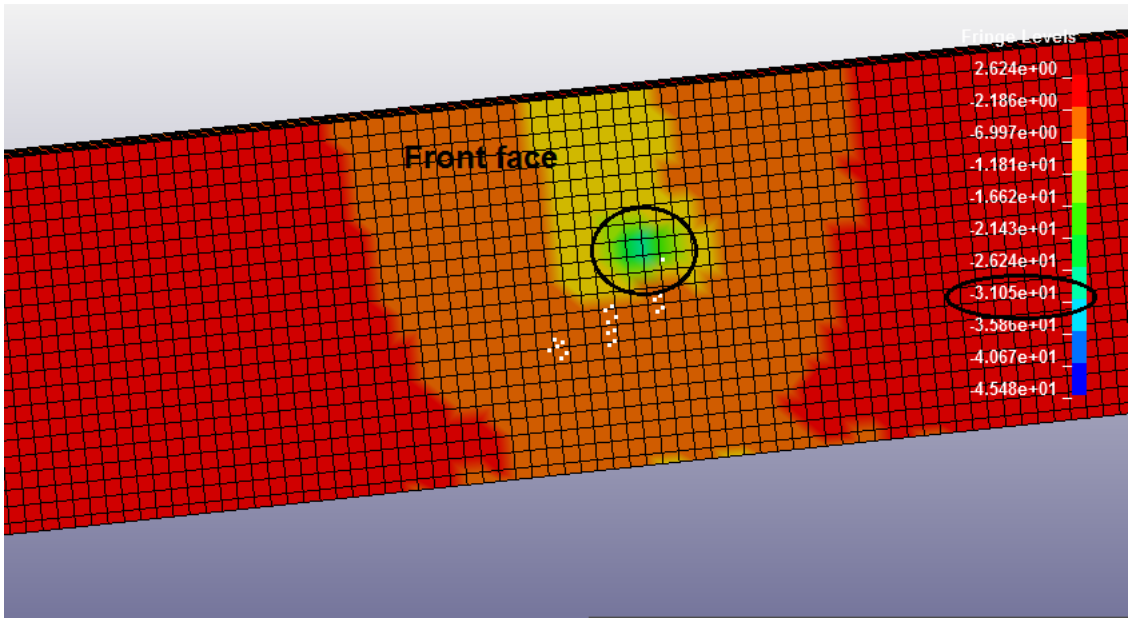

Figure 177: First impact compression effects on Rectangular – 8 inch Barrier – 3d model – front face

7.1.1.3.1.2 Tension Side

The maximum stress in tension side of the barrier is shown in the Figure 178. The maximum tensile stress at the moment of first impact was 2.62 Mpa.

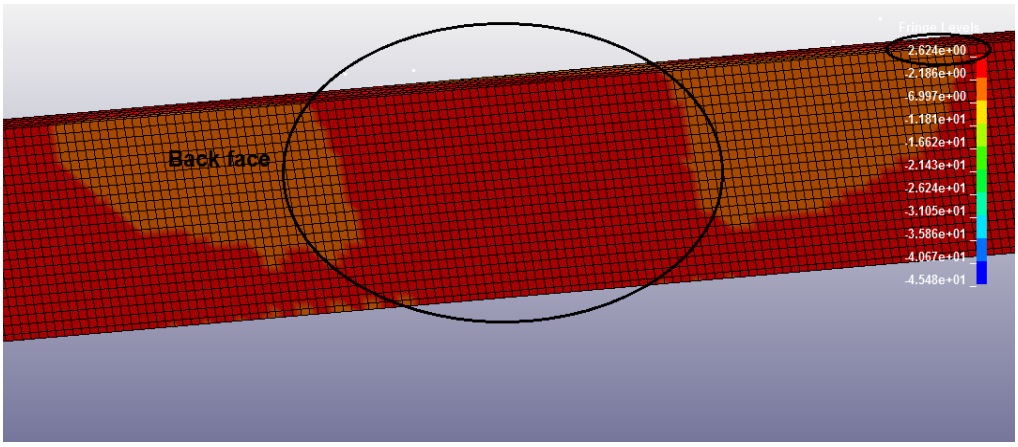

Figure 178: First impact tension effect on Rectangular – 8 inch barrier – 3d model – back face

7.1.1.3.2 Maximum Stress in the Deck Overhang

7.1.1.3.2.1 Compression Side

Maximum stress in compression side of the deck overhang is shown in Figure ….

Maximum compression at first impact at the barrier was 9.31 Mpa.

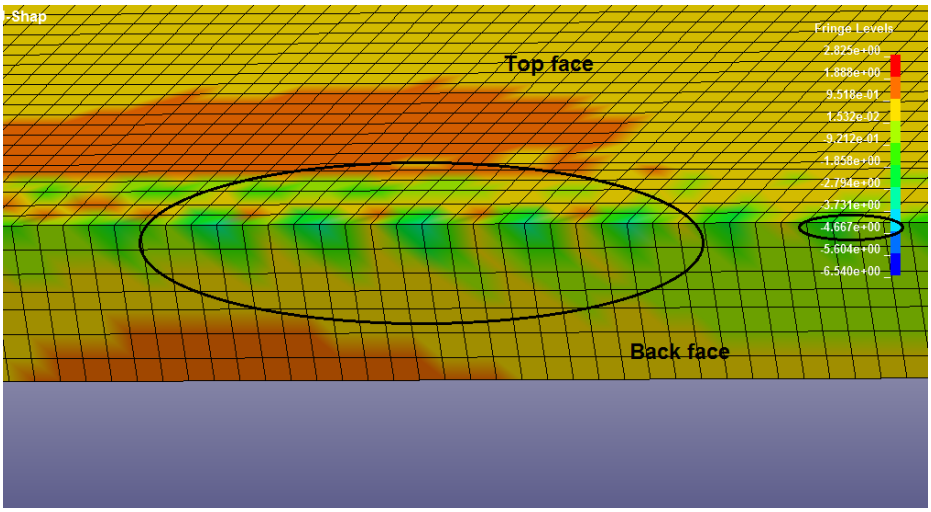

Figure 179: Rectangular – 8 inch barrier first impact in compression side of the deck overhang – top and back face

7.1.1.3.2.2 Tension Side

The maximum stress in tension side of the deck overhang is shown in Figure 180. The maximum tensile stress at the moment of first impact was 1.89 Mpa.

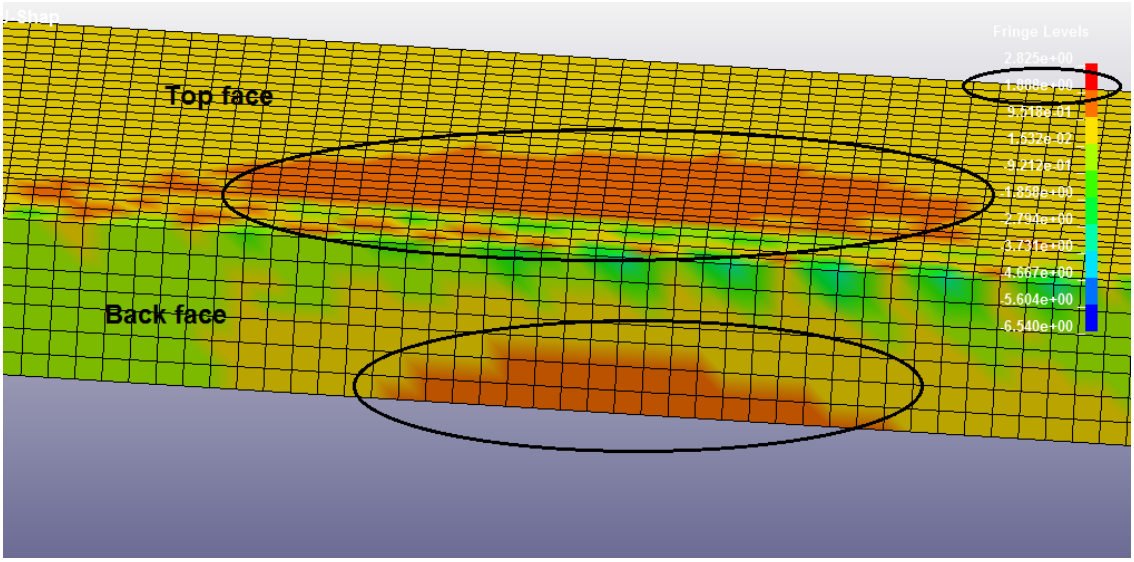

Figure 180: Rectangular – 8 inch barrier first impact in tension side of the deck overhang – top and back face

7.1.1.3.3 Maximum Stress in Reinforcement bars

7.1.1.3.3.1 Tension Side

Reinforcement bars are front hairpin dowels that connect barrier to deck overhang. As seen in Figure 181, maximum tensile reinforcement bars are #4 vertical reinforcement bars. Hence, the tensile stress is:

3.64e4 N / 129 mm^2 = 282.17 MPa = 40.93 ksi

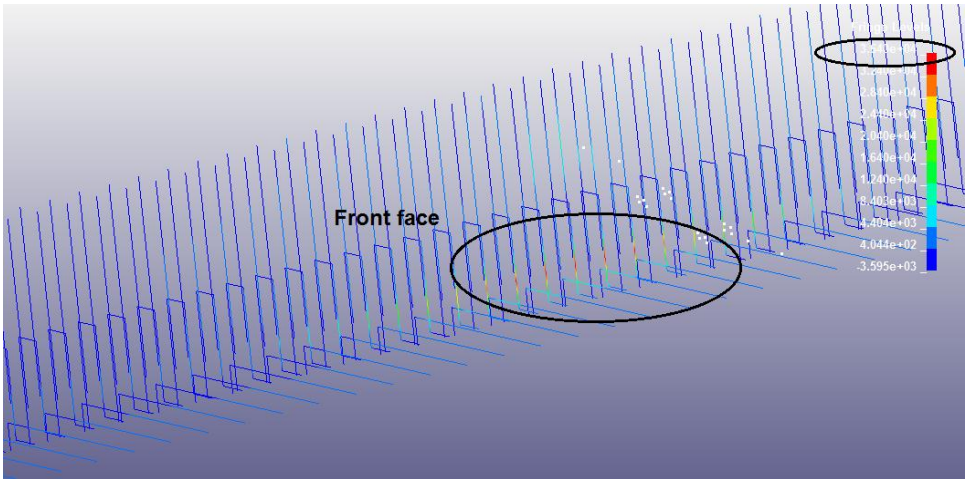

Figure 181: Axial force of the reinforcement bar in tension side at the moment of first impact: Rectangular – 8 inch – front face

7.1.1.3.3.2 Compression Side

As seen in Figure 182, maximum compression reinforcement bars are #3 horizontal reinforcement bars located at the middle and top face of the barrier. Hence, the compressive stress is:

3.79e3 N / 71 mm^2 = 53.38 MPa = 7.74ksi

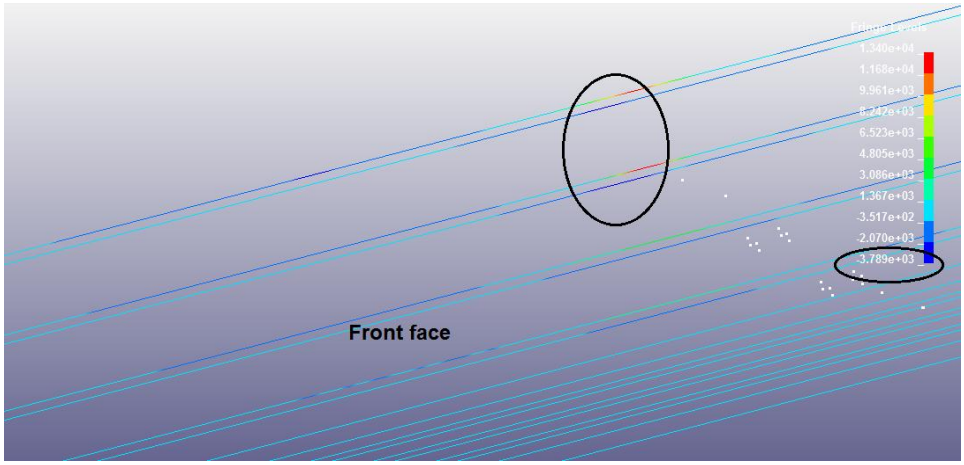

Figure 182: Axial force of the reinforcement bar in compression side at the moment of first impact: Rectangular – 8 inch – front face

7.1.1.4 Rectangular – 6 inch Barrier

Figure 183 represents the truck before it starts to hit the barrier.

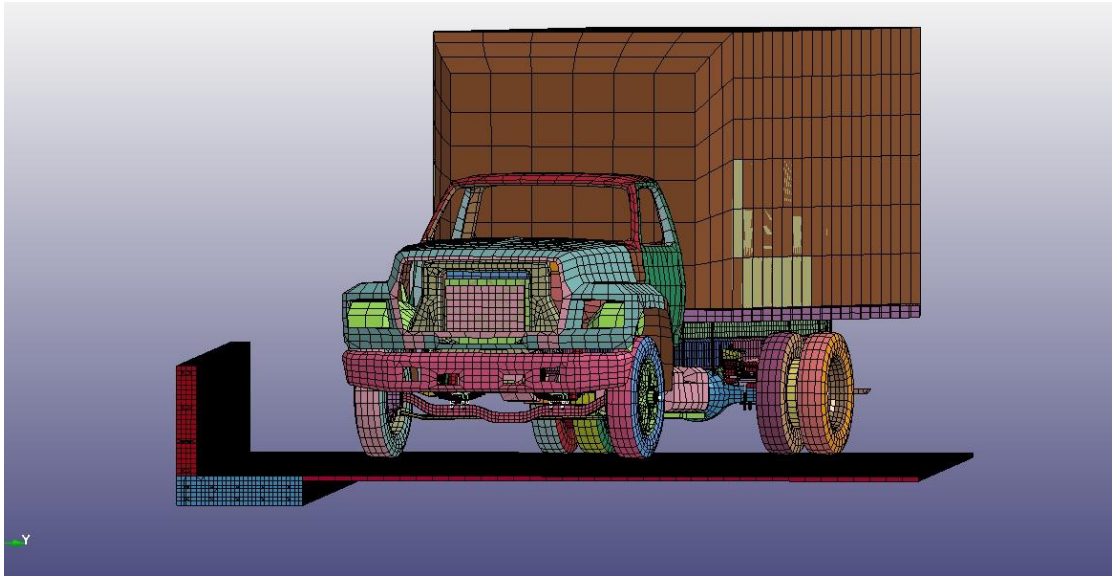

Figure 183: Rectangular – 6 inch geometry model with NCAC single unit truck

7.1.1.4.1 Maximum Stress in the Barrier

7.1.1.4.1.1 Compression Side

The maximum stress in compression side of the barrier is caused by the front bumper of the truck as shown in Figure 184, maximum compression at first impact on the barrier was 27.84 Mpa.

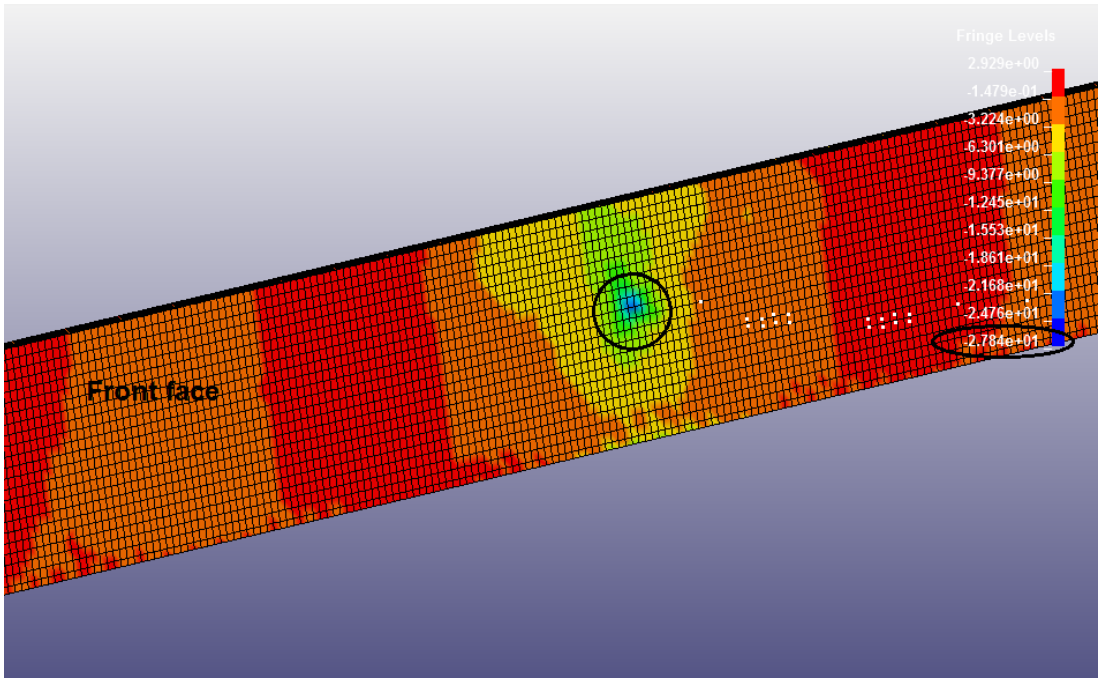

Figure 184: First impact compression effects on Rectangular – 6 inch barrier – 3d model – front face

7.1.1.4.1.2 Tension Side

The maximum stress in the tension side of the barrier is shown in the Figure 185.

The maximum tensile stress at the moment of first impact was 2.8 Mpa.

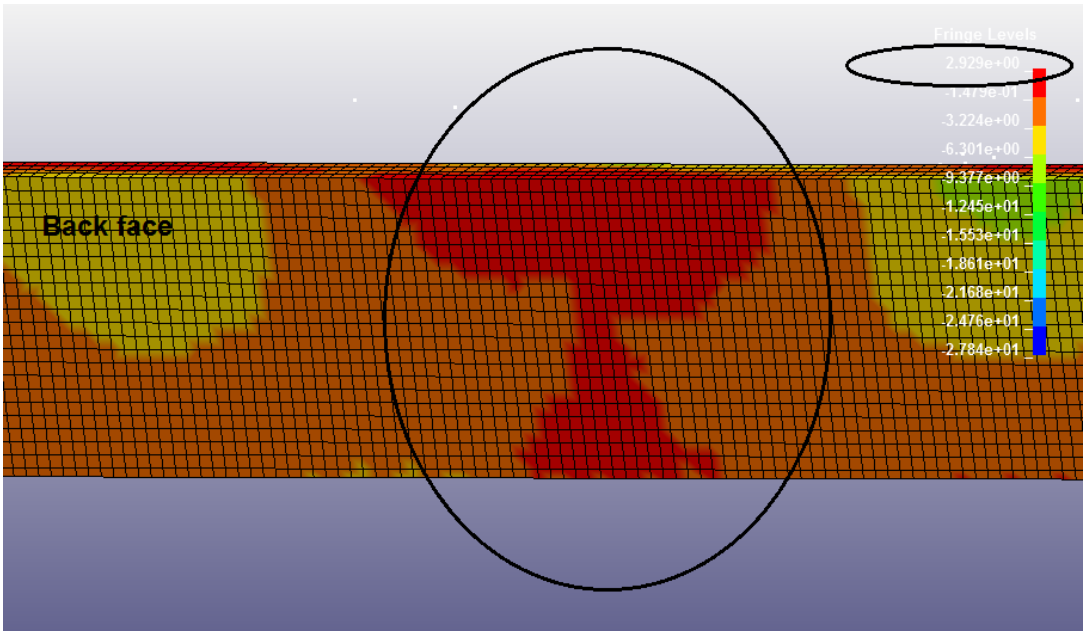

Figure 185: First impact tension effect on Rectangular – 6 inch barrier – 3d model – back face

7.1.1.4.2 Maximum Stress in the Deck Overhang

7.1.1.4.2.1 Compression Side

The maximum stress in compression side of the deck overhang is shown in Figure 186. Maximum compression at first impact on the barrier was 7.18 Mpa.

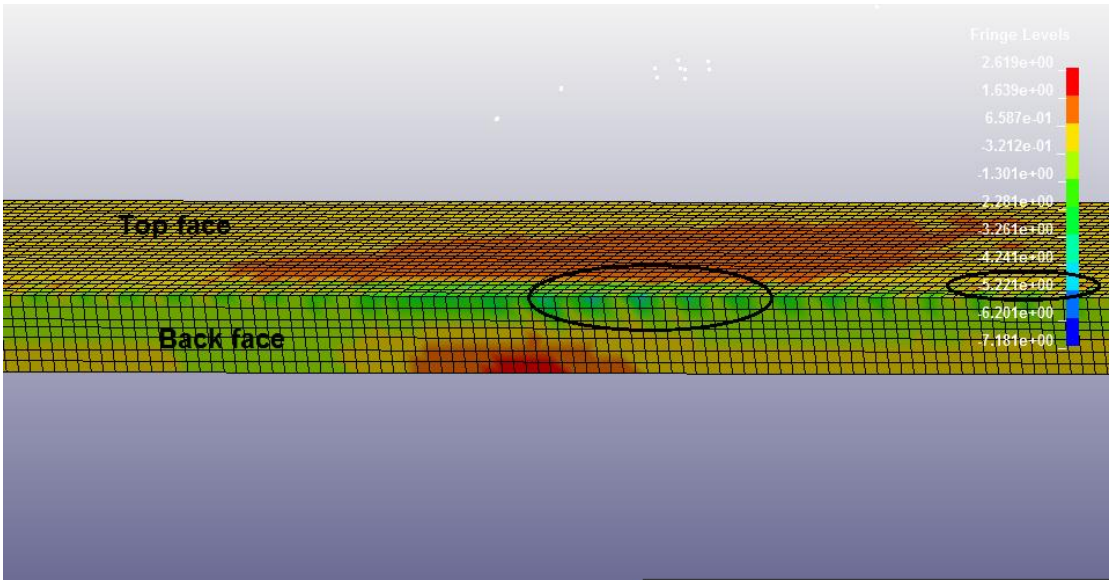

Figure 186: Rectangular – 6 inch Barrier first impact in compression side of the deck overhang – top and back face

7.1.1.4.2.2 Tension Side

The maximum stress on tension side of the deck overhang is shown in Figure 187.

The maximum tensile stress at the moment of first impact was 2.62 Mpa.

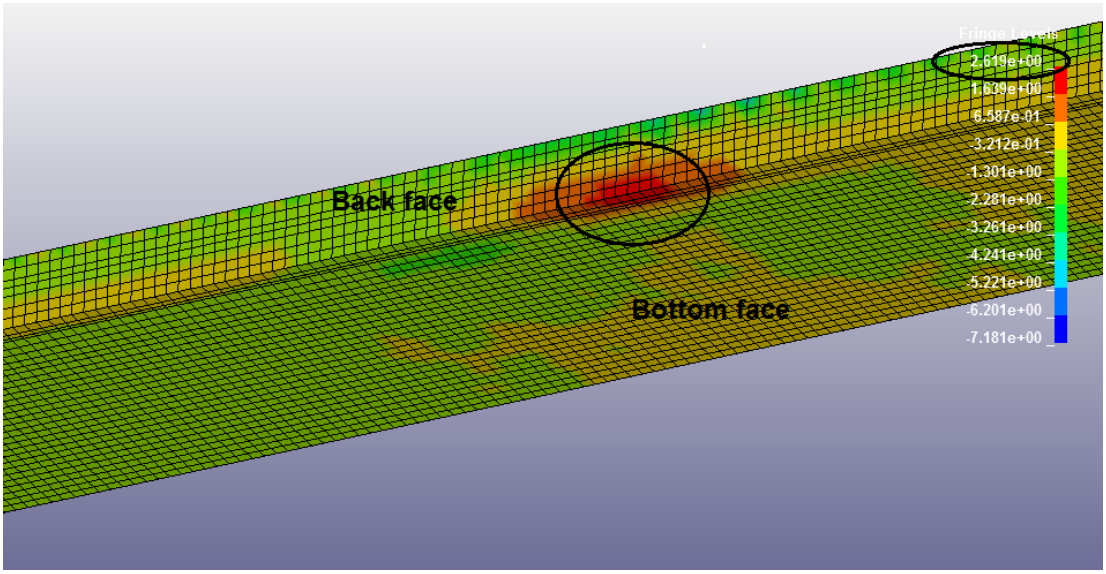

Figure 187: Rectangular – 6 inch barrier first impact in tension side of the deck overhang – back and bottom face

7.1.1.4.3 Maximum Stress in Reinforcement bars

7.1.1.4.3.1 Tension side

Reinforcement bars are front hairpin dowels that connect barriers to deck overhangs. As seen in Figure 188, the maximum tensile reinforcement bars are the #4 vertical reinforcement bars. Hence, the tensile stress is:

4.95e4 N / 129 mm^2 = 383.72 MPa = 55.65 ksi

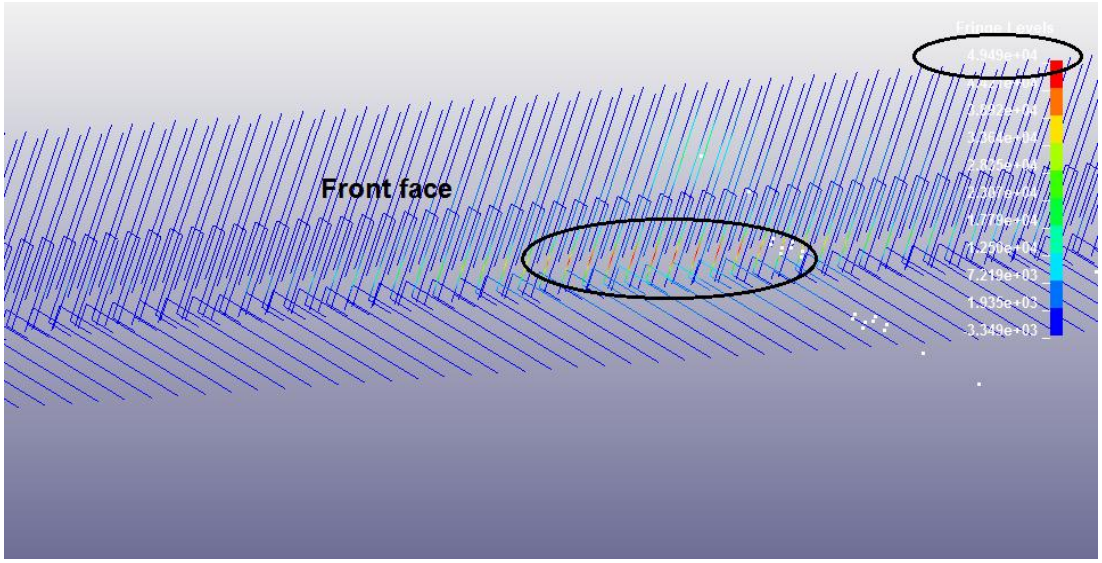

Figure 188: Axial force of the reinforcement bar in tension side at the moment of first impact: Rectangular – 6 inch – front face

7.1.1.4.3.2 Compression Side

As seen in Figure 189, the maximum compression reinforcement bars are horizontal #3 reinforcement bar and are located at the bottom, middle and top face of the barrier. Hence, the compressive stress is:

3.67e3 N / 71 mm^2 = 40.56 MPa = 5.88ksi

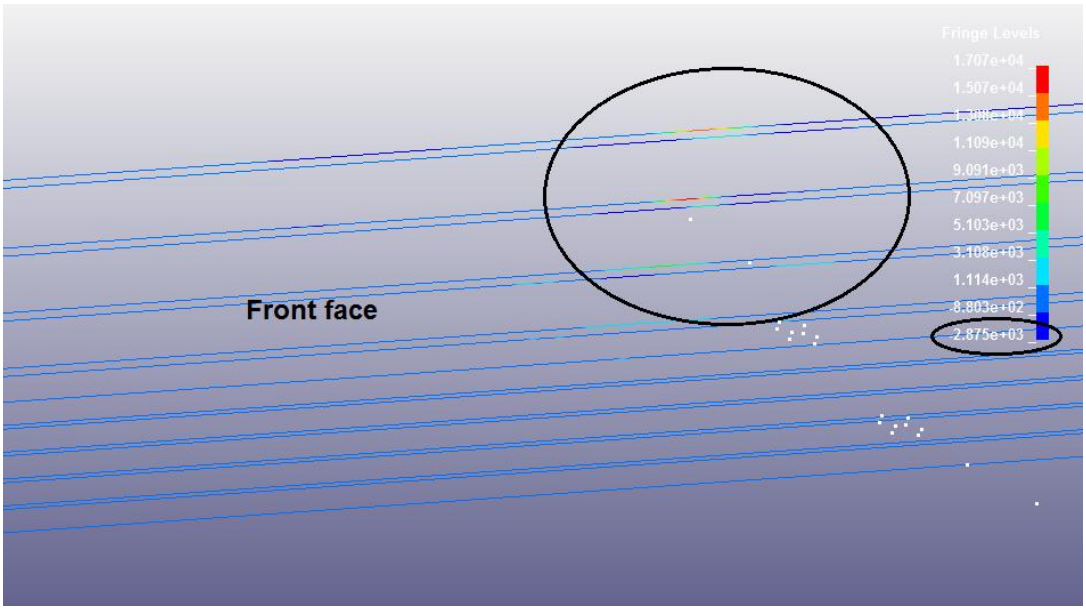

Figure 189: Axial force of the reinforcement bar in compression side at the moment of first impact: Rectangular – 6 inch – front face

7.1.1.5 Modified Single-Slope Barrier

Figure 190 represents the truck before it starts to hit the barrier.

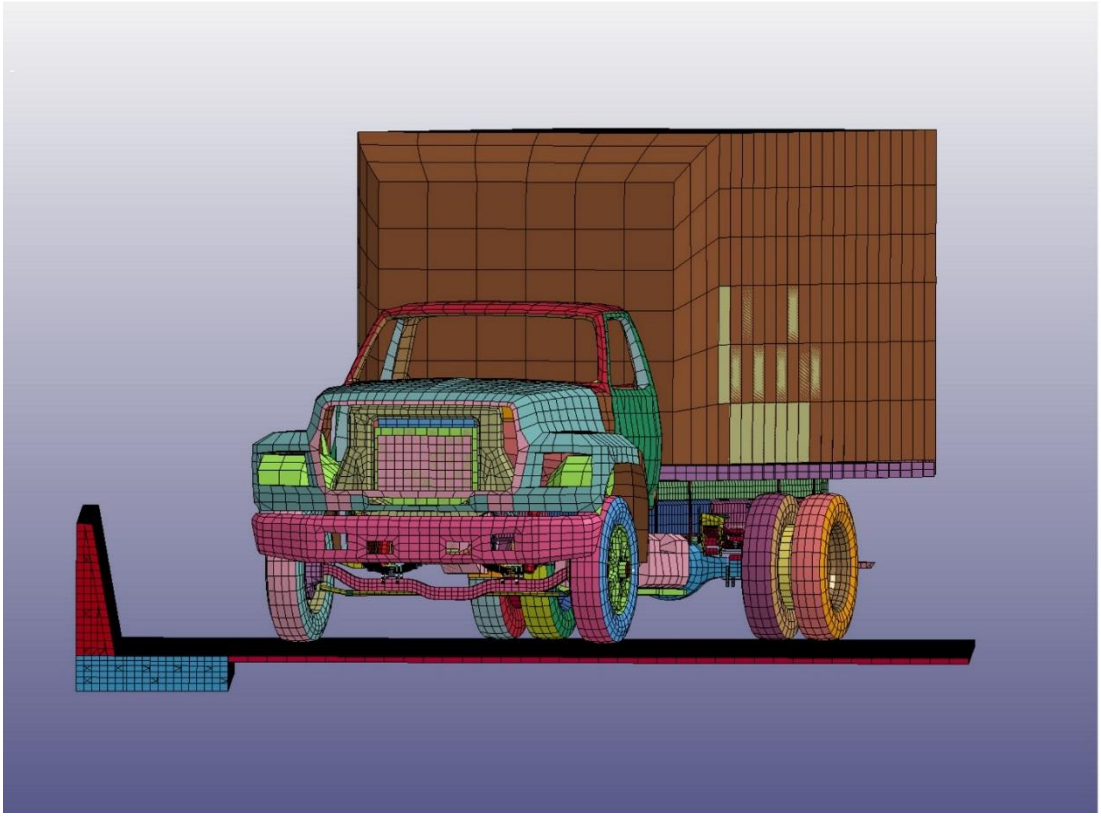

Figure 190: Modified single-slope geometry model with NCAC single unit truck

7.1.1.5.1 Maximum Stress in the Barrier

7.1.1.5.1.1 Compression Side

Figure 191 illustrates the maximum stress in compression side of the barrier caused by the front bumper of the truck. Maximum compression at first impact on the barrier was 25.26 Mpa.

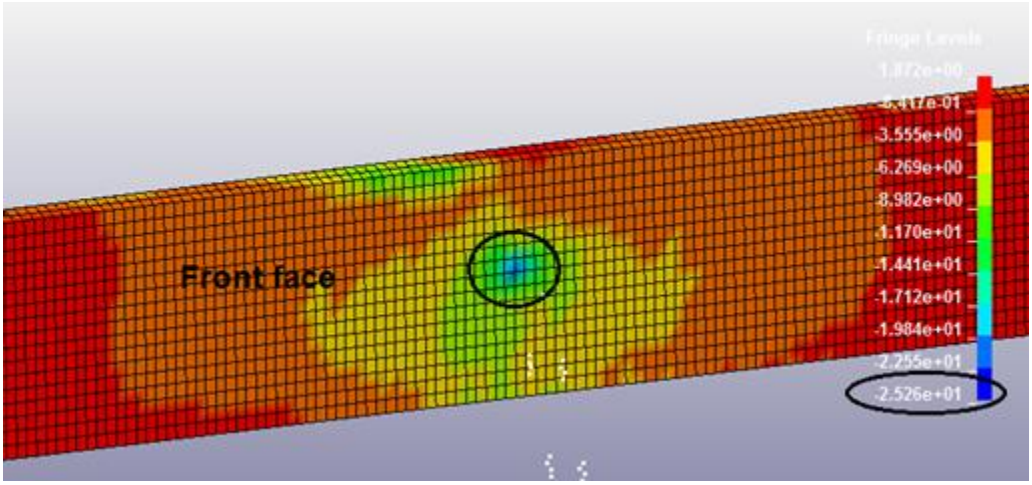

Figure 191: First impact compression effects on modified single-slope barrier – 3d model – front face

7.1.1.5.1.2 Tension Side

Figure 192 shows the maximum stress in tension side of the barrier. The maximum tensile stress at the moment of first impact was 1.87 Mpa.

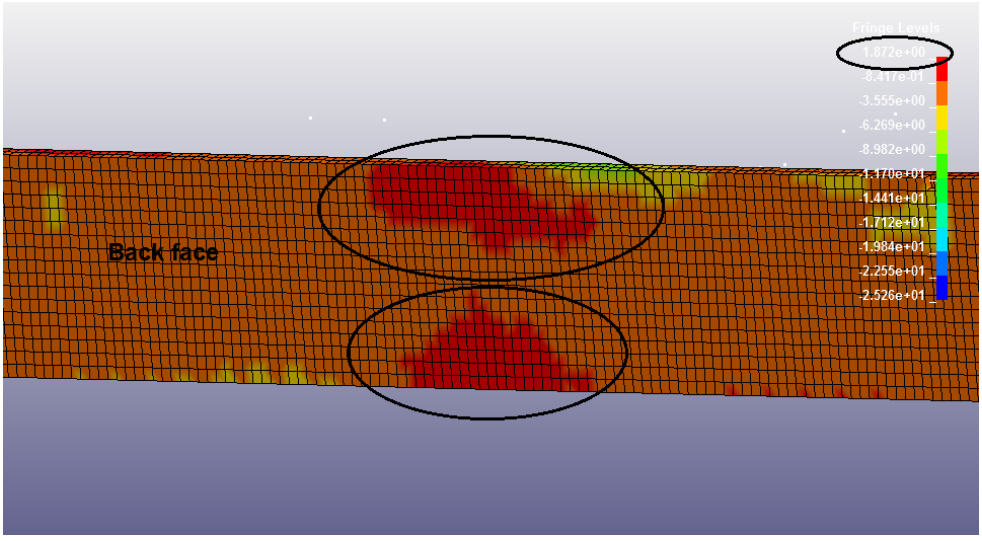

Figure 192: First impact tension effect on modified single-slope barrier – 3d model – back face

7.1.1.5.2 Maximum Stress in the Deck Overhang

7.1.1.5.2.1 Compression Side

Figure 193 shows the maximum stress in compression side of the deck. Maximum compression at first impact on the barrier was 9.31 Mpa.

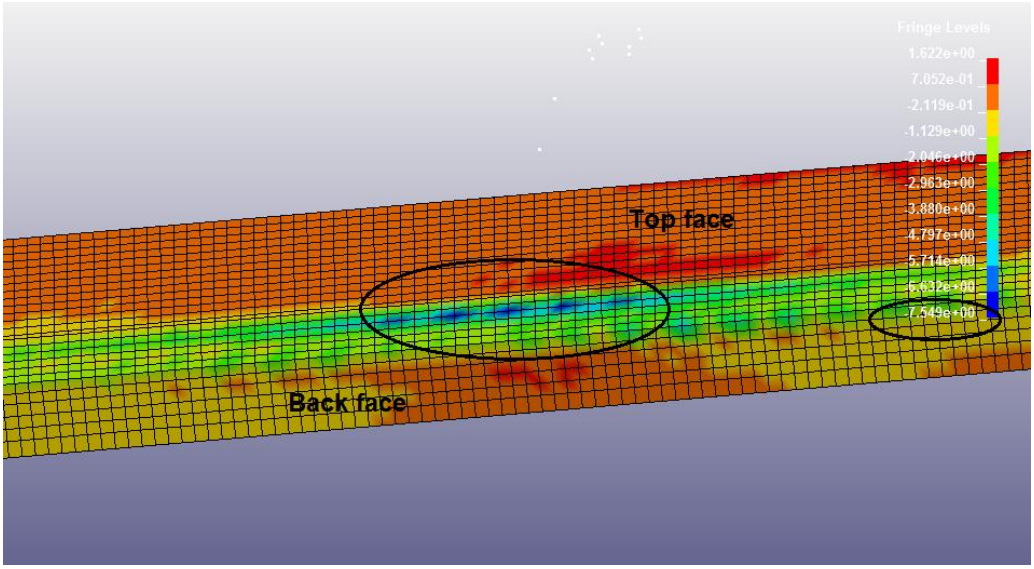

Figure 193: Modified single-slope barrier first impact in compression side of the deck overhang – top and back face

7.1.1.5.2.2 Tension Side

Figure 194 shows the maximum stress in tension side of the deck overhang The maximum tensile stress at the moment of first impact was 2.92 Mpa.

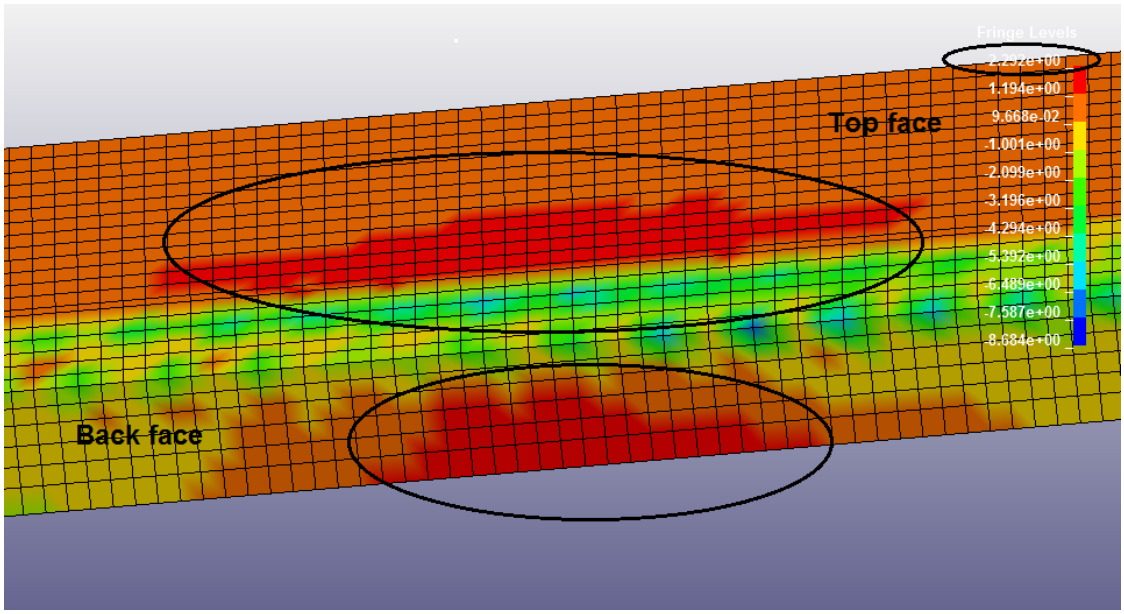

Figure 194: Modified single-slope barrier first impact in tension side of the deck overhang – top and back face

7.1.1.5.3 Maximum Stress in Reinforcement bars

7.1.1.5.3.1 Tension Side

Reinforcement bars are front hairpin dowels that connect barrier to deck overhang. As seen in Figure 195, the maximum tensile reinforcement bars are the #4 vertical reinforcement bars. Hence, the tensile stress is:

4.10e4 N / 129 mm^2 = 317.83 MPa = 40.10 ksi

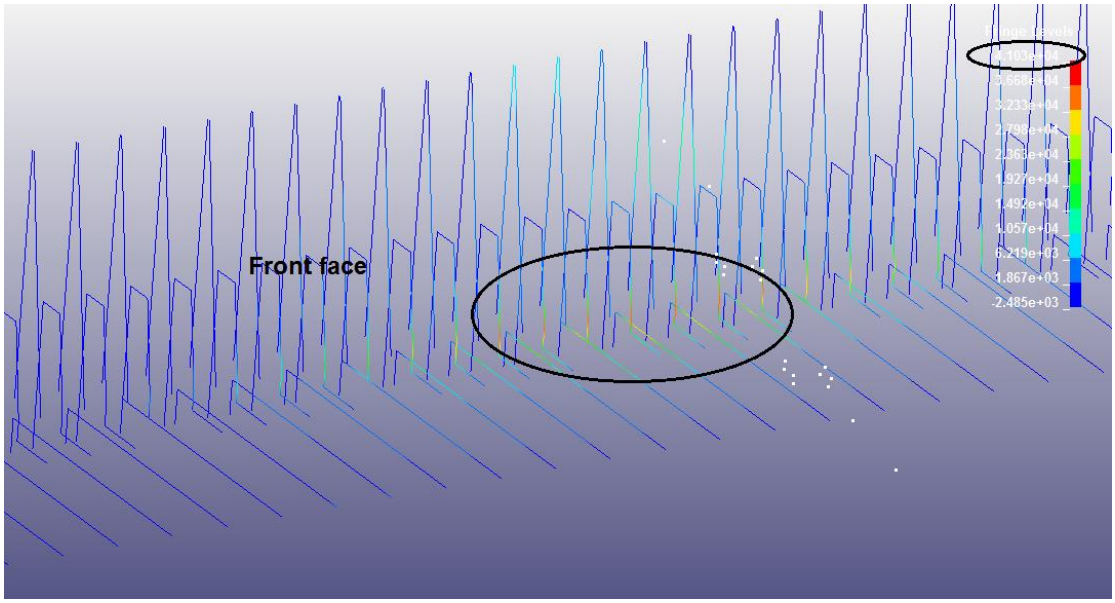

Figure 195: Axial force of the reinforcement bar in tension side at the moment of first impact: Modified single-slope – front face

7.1.1.5.3.2 Compression Side

As seen in Figure 196, the maximum compression reinforcement bars are the horizontal #3 reinforcement bars and are located at the bottom, middle and top face of the barrier. Hence, the compressive stress is:

2.08e3 N / 71 mm^2 = 29.30 MPa = 4.25ksi

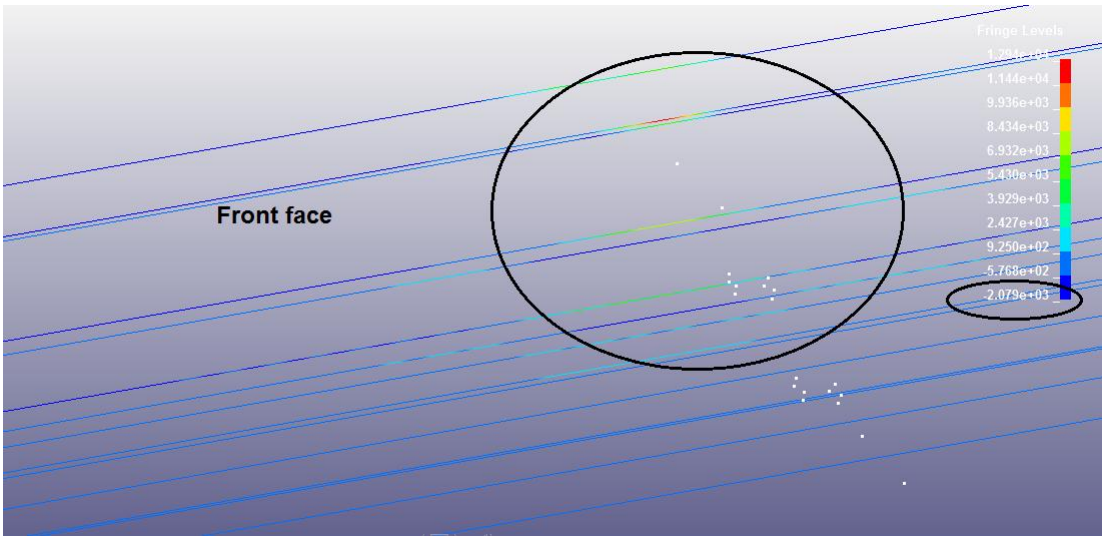

Figure 196: Axial force of the reinforcement bar in compression side at the moment of first impact – Modified single-slope – front face

7.1.1.6 Inverted modified Single-Slope Barrier

Figure 197 represents the truck before it starts to hit the barrier.

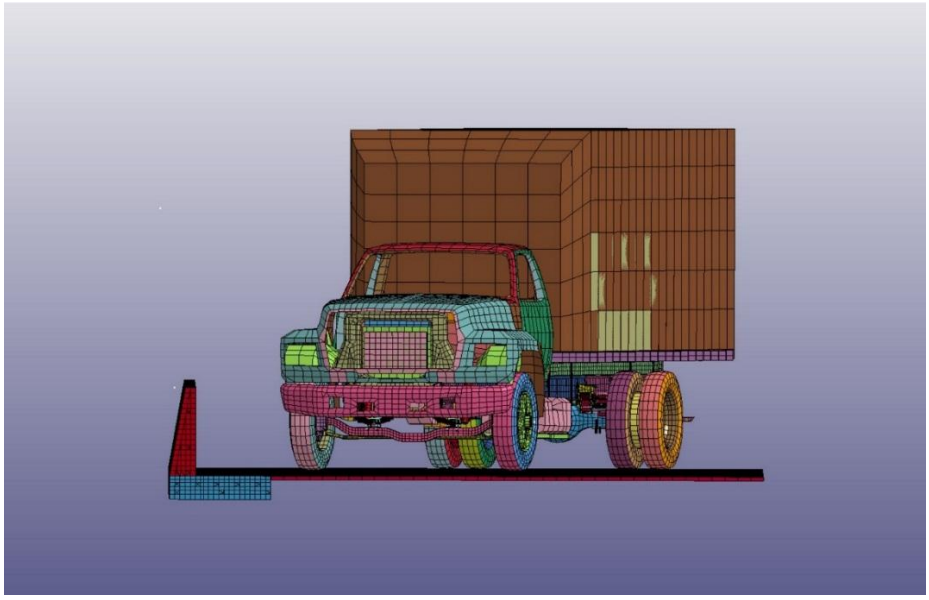

Figure 197: Inverted modified single-slope geometry model with NCAC single unit truck

7.1.1.6.1 Maximum Stress in the Barrier

7.1.1.6.1.1 Compression Side

Figure 198 shows the maximum stress in compression side of the barrier caused by front bumper of the truck. Maximum compression at first impact on the barrier was 16.69 Mpa.

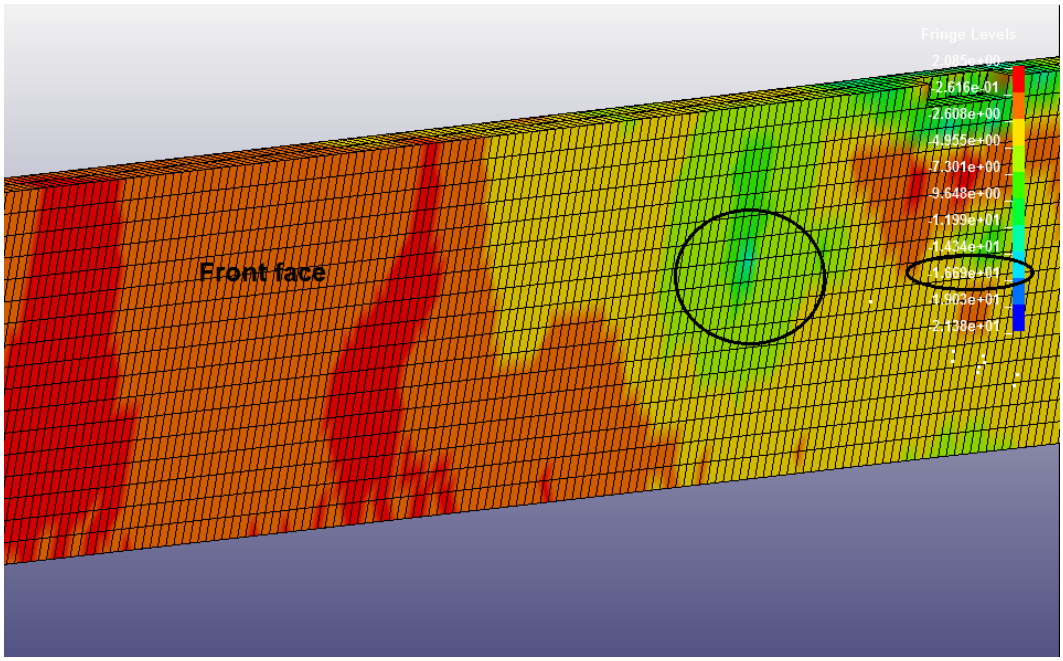

Figure 198: First impact compression effects on inverted modified single-slope barrier – 3d model – front face

7.1.1.6.1.2 Tension Side

Figure 199 shows the maximum stress in the tension side of the barrier. The maximum tensile stress at the moment of first impact was 2.09 Mpa.

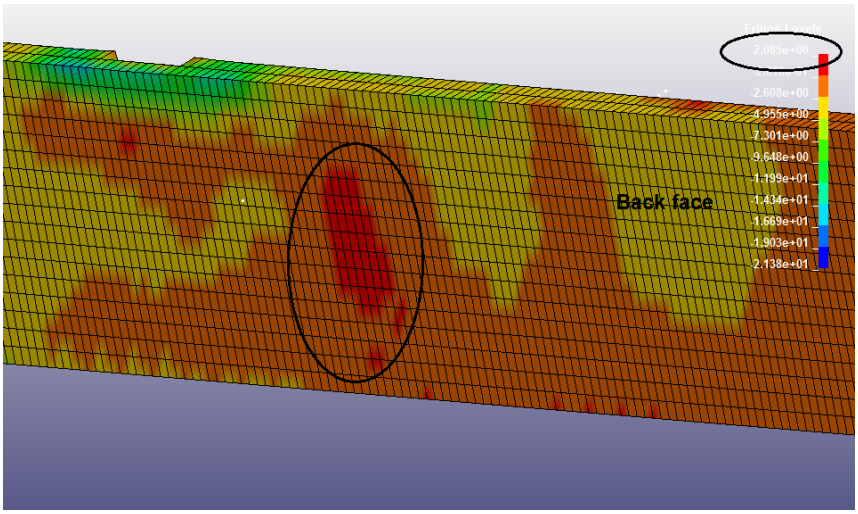

Figure 199: First impact tension effect on inverted modified single-slope barrier – 3d model – back face

7.1.1.6.2 Maximum stress in the deck overhang

7.1.1.6.2.1 Compression Side

Figure 200 shows the maximum stress in the compression side of the deck overhang.. Maximum compression at first impact on the barrier was 8.94 Mpa.

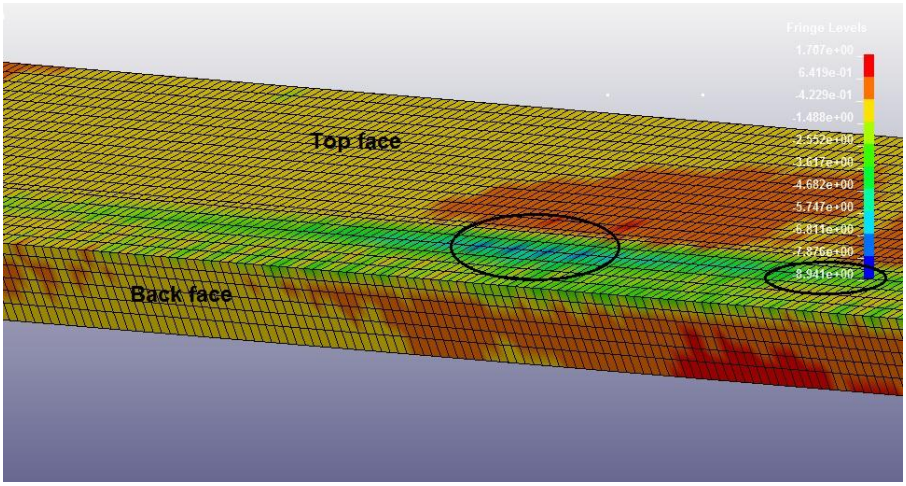

Figure 200: Inverted modified single-slope barrier first impact in compression side of the deck overhang – top and back face

7.1.1.6.2.2 Tension Side

Figure 201 shows the maximum stress in the tension side of the deck overhang. The maximum tensile stress at the moment of first impact was 1.82 Mpa.

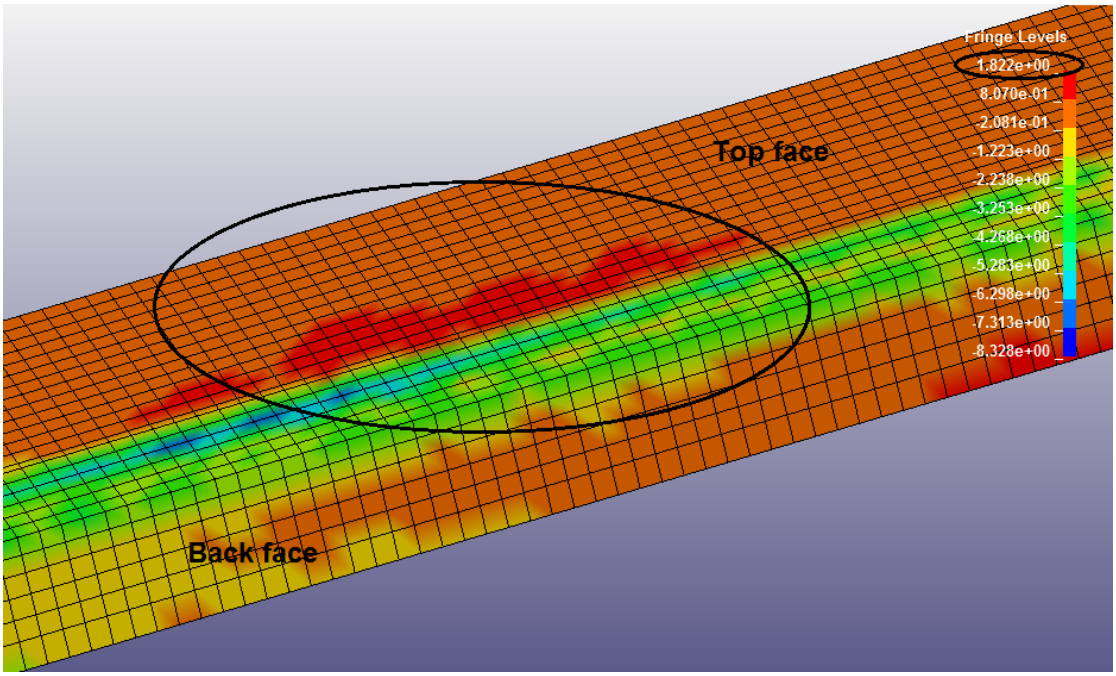

Figure 201: Inverted modified single-slope barrier first impact in tension side of the deck overhang – top and back face

7.1.1.6.3 Maximum stress in reinforcement bars

7.1.1.6.3.1 Tension Side

As seen in Figure … maximum tensile reinforcement bars are #4 hairpin dowels that connect the barrier to the deck overhang. Hence, the tensile stress is:

5.78e4 N / 129 mm^2 = 448.06 MPa = 64.99 ksi

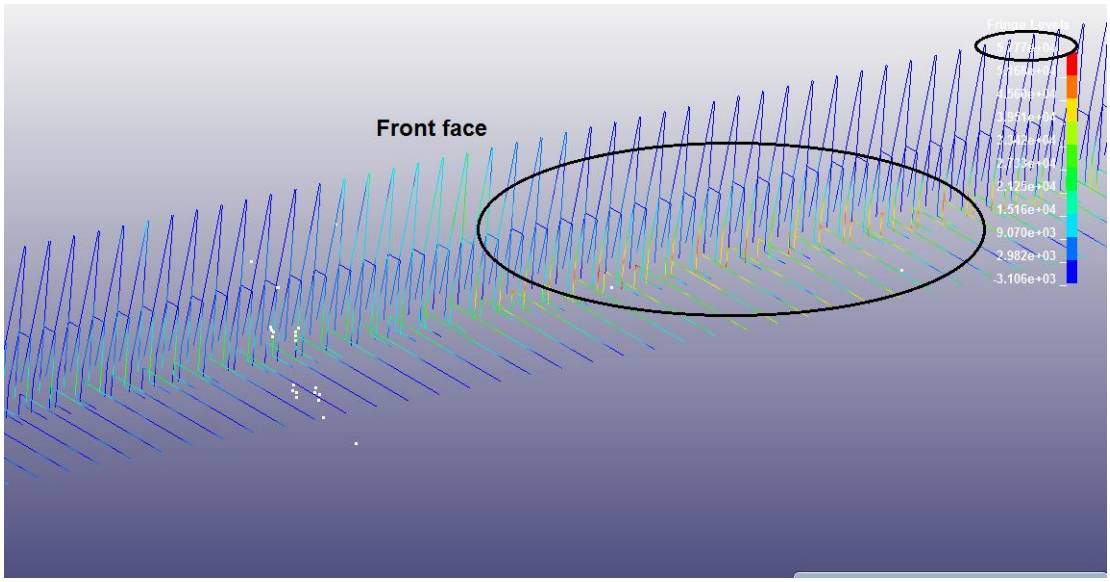

Figure 202: Axial force of the reinforcement bar in tension side at the moment of first impact: Inverted modified single-slope – front face

7.1.1.6.3.2 Compression side

As seen in Figure 203, maximum compression reinforcement bars are horizontal and #3 and located at the top of the deck overhang. Hence, the compressive stress is:

1.01e4 N / 71 mm^2 = 142.25 MPa = 20.63ksi

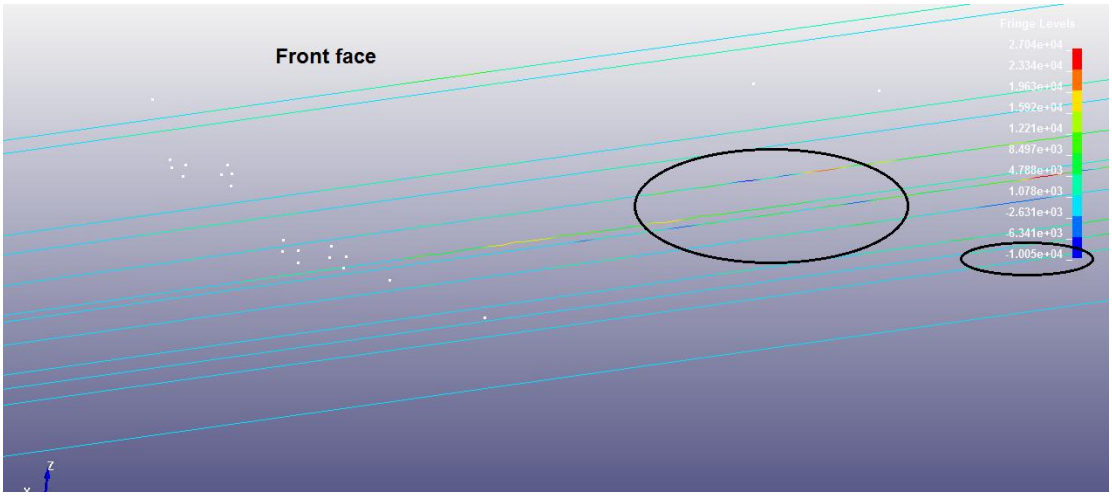

Figure 203: Axial force of the reinforcement bar in compression side at the moment of first impact: Inverted modified single-slope – front face

7.1.2 Maximum Deflection

This sub-chapter showed the maximum deflection of the barrier and deck overhang based on single unit truck's first impact.

7.1.2.1 New Jersey Barrier

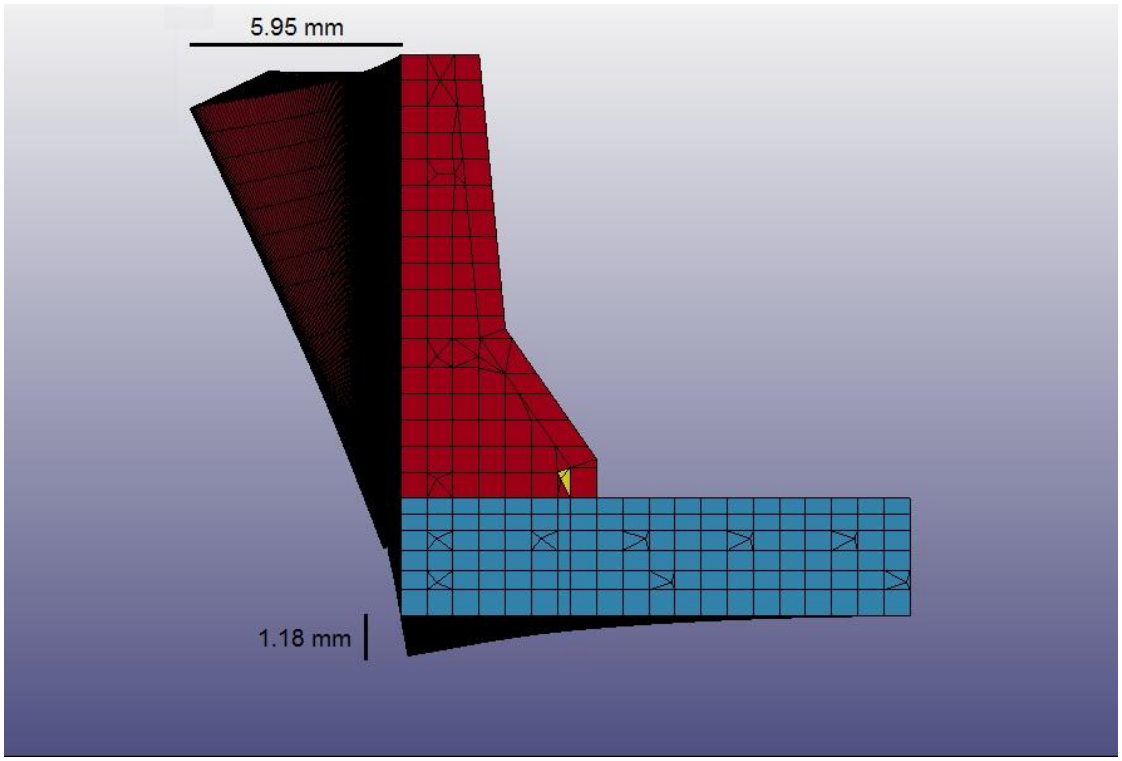

Figure 204: Maximum deflection of barrier and deck overhang – New Jersey

7.1.2.1.1 Maximum Deflection in Barrier

As seen in Figure 205, the maximum deflection in the barrier at moment .205 sec was 5.95 mm or 0.23 inches.

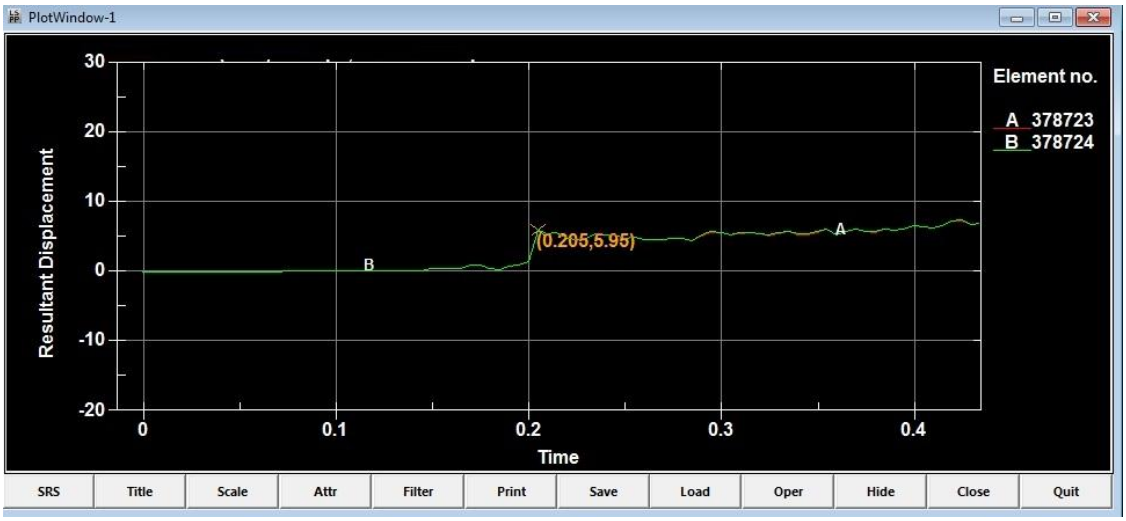

Figure 205: Maximum deflection of the barrier at first impact – New Jersey geometry

7.1.2.1.2 Maximum deflection in deck overhang

As seen in Figure 206, the maximum deflection in the deck overhang at moment 0.21 sec was 1.18 mm or 0.05 inches.

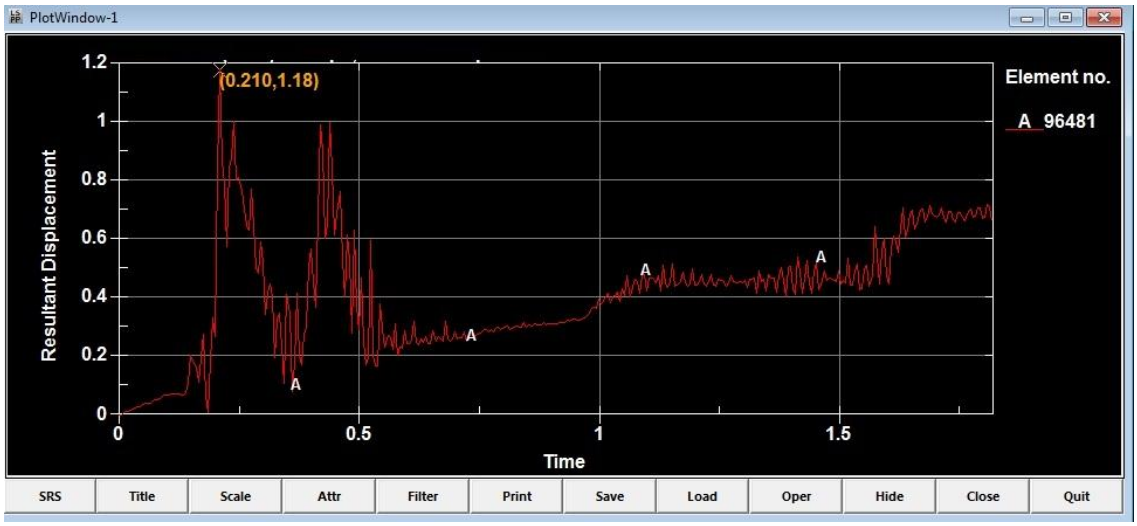

Figure 206: Maximum deflection of the deck overhang at first impact – New-Jersey geometry

This sub-chapter showed the maximum deflection of the barrier and deck overhang based on single unit truck's first impact.

7.1.2.2 Modified New Jersey Barrier

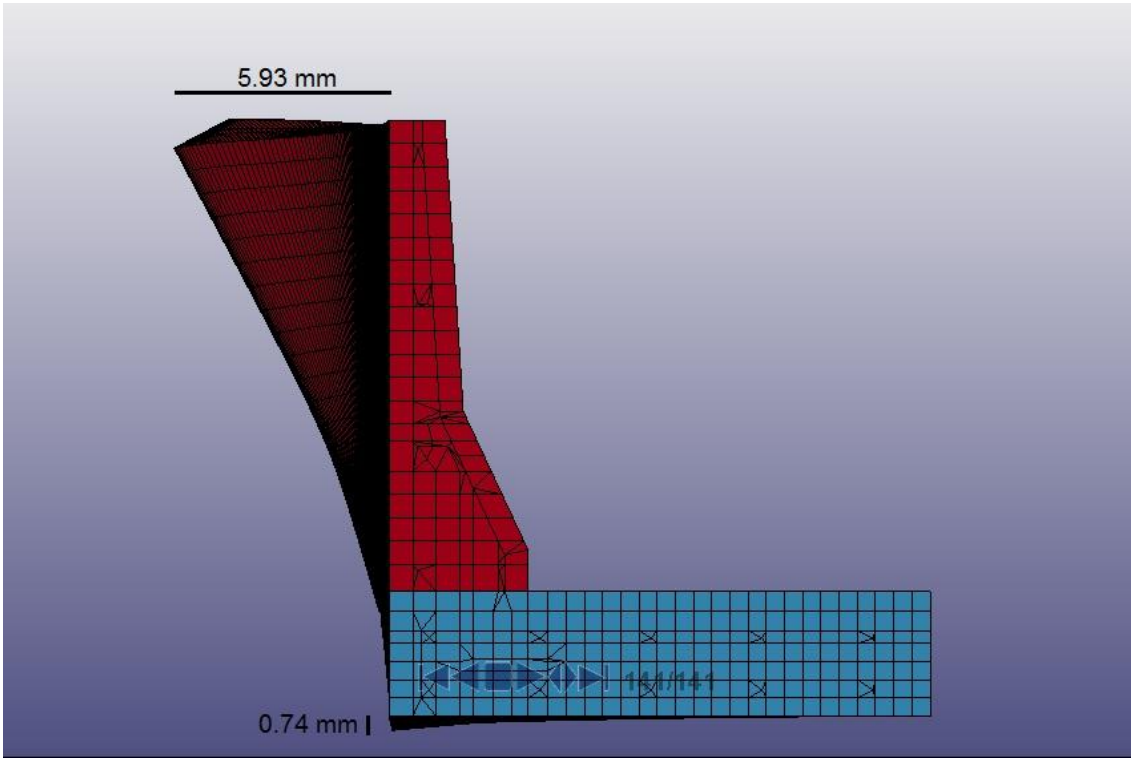

Figure 207: Maximum deflection of barrier and deck overhang – modified New Jersey

7.1.2.2.1 Maximum Deflection in Barrier

As seen in Figure 208, maximum deflection in the barrier at moment 0.23 sec was 5.93 mm or 0.23 inches.

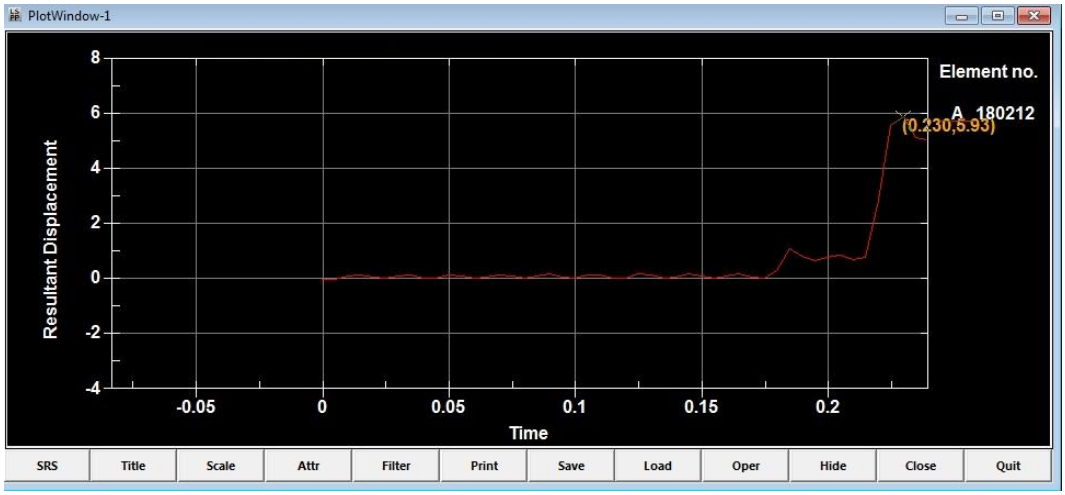

Figure 208: Maximum deflection of the barrier at first impact – modified New Jersey geometry

7.1.2.2.2 Maximum Deflection in Deck Overhang

As seen in Figure 209, maximum deflection in the deck overhang at moment 0.225 sec was 0.74 mm or 0.03 inches.

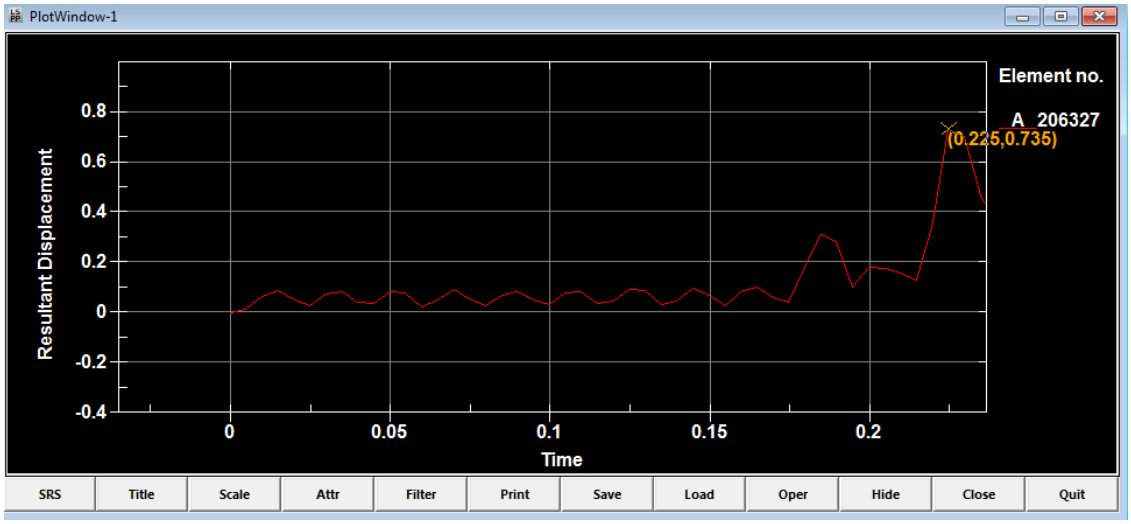

Figure 209: Maximum deflection of the deck overhang at first impact – modified New Jersey geometry

7.1.2.3 Rectangular – 8 Inch Barrier

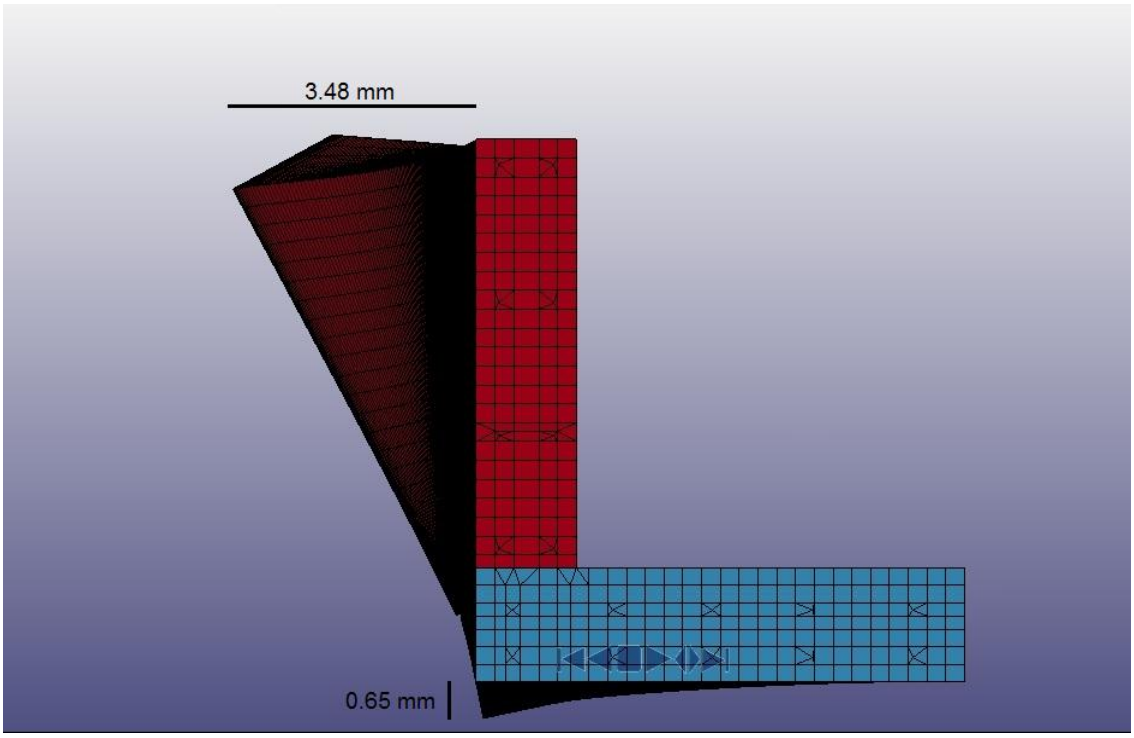

Figure 210: Maximum deflection of barrier and deck overhang: Rectangular – 8 inch

7.1.2.3.1 Maximum Deflection in Barrier

As seen in Figure 211, maximum deflection in the barrier at moment 0.17 sec was 3.48 mm or 0.14 inches.

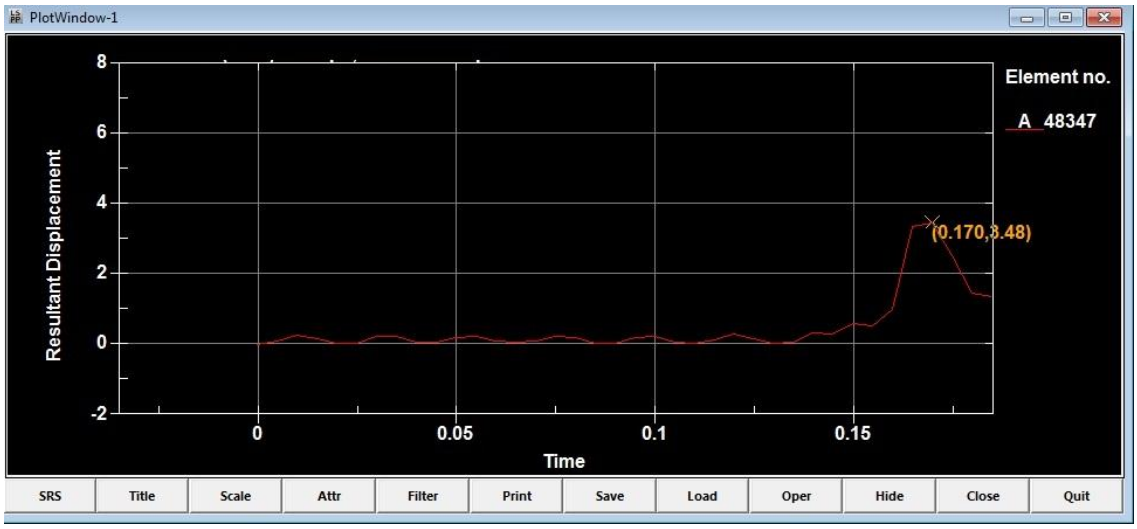

Figure 211: Maximum deflection of the barrier at first impact: Rectangular – 8 inch geometry

7.1.2.3.2 Maximum deflection in deck overhang

As seen in Figure 212, the maximum deflection in the deck overhang at moment 0.17 sec was 0.65 mm or 0.03 inches.

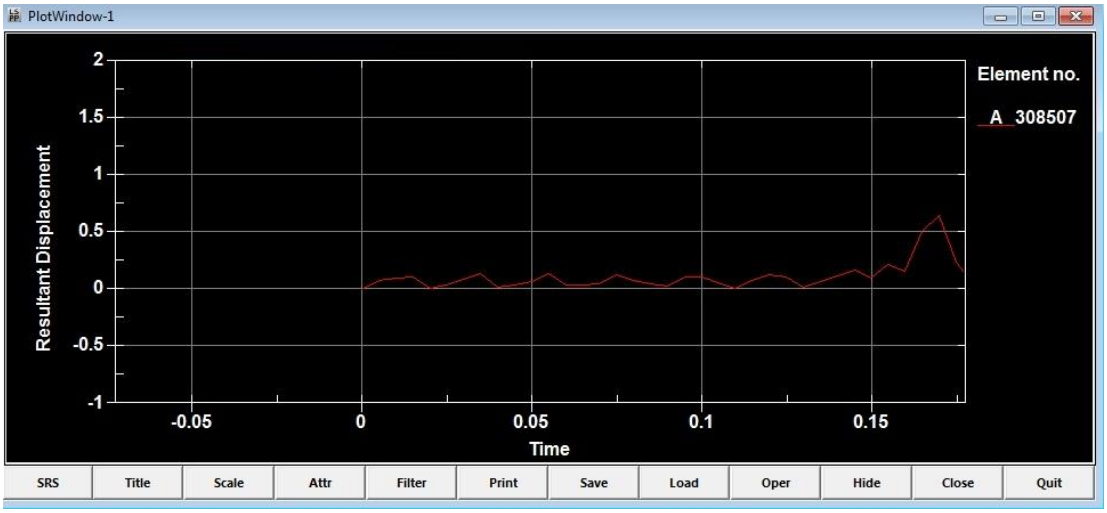

Figure 212: Maximum deflection of the deck overhang at first impact: Rectangular - 8 inch geometry

7.1.2.4 Rectangular – 6 Inch Barrier

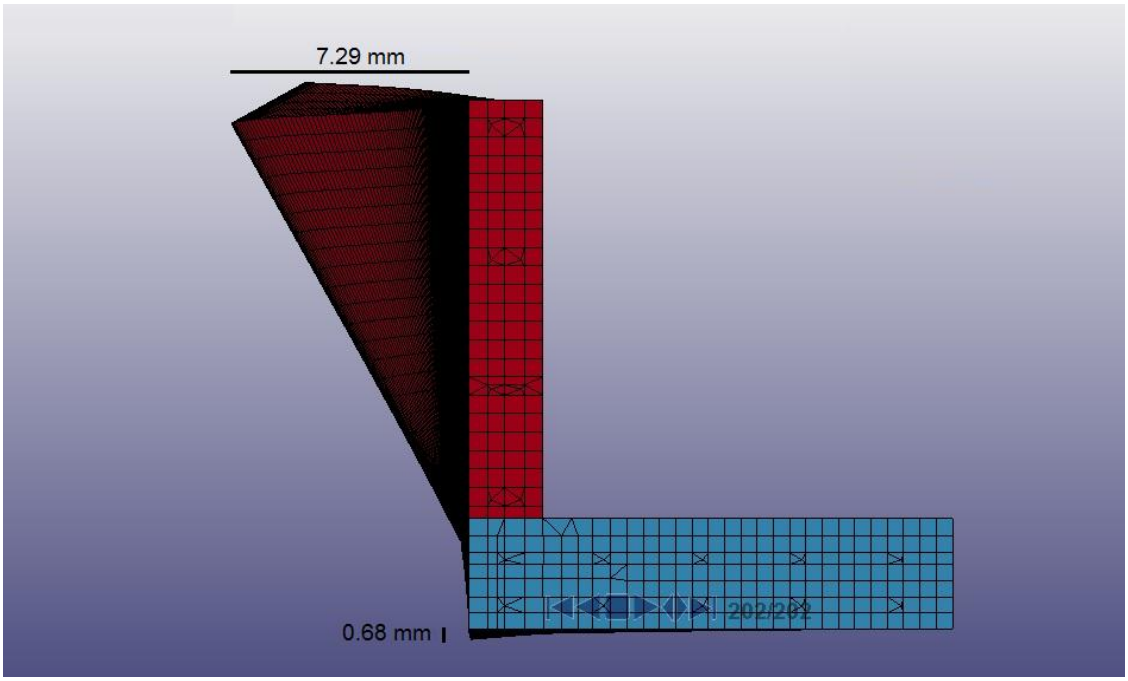

Figure 213: Maximum deflection of barrier and deck overhang: Rectangular – 6 inch

7.1.2.4.1 Maximum Deflection in Barrier

As seen in Figure 214, the maximum deflection in the barrier at moment 0.18 sec was 7.29 mm or 0.29 inches.

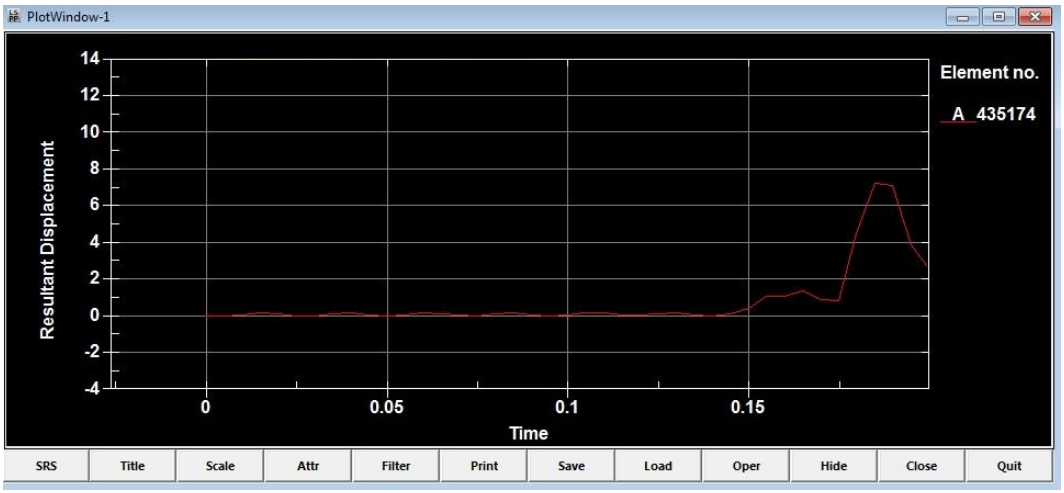

Figure 214: Maximum deflection of the barrier at first impact: Rectangular – 6 inch geometry

7.1.2.4.2 Maximum deflection in deck overhang

As seen in Figure 215, the maximum deflection in the deck overhang at moment 0.19 sec was 0.68 mm or 0.03 inches.

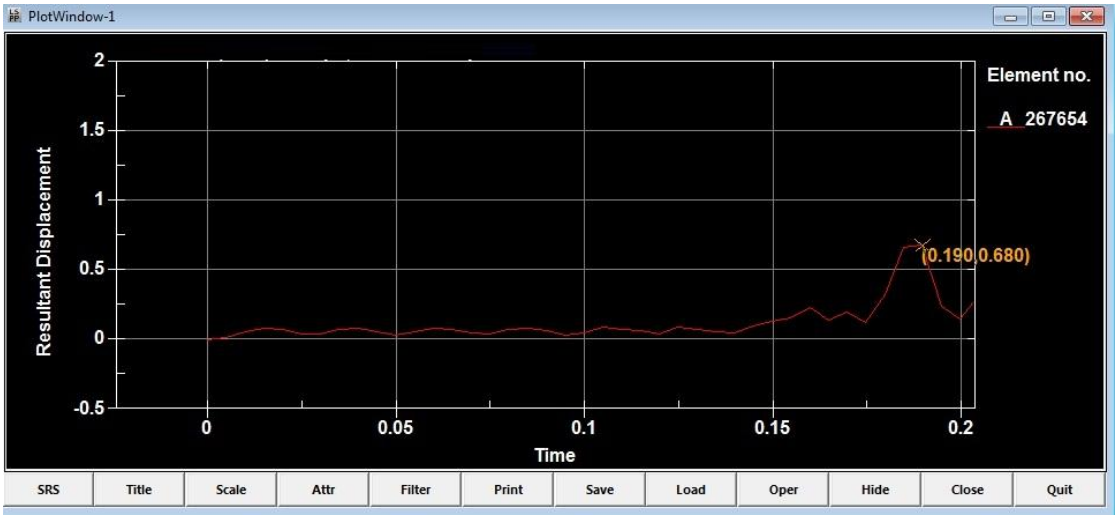

Figure 215: Maximum deflection of the deck overhang at first impact: Rectangular – 6 inch geometry

7.1.2.5 Modified single-slope barrier

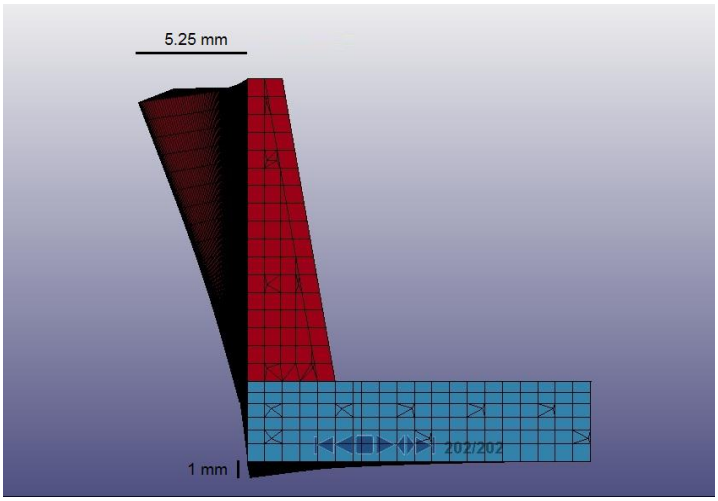

Figure 216: Maximum deflection of barrier and deck overhang: Modified single-slope

7.1.2.5.1 Maximum deflection in barrier

As shown in Figure 217, maximum deflection in the barrier at moment 0.195 sec was 5.25 mm or 0.21 inches.

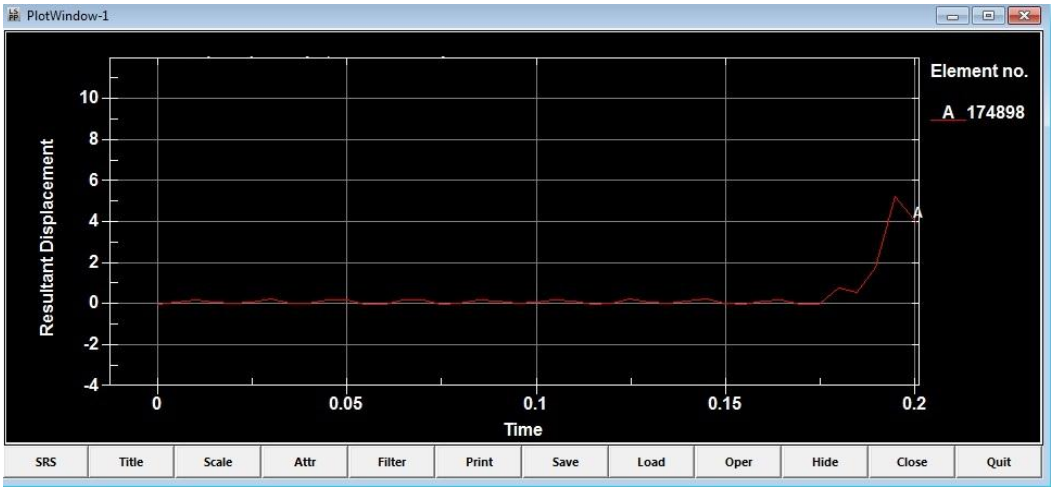

Figure 217: Maximum deflection of the barrier at first impact: Modified single-slope geometry

7.1.2.5.2 Maximum deflection in deck overhang

As seen in Figure 218, the maximum deflection in the deck overhang at moment 0.20 sec was 1 mm or 0.04 inches.

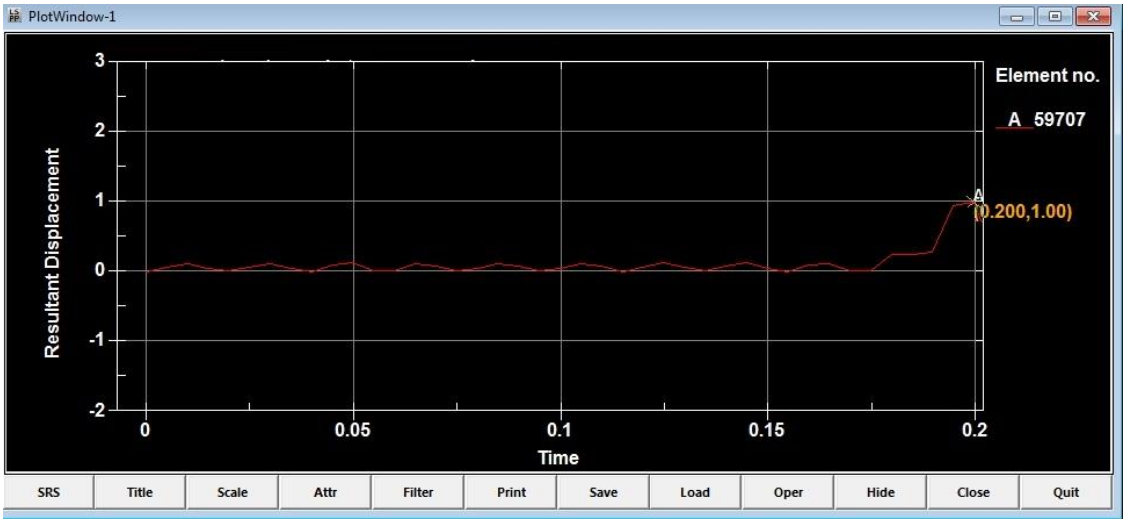

Figure 218: Maximum deflection of the deck overhang at first impact: Modified single-slope geometry

7.1.2.6 Inverted modified single-slope barrier

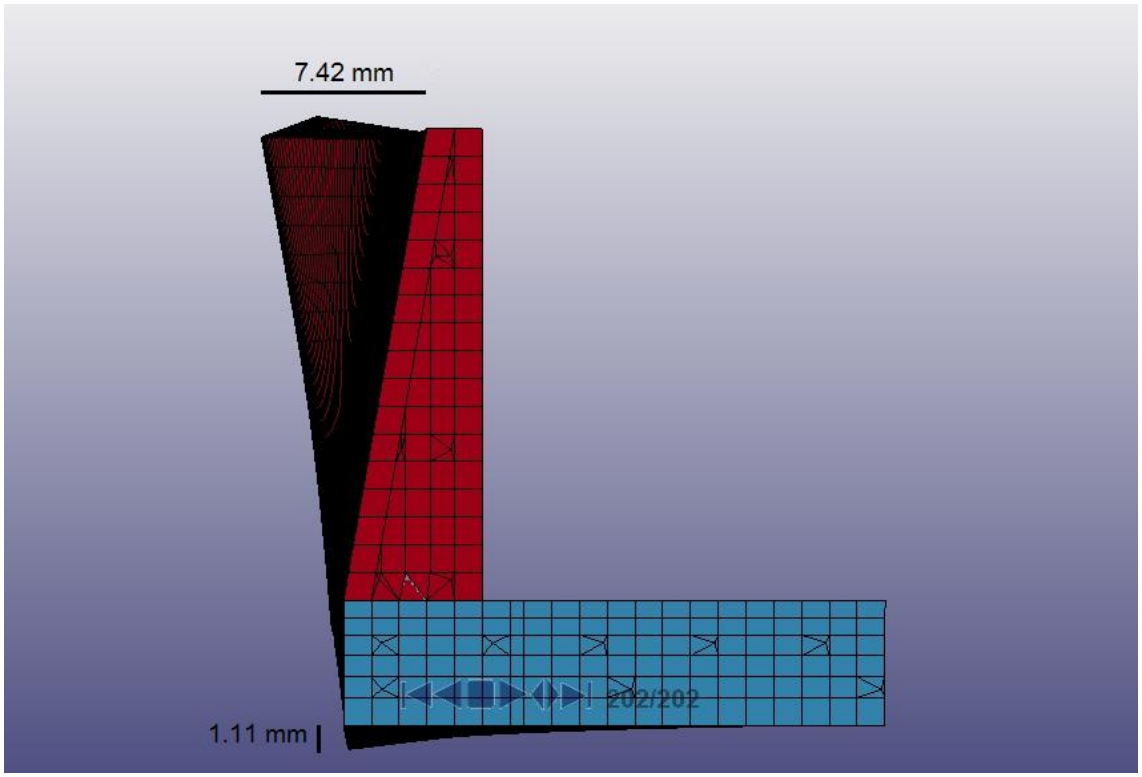

Figure 219: Maximum deflection of barrier and deck overhang: Inverted modified single-slope

7.1.2.6.1 Maximum deflection in barrier

As seen in Figure 218, the maximum deflection in the barrier at moment 0.235 sec was 7.42 mm or 0.29 inches.

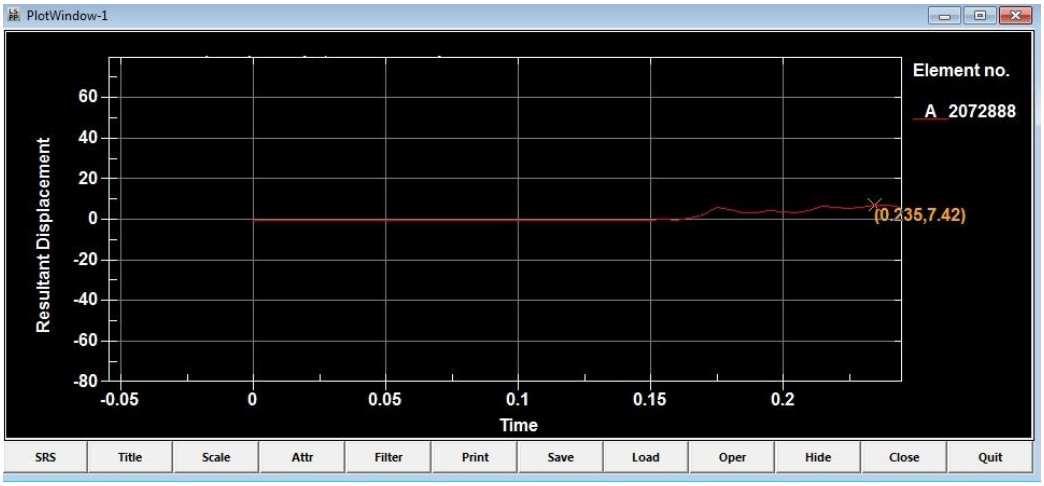

Figure 220: Maximum deflection of the barrier at first impact: Inverted modified single-slope geometry

7.1.2.6.2 Maximum deflection in deck overhang

As seen in Figure 221, the maximum deflection in the deck overhang at moment 0.24 sec was 1.11 mm or 0.04 inches.

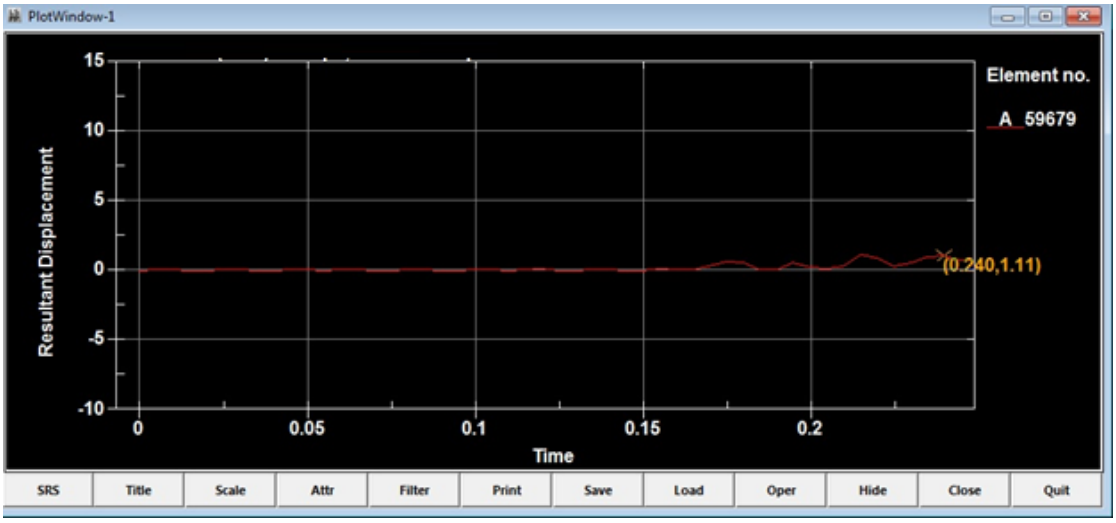

Figure 221: Maximum deflection of the deck overhang at first impact: Inverted modified single-slope geometry

7.2 Second Impact

7.2.1 Maximum Stress

As mentioned before in Sub-Chapter 7.1.1, this section will seek to determine the maximum stress in barriers with different geometries at the moment of second impact. Although the vehicle engine is located in front of the truck, since the back of the truck has sharp edges at the bumper, it is very important to study the barrier and deck overhang behavior after second impact.

7.2.1.1 New Jersey Barrier

7.2.1.1.1 Maximum Stress in the Barrier

7.2.1.1.1.1 Compression Side

Figure 222 shows the maximum stress in the compression side of the barrier caused by the rear bumper of the truck. Maximum compression at second impact on the barrier was 22.78Mpa.

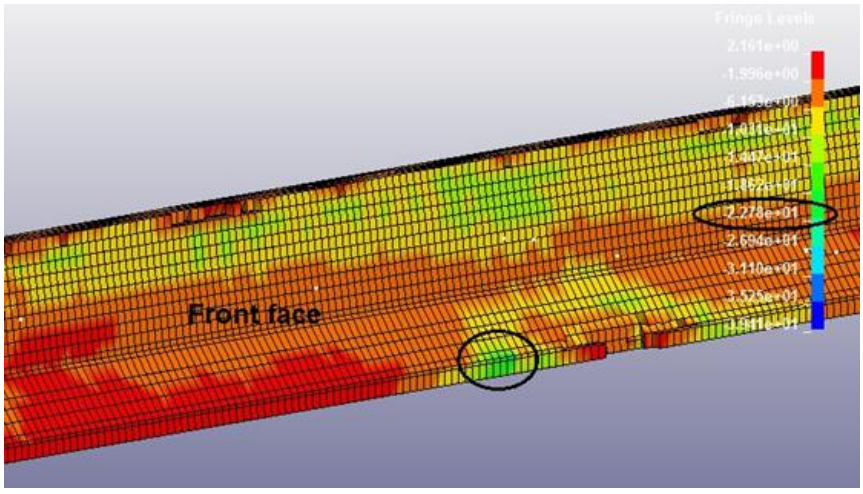

Figure 222: Second impact compression effects on New Jersey barrier: 3d model – front face

7.2.1.1.1.2 Tension Side

Figure 223 shows the maximum stress in the tension side of the barrier. The maximum tensile stress at the moment of second impact was 2.16 Mpa.

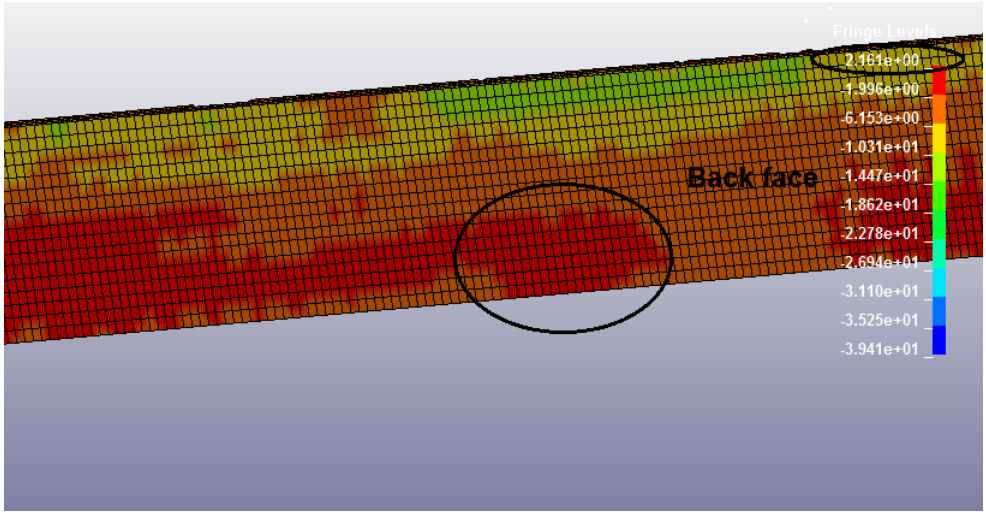

Figure 223: Second impact tension effect on New Jersey barrier: 3d model – back face

7.2.1.1.2 Maximum Stress in the Deck Overhang

7.2.1.1.2.1 Compression Side

Figure 224, shows the maximum stress in compression side of the deck overhang. Maximum compression at the second impact on the barrier was 12.97 Mpa.

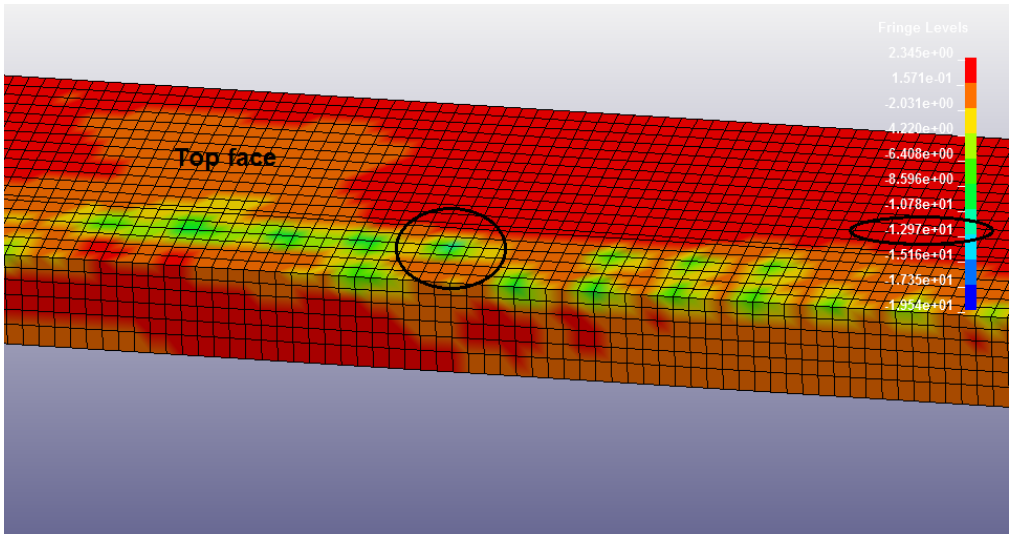

Figure 224: New-Jersey barrier second impact in compression side of the deck overhang: top face

7.2.1.1.2.2 Tension side

Figure 225 shows the maximum stress in the tension side of the deck overhang. The maximum tensile stress in the moment of second impact was 2.35Mpa.

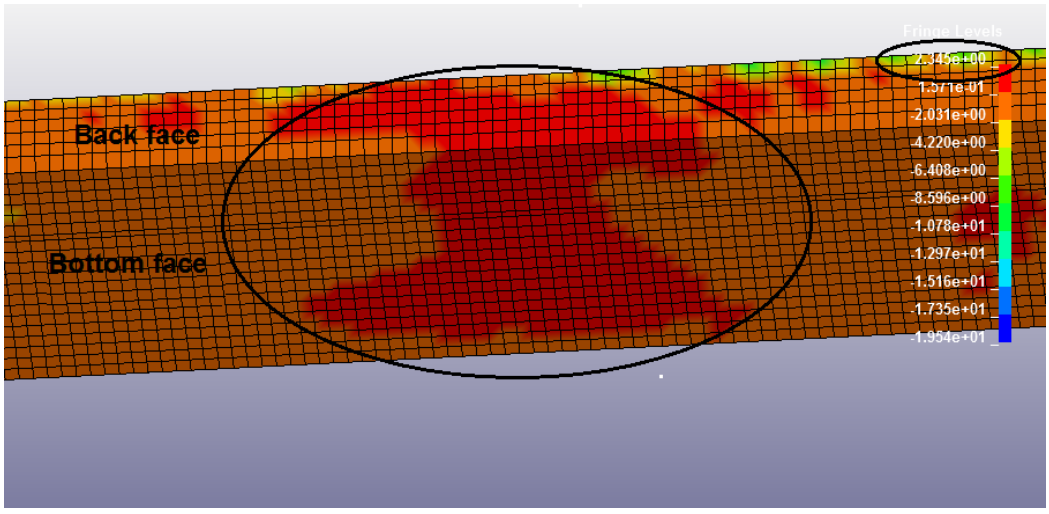

Figure 225: New-Jersey barrier second impact in tension side of the deck overhang: bottom and back face

7.2.1.1.3 Maximum stress in reinforcement bars

7.2.1.1.3.1 Tension side

Reinforcement bars are located in the top and front side of the barrier As seen in Figure 226, the maximum tensile reinforcement bars are the #4 vertical reinforcement bars.. Hence, the tensile stress is:

5.23e4 N / 129 mm^2 = 405.43 MPa = 58.80ksi

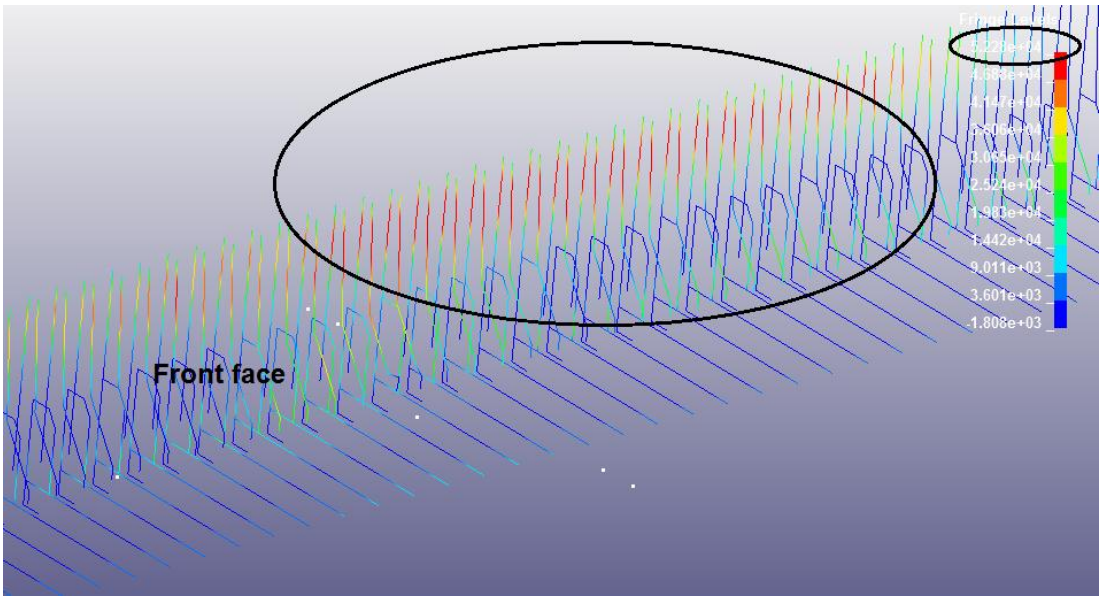

Figure 226: Axial force of the reinforcement bar in tension side at the moment of second impact: New-Jersey barrier – front face

7.2.1.1.3.2 Compression side

As seen in Figure 227, the maximum compression to the reinforcement bars is at the #3 horizontal reinforcement bar at the bottom face of the barrier. Hence, the compressive stress is:

3.67e3 N / 71 mm^2 = 90.42 MPa = 13.11ksi

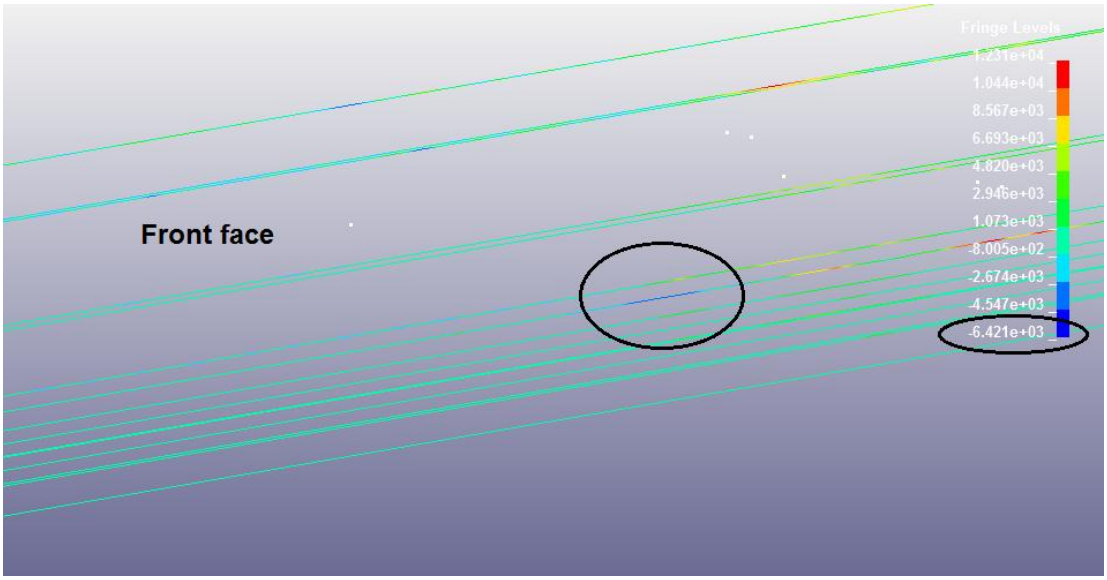

Figure 227: Axial force of the reinforcement bar in compression side at the moment of second impact: New Jersey – front face

7.2.1.2 Modified New-Jersey barrier

7.2.1.2.1 Maximum stress in the barrier

As seen in Figure 228, at the moment of second impact, all elements turn into red. Although determining the exact location of elements in compression and tension is not possible, all elements fell within the range of 26.57 MPa and 2.39 Mpa.

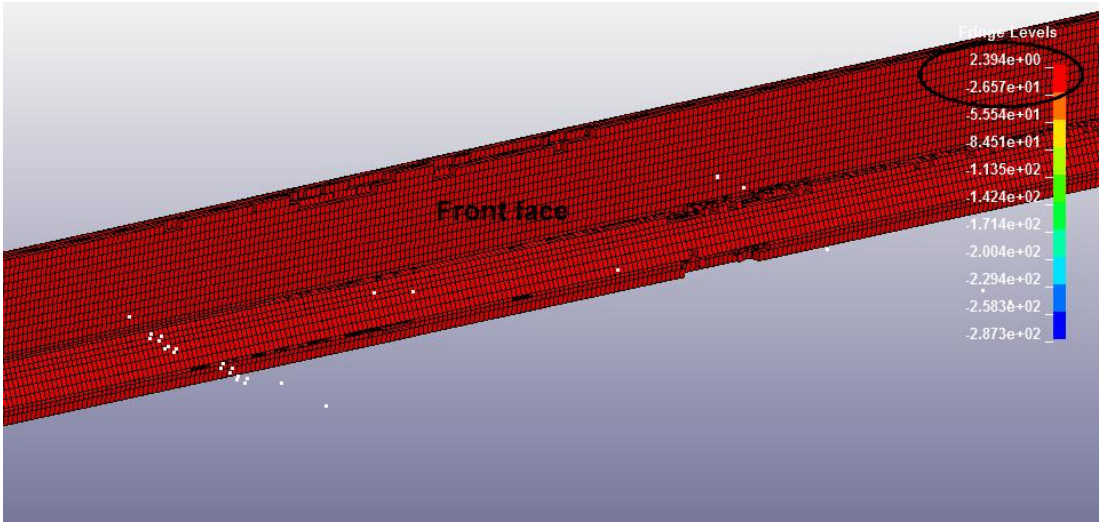

Figure 228: Second impact compression and tension effects on modified New-Jersey barrier: 3d model – front face

7.2.1.2.1.1 Compression side

Maximum compressive stress at the barrier was 26.57 Mpa

7.2.1.2.1.2 Tension side

Maximum tensile stress at the barrier was 2.39 Mpa

7.2.1.2.2 Maximum stress in the deck overhang

7.2.1.2.2.1 Compression side

Figure 229 shows the maximum stress in compression side of the deck overhang.

Maximum compression at second impact on the barrier was 31.11Mpa.

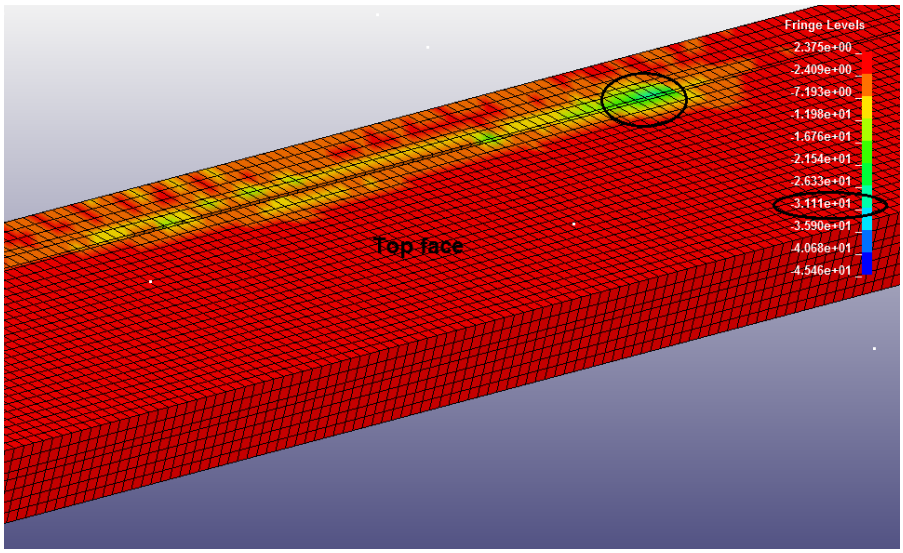

Figure 229: Modified New Jersey barrier second impact in compression side of the deck overhang: top face

7.2.1.2.2.2 Tension Side

Figure 230 shows the maximum stress in tension side of the deck overhang. The maximum tensile stress at the moment of second impact was 2.38 Mpa.

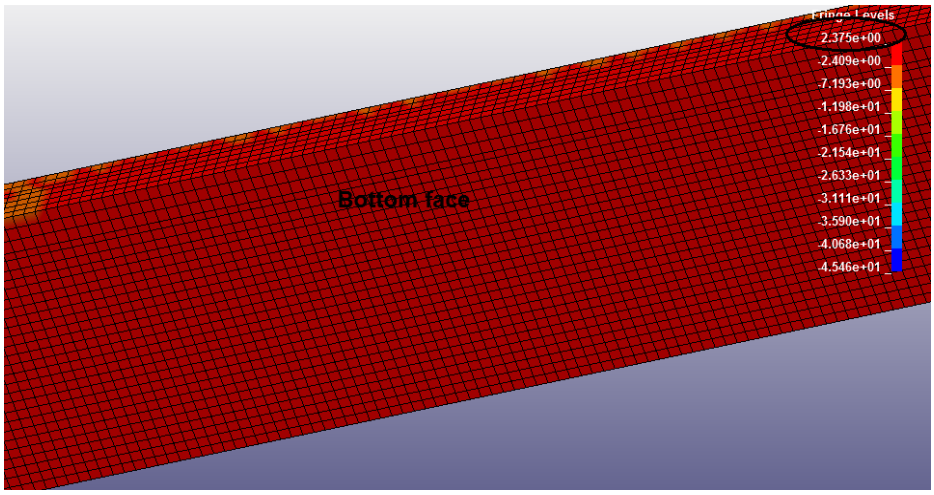

Figure 230: Modified New-Jersey barrier second impact in tension side of the deck overhang: bottom face

7.2.1.2.3 Maximum Stress in Reinforcement bars

7.2.1.2.3.1 Tension Side

As seen in Figure 231, the maximum tension for reinforcement bars is with the #4 vertical reinforcement bars located at the middle of the barrier and front face, respectively. Consequently, the tensile stress is:

6.17e4 N / 129 mm^2 = 478.29MPa = 69.37ksi

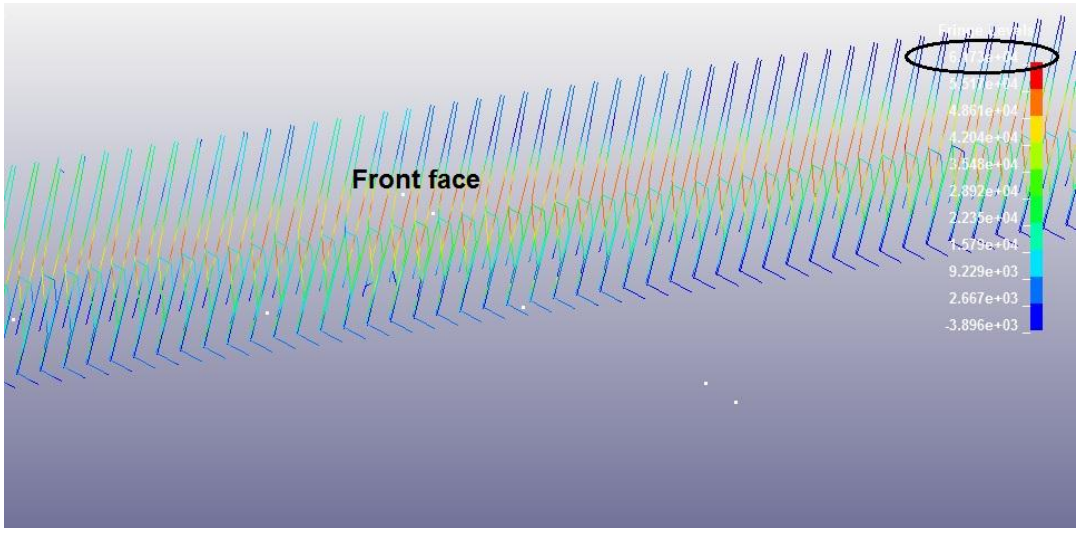

Figure 231: Axial force of the reinforcement bar in tension side at the moment of second impact: Modified New Jersey barrier – front face

7.2.1.2.3.2 Compression side

As seen in Figure 232, the maximum compression reinforcement bars are the #3 horizontal reinforcement bars at the top face of the barrier. Hence, the compressive stress is:

1.01e4 N / 71 mm^2 = 142.25 MPa = 20.63ksi

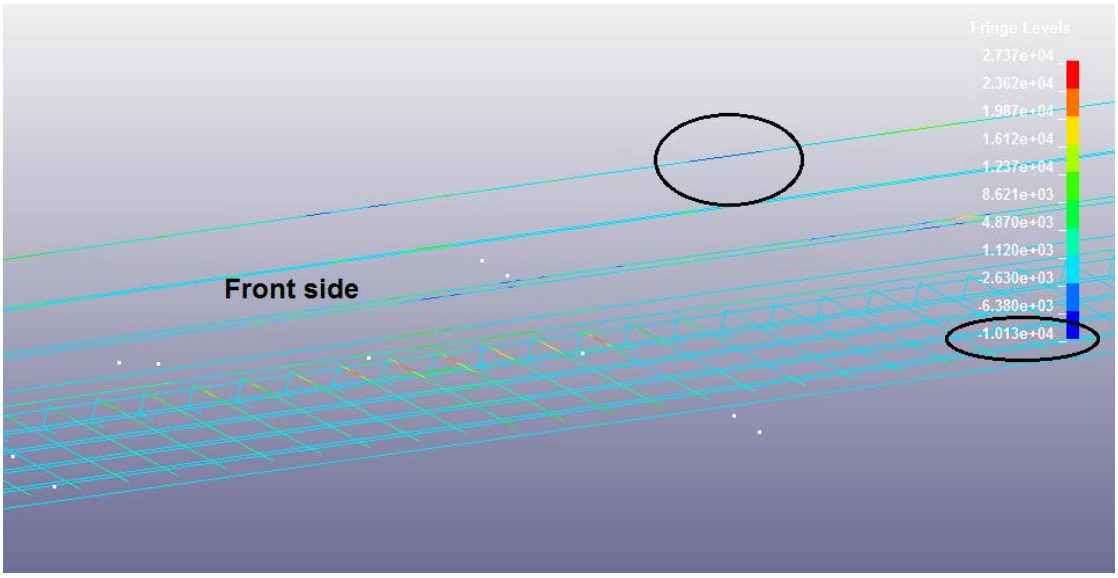

Figure 232: Axial force of the reinforcement bar in compression side at the moment of second impact: Modified New Jersey barrier – front face

7.2.1.3 Rectangular – 8 inch barrier

7.2.1.3.1 Maximum stress in the barrier

7.2.1.3.1.1 Compression side

Figure 233 shows the maximum stress in compression side of the barrier caused by the rear bumper of the truck. Maximum compression at second impact at the barrier was 30.96Mpa.

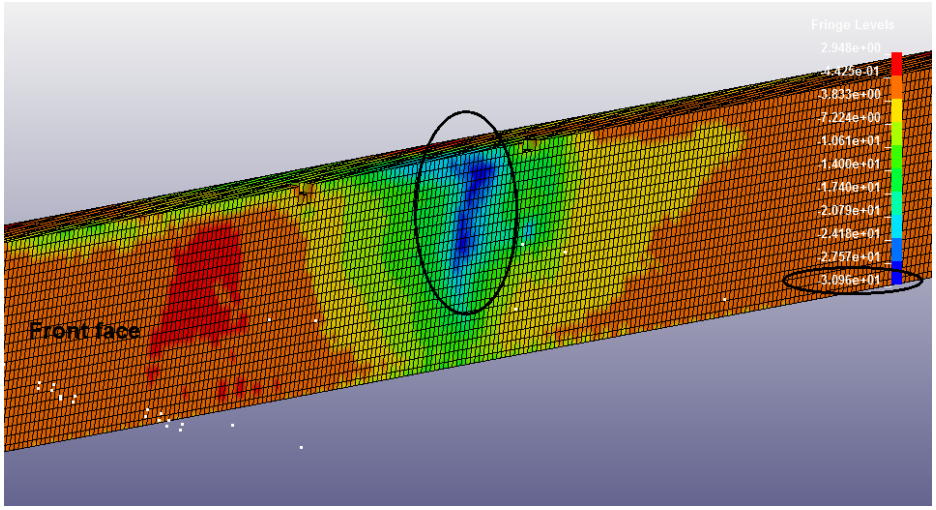

Figure 233: Second impact compression effects on Rectangular – 8 inch barrier: 3d model – front face

7.2.1.3.1.2 Tension side

Figure 234 shows the maximum stress in tension side of the barrier has been shown in the Figure ... The maximum tensile stress at the moment of second impact was 2.95 Mpa.

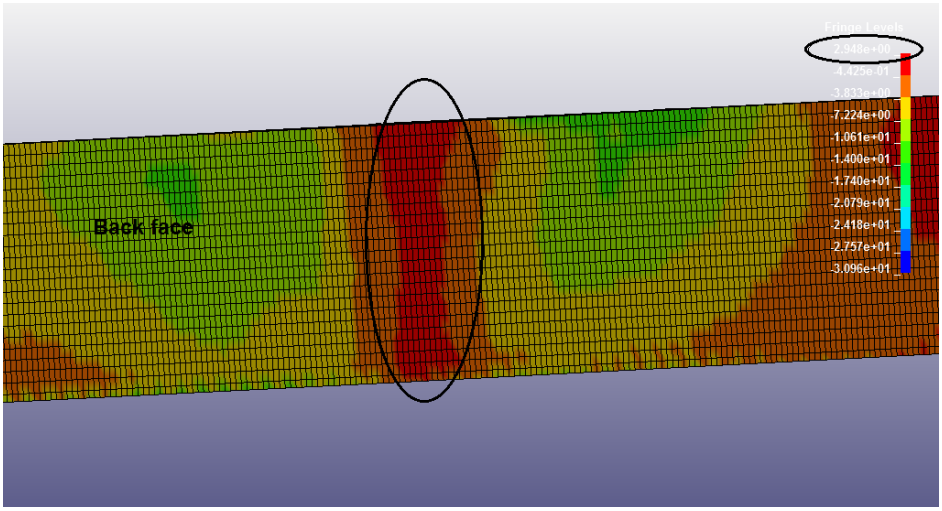

Figure 234: Second impact tension effect on Rectangular – 8 inch barrier: 3d model – back face

7.2.1.3.2 Maximum stress in the Deck Overhang

7.2.1.3.2.1 Compression side

Figure 235 shows the maximum stress in compression side of the deck overhang..

Maximum compression at second impact on the barrier was 12.15Mpa.

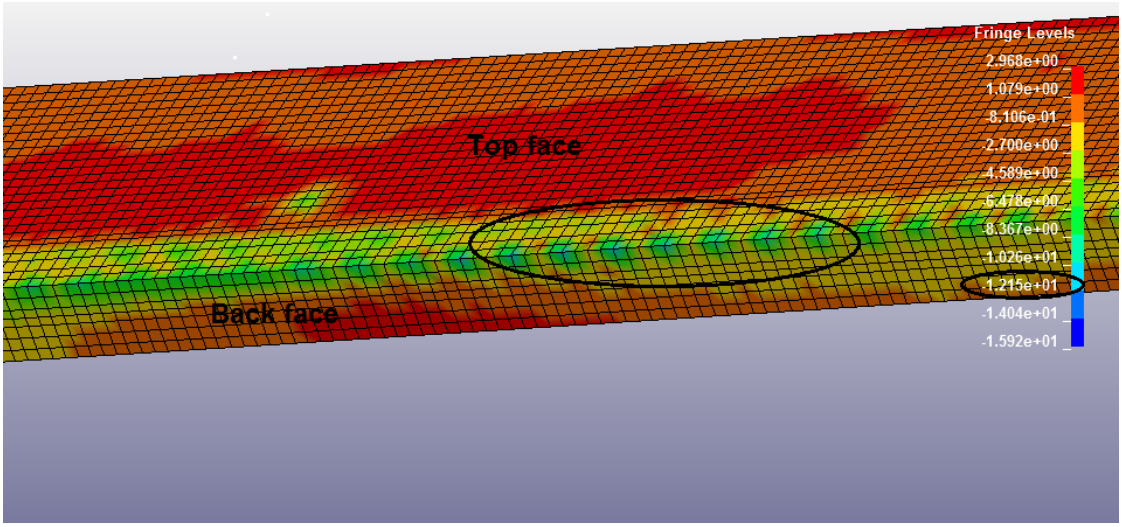

Figure 235: Rectangular – 8 inch barrier second impact in compression side of the deck overhang: top and back face

7.2.1.3.2.2 Tension side

Figure 236 shows the maximum stress in tension side of the deck overhang. The maximum tensile stress at the moment of second impact was 2.97 Mpa.

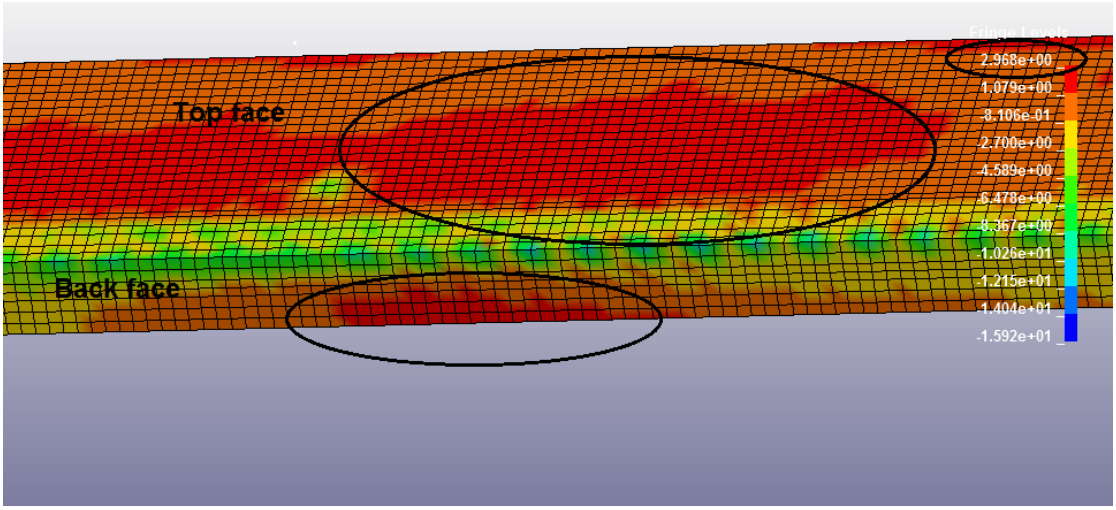

Figure 236: Rectangular – 8 inch barrier second impact in tension side of the deck overhang: top and back face

7.2.1.3.3 Maximum stress in reinforcement bars

7.2.1.3.3.1 Tension Side

Reinforcement bars are front hairpin dowels that connect barriers to deck overhangs. As seen in Figure 237, the maximum tensile reinforcement bars are #4 vertical reinforcement bars. Consequently, the tensile stress is:

5.38e4 N / 129 mm^2 = 417.05 MPa = 60.49ksi

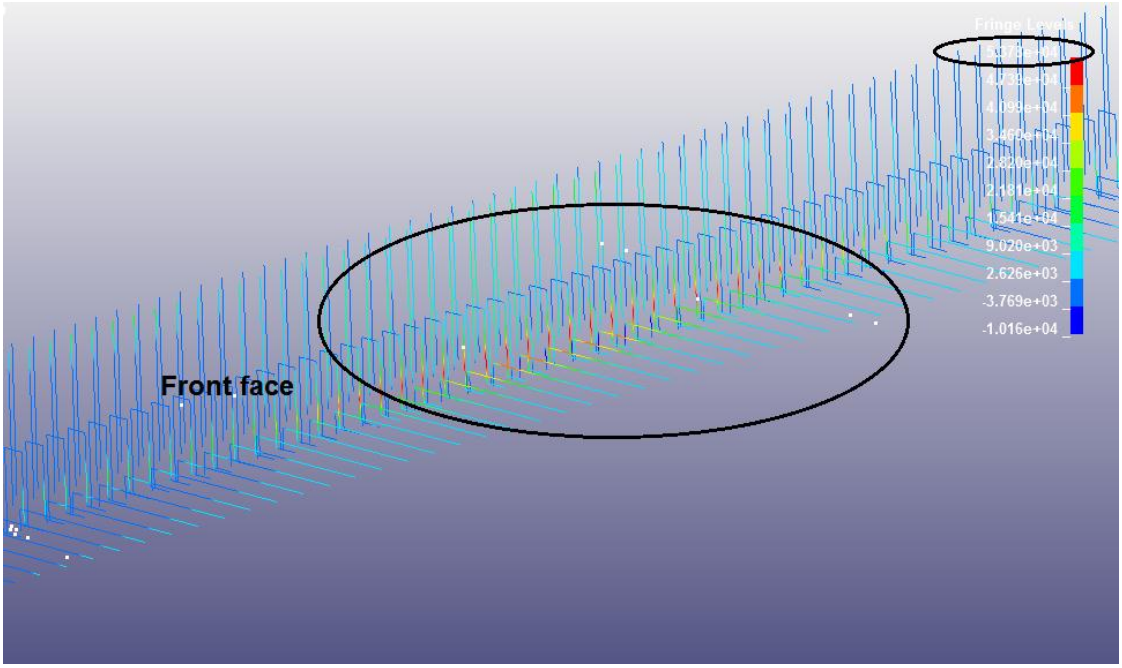

Figure 237: Axial force of the reinforcement bar in tension side at the moment of second impact: Rectangular – 8 inch – front face

7.2.1.3.3.2 Compression Side

As seen in Figure 238, the maximum compression reinforcement bars are the #3 horizontal reinforcement bars located at the middle and top face of the barrier. Thus, the compressive stress is:

3.60e3 N / 71 mm^2 = 50.70 MPa = 7.35ksi

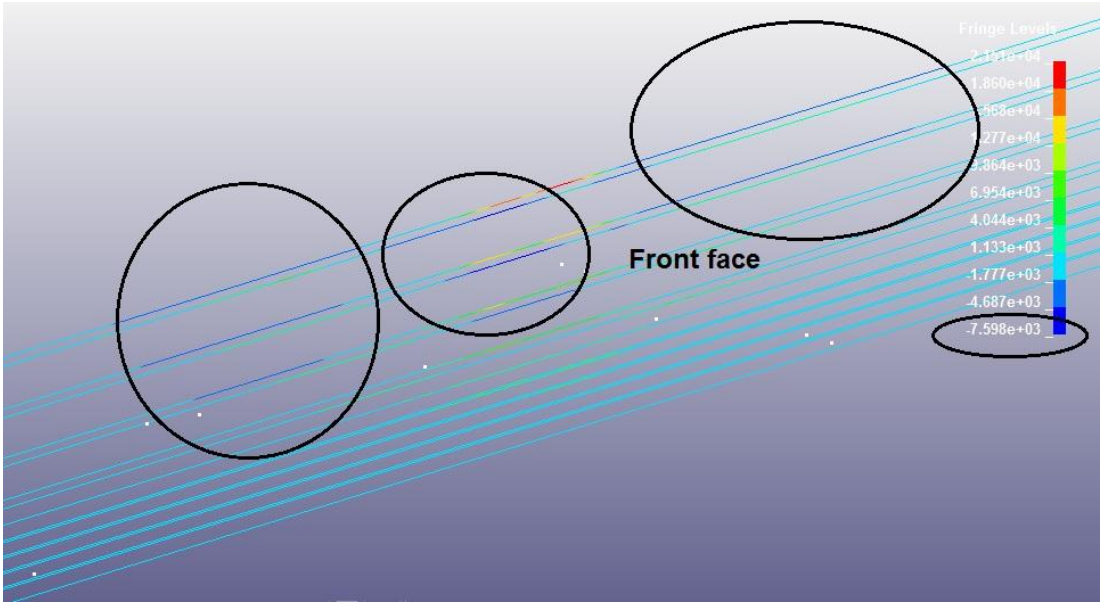

Figure 238: Axial force of the reinforcement bar in compression side at the moment of second impact: Rectangular – 8 inch – front face

7.2.1.4 Rectangular – 6 Inch Barrier

7.2.1.4.1 Maximum stress in the barrier

7.2.1.4.1.1 Compression side

Figure 239 shows the maximum stress in compression side of the barrier caused by the rear bumper of the truck. The maximum compression at second impact on the barrier was 42.89 Mpa.

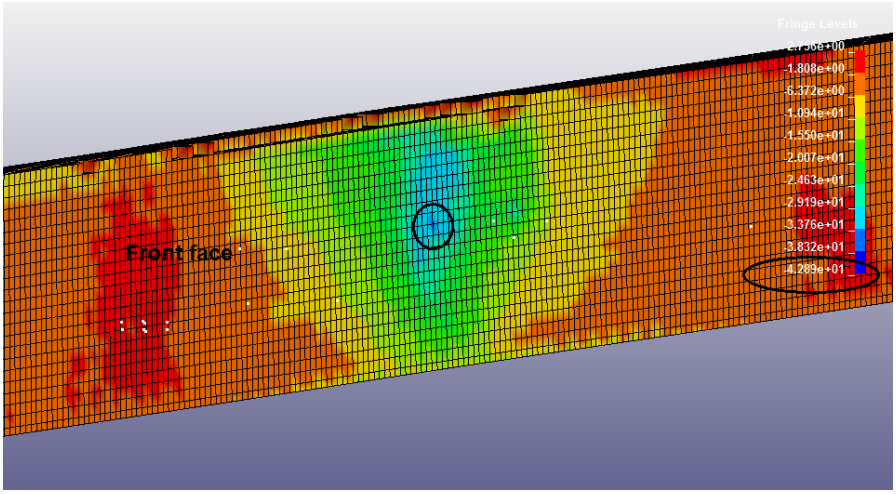

Figure 239: Second impact compression effects on Rectangular – 6 inch Barrier: 3d model – front face

7.2.1.4.1.2 Tension side

Figure 240 shows the maximum stress in tension side of the barrier. The maximum tensile stress at the moment of second impact was 2.76Mpa.

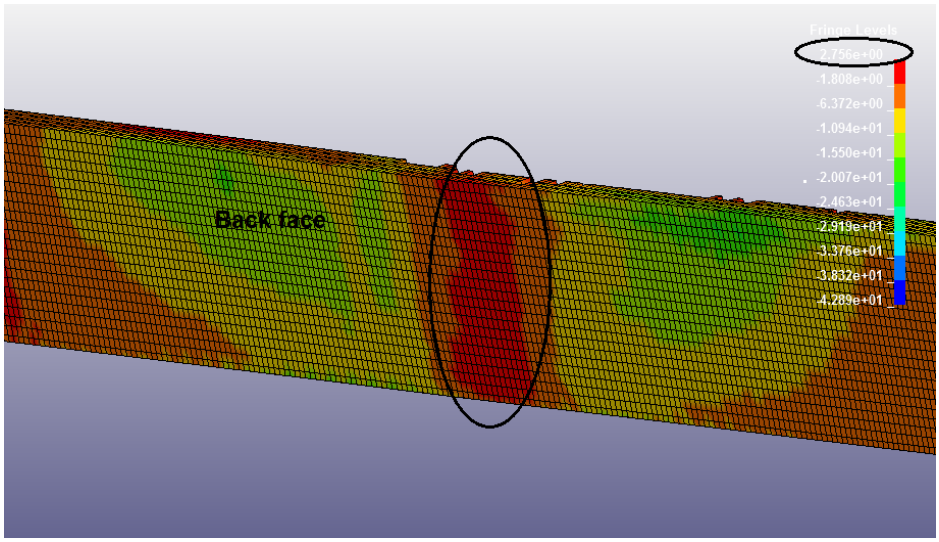

Figure 240: Second impact tension effect on Rectangular 6 inch barrier: 3d model – back face

7.2.1.4.2 Maximum stress in the deck overhang

7.2.1.4.2.1 Compression Side

Figure 241 shows the maximum stress in compression side of the deck overhang . The maximum compression at second impact on the barrier was 21.14Mpa.

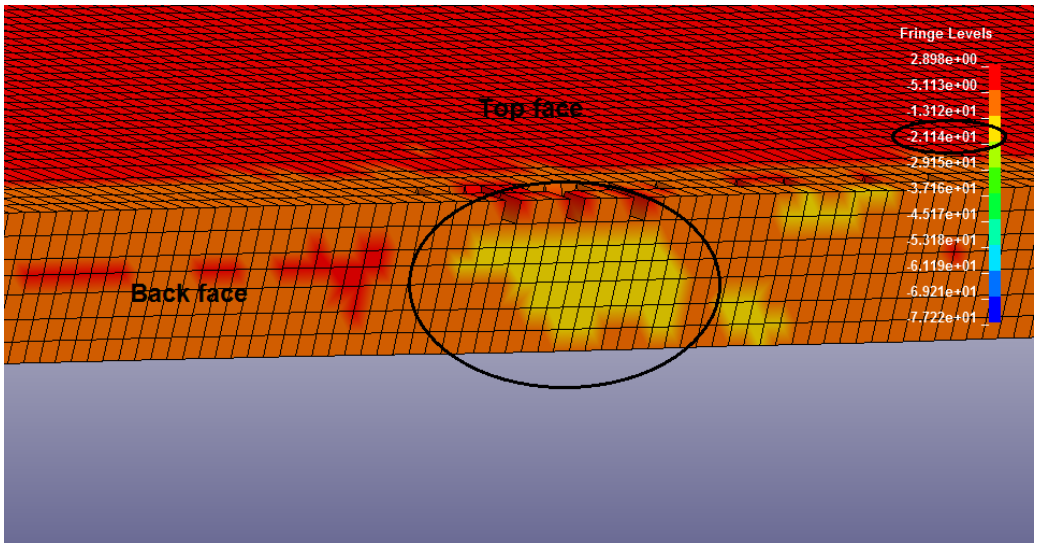

Figure 241: Rectangular – 6 inch barrier second impact in compression side of the deck overhang: top and back face

7.2.1.4.2.2 Tension side

Figure 242 shows the maximum stress in tension side of the deck overhang. The maximum tensile stress at the moment of second impact was 2.90 Mpa.

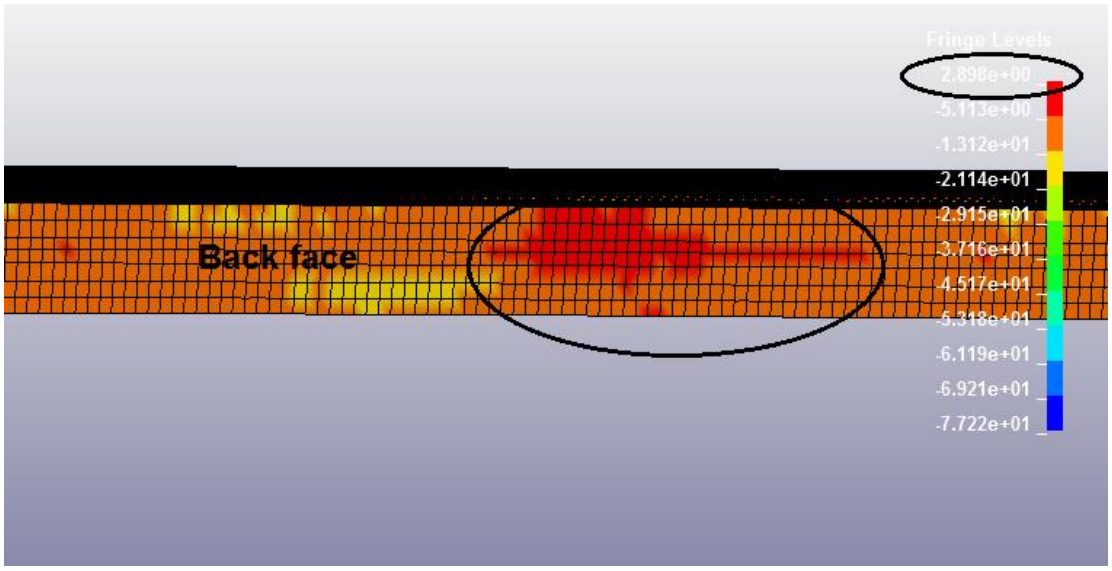

Figure 242: Rectangular – 6 inch barrier second impact in tension side of the deck overhang: back face

7.2.1.4.3 Maximum stress in reinforcement bars

7.2.1.4.3.1 Tension Side

As seen in Figure 243, the maximum tensile reinforcement bars are the #4 vertical reinforcement bars. Reinforcement bars are front hairpin dowels that connect barrier to deck overhang. Therefore, the tensile stress is:

5.47e4 N / 129 mm^2 = 424.03 MPa = 61.50ksi

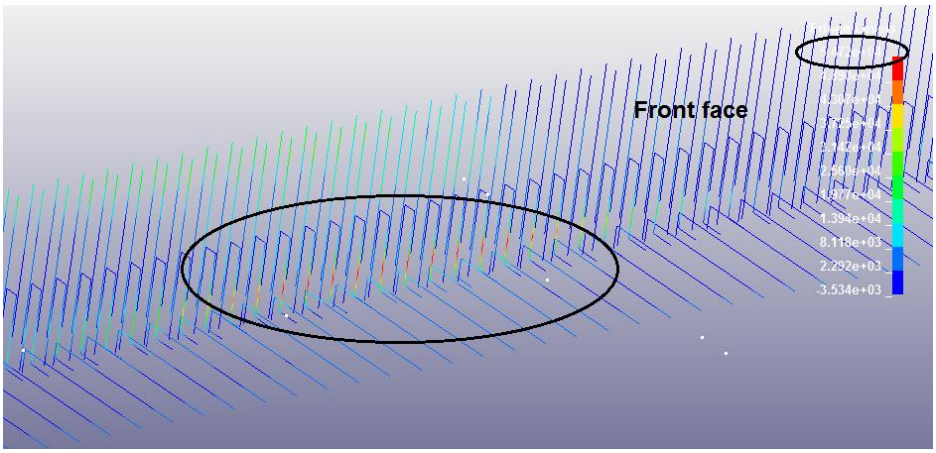

Figure 243: Axial force of the reinforcement bar in tension side at the moment of second impact: Rectangular – 6 inch – front face

7.2.1.4.3.2 Compression side

As seen in Figure 244, the maximum compression reinforcement bars are the #3 horizontal reinforcement bars located at the bottom face of the barrier. Thus, the compressive stress is:

1.60e4 N / 71 mm^2 = 225.35 MPa = 32.68ksi

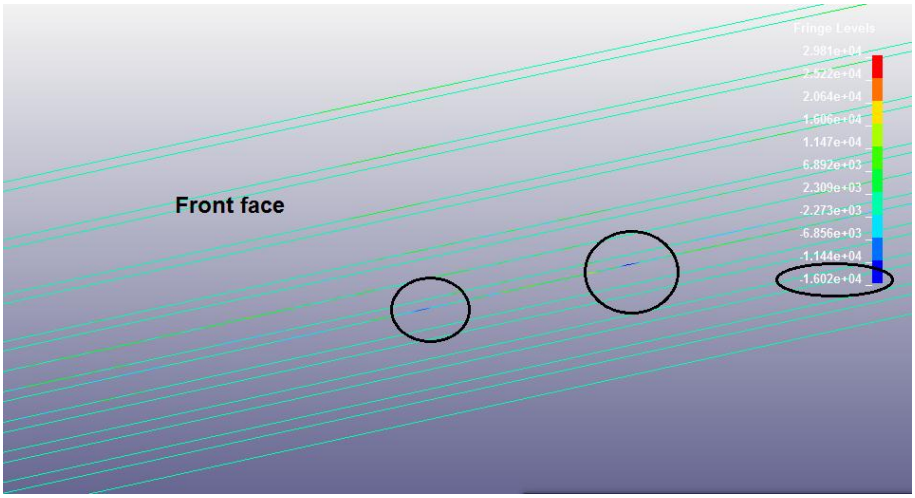

Figure 244: Axial force of the reinforcement bar in compression side at the moment of second impact: Rectangular – 6 inch – front face

7.2.1.5 Modified single-slope barrier

7.2.1.5.1 Maximum stress in the barrier

7.2.1.5.1.1 Compression Side

Figure 245 shows the maximum stress in compression side of the barrier caused by the rear bumper of the truck. Maximum compression at second impact at the barrier was 22.65Mpa.

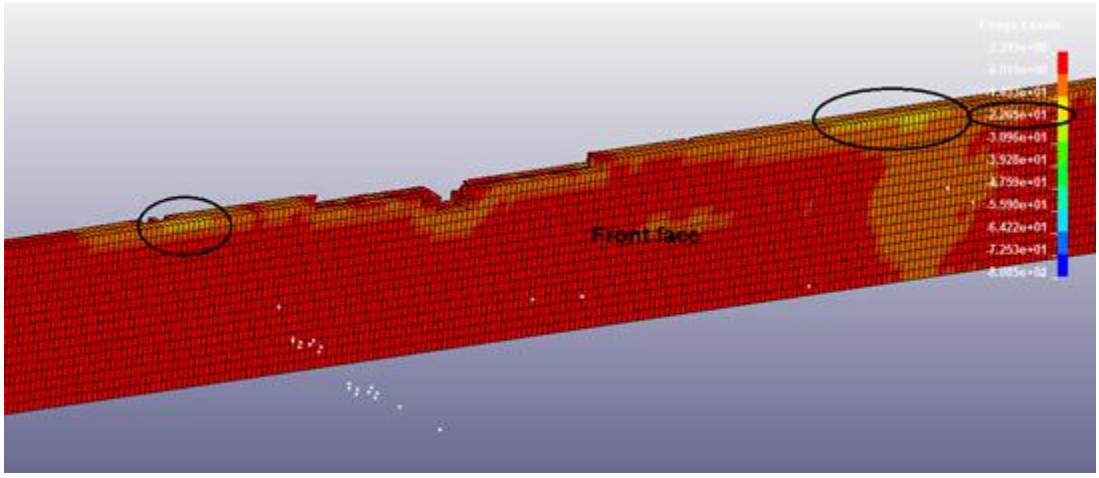

Figure 245: Second impact compression effects on modified single-slope barrier: 3d model – front face

7.2.1.5.1.2 Tension side

Figure 246 shows the maximum stress in tension side of the barrier. The maximum tensile stress in the moment of second impact was 2.30Mpa.

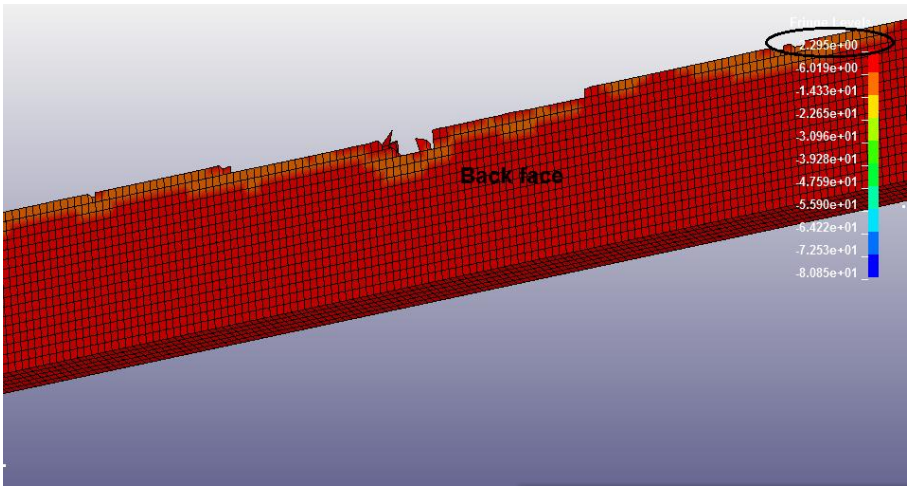

Figure 246: Second impact tension effect on modified single-slope barrier: 3d model – back face

7.2.1.5.2 Maximum stress in the deck overhang

7.2.1.5.2.1 Compression side

Figure 247 shows the maximum stress in compression side of the deck overhang.

Maximum compression at second impact on the barrier was 14.30Mpa.

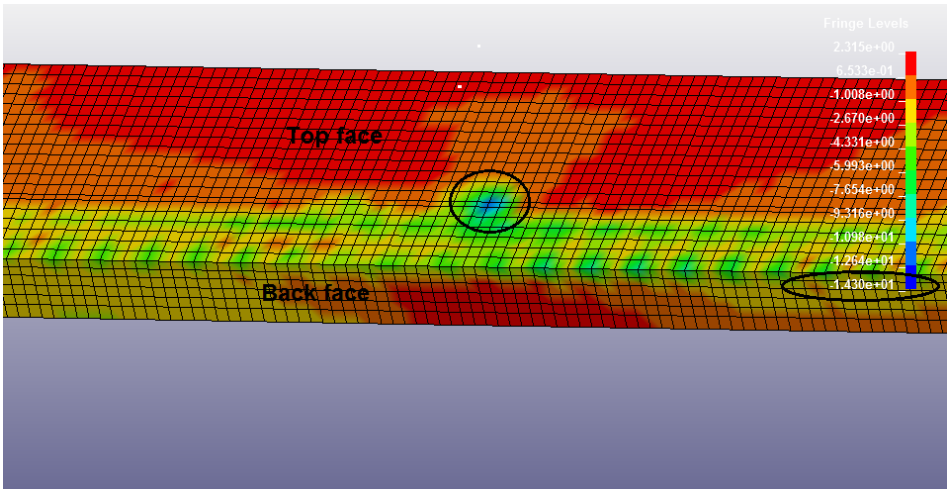

Figure 247: Modified single-slope barrier second impact in compression side of the deck overhang: top and back face

7.2.1.5.2.2 Tension side

Figure 248 shows the maximum stress in tension side of the deck overhang. The maximum tensile stress at the moment of second impact was 2.32Mpa.

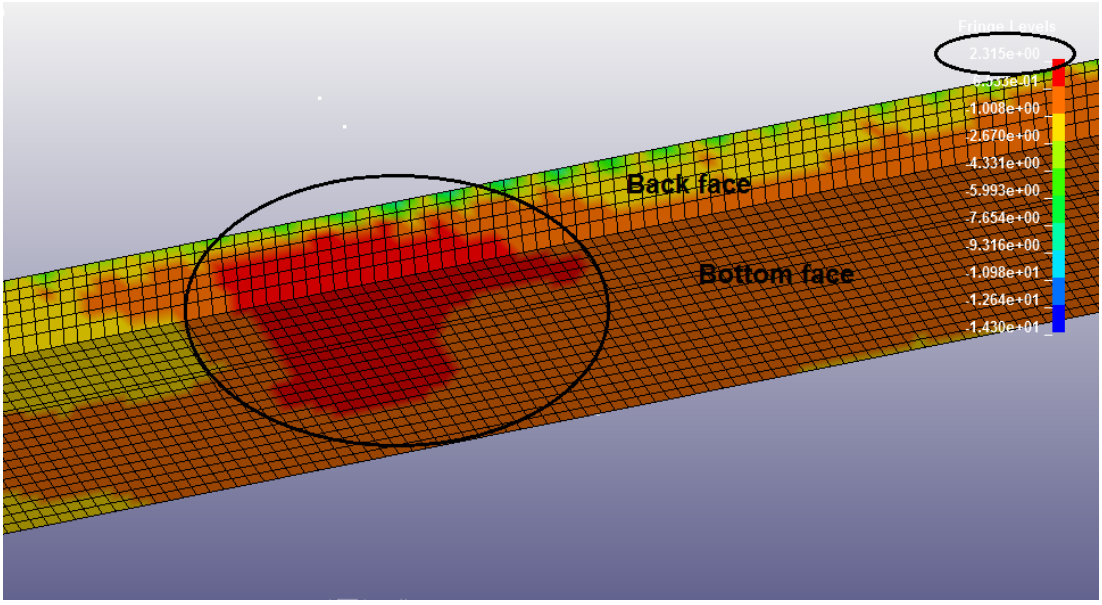

Figure 248: Modified single-slope barrier second impact in tension side of the deck overhang: bottom and back face

7.2.1.5.3 Maximum stress in reinforcement bars

7.2.1.5.3.1 Tension side

As seen in Figure 249, the maximum tensile reinforcement bars are the #4 vertical reinforcement bars. Reinforcement bars are front hairpin dowels that connect barrier to deck overhang. Hence, the tensile stress is:

4.58e4 N / 129 mm^2 = 355.04 MPa = 51.49ksi

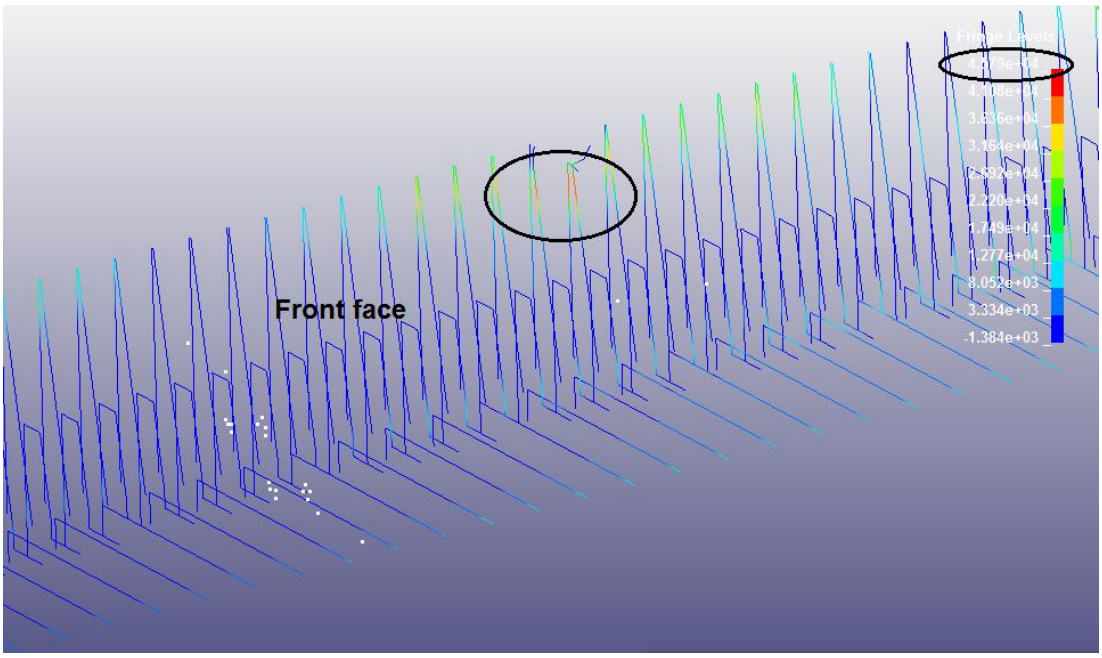

Figure 249: Axial force of the reinforcement bar in tension side at the moment of second impact: Modified single-slope – front face

7.2.1.5.3.2 Compression side

As seen in Figure 250, the maximum compression reinforcement bars are the horizontal #3 reinforcement bars located at the bottom, middle and top face of the barrier. Hence, the compressive stress is:

4.48e3 N / 71 mm^2 = 63.10 MPa = 9.15ksi

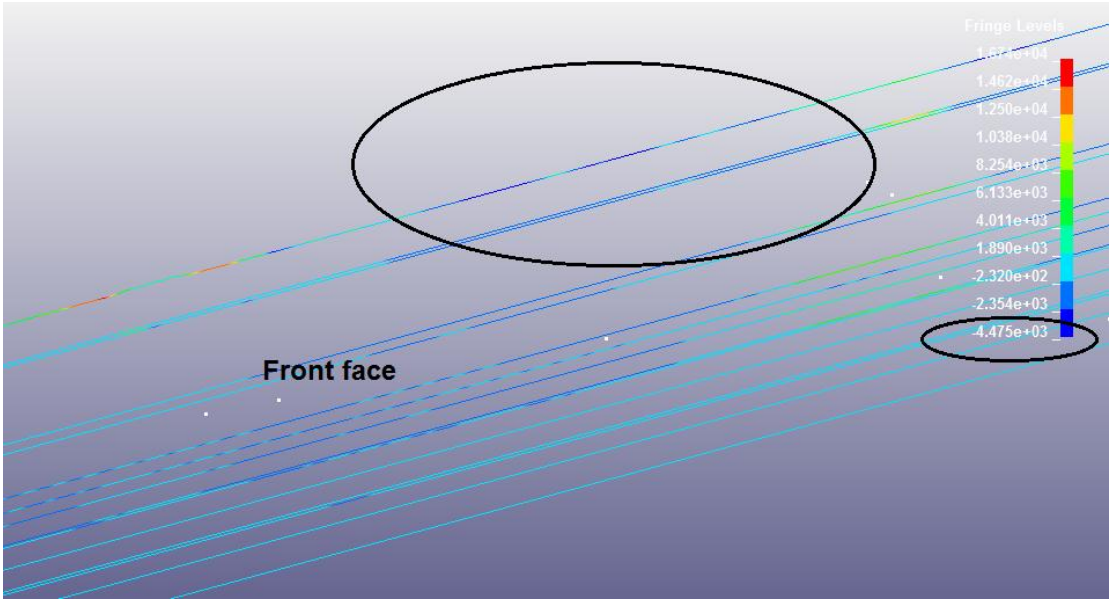

Figure 250: Axial force of the reinforcement bar in compression side at the moment of second impact: Modified single-slope – front face

7.2.1.6 Inverted modified single-slope barrier

7.2.1.6.1 Maximum stress in the barrier

7.2.1.6.1.1 Compression side

Figure 251 shows the maximum stress in compression side of the barrier caused by the impact of the rear bumper of the truck. The maximum compression at the second impact at the barrier was 24.27Mpa.

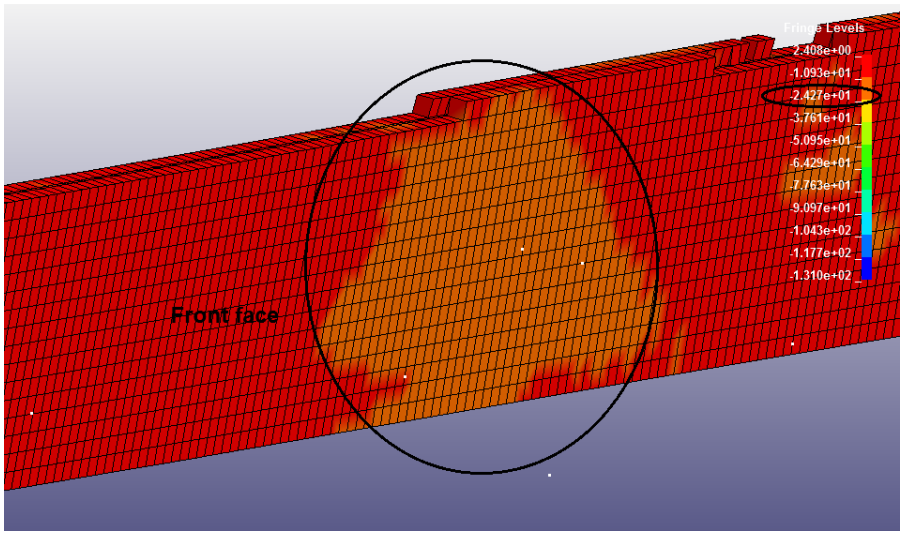

Figure 251: Second impact compression effects on inverted modified single-slope barrier: 3d model – front face

7.2.1.6.1.2 Tension side

Figure 252 shows the maximum stress in tension side of the barrier. The maximum tensile stress at the moment of second impact was 2.41Mpa.

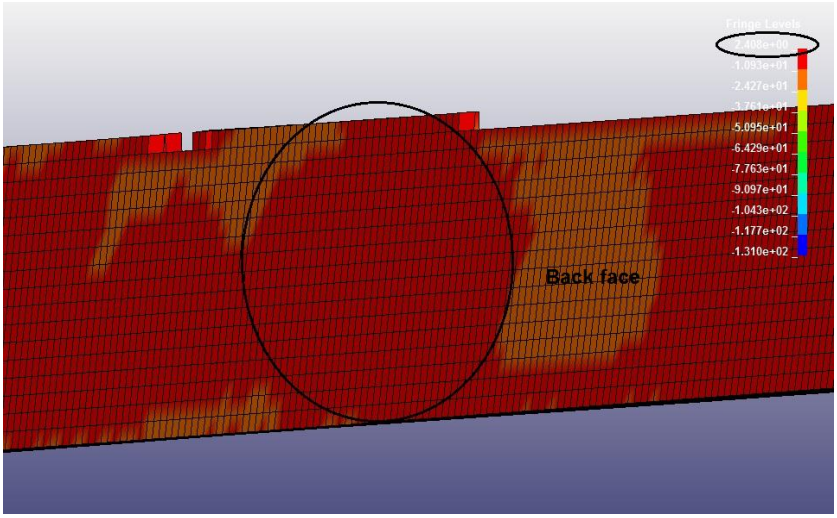

Figure 252: Second impact tension effect on inverted modified single-slope barrier: 3d model – back face

7.2.1.6.2 Maximum stress in the deck overhang

7.2.1.6.2.1 Compression side

Figure 253 shows the maximum stress in compression side of the deck overhang. Maximum compression at second impact on the barrier was 21.37 Mpa.

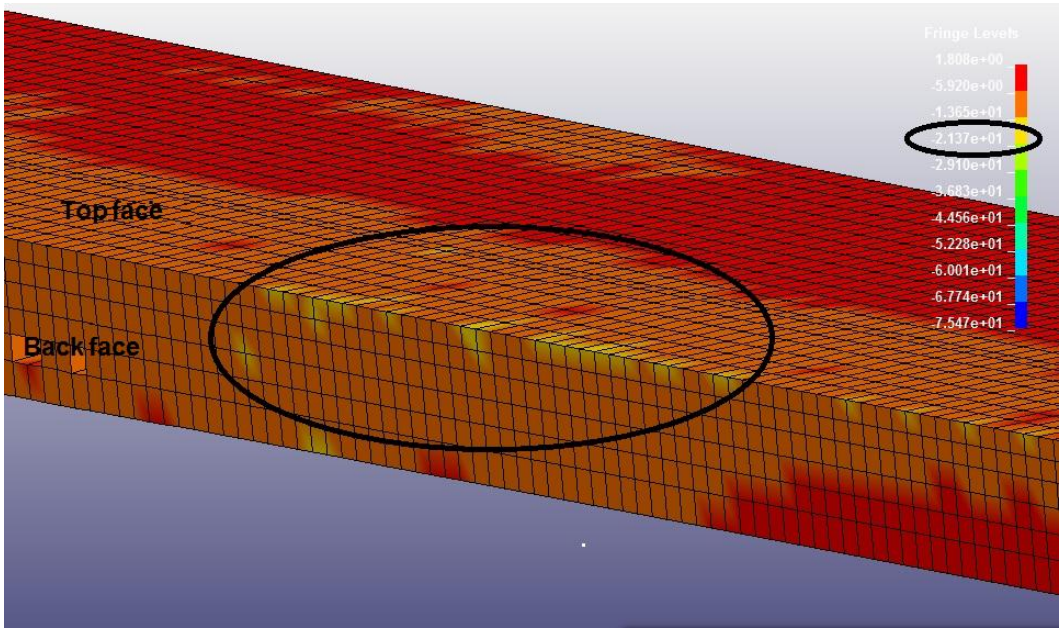

Figure 253: Inverted modified single-slope barrier second impact in compression side of the deck overhang: top and back face

7.2.1.6.2.2 Tension side

Figure 254 shows the maximum stress in tension side of the deck overhang. The maximum tensile stress at the moment of second impact was 2.37 Mpa.

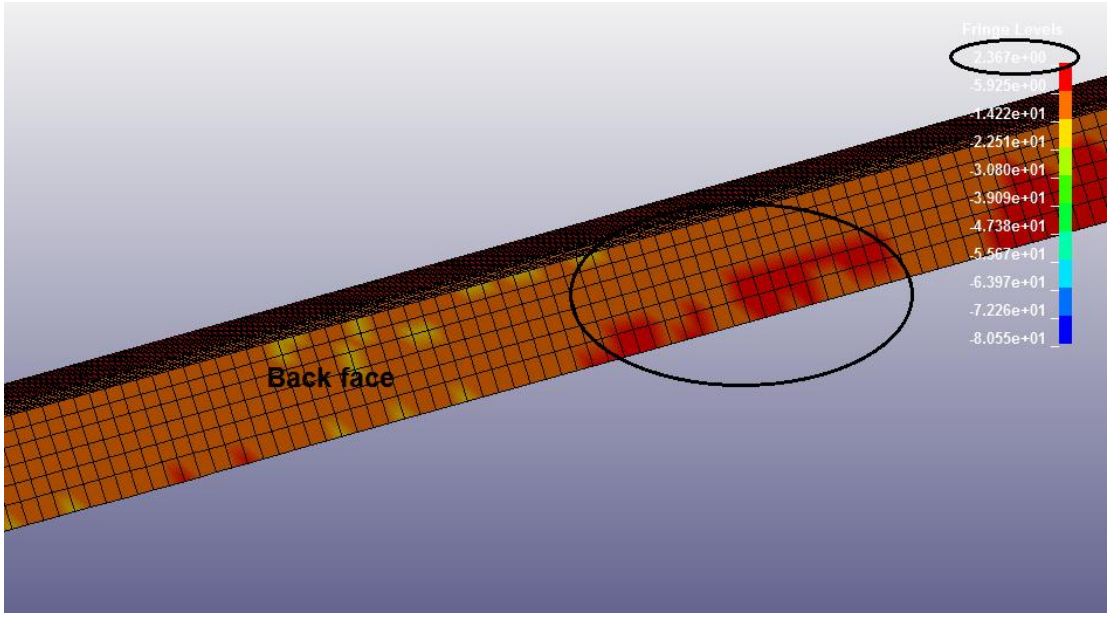

Figure 254: Inverted modified single-slope barrier second impact in tension side of the deck overhang: top and back face

7.2.1.6.3 Maximum stress in reinforcement bars

7.2.1.6.3.1 Tension side

As seen in Figure 255, the maximum tensile reinforcement bars are the #4 hairpin dowels that connect the barrier to the deck overhang and the topside reinforcement bars located in the deck overhang. Hence, the tensile stress is:

6.00e4 N / 129 mm^2 = 465.12 MPa = 67.46ksi

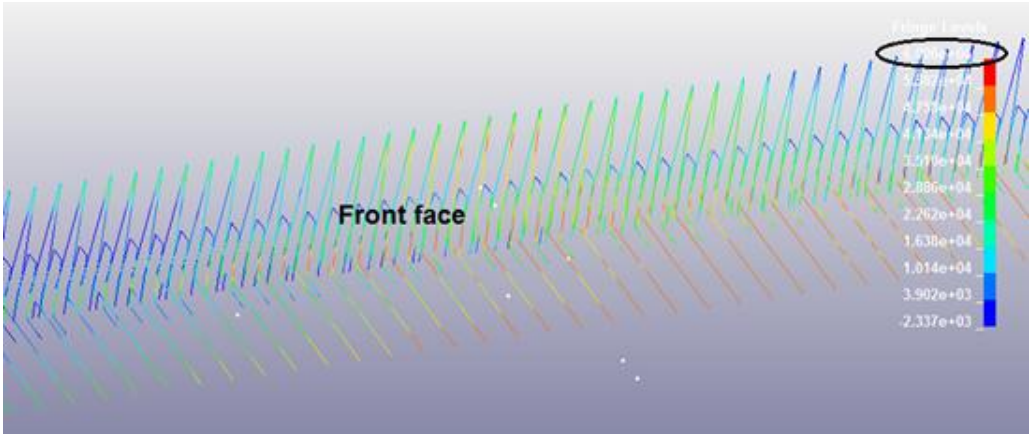

Figure 255: Axial force of the reinforcement bar in tension side at the moment of second impact: Inverted modified single-slope – front face

7.2.1.6.3.2 Compression side

As seen in Figure 256, the maximum compression reinforcement bars are #3 horizontal and located at the top of the deck overhang. Consequently, the compressive stress is:

1.19e4 N / 71 mm^2 = 167.61 MPa = 24.31ksi

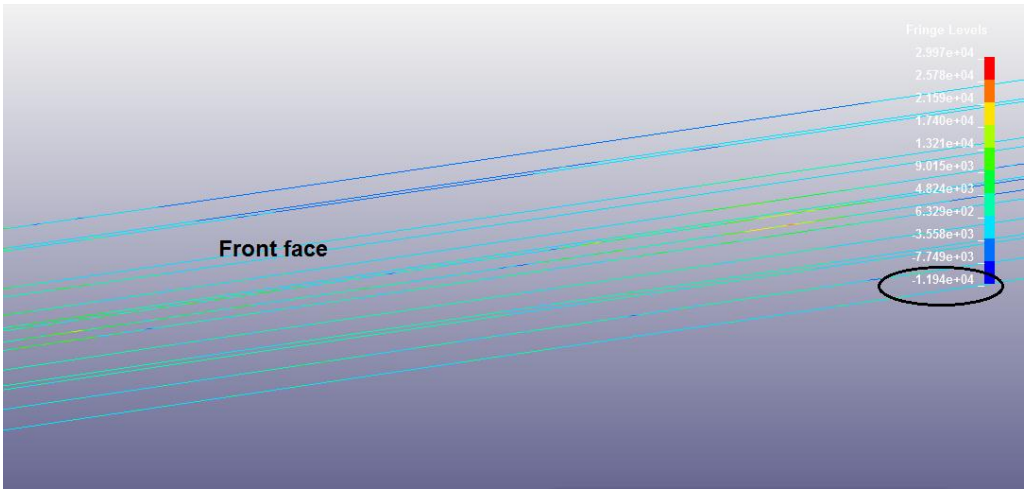

Figure 256: Axial force of the reinforcement bar in compression side at the moment of second impact: Inverted modified single-slope – front face

7.2.2 Maximum Deflection

This Sub-Chapter shows the maximum deflection of the barrier and deck overhang based on single unit truck second impact.

7.2.2.1 New Jersey Barrier

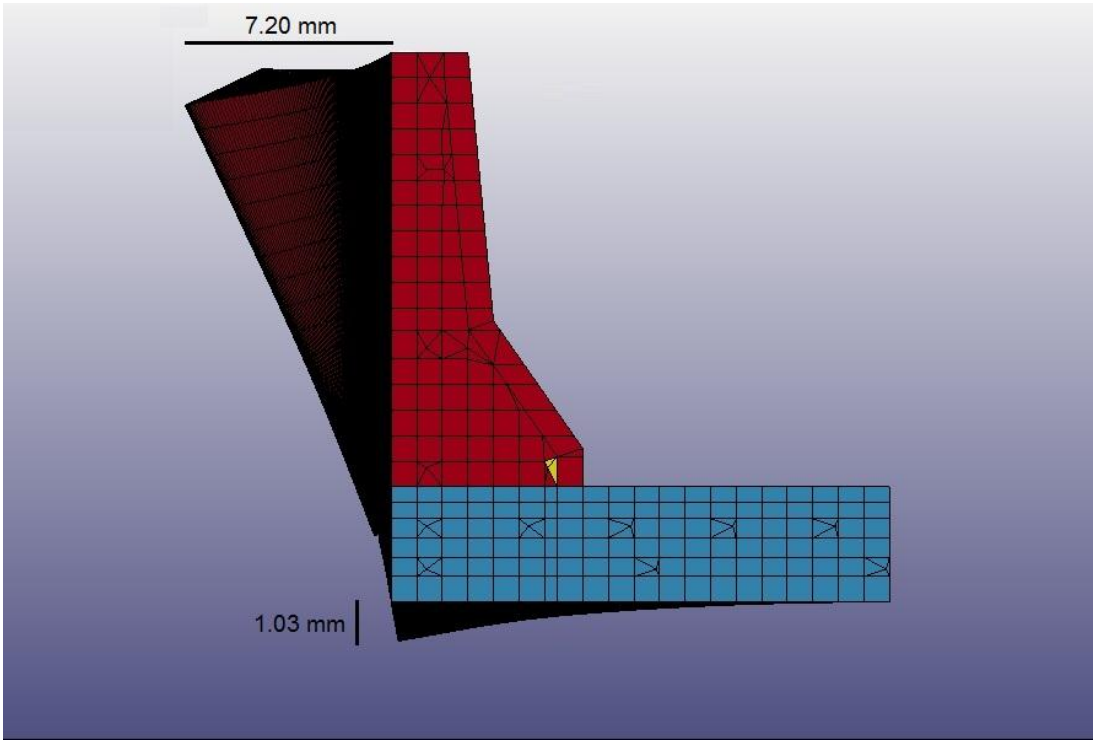

Figure 257: Maximum deflection of barrier and deck overhang – New Jersey

7.2.2.1.1 Maximum deflection in barrier

As seen in Figure 258, maximum deflection in the barrier in moment .44 sec was 7.20 mm or 0.28 inches.

Figure 258: Maximum deflection of the barrier at second impact – New Jersey geometry

7.2.2.1.2 Maximum deflection in deck overhang

As seen in Figure 259, maximum deflection in the deck overhang at moment 0.44 sec was 1.03 mm or 0.04 inches.

Figure 259: Maximum deflection of the deck overhang at second impact – New Jersey geometry

This Sub-Chapter shows the maximum deflection of the barrier and deck overhang based on single unit truck second impact.

7.2.2.2 Modified New-Jersey Barrier

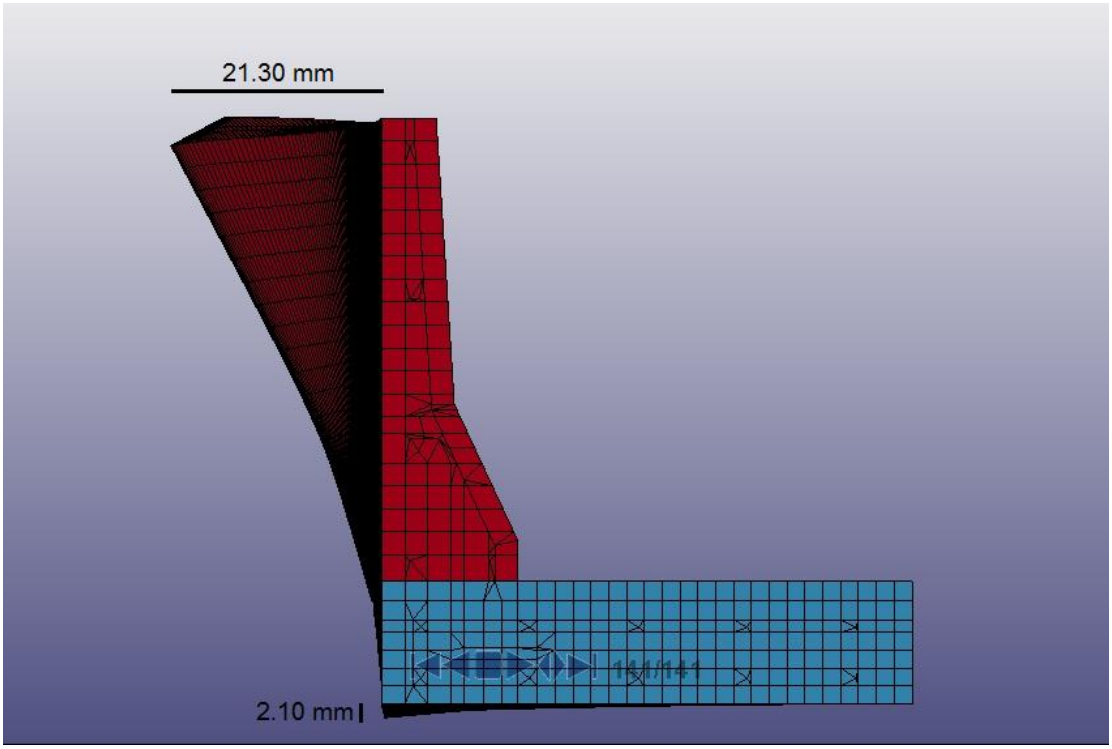

Figure 260: Maximum deflection of barrier and deck overhang – modified New Jersey

7.2.2.2.1 Maximum Deflection in Barrier

As seen in Figure 261, maximum deflection in the barrier in moment 0.455 sec was 21.30 mm or 0.84 inches.

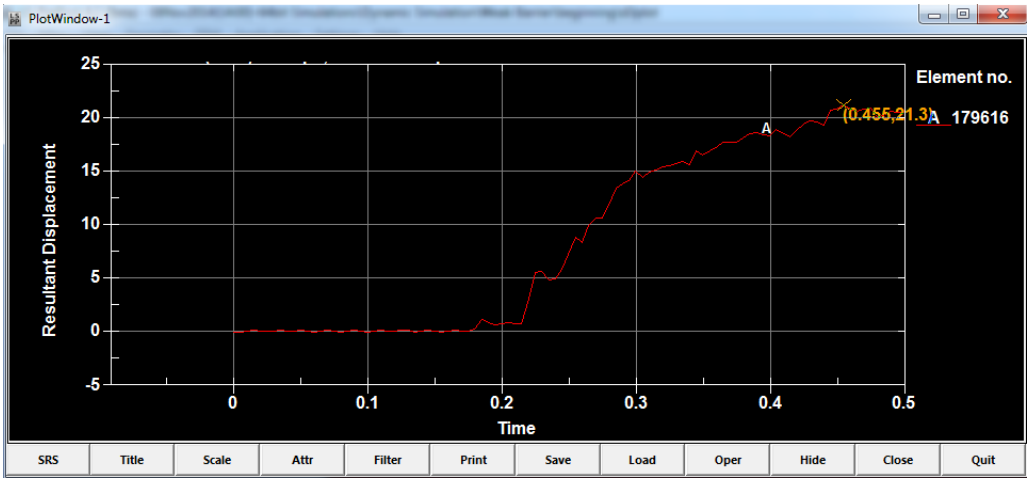

Figure 261: Maximum deflection of the barrier at second impact – modified New Jersey geometry

7.2.2.2.2 Maximum deflection in deck overhang

As seen in Figure 262, maximum deflection in the deck overhang at moment 0.46 sec was 2.10 mm or 0.08 inches.

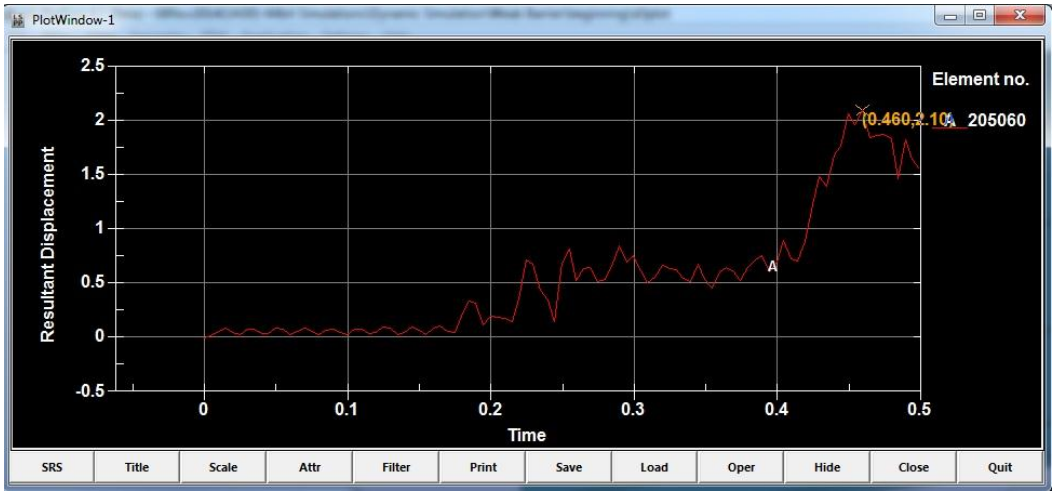

Figure 262: Maximum deflection of the deck overhang at second impact – modified New Jersey geometry

7.2.2.3 Rectangular – 8 inch Barrier

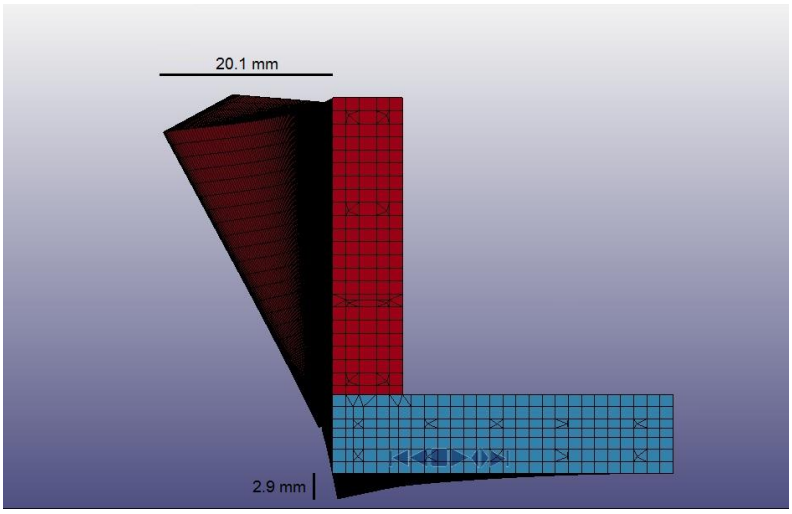

Figure 263: Maximum deflection of barrier and deck overhang – Rectangular – 8 inch

7.2.2.3.1 Maximum deflection in barrier

As seen in Figure 264, maximum deflection in the barrier at moment 0.415 sec was 20.1 mm or 0.79 inches.

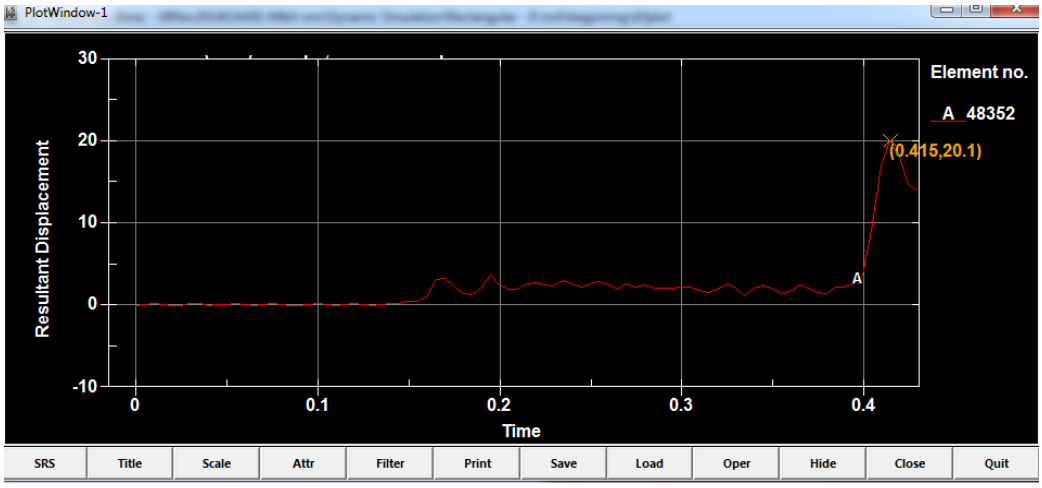

Figure 264: Maximum deflection of the barrier at second impact: Rectangular – 8 inch geometry

7.2.2.3.2 Maximum deflection in deck overhang

As seen in Figure 265, maximum deflection in the deck overhang at moment 0.415 sec was 2.9 mm or 0.11 inches.

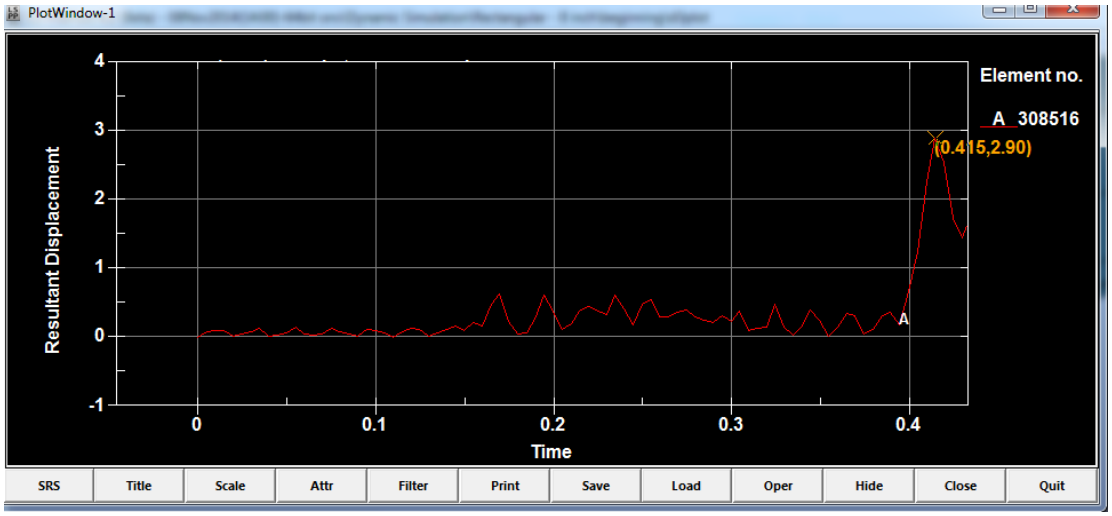

Figure 265: Maximum deflection of the deck overhang at second impact: Rectangular – 8 inch geometry

7.2.2.4 Rectangular – 6 inch Barrier

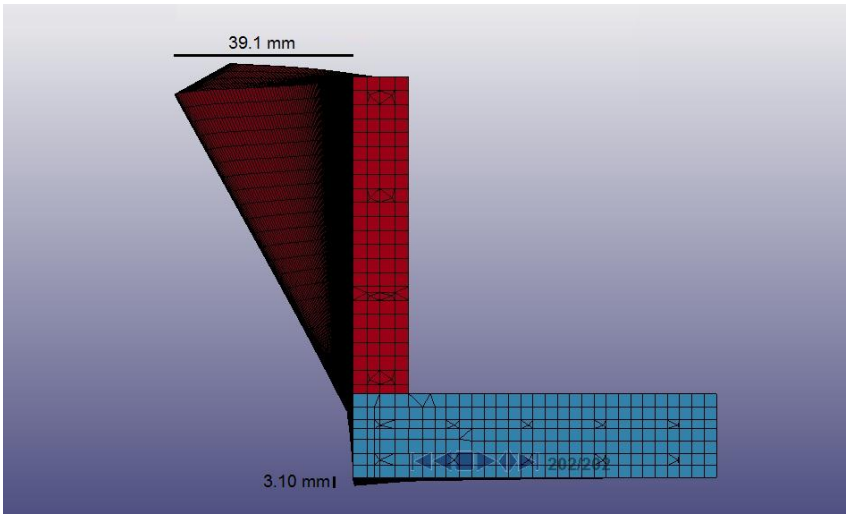

Figure 266: Maximum deflection of barrier and deck overhang: Rectangular – 6 inch

7.2.2.4.1 Maximum Deflection in Barrier

As seen in Figure 267, maximum deflection in the barrier at moment 0.435 sec was 39.1 mm or 1.54 inches.

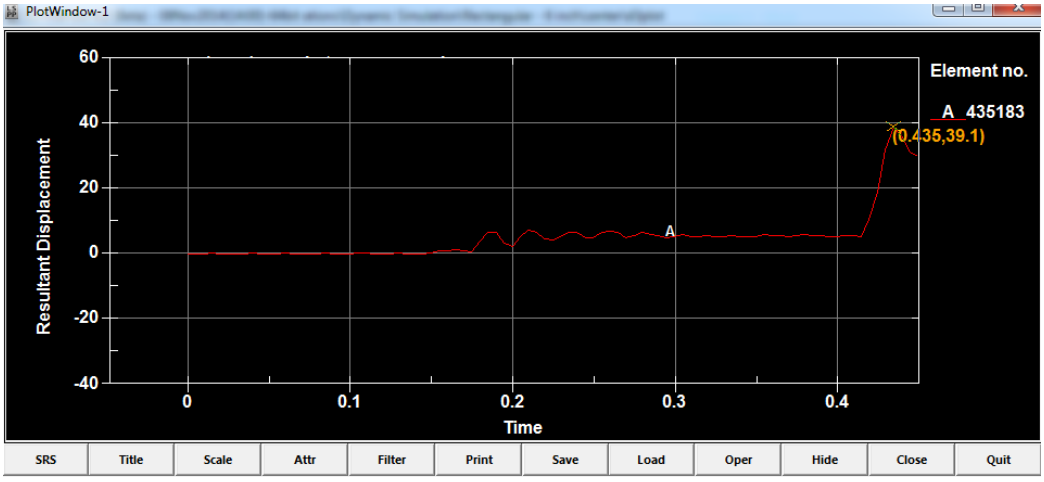

Figure 267: Maximum deflection of the barrier at second impact: Rectangular – 6 inch geometry

7.2.2.4.2 Maximum Deflection in Deck Overhang

As seen in Figure 268, maximum deflection in the deck overhang at moment 0.435 sec was 3.10 mm or 0.12 inches.

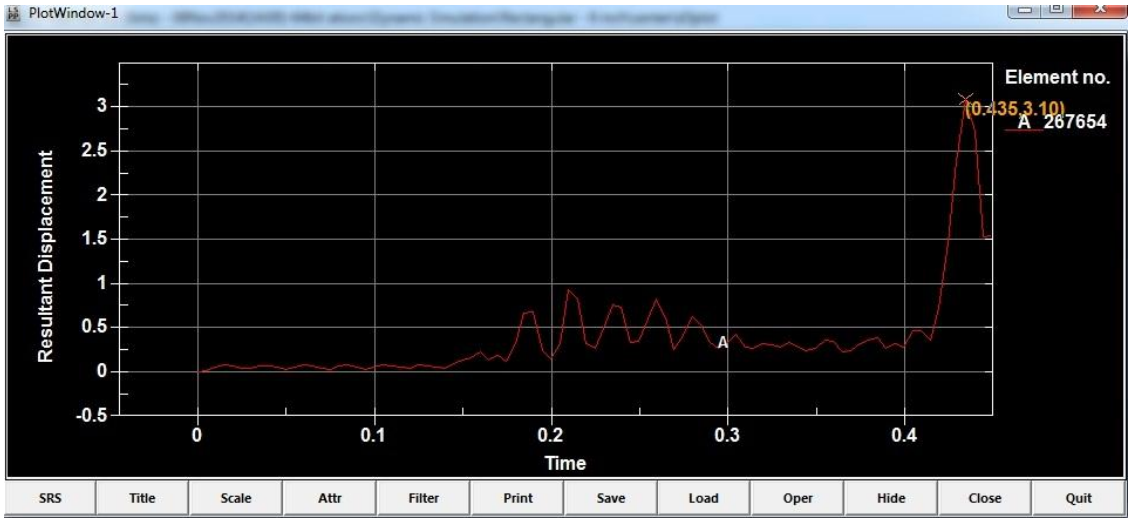

Figure 268: Maximum deflection of the deck overhang at second impact: Rectangular – 6 inch geometry

7.2.2.5 Modified Single-Slope barrier

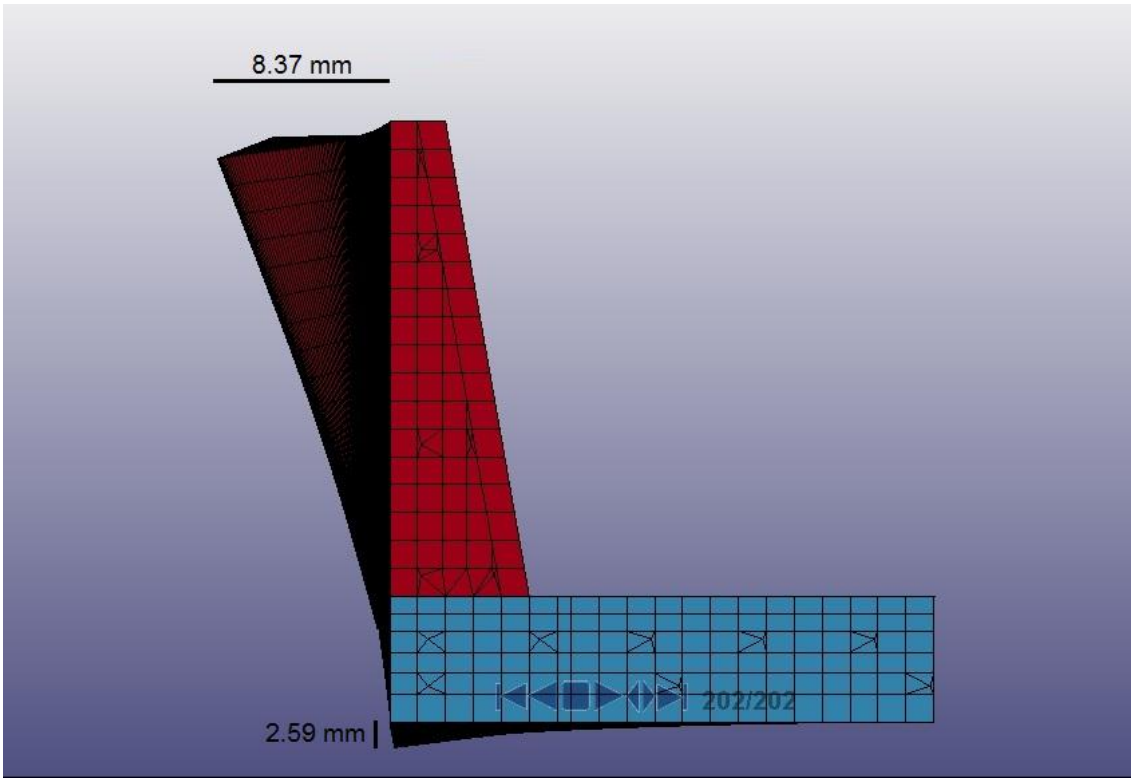

Figure 269: Maximum deflection of barrier and deck overhang: Modified single-slope

7.1.2.5.1 Maximum deflection in barrier

As seen in Figure 270, maximum deflection in the barrier at moment 0.45 sec was 8.37 mm or 0.33 inches.

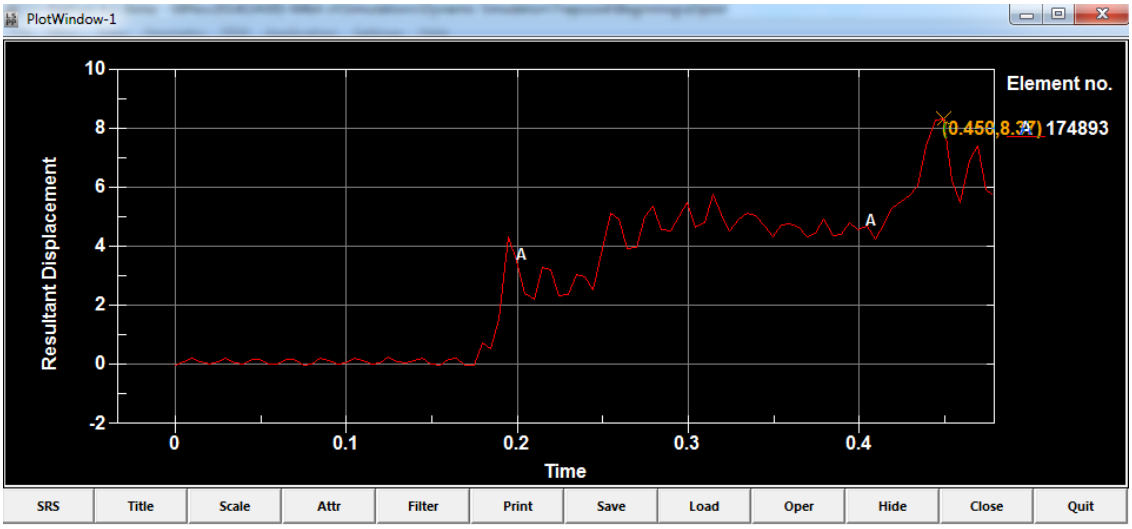

Figure 270: Maximum deflection of the barrier at second impact – Modified single-slope geometry

7.2.2.5.2 Maximum deflection in deck overhang

As seen in Figure 271, maximum deflection in the deck overhang at moment 0.45 sec was 2.59 mm or 0.10 inches.

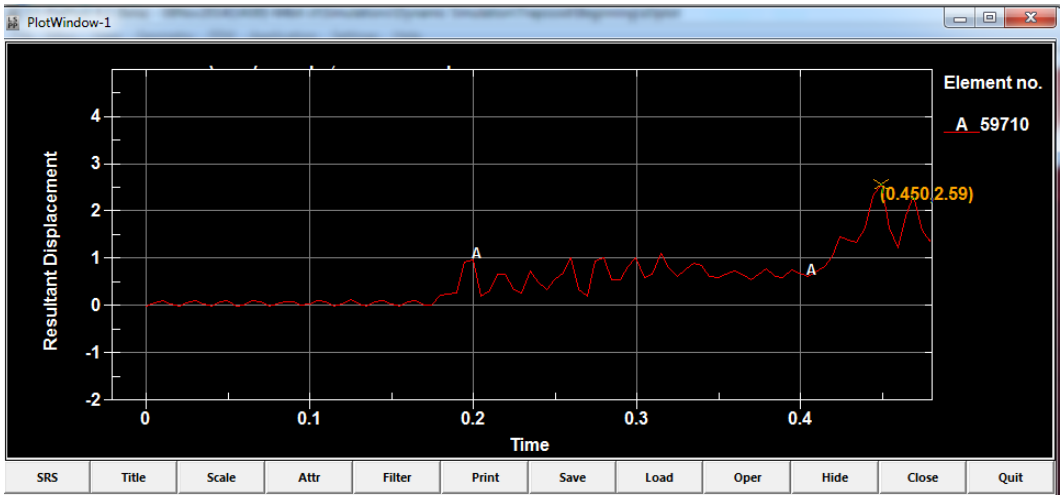

Figure 271: Maximum deflection of the deck overhang at second impact: Modified single-slope geometry

7.2.2.6 Inverted modified single-slope barrier

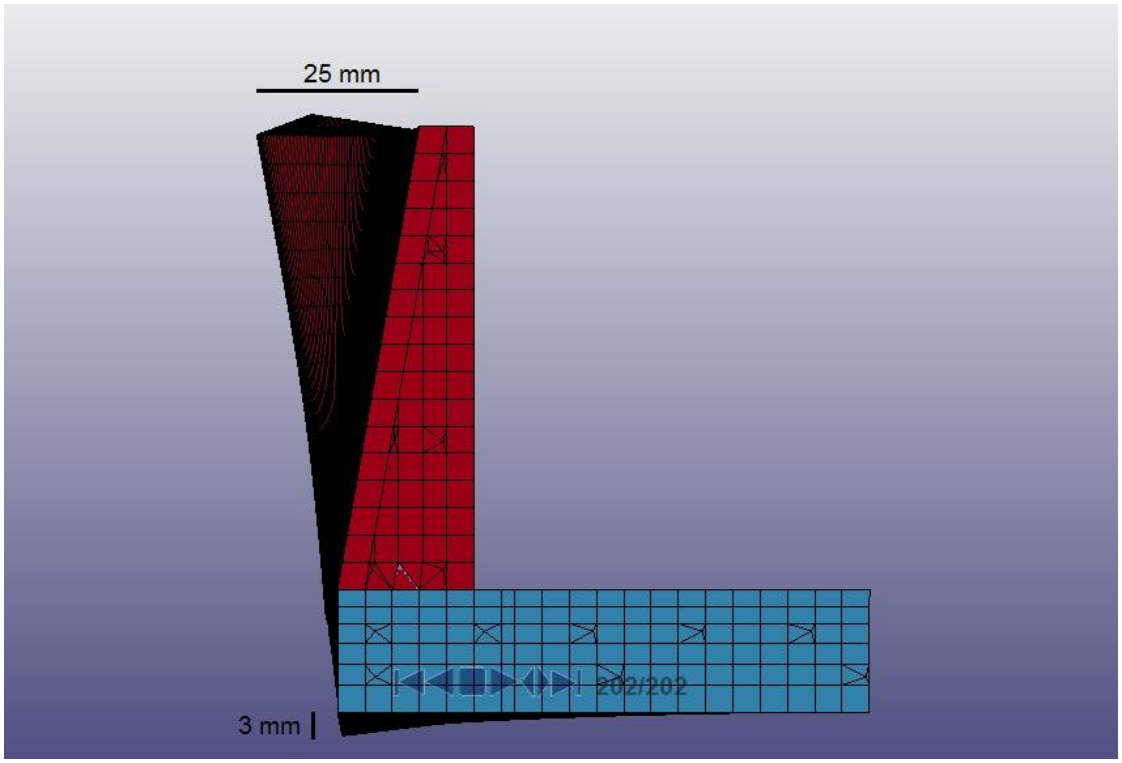

Figure 272: Maximum deflection of barrier and deck overhang: Inverted modified single-slope

7.2.2.6.1 Maximum deflection in barrier

As seen in Figure 273, maximum deflection in the barrier at moment 0.425 sec was 25 mm or to 0.98 inches.

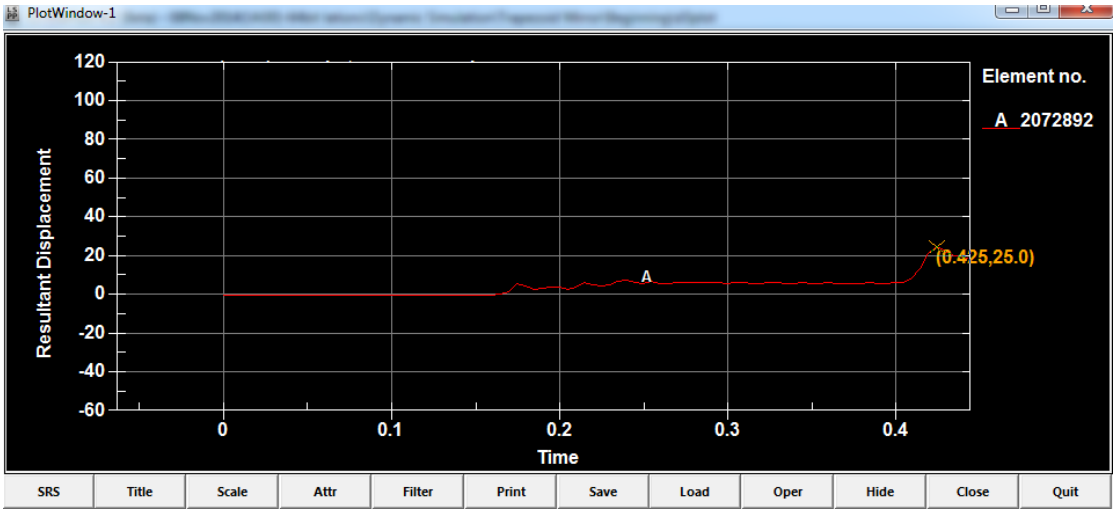

Figure 273: Maximum deflection of the barrier at second impact: Inverted modified single-slope geometry

7.2.2.6.2 Maximum deflection in deck overhang

As seen in Figure 274, maximum deflection in the deck overhang at moment 0.425 sec was 3 mm or 0.12 inches.

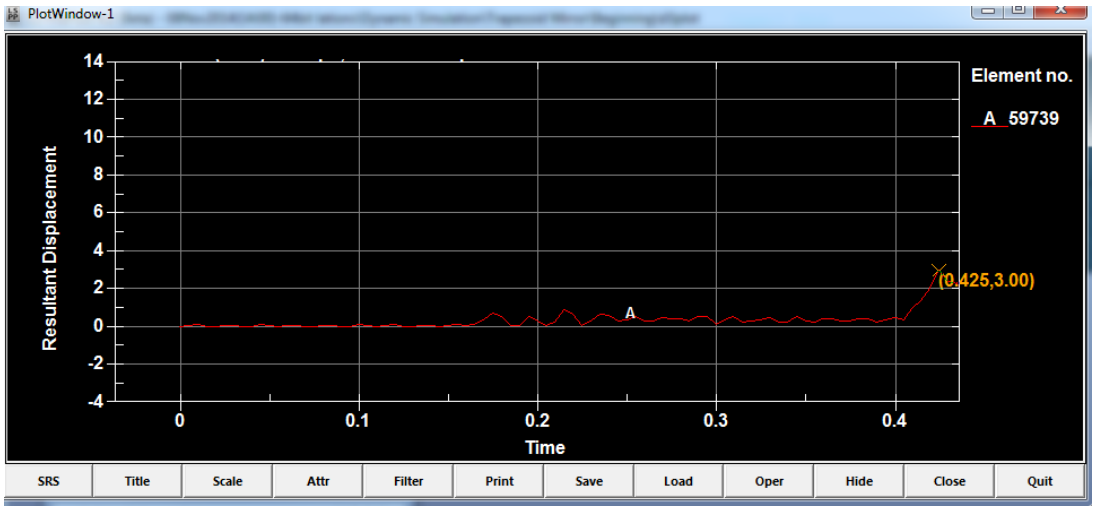

Figure 274: Maximum deflection of the deck overhang at second impact – Inverted modified single-slope geometry

7.3 Internal Energy Absorption

This sub-chapter determined the contribution of energy absorption by each portion in the system. By considering a certain amount of time, after first and second impact, for each geometry, it is possible to determine the percentage of internal energy absorbed by the vehicle, the barrier, the deck overhang, and the reinforcement bars. As previously mentioned, first impact for different geometries occurred within a 0.065-second tolerance. This variation is based on different geometries having different thicknesses so as to slightly alter the moment of impact by the truck. As well, the maximum time between the second and first impact - 0.255 seconds - occurred in "Modified Single Slope" and "Rectangular – 6 inch" geometries. Therefore, the research will consider the internal energy at "the moment of second impact (+ 0.18 second)". The purpose for adding this 0.18-second is to insure that the energy of the second impact is fully absorbed by all components and all reinforcement bars have less than 6% strain. Based on this assumption, the moment of measuring energy for geometries would be:

New-Jersey geometry: 0.62 sec

Modified New-Jersey geometry: 0.635 sec

Rectangular – 8 inch geometry: 0.595 sec

Rectangular – 6 inch geometry: 0.615 sec

Modified single-slope: 0.63 sec

Inverted modified single-slope: 0.605 sec

This research tried to determine the internal energy absorbed by each component at the same time within different barriers, but the barrier geometries are different. Consequently, the vehicle's "first impact", "second impact", and "sliding between first and second impact" are different in nature for these geometries. For instance, by comparing the first impact in "New Jersey barrier" with "rectangular - 8 inch barrier," it is obvious that at the first impact with "New-Jersey barrier", both tire and front bumper impact the barrier at the same time, but in "rectangular - 8 inch barrier", only the front bumper impacts the barrier at the moment of first impact. Hence, calculating the absolute time of the first and second impact is not possible, but with an acceptable tolerance, it is possible to determine them and calculate the internal energy absorbed by each component.

7.3.1 New-Jersey

7.3.1.1 Truck

Figure 275 represents the internal energy graph of the truck for New Jersey geometry.

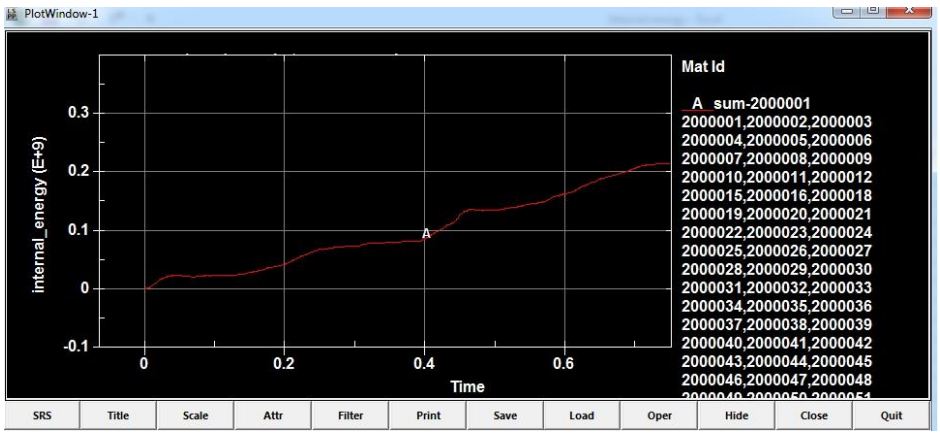

Figure 275: Internal energy of the truck – New Jersey geometry

As seen above, the internal energy of the truck at 0.62 sec is 1.73e8 n-mm.

7.3.1.2 Barrier

Figure 276 represents the internal energy graph of the barrier for New Jersey geometry.

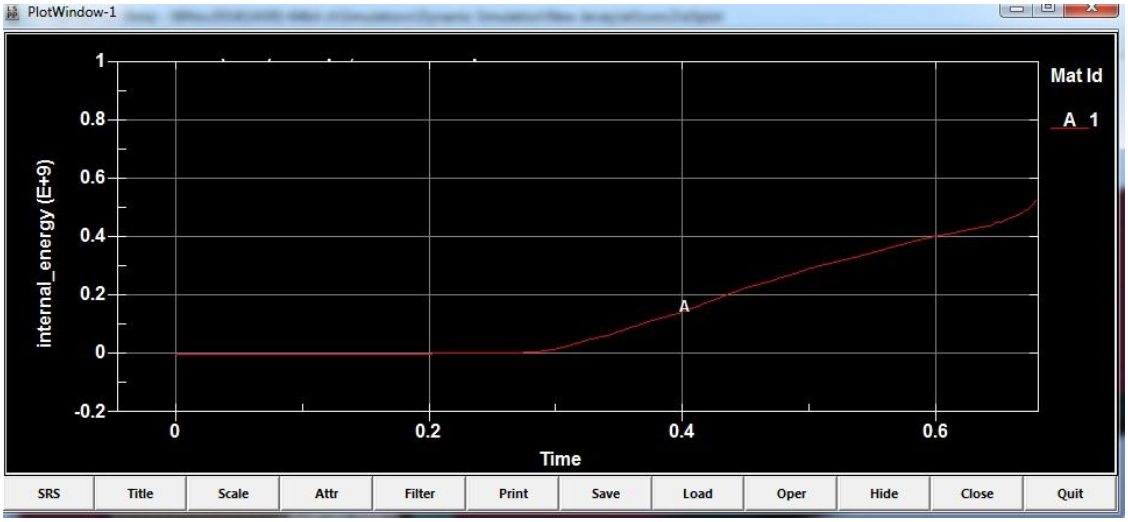

Figure 276: Internal energy of the barrier – New Jersey geometry

As seen above, the internal energy of the barrier at 0.62 sec is 4.22e8 n-mm.

7.3.1.3 Deck Overhang

Figure 277 represents the internal energy graph of the deck overhang for New Jersey geometry.

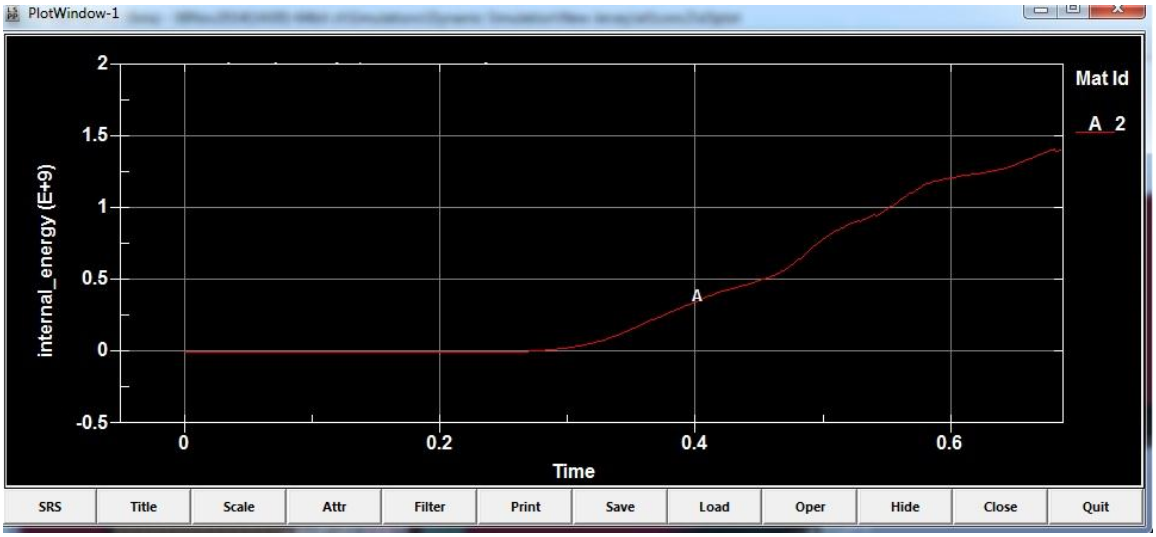

Figure 277: Internal energy of the deck overhang – New Jersey geometry

As seen above, the internal energy of the barrier at 0.62 sec is 1.24e9 n-mm.

7.3.1.4 Reinforcement bars

Figure 278 represents the internal energy graph of the reinforcement bars for New Jersey geometry.

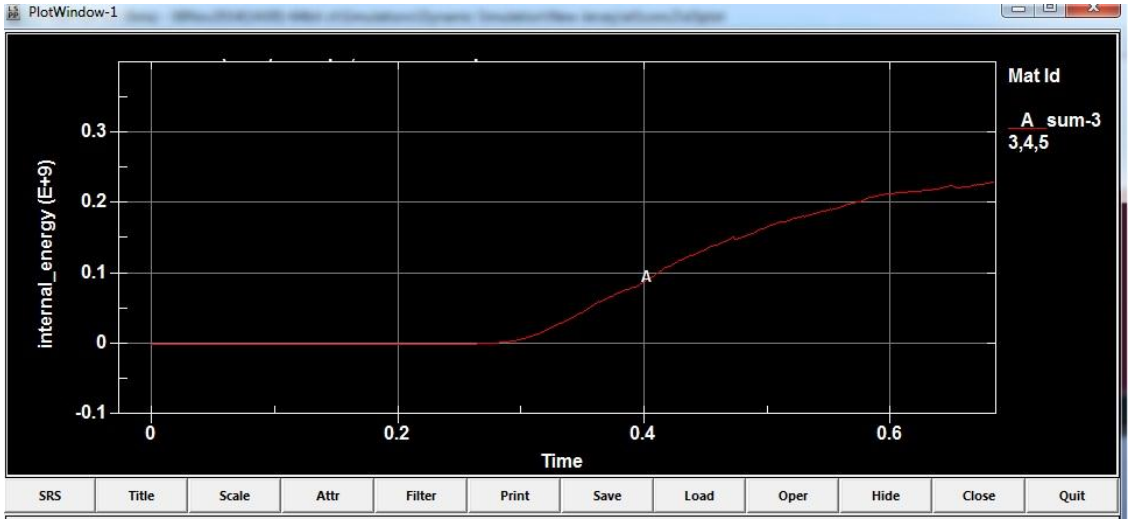

Figure 278: Internal energy of the reinforcement bars – New Jersey geometry

As seen above, the internal energy of the reinforcement bars at 0.62 sec is 2.18e8 n-mm.

7.3.2 Modified New Jersey

7.3.2.1 Truck

Figure 279 represents the internal energy graph of the truck for modified New Jersey geometry.

Figure 279: Internal energy of the truck – modified New Jersey geometry

As seen above, the internal energy of the truck at 0.635 sec is 1.68e8 n-mm.

7.3.2.2 Barrier

Figure 280 represents the internal energy graph of the barrier for modified New Jersey geometry.

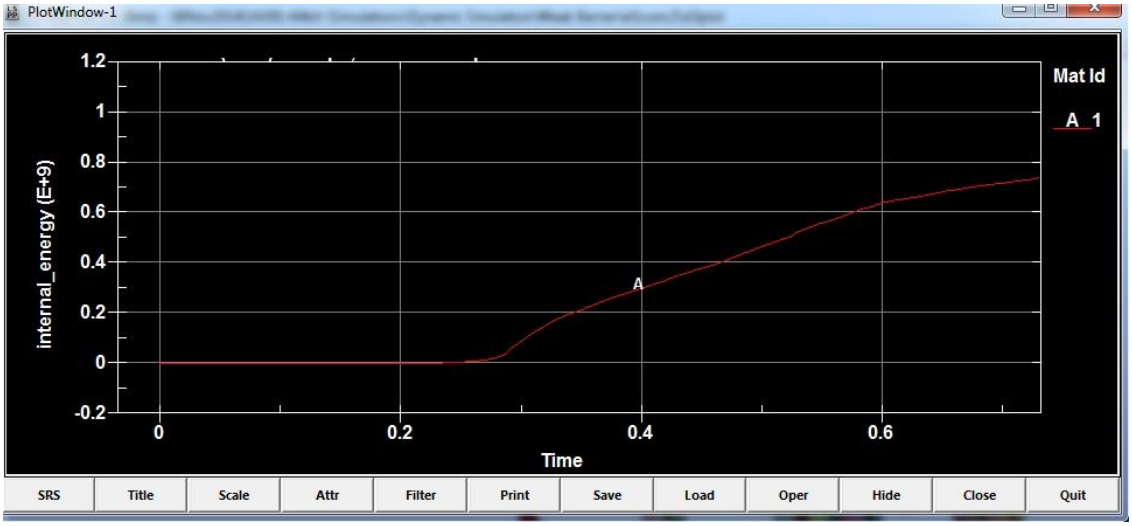

Figure 280: Internal energy of the barrier – modified New Jersey geometry

As seen above, the internal energy of the barrier at 0.635 sec is 6.70e8 n-mm.

7.3.2.3 Deck Overhang

Figure 281 represents the internal energy graph of the deck overhang for modified New Jersey geometry.

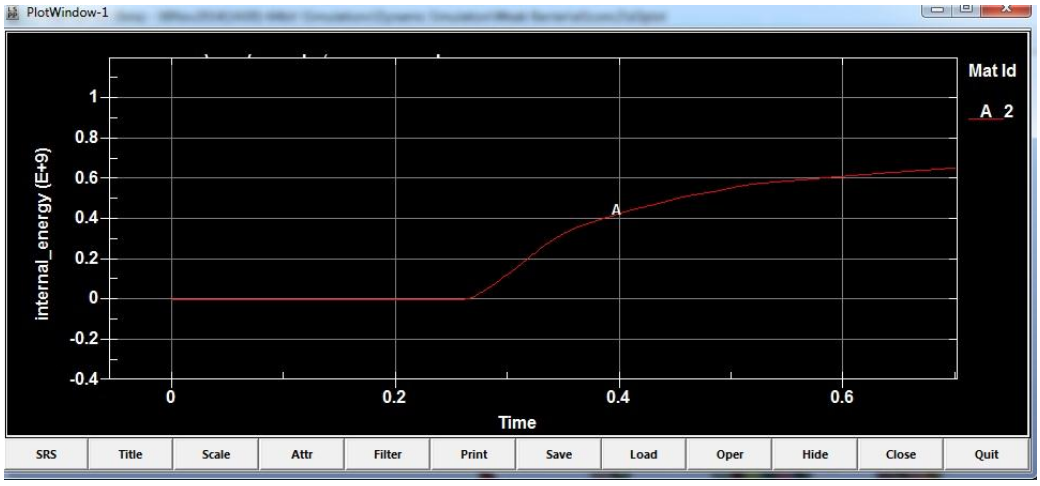

Figure 281: Internal energy of the deck overhang – modified New Jersey geometry

As seen above, the internal energy of the barrier at 0.635 sec is 6.3e8 n-mm.

7.3.2.4 Reinforcement bars

Figure 282 represents the internal energy graph of the reinforcement bars for modified New Jersey geometry.

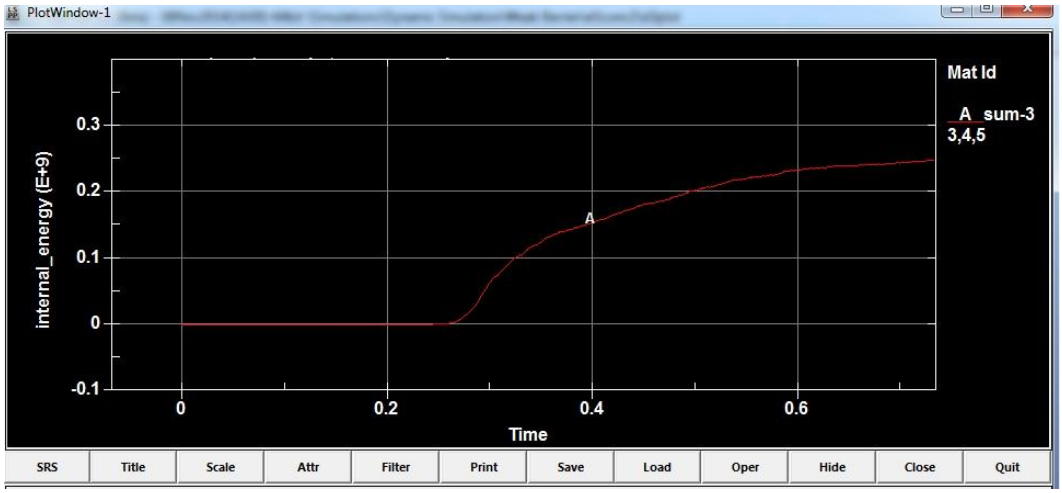

Figure 282: Internal energy of the reinforcement bars – modified New Jersey geometry

As seen in above, the internal energy of the reinforcement bars at 0.635 sec is 2.39e8 n-mm.

7.3.3 Rectangular – 8 inch

7.3.3.1 Truck

Figure 283 represents the internal energy graph of the truck for rectangular – 8 inch geometry.

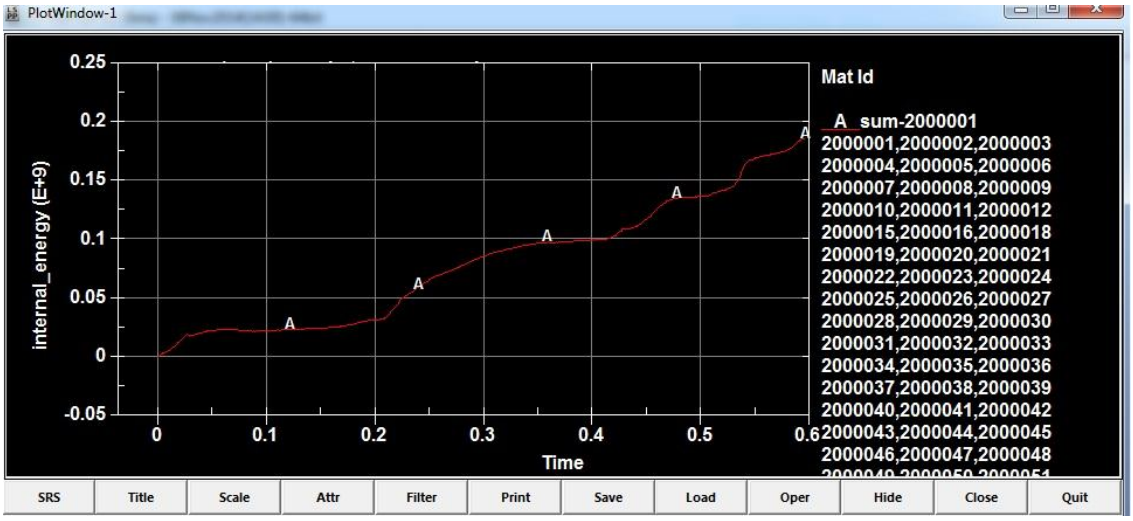

Figure 283: Internal Energy of the Truck – Rectangular 8 inch geometry

As seen above, the internal energy of the truck at 0.595 sec is 1.86e8 n-mm.

7.3.3.2 Barrier

Figure 284, represents the internal energy graph of the barrier for rectangular – 8 inch geometry.

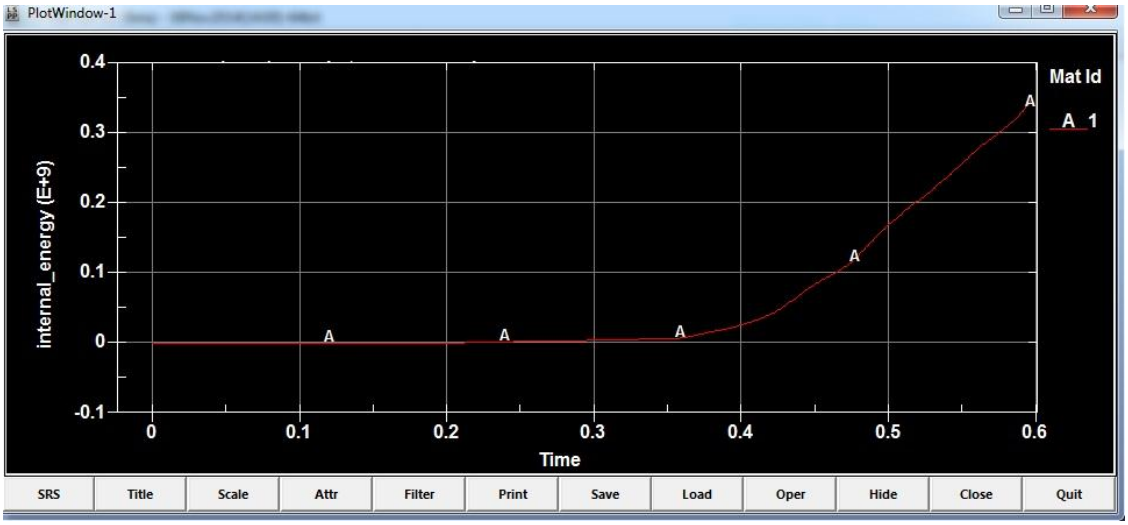

Figure 284: Internal energy of the barrier –rectangular – 8 inch geometry

As seen above, the internal energy of the barrier at 0.595 sec is 3.40e8 n-mm.

7.3.3.3 Deck Overhang

Figure 285 represents the internal energy graph of the deck overhang for rectangular – 8 inch geometry.

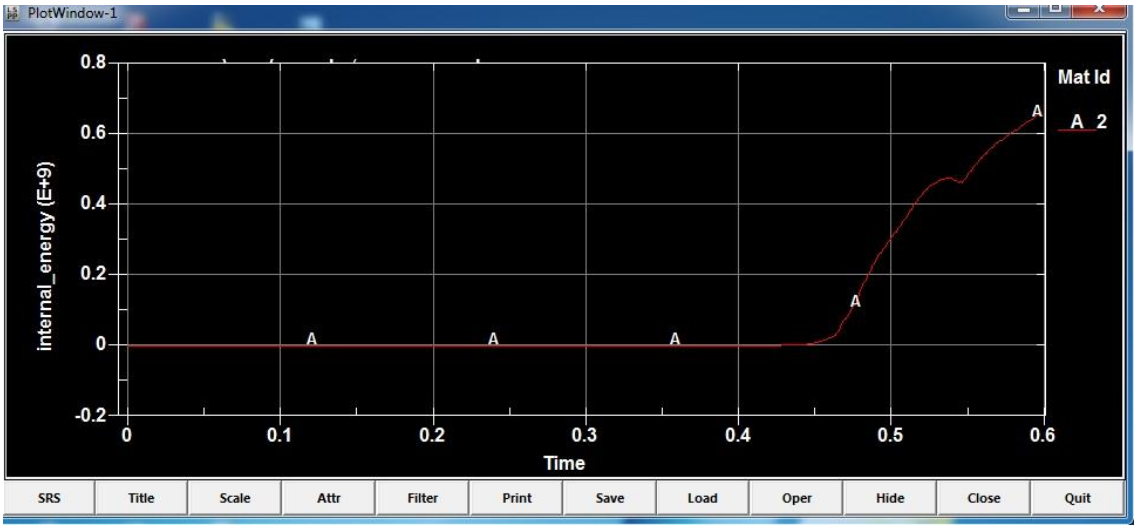

Figure 285: Internal energy of the deck overhang – rectangular – 8 inch geometry

As seen above, the internal energy of the barrier at 0.595 sec is 6.50e8 n-mm.

7.3.3.4 Reinforcement bars

Figure 286 represents the internal energy graph of the reinforcement bars for rectangular – 8 inch geometry.

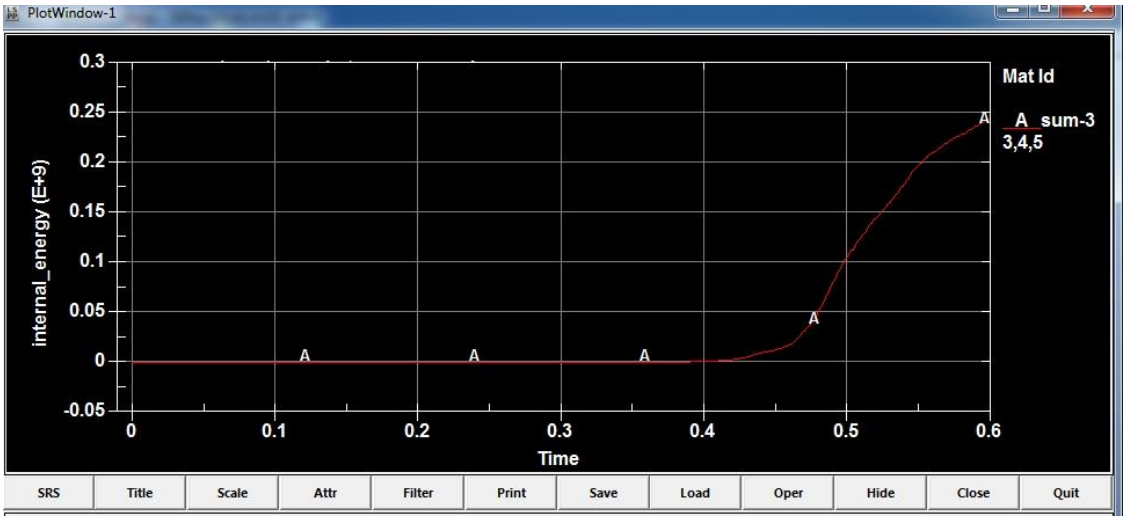

Figure 286: Internal energy of the reinforcement bars – rectangular – 8 inch geometry

As seen above, the internal energy of the reinforcement bars at 0.595 sec is 2.40e8 n-mm.

7.3.4 Rectangular – 6 inch

7.3.4.1 Truck

Figure 287 represents the internal energy graph of the truck for rectangular – 6 inch geometry.

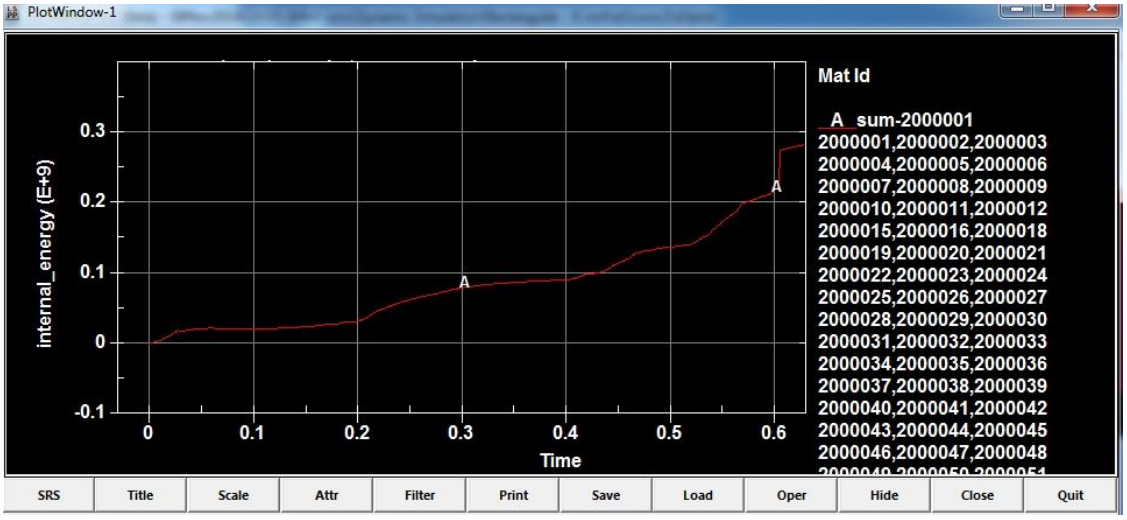

Figure 287: Internal energy of the Truck – Rectangular – 6 inch geometry

As seen above, the internal energy of the truck at 0.615 sec is 2.79e8 n-mm.

7.3.4.2 Barrier

Figure 288 represents the internal energy graph of the barrier for rectangular – 6 inch geometry.

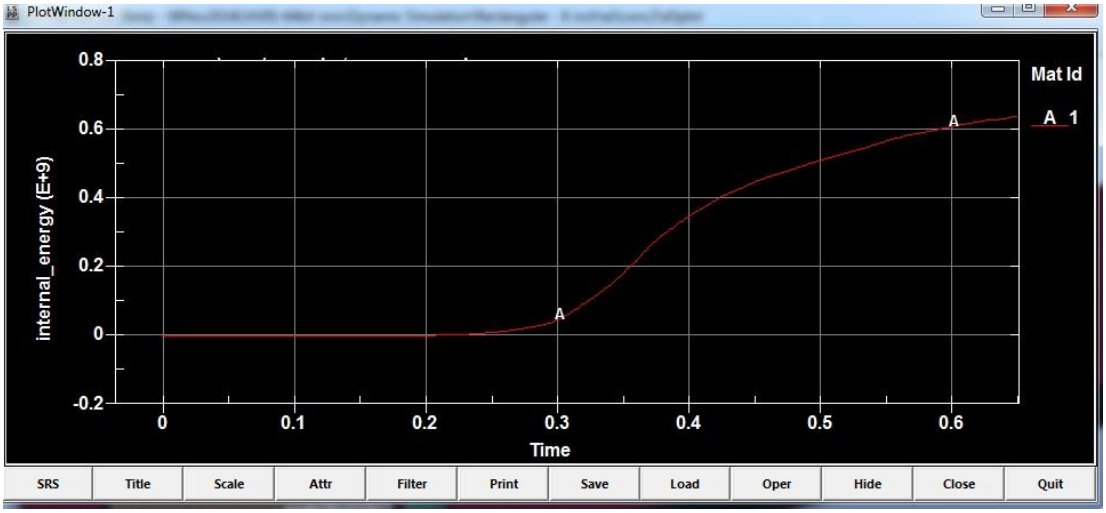

Figure 288: Internal energy of the Barrier – Rectangular – 6 inch geometry

As seen above, the internal energy of the barrier at 0.615 sec is 6.21e8 n-mm.

7.3.4.3 Deck Overhang

Figure 289 represents the internal energy graph of the deck overhang for rectangular – 6 inch geometry.

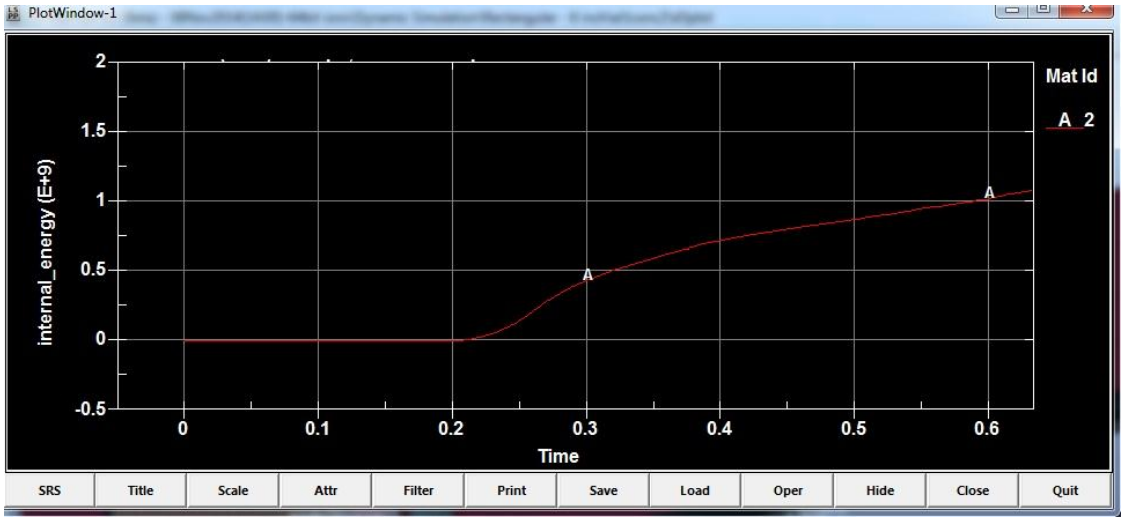

Figure 289: Internal energy of the deck overhang – rectangular – 6 inch geometry

As seen above, the internal energy of the barrier at 0.615 sec is 1.06e9 n-mm.

7.3.4.4 Reinforcement bars

Figure 290 represents the internal energy graph of the reinforcement bars for rectangular – 6 inch geometry.

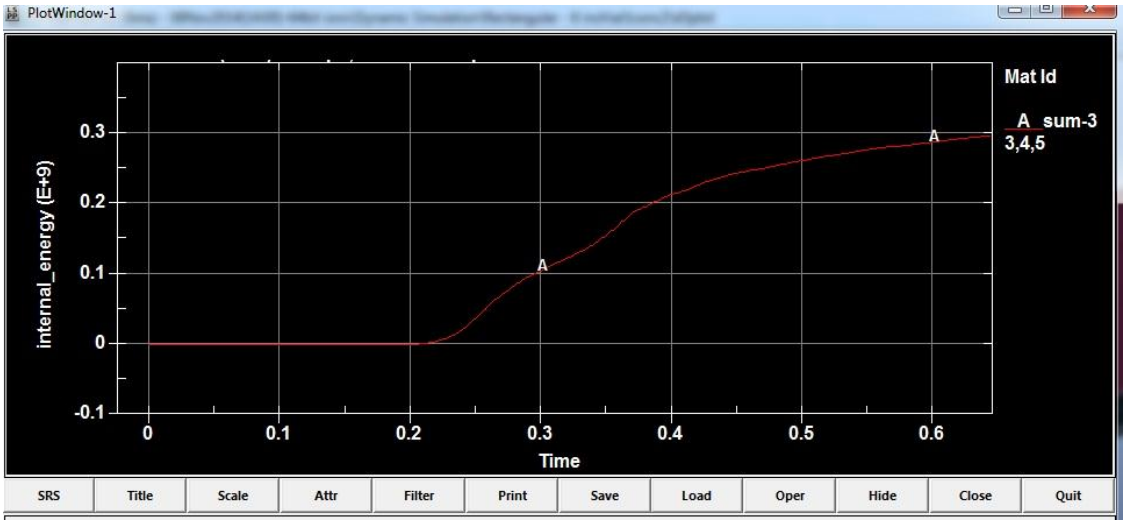

Figure 290: Internal energy of the reinforcement bars – rectangular – 6 inch geometry

As seen above, the internal energy of the reinforcement bars at 0.615 sec is 2.92e8 n-mm.

7.3.5 Modified single-slope

7.3.5.1 Truck

Figure 291 represents the internal energy graph of the truck for modified single-slope geometry.

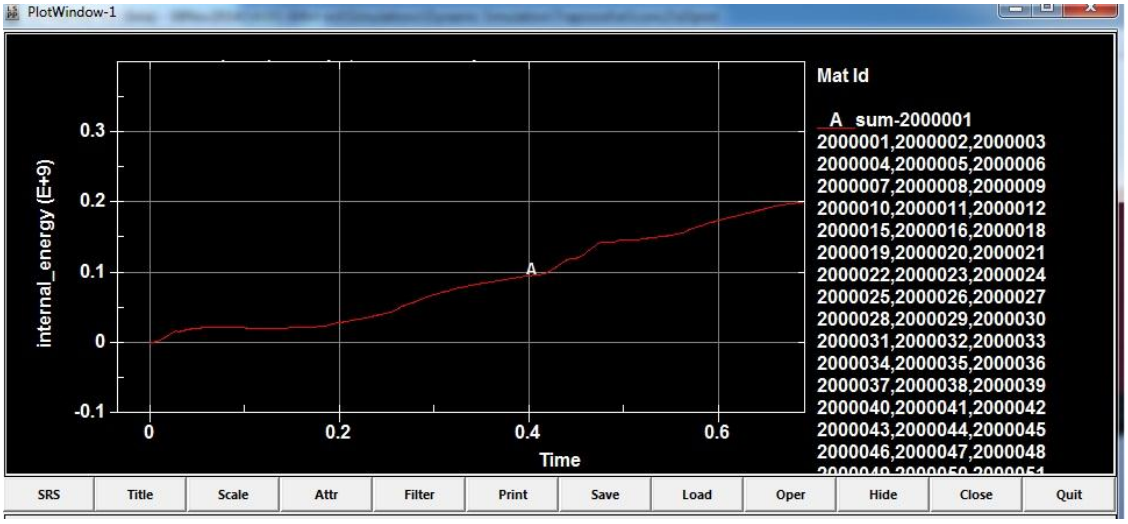

Figure 291: Internal energy of the truck – modified single-slope

As seen above, the internal energy of the truck at 0.63 sec is 1.85e8 n-mm.

7.3.5.2 Barrier

Figure 292 represents the internal energy graph of the barrier for modified single-slope geometry.

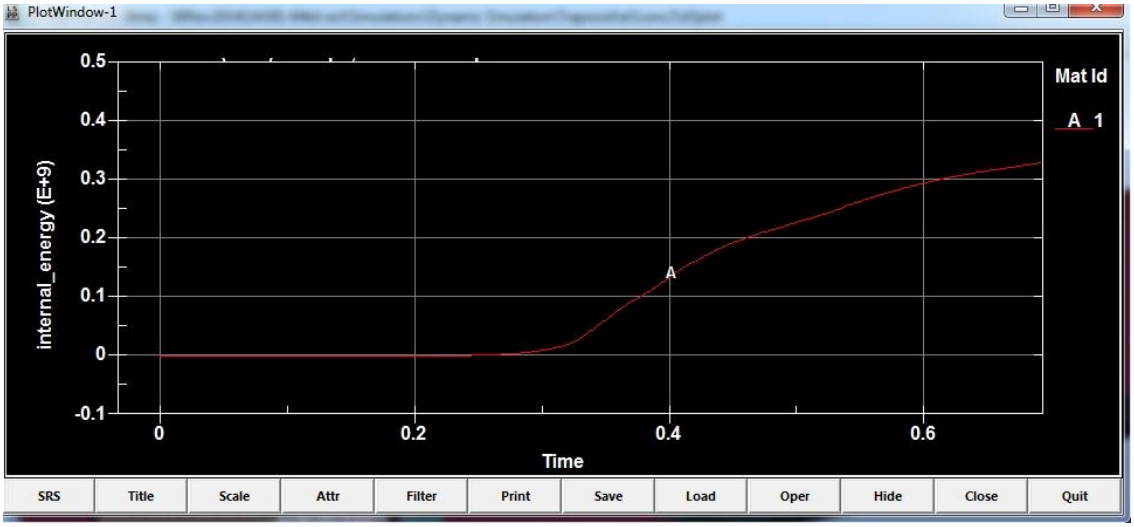

Figure 292: Internal energy of the barrier – modified single-slope

As seen above, the internal energy of the barrier at 0.63 sec is 3.08e8 n-mm.

7.3.5.3 Deck Overhang

Figure 293 represents the internal energy graph of the deck overhang for modified single-slope.

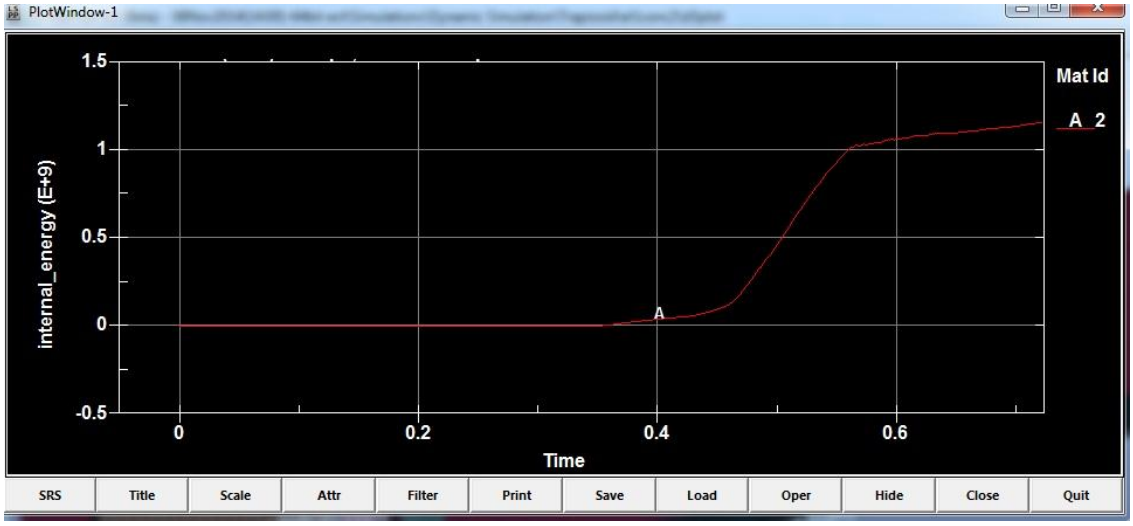

Figure 293: Internal energy of the deck overhang – modified single-slope

As seen above, the internal energy of the barrier at 0.63 sec is 1.09e9 n-mm.

7.3.5.4 Reinforcement bars

Figure 294 represents the internal energy graph of the reinforcement bars for modified single-slope.

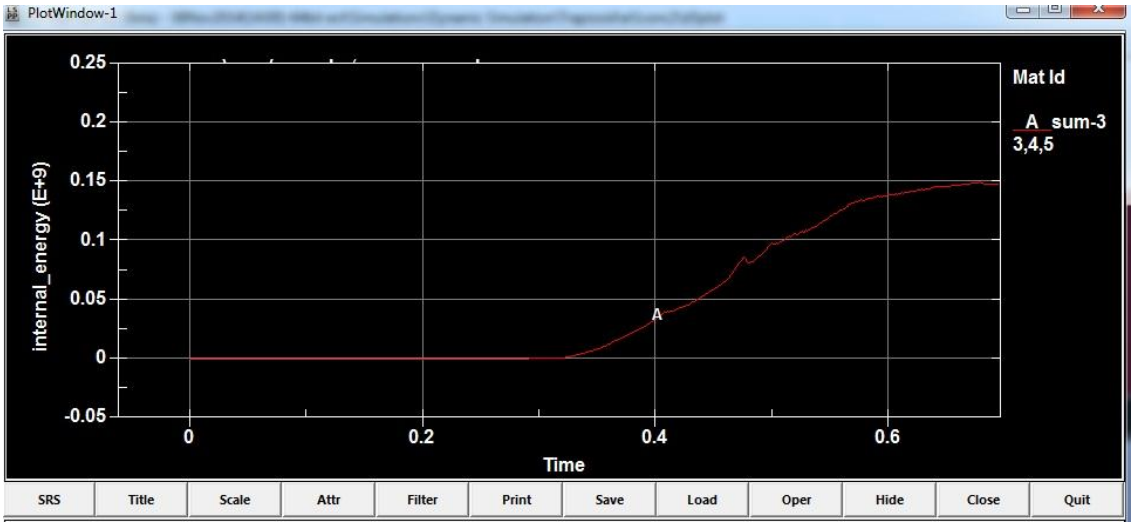

Figure 294: Internal energy of the reinforcement bars – modified single-slope

As seen above, the internal energy of the reinforcement bars at 0.63 sec is 1.44e8 n-mm.

7.3.6 Inverted Modified Single-Slope

7.3.6.1 Truck

Figure 295 represents the internal energy graph of the truck for inverted modified single-slope geometry.

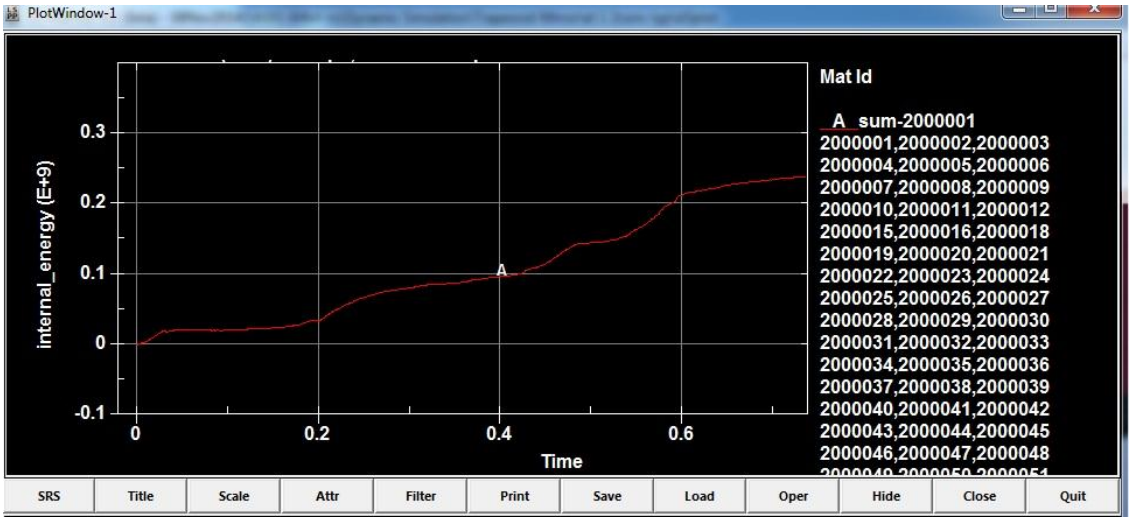

Figure 295: Internal energy of the truck – inverted modified single-slope

As seen above, the internal energy of the truck at 0.605 sec is 2.15e8 n-mm.

7.3.6.2 Barrier

Figure 296 represents the internal energy graph of the barrier for inverted modified single-slope geometry.

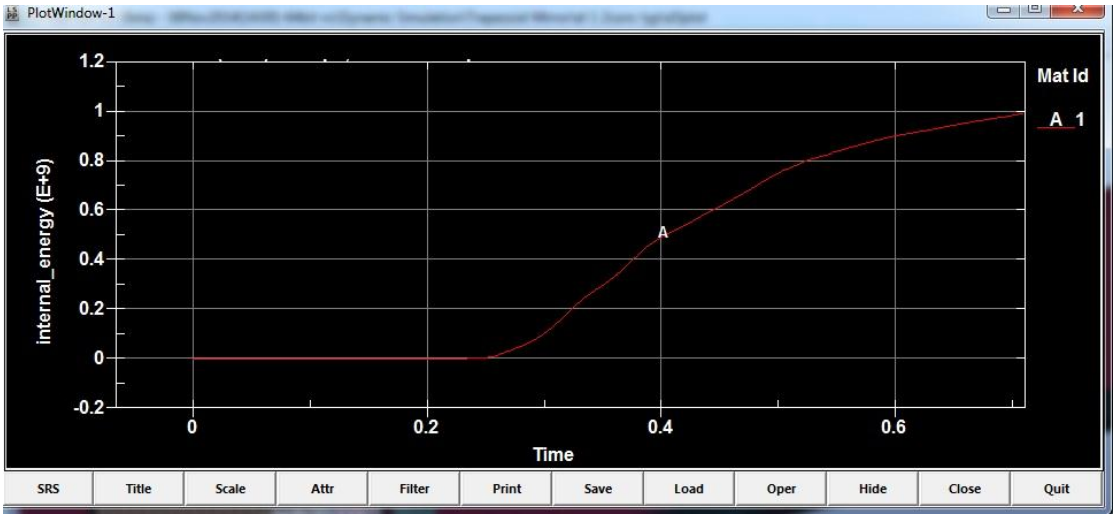

Figure 296: Internal energy of the barrier – inverted modified single-slope

As seen above, the internal energy of the barrier at 0.605 sec is 9.08e8 n-mm.

7.3.6.3 Deck Overhang

Figure 297 represents the internal energy graph of the deck overhang for inverted modified single-slope.

Figure 297: Internal energy of the deck overhang – inverted modified single-slope

As seen above, the internal energy of the barrier at 0.605 sec is 2.10e9 n-mm.

7.3.6.4 Reinforcement bars

Figure 298 represents the internal energy graph of the reinforcement bars for inverted modified single-slope

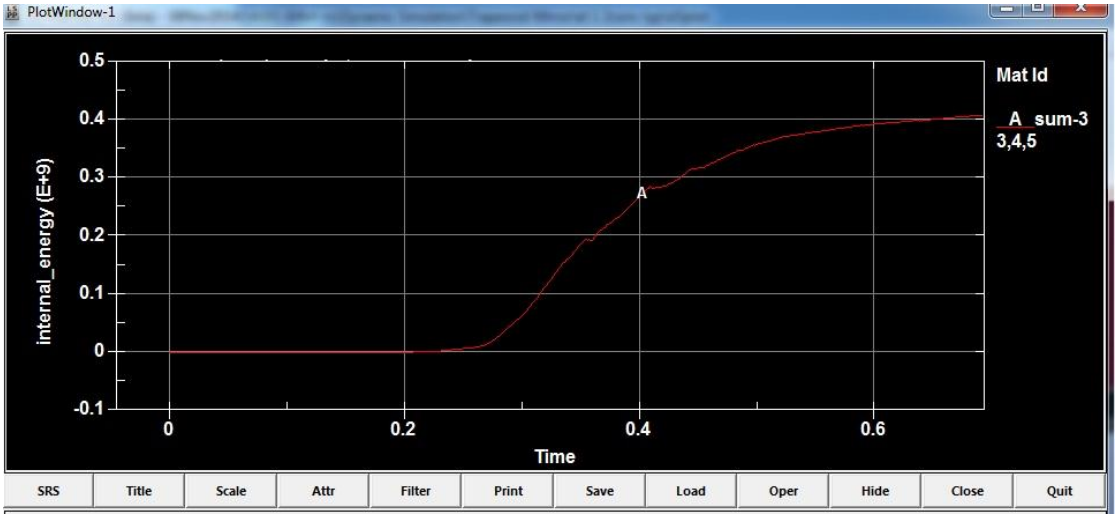

Figure 298: Internal energy of the reinforcement bars – inverted modified single-slope

As seen above, the internal energy of the reinforcement bars at 0.605 sec is 3.95e8 n-mm.

8 RESULTS AND DISCUSSION

The purpose of this chapter is to (1) compare all barriers in static simulation in order to perform the best geometry which does not only provide enough safety, but also proves to be more economical than New Jersey barrier; (2) compare all barriers in dynamic simulation in order to find the most efficient geometry in terms of production cost and safety; (3) compare static simulation with dynamic simulation for all geometries; (4) demonstrate the damage to the barriers and deck overhangs caused by dynamic impact, and (5) demonstrate the vehicle rolling over on all barriers to determine the most efficient geometry with maximum safety.

Due to the compatibility of barrier and truck interaction, a fine mesh detailed finite element analysis model was developed.

In order to demonstrate the accuracy of the aforementioned FE model, several tests were conducted in “Evaluation of LS-DYNA Concrete Material 159” report. Since the results matched closely with the FE results, by considering the same materials and definitions, it is possible to obtain reliable results with an acceptable amount of tolerance.

It is important to mention that there is no specific guidelines to design barriers based on dynamic impact that considers all criteria such as vehicle deformation, stress distribution, and the behavior of the vehicle after impact. Hence, a factual way to observe and calculate all of the above is to simulate and run finite element analysis models.

In order to propose the best geometry by considering all safety criteria, five different geometries were considered.

8.1 Static simulation results comparison

8.1.1 Maximum stress

8.1.1.1 Maximum stress in barriers

8.1.1.1.1 Compression side

Figure 299 represents the maximum stress on barriers in compression side, or front face of the barrier.

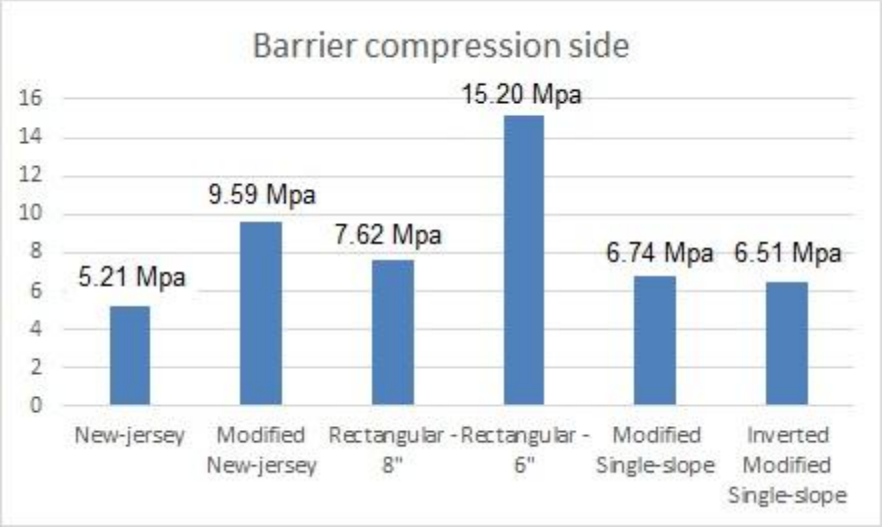

Figure 299: Maximum stress in compression side of barriers

As seen in Figure 299 the maximum stress is exhibited by the rectangular – 6 inch geometry, and is equal to 15.20 Mpa. Since this number is less than 30.44 Mpa, none of the barriers reached or exceeded yield compression of the concrete.

8.1.1.1.2 Tension side

Figure 300 represents the maximum stress on barriers in tension side, or back face, of the barrier.

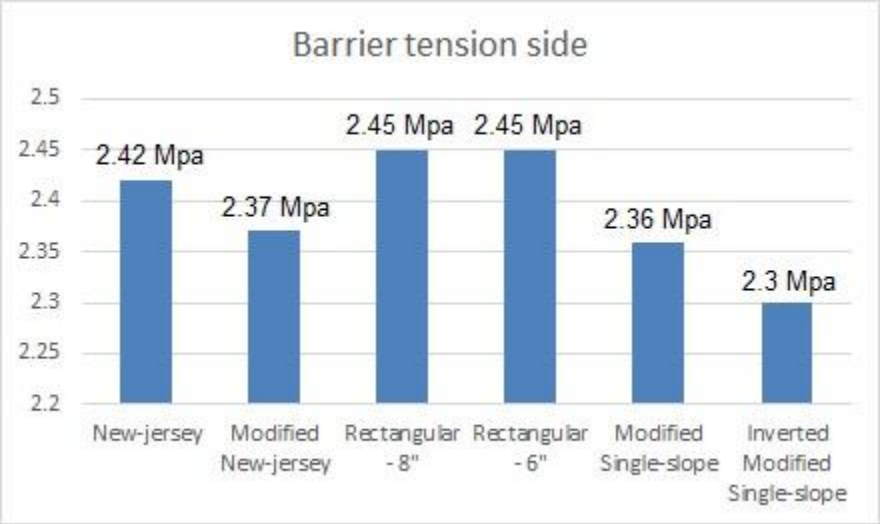

Figure 300: Maximum stress in tension side of barriers

As seen above, the maximum stress is exhibited by the rectangular – 6 and 8 inch geometries, and is equal to 2.45 Mpa. Chapter 3 of this research mentioned that module of rupture for barrier concrete based on ACI 318-14 is equal to 3.44 MPa (498.34 psi). Since this number is less than 3.44 Mpa, none of the barriers reached or exceeded module of rupture.

8.1.1.2 Maximum stress in deck overhang

8.1.1.2.1 Compression side

Figure 301 represents the maximum stress on deck overhang in compression side, or bottom face, of deck overhang.

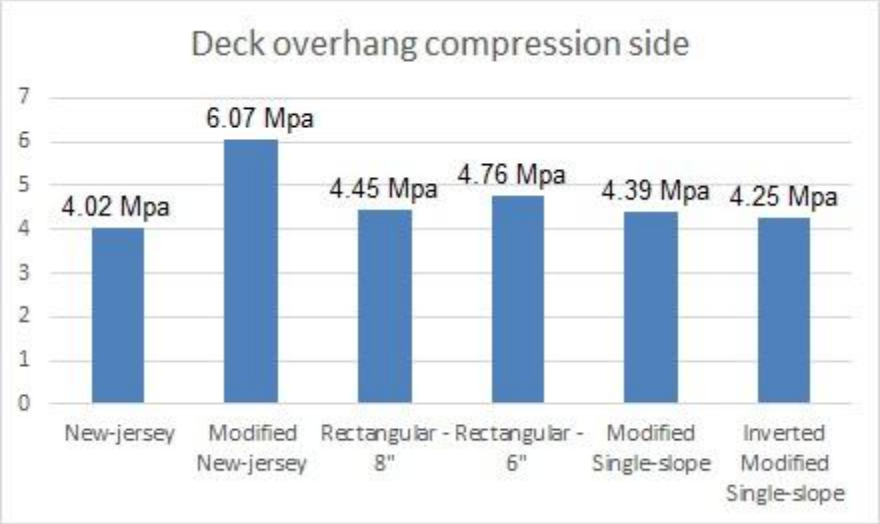

Figure 301: Maximum stress in compression side of deck overhang

As seen above, the maximum stress belongs to modified New Jersey geometry, and is equal to 6.07 Mpa. Since this number is less than 35.52 Mpa, none of the barriers reached or exceeded yield compression of the concrete.

8.1.1.2.2 Tension side

Figure 302 represents the maximum stress on deck overhang in tension side, or top face of deck overhang.

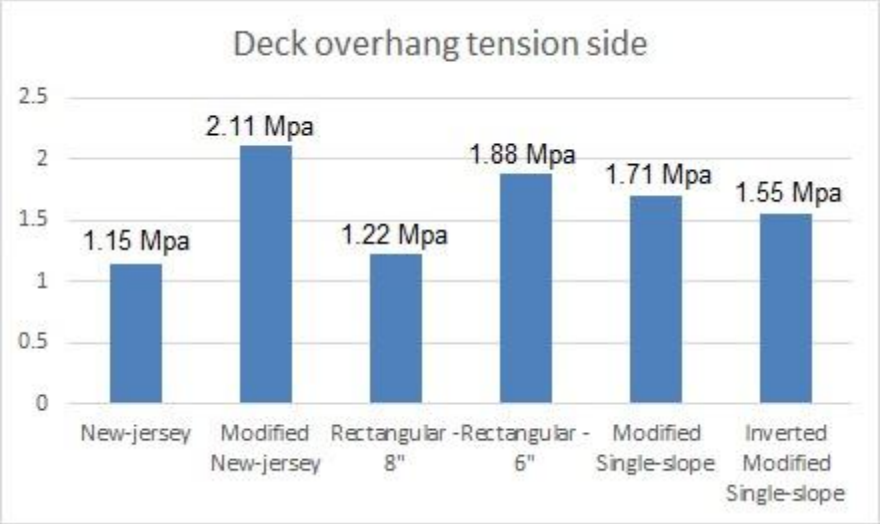

Figure 302: Maximum stress in tension side of barriers

As seen above, the maximum stress belongs to modified New Jersey geometry, and is equal to 2.11 Mpa. Chapter 3 of this research mentioned that module of rupture for barrier concrete based on ACI 318-14 is equal to 3.71 MPa (538.33 psi). Since this number is less than 3.44 Mpa, none of the barriers reached or exceeded module of rupture.

8.1.1.3 Maximum stress in reinforcement bars

8.1.1.3.1 Compression side

Figure 303 represents the maximum stress on reinforcement bars in compression, or back face, of barrier.

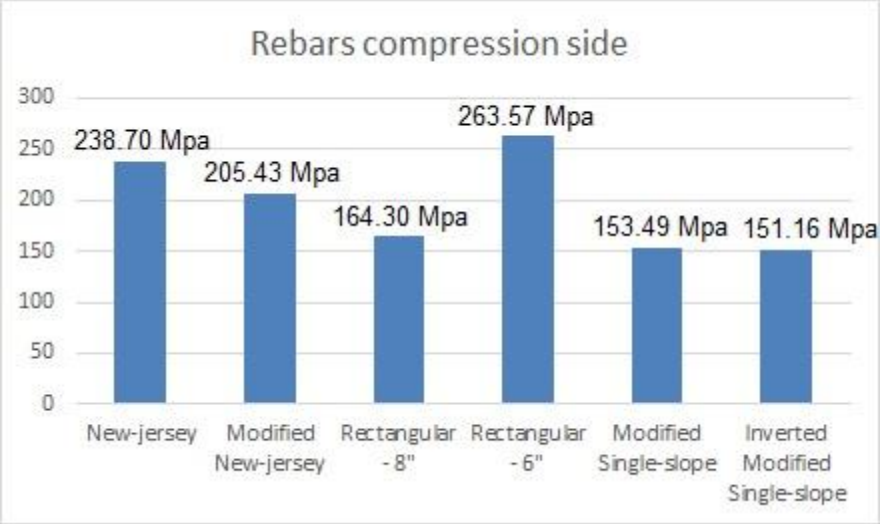

Figure 303: Maximum stress for reinforcement bars in compression

As seen above, the maximum stress belongs to rectangular – 6 inch geometry, and is equal to 263.57 Mpa. Since the yield point for steel in compression and tension side considered as 413.69 Mpa, none of the reinforcement bars reached or exceeded the yield point of the steel.

8.1.1.3.2 Tension side

Figure 304 represents the maximum stress on reinforcement bars in tension side, or front face of barrier.

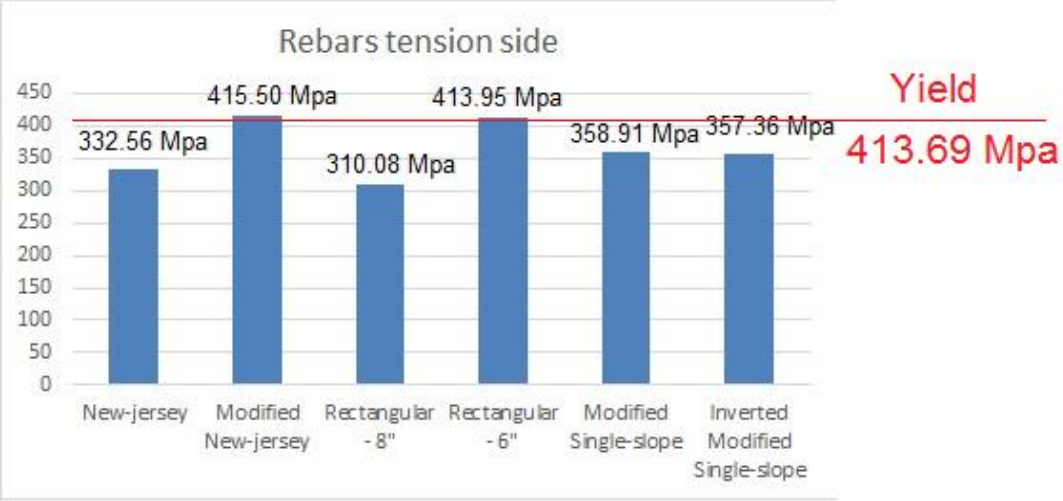

Figure 304: Maximum stress for reinforcement bars in tension

As seen above, the maximum stress belongs to modified New Jersey and rectangular – 6 inch geometries, and is equal to 415.50 and 413.95 MPa respectively. Since the yield point for steel in compression and tension side is considered as 413.69 Mpa, the said reinforcement bars passed the yield point and entered into plasticity mode.

8.1.2 Maximum Deflection

Figure 305 and 306 show the maximum deflection in barrier and deck overhang respectively, based on a 54 kip distributed load that represents Test Level 4.

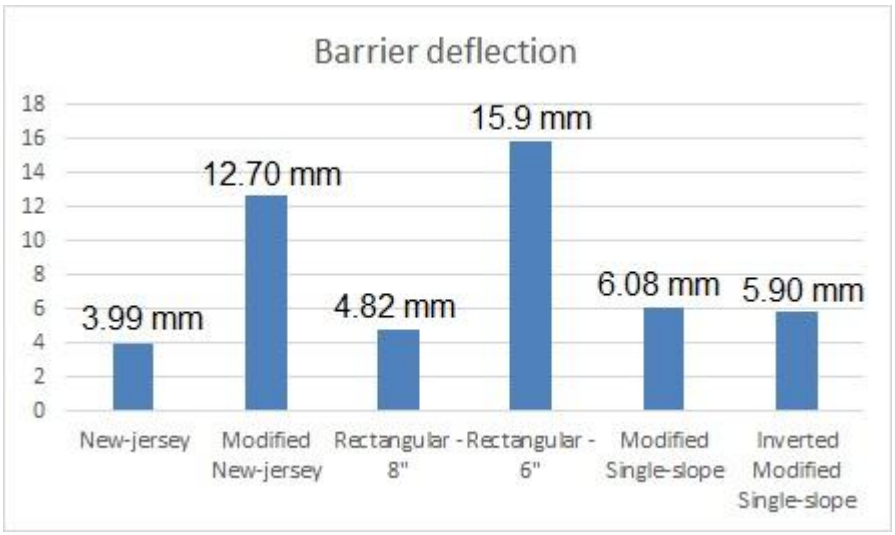

Figure 305: Maximum deflection at barriers

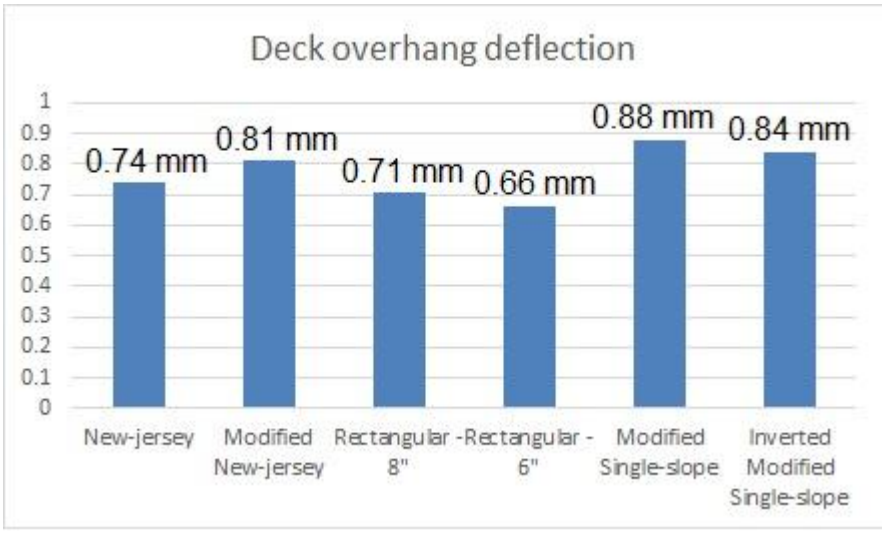

Figure 306: Maximum deflection in deck overhang

The maximum deflection for the barriers was exhibited in modified New Jersey and rectangular – 6 inch barrier and was equal to 12.7 mm and 15.9 mm respectively. In

the deck overhang, almost all geometries had a similar range of between 0.66 and 0.88 mm.

8.2 Dynamic simulation results comparison

Compared to static simulations, in dynamic simulations, maximum tensile and compressive stress in concrete blocks are not necessarily located at the point of first or second impact. As has been discussed and shown in Chapter 5, maximum compressive and tensile stresses are located at different points in different geometries.

The optimized barrier that this research is looking for should:

- Be able to resist the impact force caused by the vehicle while it is safe and economical to manufacture.
- Keep the deflection in the barrier and deck overhang to a minimum.
- Not redirect the vehicle to the traffic lane.
- Not cause the vehicle to roll over the barrier which may cause serious damage to the traffic layers underneath.
- Minimize damage to all portions and minimize the total energy produced by the impact.

8.2.1 Maximum stress

8.2.1.1 Maximum stress in barrier

8.2.1.1.1 Compressive strength

8.2.1.1.1.1 First impact

Figure 307 represents the maximum compressive strength in barriers at moment of first impact.

Figure 307: Maximum compressive strength in barriers – First impact

As seen above, the maximum stress belongs to rectangular – 8 inch geometry, and is equal to 31.05 Mpa. Although this value is less than 31.96 Mpa, but the barrier will almost get close to the concrete compressive strength.

8.2.1.1.1.2 Second impact

Figure 308 represents the maximum compressive strength on barriers at moment of second impact.

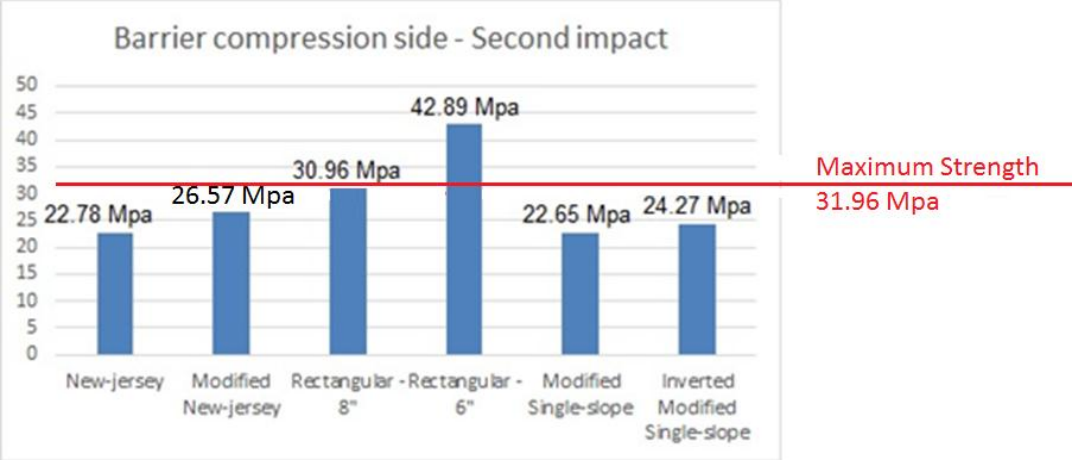

Figure 308: Maximum compressive strength in barriers – Second impact

As seen above, the maximum stress belongs to rectangular – 8 and 6 inch geometries, and are equal to 30.96 MPa and 42.89 MPa respectively. Since these values are more or close to 31.96 Mpa, these barriers will reach the concrete compressive strength at second impact and they cannot meet the first criteria for a barrier that this research is looking for, because after this number, barriers will lose serviceability.

8.2.1.1.2 Tensile strength

8.2.1.1.2.1 First impact

Figure 309 represents the maximum tensile strength of barriers at moment of first impact.

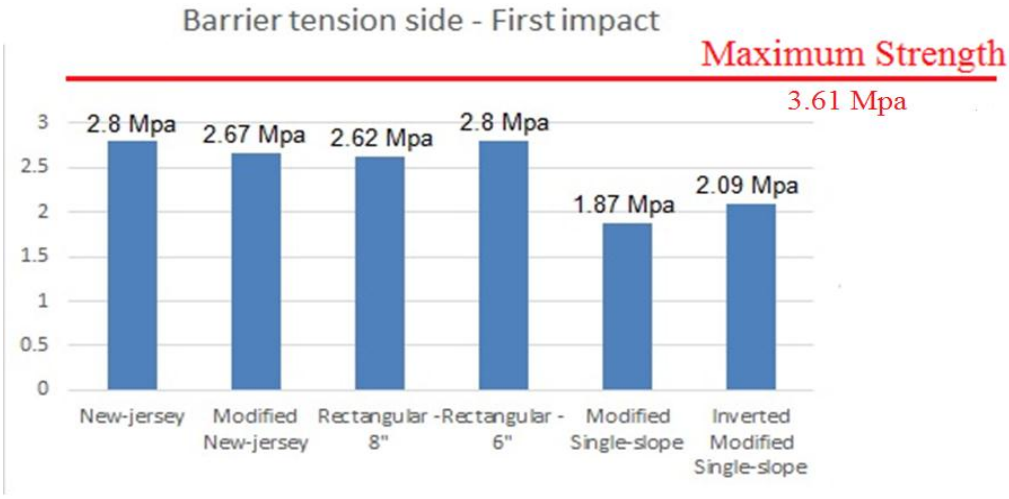

Figure 309: Maximum tensile strength in barriers – First impact

As seen above, all of the barriers have a tensile strength range of between 1.87 MPa and 2.8 MPa at the moment of first impact. Since all values are below 3.61 Mpa, none of the barriers would reach tensile strength limits or crack.

8.2.1.1.2.2 Second impact

Figure 310 represents the maximum tensile strength of barriers at the moment of second impact.

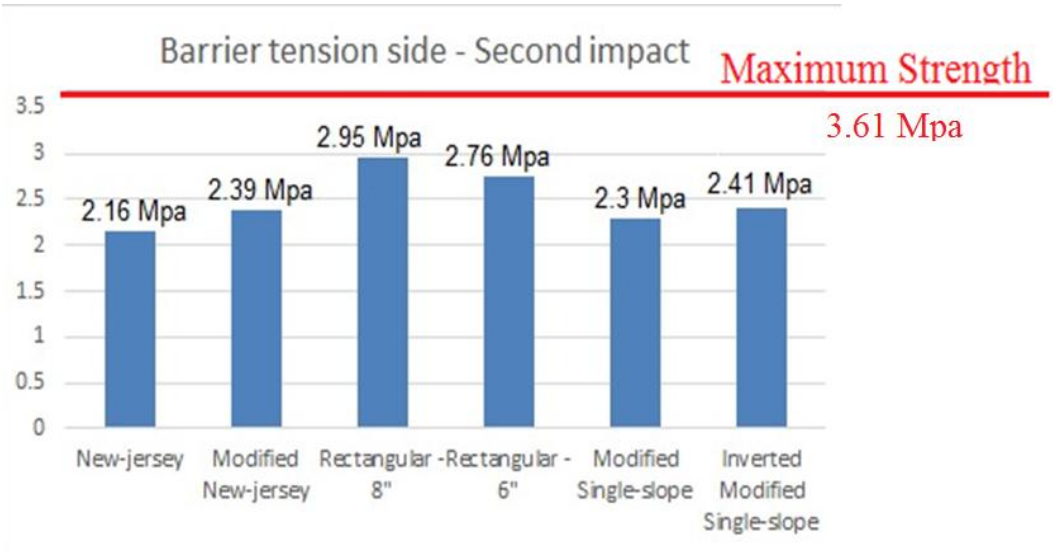

Figure 310: Maximum tensile strength in barriers – Second impact

As seen above, at the moment of second impact, all of the barriers have a tensile strength range of between 2.16 MPa and 2.95 Mpa. Since all values are less than 3.61 Mpa, none of the barriers would reach tensile strength limits or crack.

8.2.1.2 Maximum stress in deck overhang

8.2.1.2.1 Compressive strength

8.2.1.2.1.1 First impact

Figure 311 represents the maximum compressive strength of deck overhang at the moment of first impact.

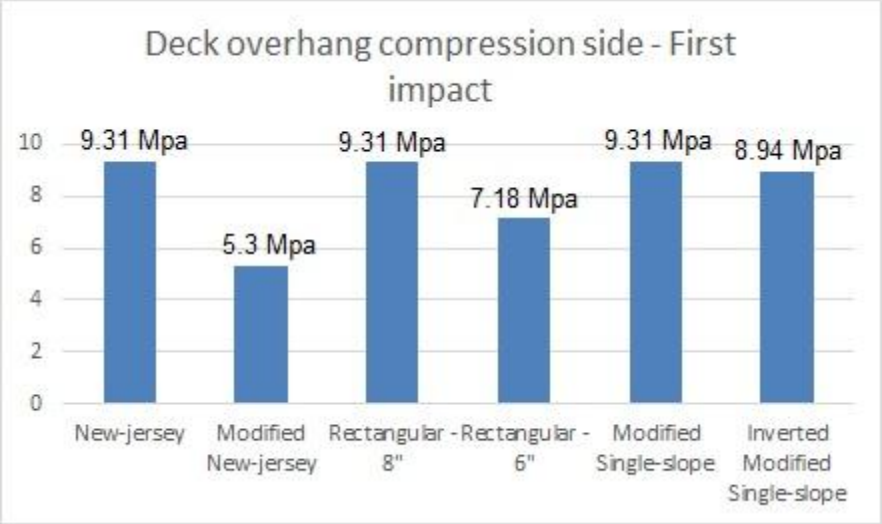

Figure 311: Maximum compressive strength in deck overhang – First impact

As seen above, the maximum stress belongs to New Jersey, rectangular – 8 inch, and modified single-slope geometries, and is equal to 9.31 Mpa. Since this value is less than 37.30 Mpa, these barriers will not reach the concrete compressive strength limit at first impact.

8.2.1.2.1.2 Second impact

Figure 312 represents the maximum compressive strength in deck overhang at the moment of second impact.

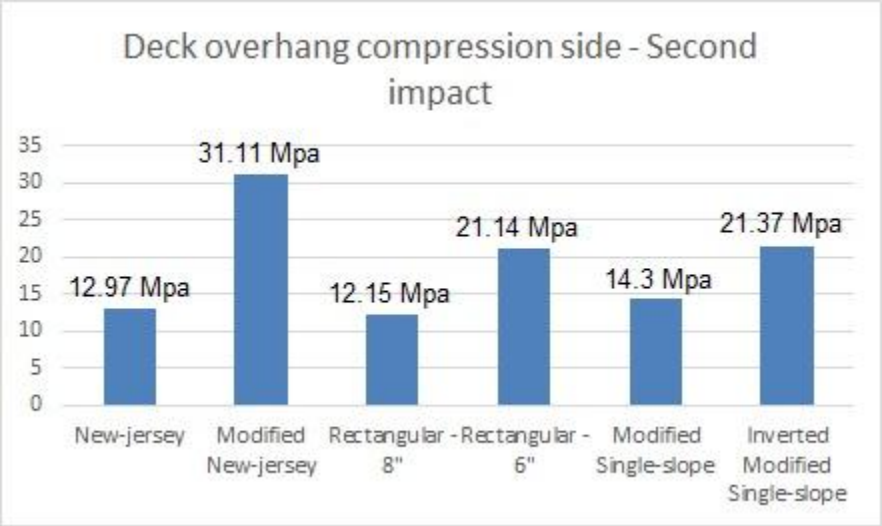

Figure 312: Maximum compressive strength in deck overhang – Second impact

As seen above, the maximum stress belongs to modified New Jersey geometry, and is equal to 31.11 Mpa. Although this value is fairly close to but less than 37.30 MPa - the compressive strength of the concrete in deck overhang - this geometry might lose its serviceability after the second impact.

8.2.1.2.2 Tensile strength

8.2.1.2.2.1 First impact

Figure 313 represented the maximum tensile strength in deck overhang at the moment of first impact.

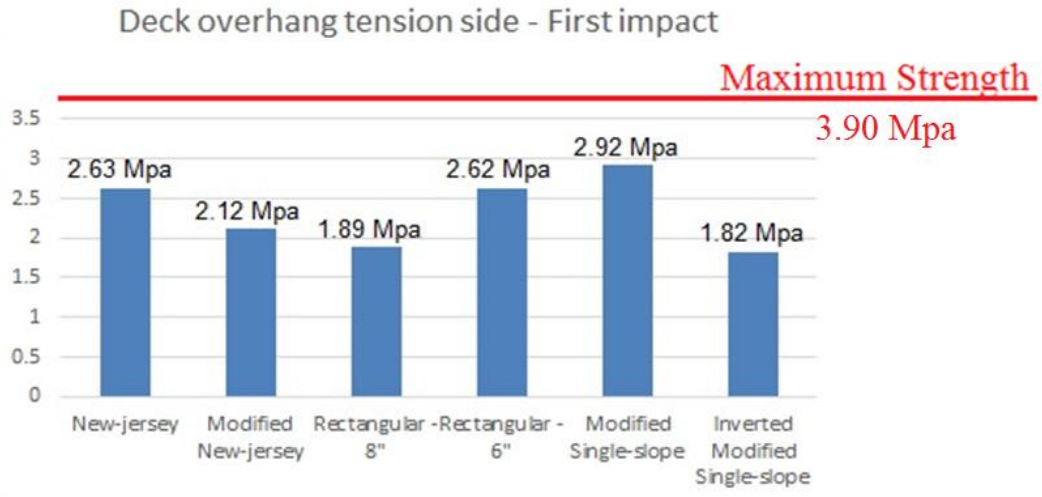

Figure 313: Maximum tensile strength in deck overhang – First impact

As depicted above, at the moment of first impact, all of the deck overhangs have a tensile strength range of between 1.82 MPa and 2.92 Mpa. Since all values are less than 3.90 Mpa, none of the deck overhangs would not reach tensile strength limits or crack.

8.2.1.2.2.2 Second impact

Figure 314 represented the maximum tensile strength in deck overhang at the moment of second impact.

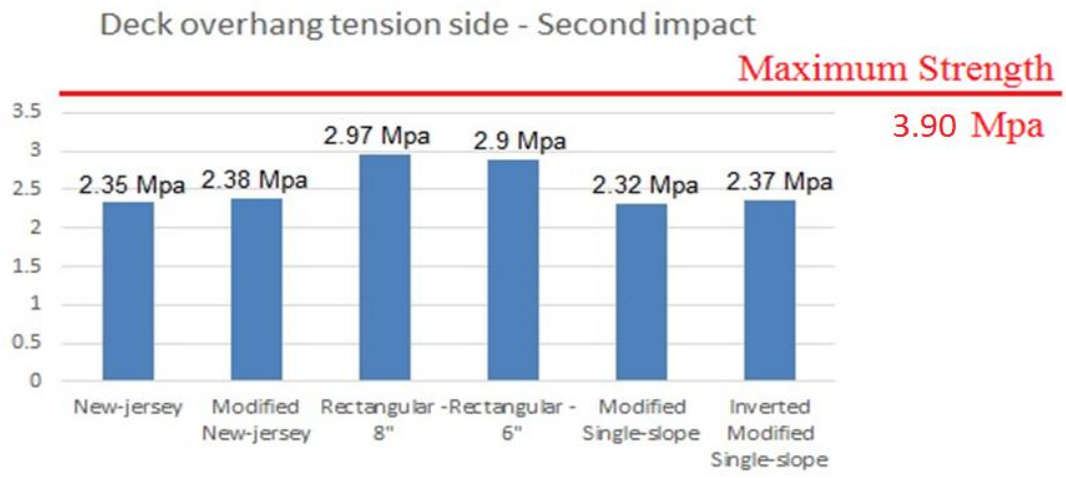

Figure 314: Maximum tensile strength in deck overhang – Second impact

As seen above, at the moment of second impact, all of the barriers have a tensile strength range of between 2.32 MPa and 2.97 Mpa. Since all values are less than 3.90 Mpa, none of the barriers would reach tensile strength limits or crack.

8.2.1.3 Maximum stress at reinforcement bars

8.2.1.3.1 Compressive strength

8.2.1.3.1.1 First impact

Figure 315 represents the maximum compressive strength of the reinforcement bars at the moment of first impact.

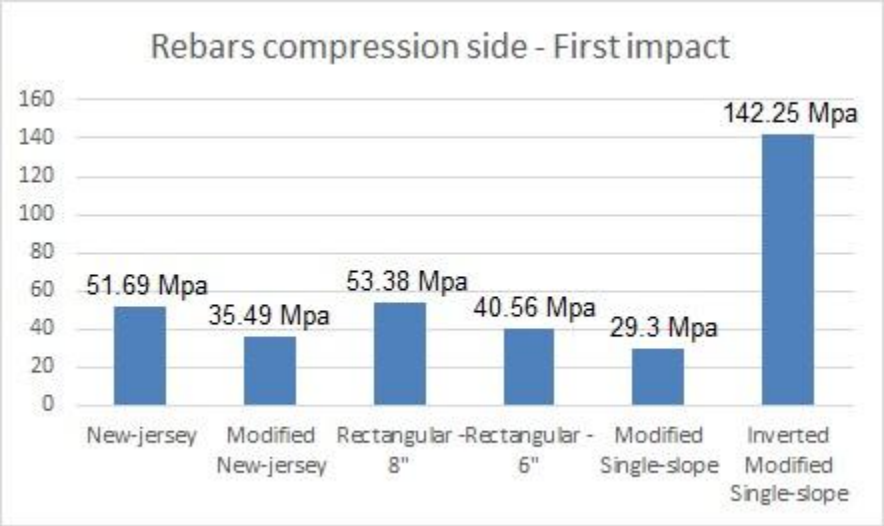

Figure 315: Maximum compressive strength of reinforcement bars – First impact

As seen above, the maximum capacity for stress belongs to inverted modified single-slope geometry, and is equal to 142.25 Mpa. Since this value is less than 413.69 MPa (60 ksi), reinforcement bars will not reach the concrete compressive strength at first impact.

8.2.1.3.1.2 Second impact

Figure 316 represents the maximum compressive strength of reinforcement bars at the moment of second impact.

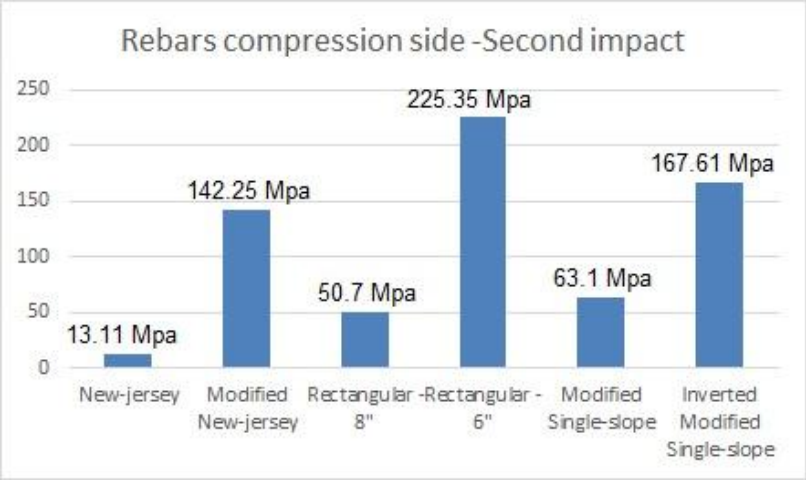

Figure 316: Maximum compressive strength of reinforcement bars – Second impact

As seen above, the maximum capacity for stress belongs to modified New Jersey, rectangular – 6 inch, and inverted modified single-slope geometries, and are equal to 142.25, 225.35, 167.61 MPa respectively. All of these values are less than 413.69 MPa (60 ksi), and consequently, none of the reinforcement bars would reach compressive strength limits.

8.2.1.3.2 Tensile strength

8.2.1.3.2.1 First impact

Figure 317 represents the maximum tensile strength of reinforcement bars at the moment of first impact.

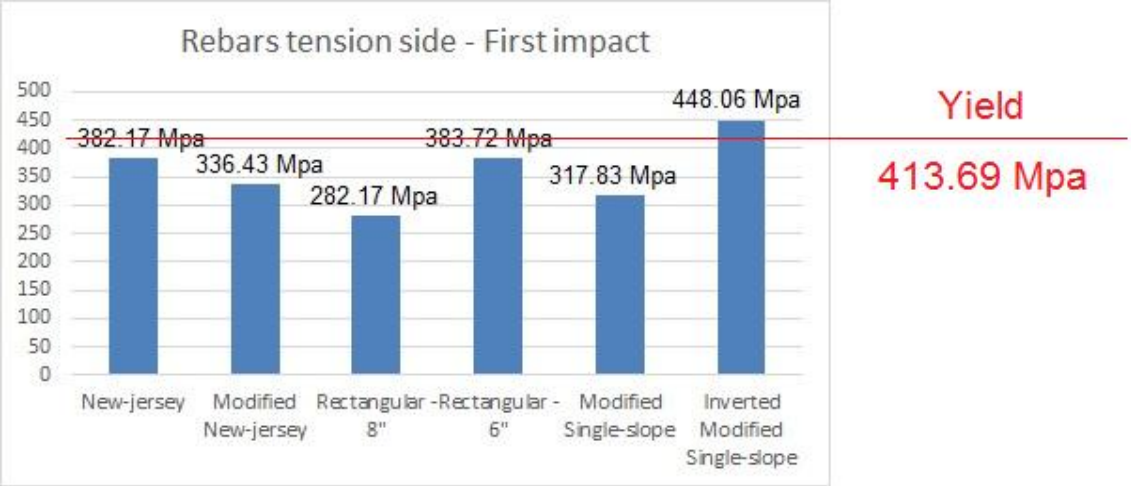

Figure 317: Maximum tensile strength in reinforcement bars – First impact

As seen in above, only the Inverted Modified Single-Slope geometry reached and exceeded the yield point. Therefore, the Inverted Modified Single-Slope might not be serviceable after the first impact and cannot meet the first criteria of this research.

8.2.1.3.2.2 Second impact

Figure 318 represents the maximum tensile strength of reinforcement bars at the moment of second impact.

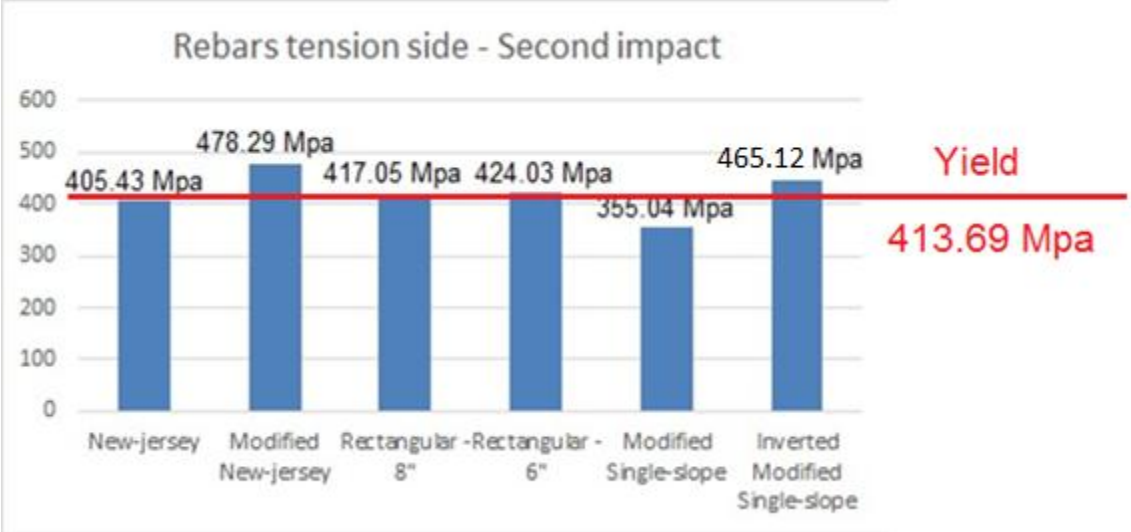

Figure 318: Maximum tensile strength of reinforcement bars – Second impact

As realized above, with the exception of the New Jersey and modified single-slope geometries, all other barriers and reinforcement bars reach and exceed the yield stress point.

8.2.2 Maximum deflection

8.2.2.1 First impact

Figure 319 and 320 exhibited the maximum deflection in barrier and deck overhang respectively, based on Test Level 4 single unit truck at the moment of first impact.

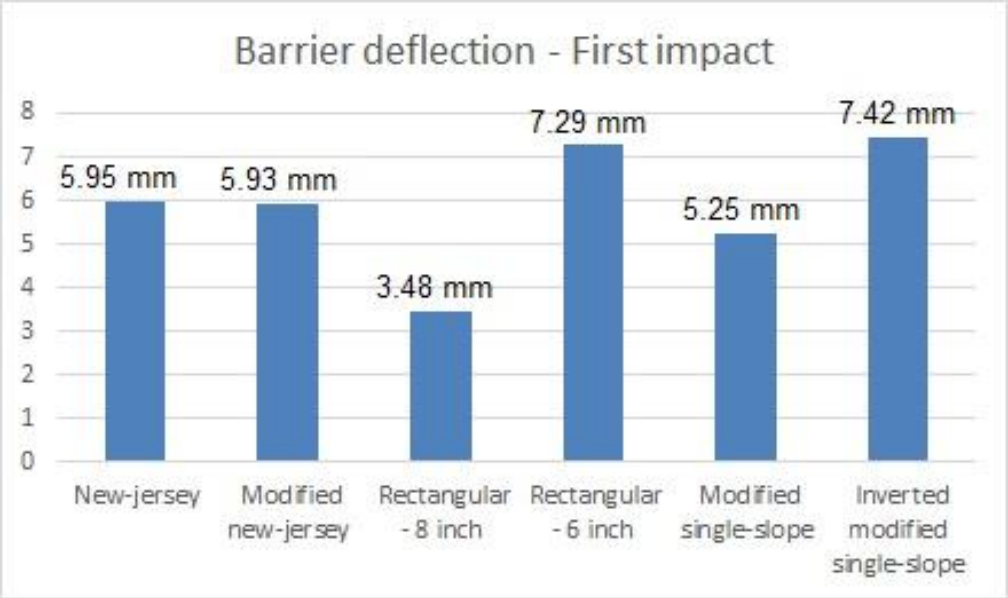

Figure 319: Maximum deflection at barriers – first impact

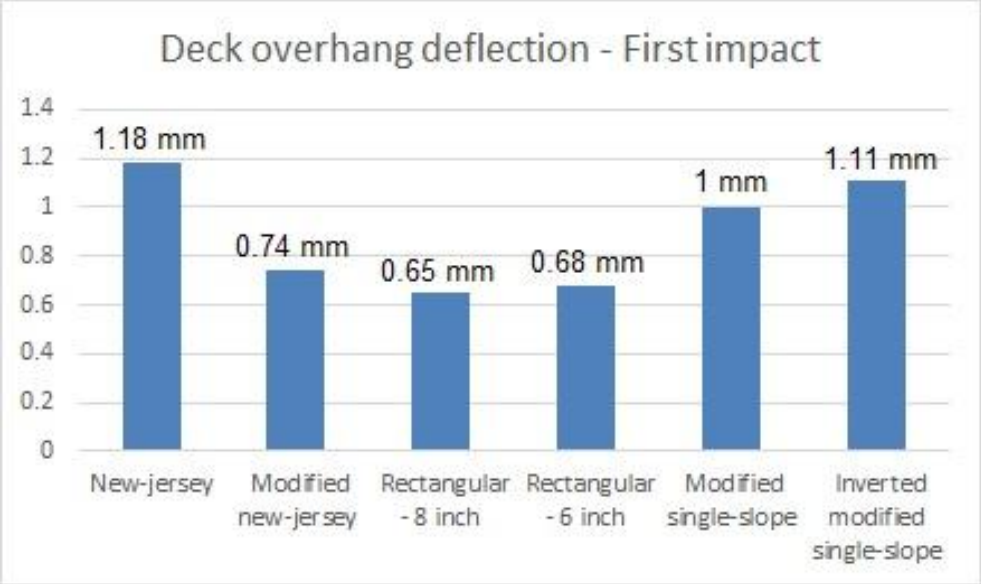

Figure 320: Maximum deflection in deck overhang – first impact

The maximum deflection of the barriers at moment of first impact was in the rectangular – 6 inch barrier and inverted modified single-slope geometries. Deflection was measured at 7.29 mm and 7.42 mm respectively. In the deck overhang, almost all geometries had a consistent range of between 0.65 mm and 1.18 mm.

8.2.2.2 Second Impact

Figure 231 and 322 showed the maximum deflection in barrier and deck overhang respectively, based on Test Level 4 single unit truck at the moment of second impact.

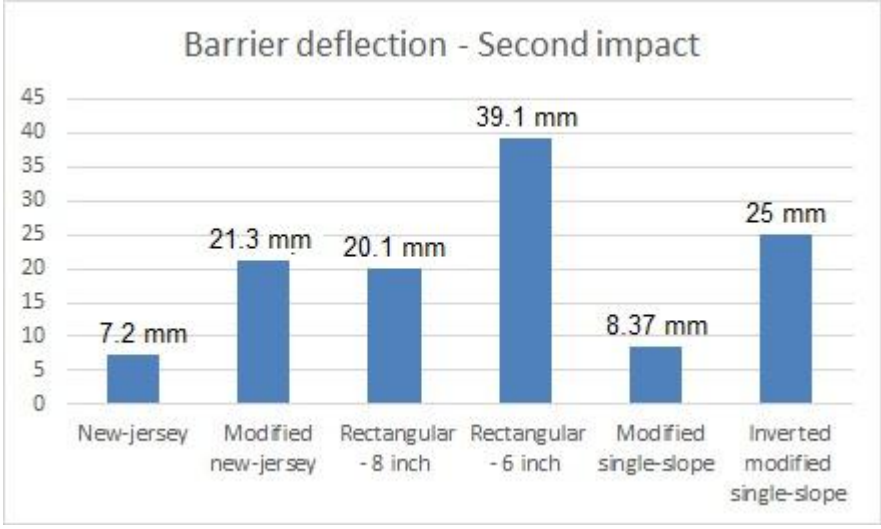

Figure 321: Maximum deflection at barriers – second impact

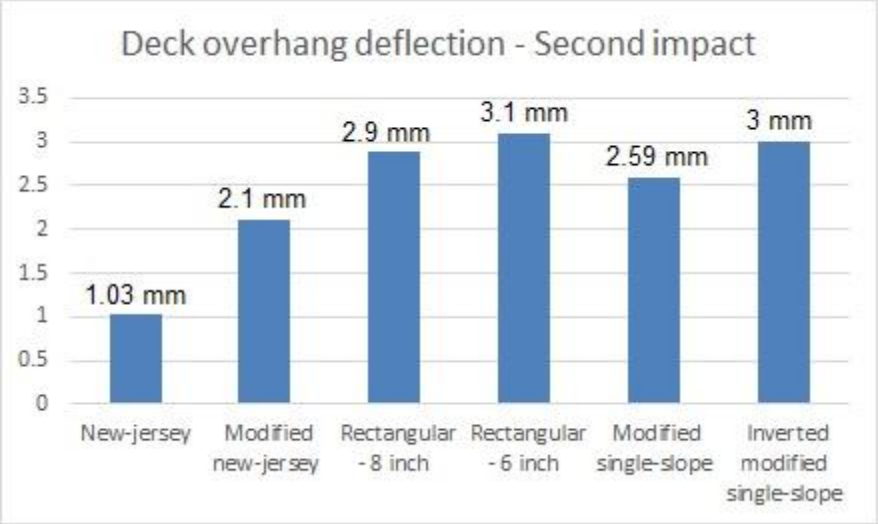

Figure 322: Maximum deflection at deck overhang – second impact

Except for the New Jersey and modified single-slope geometries, all other barriers had deflection of more than 20 mm. The maximum deflection was for the rectangular – 6 inch and equal to 39.1 mm.

As for the deck overhang, the greater part of the geometries had the same range: between 1.03 mm and 3.1 mm. Although the deflection at the deck overhang, for all geometries, are almost acceptable, since the deflection at the barrier in all geometries – with the exception of the New Jersey and the modified single-slope - is too high, they will not meet the second criteria of this research, namely, to keep the deflection minimal.

8.2.3 Internal Energy Comparison

Internal energy absorption is explained in previous chapters. In order to find the most efficient and economical geometry, this chapter compared all internal energy absorption by classifying them into two different categories. The first category compared internal energy between different geometries but the same component, and the second

category compared internal energy absorbed by each geometry via all components. All internal energies were extracted from LS-DYNA graphs at the moment of "second impact + 0.18 second"

8.2.3.1 Internal energy absorbed by each component

Figure 323 to 326 represented the internal energy absorbed by each component in all geometries.

Figure 323: Internal energy absorbed by vehicle at all geometries

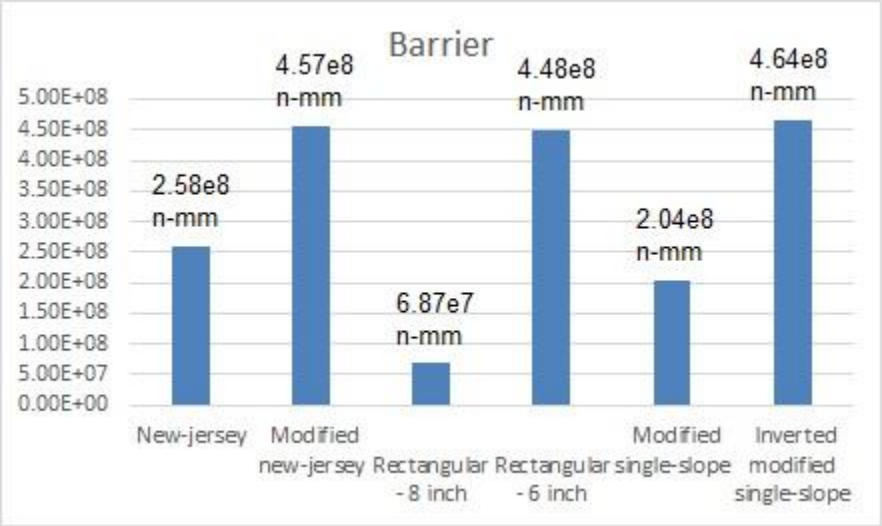

Figure 324: Internal energy absorbed by barrier at all geometries

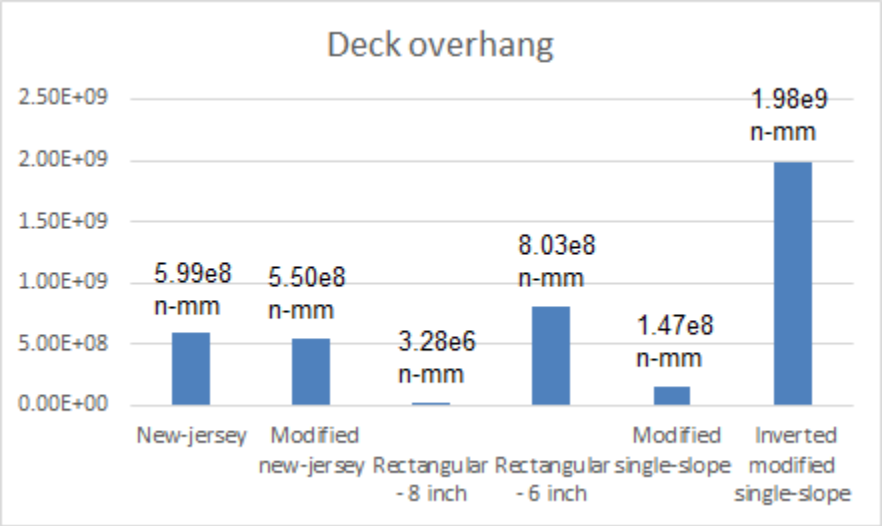

Figure 325: Internal energy absorbed by deck overhang at all geometries

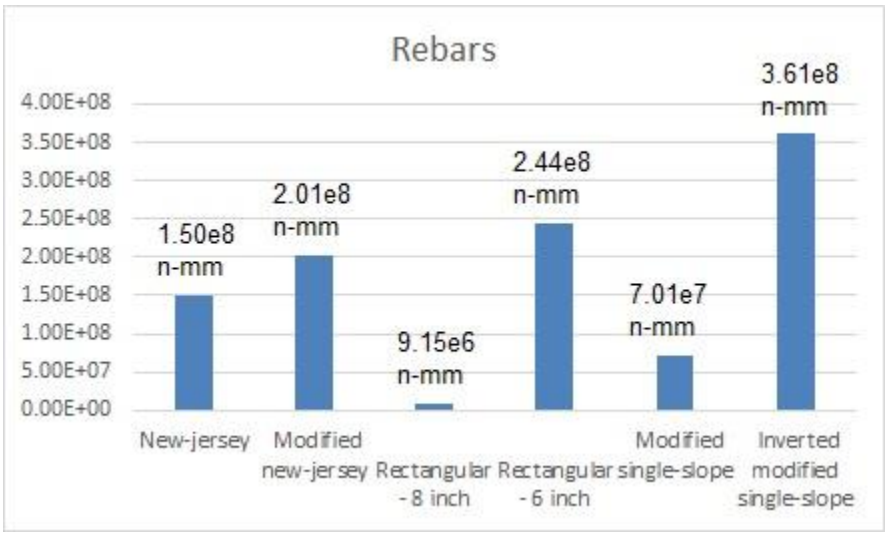

Figure 326: Internal energy absorbed by reinforcement bars at all geometries

The internal energy absorbed by the vehicle in all geometries does not vary greatly; however, the maximum energy absorbed by the vehicle was during its impact with the modified New Jersey barrier

The maximum energy absorbed by the barrier was almost the same using modified New Jersey, rectangular – 6 inch, and inverted modified single slope geometries.

The maximum energy absorbed by deck overhang was accomplished with inverted modified New Jersey geometry, but with a significant difference than other barriers. This comparison shows that this barrier is not thick nor efficient enough, which causes the deck overhang to experience a lot of damage

The maximum energy absorbed by reinforcement bars was with inverted modified New Jersey geometry but again, with significant differences from other barriers again. Research shows that this barrier is not efficient enough, which causes the reinforcement

bars to experience a lot of damage. Rectangular – 6 inch, and modified New Jersey experienced the maximum energy absorption at the reinforcement bars as well.

The evidence from this research concludes that modified New Jersey, rectangular – 6 inch geometry, and inverted modified geometry allowed for too much energy at the barrier and at the reinforcement bars. In addition, inverted modified New Jersey geometry absorbed too much energy at the deck overhang portion which might cause serious damage to this portion. These geometries cannot meet the fifth criteria that the research is looking for, namely, the goal of minimizing the energy caused by the impact, and the damage to different portions.

8.2.3.2 Internal energy absorbed by each geometry

Figure 237 to 332 represented the internal energy absorbed by each geometry in all components.

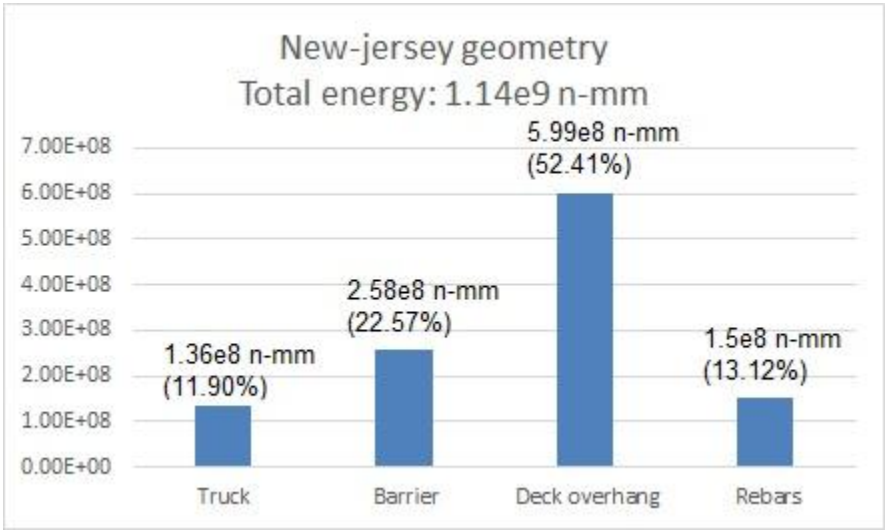

Figure 327: Internal energy absorbed via New Jersey geometry by each components

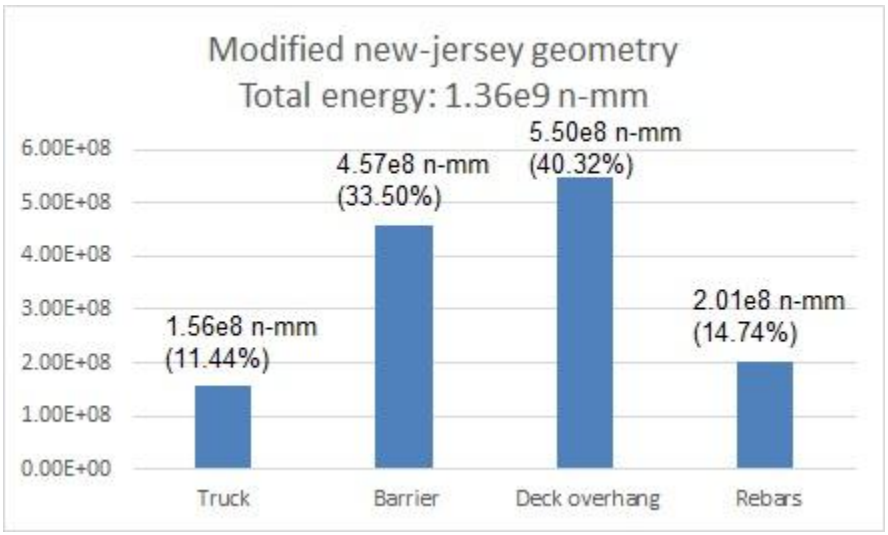

Figure 328: Internal energy absorbed via modified New Jersey geometry by each components

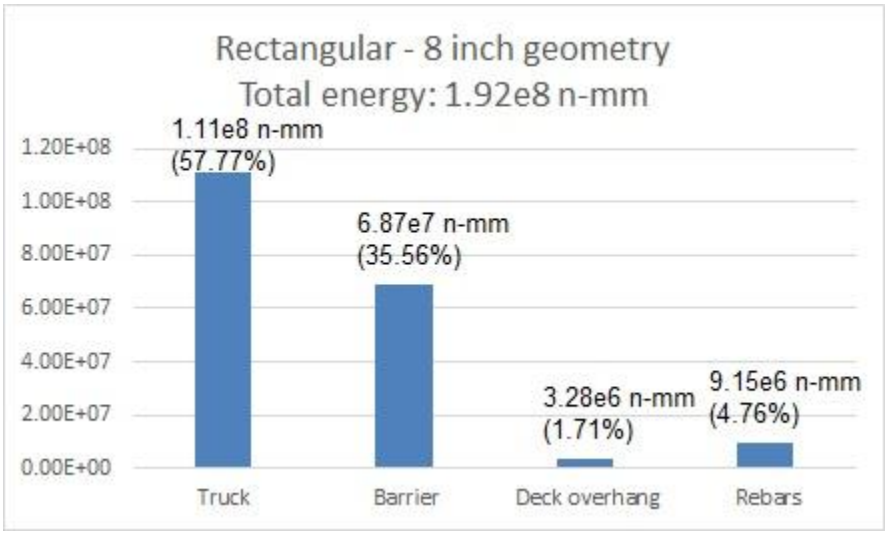

Figure 329: Internal energy absorbed via modified rectangular – 8 inch geometry by each components

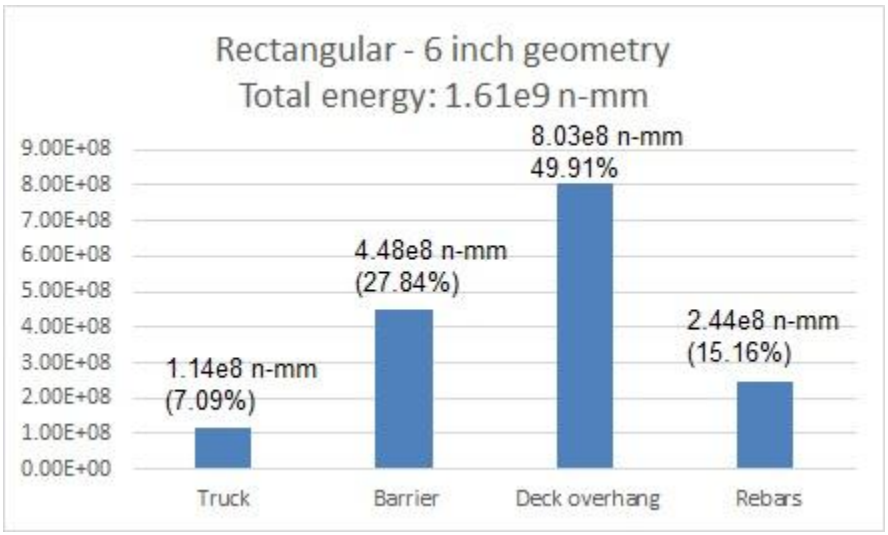

Figure 330: Internal energy absorbed via rectangular – 6 inch geometry by each components

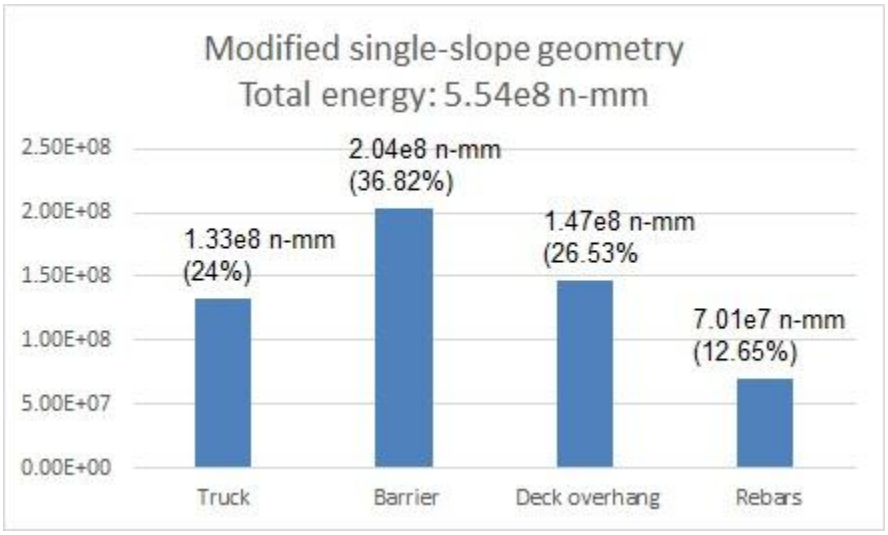

Figure 331: Internal energy absorbed via modified single-slope geometry by each components

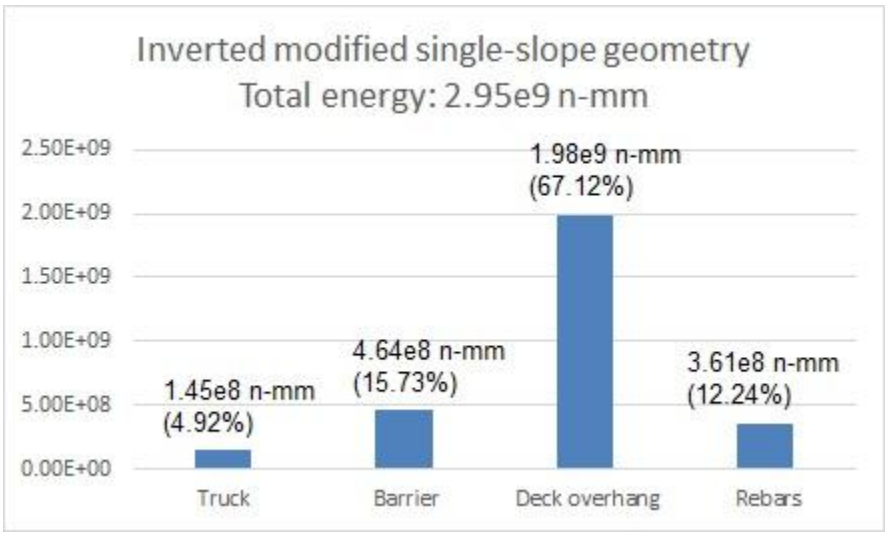

Figure 332: Internal energy absorbed via inverted modified single-slope geometry by each components

With different geometries total energy absorption by all components may vary. This is because, in some geometries, some of the impact energy is lost because of vehicle roll- over off the barrier or "taking off" from the concrete deck overhang surface. As determined by this study, the New Jersey barrier had the maximum energy absorption at the deck overhang, which constitutes almost half of the impact energy. Modified New Jersey had the maximum energy absorption at barrier and deck overhang - almost 74% of the total impact energy.

With Rectangular – 8 inch geometry, almost 60% of the energy is absorbed by the truck, with the remaining energy absorbed by the barrier.

Alternatively, in Rectangular – 6 inch geometry, although the thickness of the barrier is enough to resist the impact, it cannot absorb a lot of energy. Most of the impact

energy is absorbed by the deck overhang which might cause serious damage to this component.

The modified single-slope geometry had the most optimized energy absorption of all components. Most of the energy was absorbed by the barrier. The deck overhang and vehicle had almost the same amount of energy absorption, with the reinforcement bars having the minimum energy absorption.

The inverted modified single-slope version acted almost like the rectangular – 6 inch barrier. Since this geometry is not thick enough, a significant amount of the impact energy was absorbed by the deck overhang, which may cause significant damage to that portion.

8.3 Barrier and deck overhang damage after second impact

Figure 333 to 338, using dynamic load simulation, showed the damage imposed to all geometries after second impact.

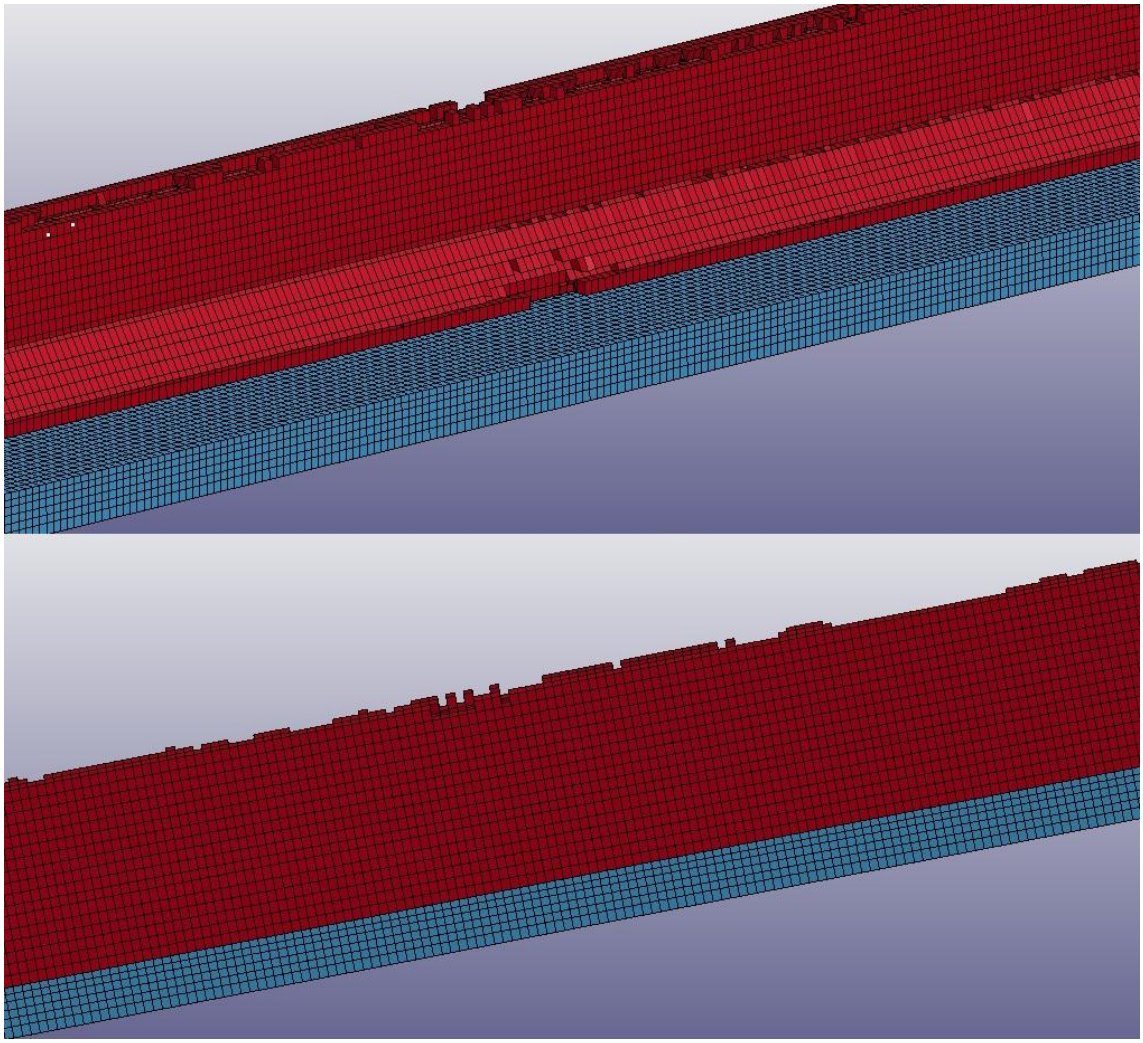

Figure 333: New Jersey geometry damage after second impact – front and back face

As seen above, after second impact, News Jersey geometry experienced minor damage to the barrier, but the deck overhang did not have any serious damage.

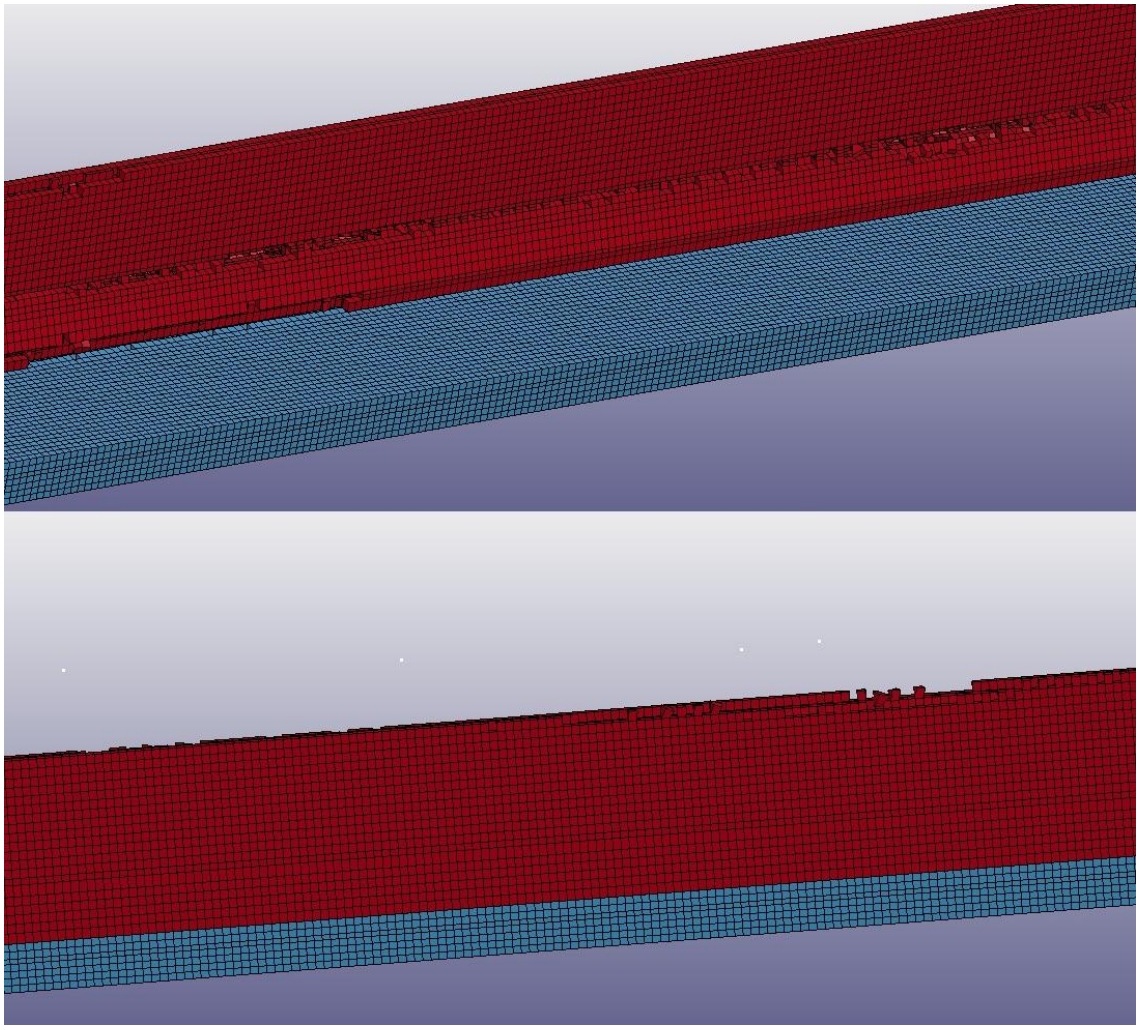

Figure 334: Modified New Jersey geometry damage after second impact – front and back face

As seen above, after second impact, the modified New Jersey geometry experienced major damages at the barrier, but the deck overhang did not have any serious damage. All elements located between top and bottom segments either destroyed or experienced major damage.

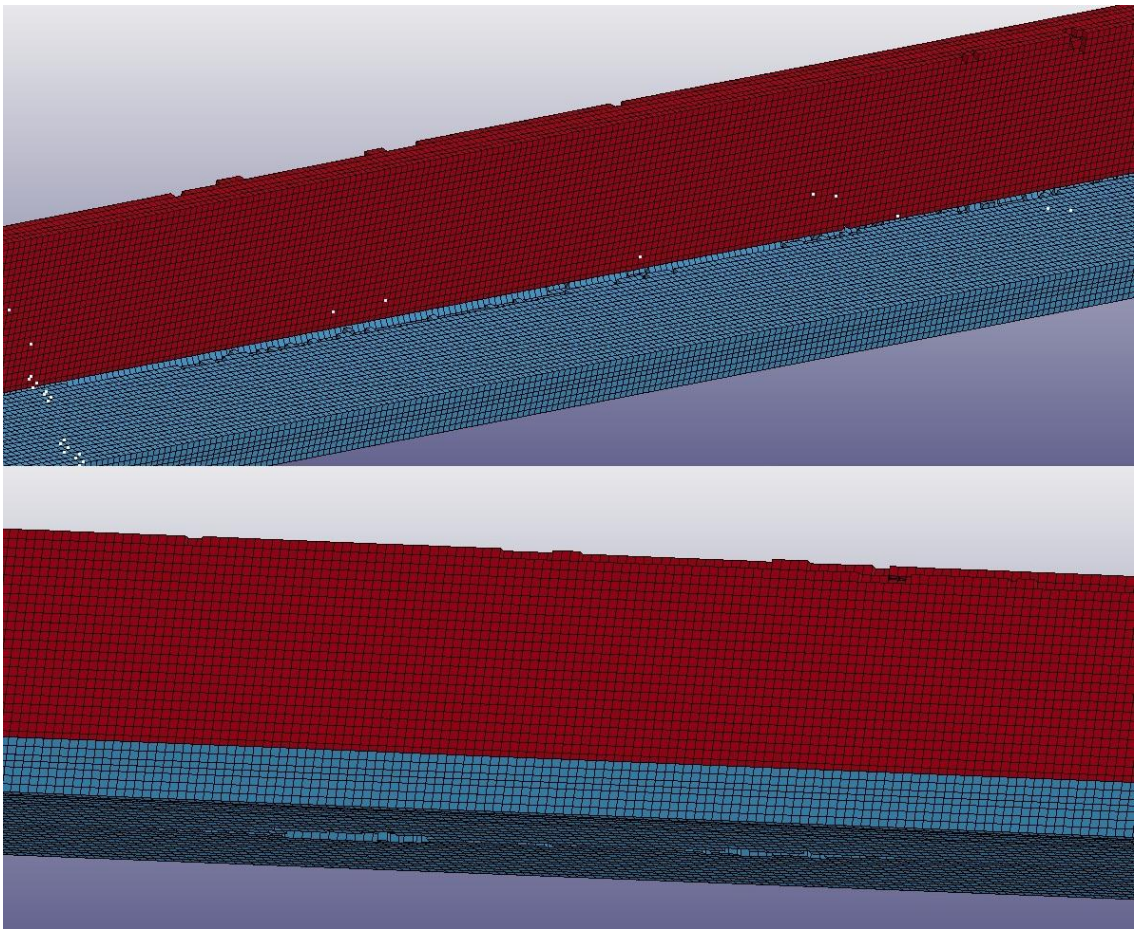

Figure 335: Rectangular – 8 inch geometry damage after second impact – front and back face

As seen above, after second impact, rectangular – 8 inch geometry experienced minor damage at the top of the barrier. In addition, the deck overhang at both top and bottom face, experienced some major damages. One could deduce that this geometry acted as “a stiff material” and could not absorb enough energy to avoid serious damages to the deck overhang.

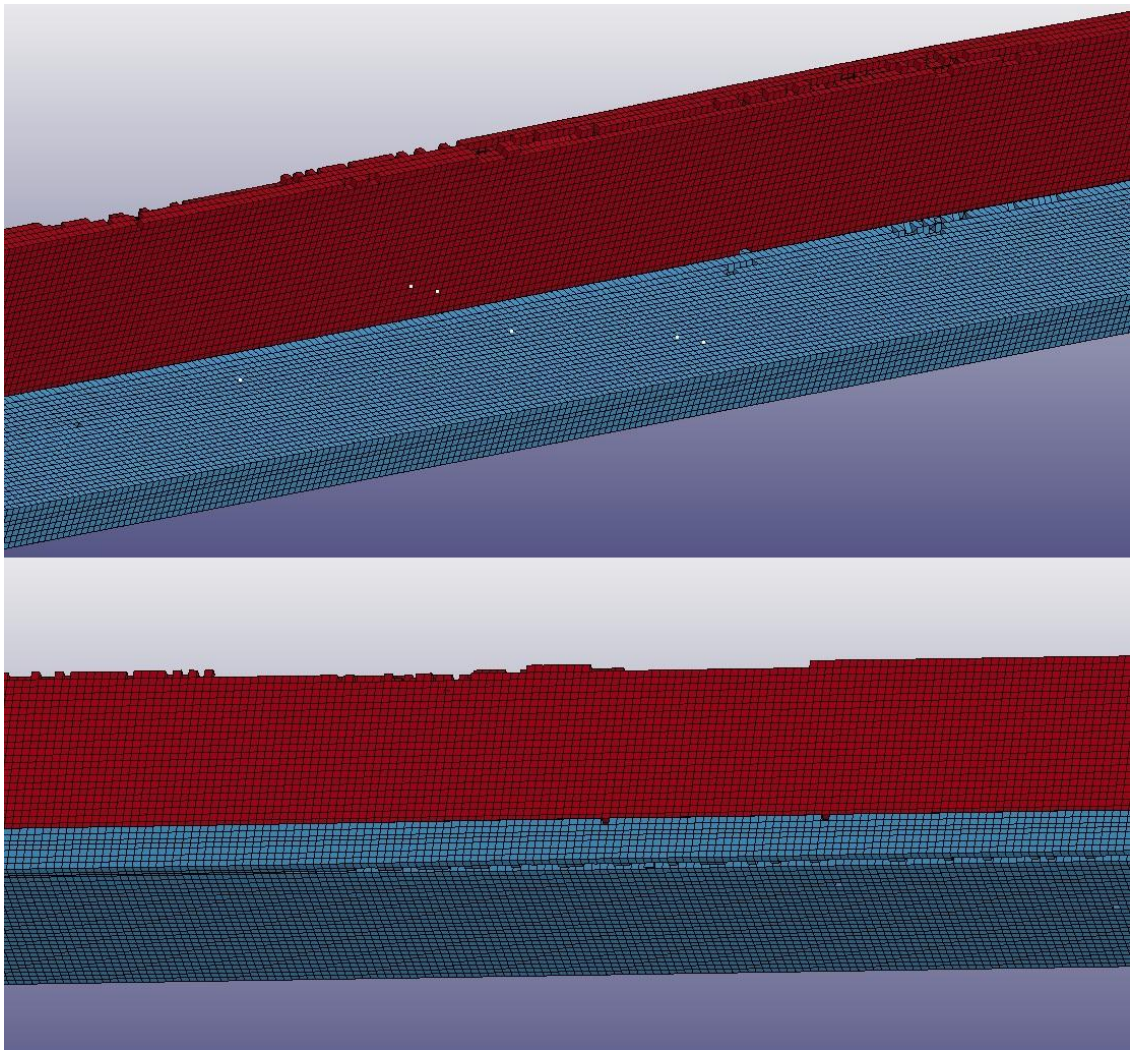

Figure 336: Rectangular – 6 inch geometry damage after second impact – front and back face

As seen above, compared with rectangular – 8 inch, this barrier not only had some major damage to the deck overhang, but also the barrier as a whole had more injury. Although the injury imposed to the barrier might be within acceptable limits; stiill, this research is looking for a geometry that allows minimum damage to deck overhang.

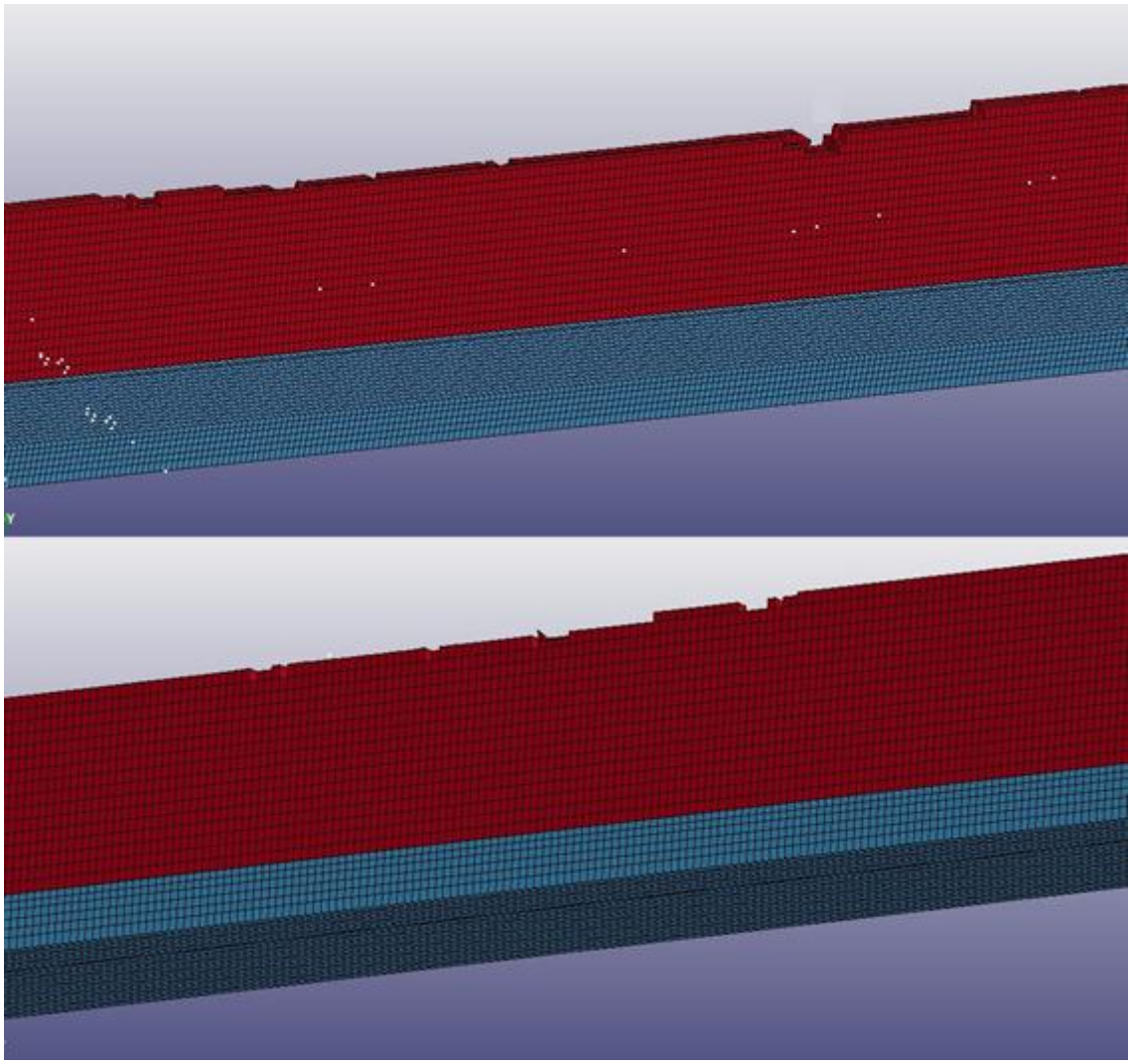

Figure 337: Modified single-slope geometry damage after second impact – front and back face

As seen above, this geometry had its maximum energy absorption within the barrier, and accordingly, the deck overhang did not have any minor or major damages.

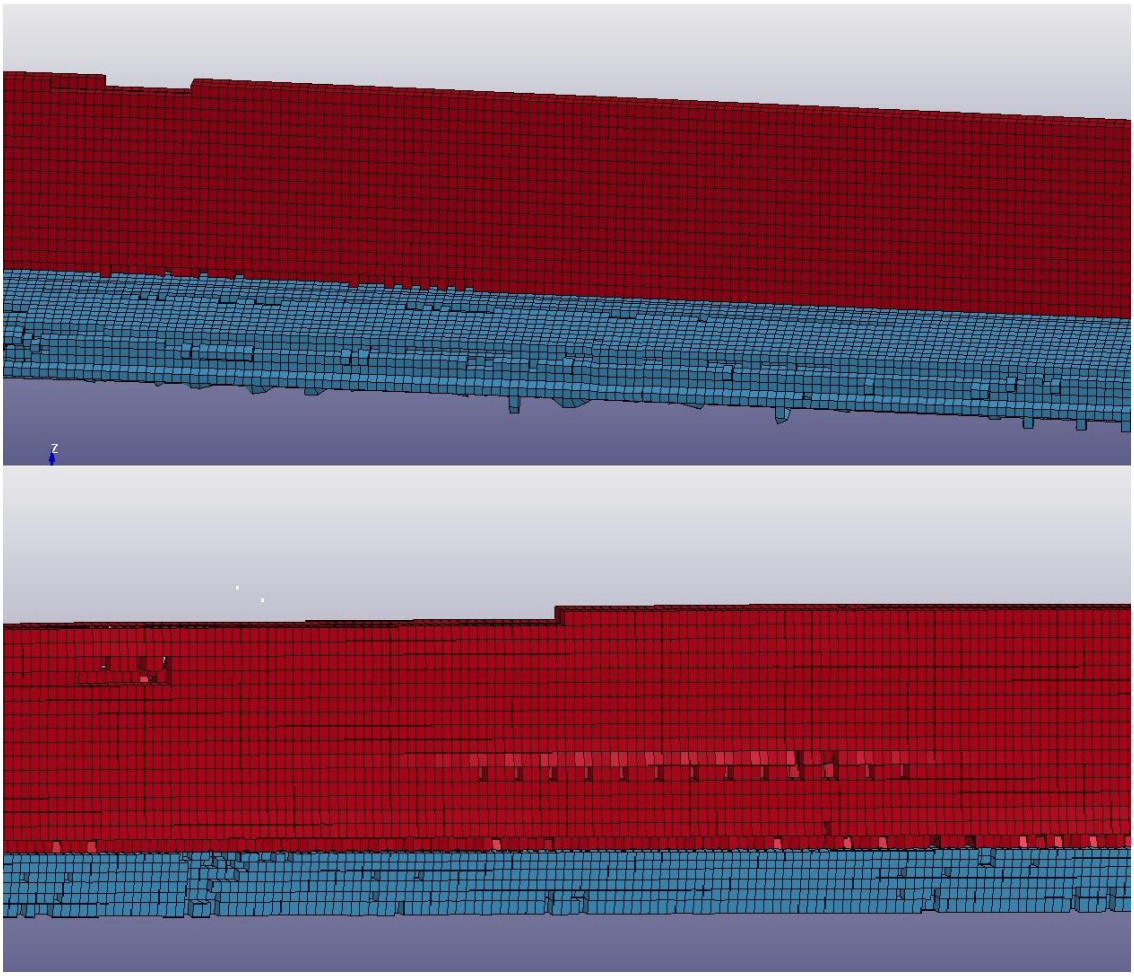

Figure 338: Inverted modified single-slope geometry damage after second impact – front and back face

As seen above, upon impact, this geometry not only produced the maximum damage to the barrier but also to the deck overhang.

Except for the New Jersey and modified single-slope geometries, all other geometries had major damage either at the barrier or the deck overhang.

8.4 Vehicle roll over

As mentioned before, vehicle roll-over is a major concern amongst barriers designers. They responded by designing taller barriers such as “Tall New-Jersey Barrier” to avoid this problem. However, this barrier production demanded additional cost to pour the concrete. This research tried to circumvent this problem by using 34 inch tall barriers, the same height as the New Jersey barrier.

Figure 339 to 342 showed the vehicle rolling over at “first impact”, “second impact”, “second impact + 0.28 second”, and “second impact + 0.815 second”.

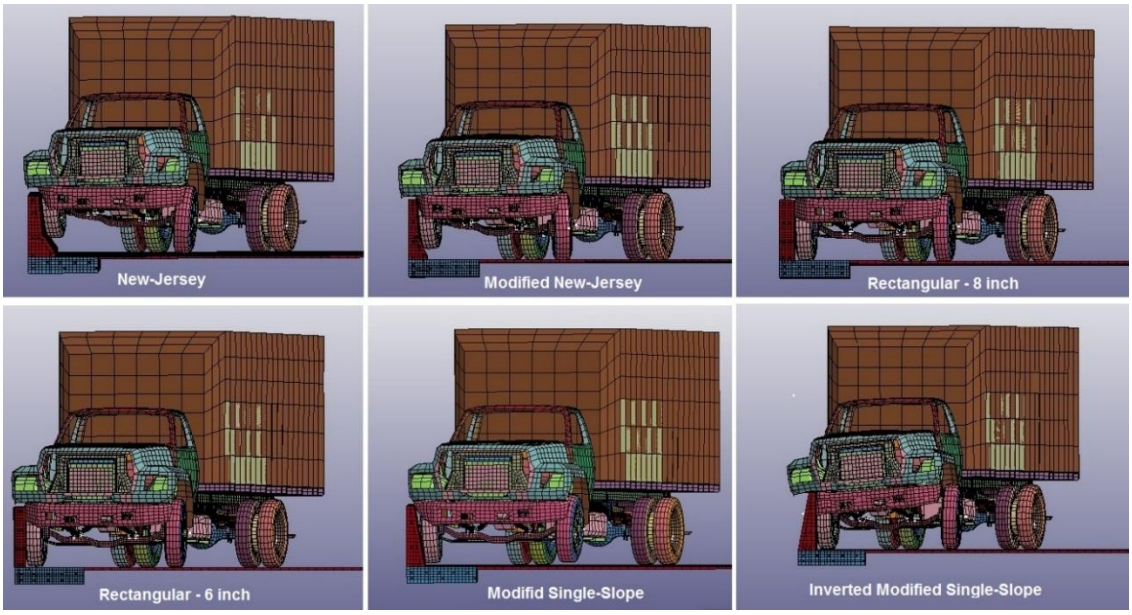

Figure 339: 3d model – first impact

As seen in the above figure, after the first impact, using dynamic load simulation vehicle front tires impacting New Jersey and modified New Jersey geometries rolled on the taper slope, which caused the front of the vehicle to lift from the bridge surface and caused an additional rolling over after second impact. Since New Jersey barrier has

lighter taper slopes, this phenomenon occurred more often with New Jersey barrier. Vehicles on all other barriers did not lift at the moment of first impact.

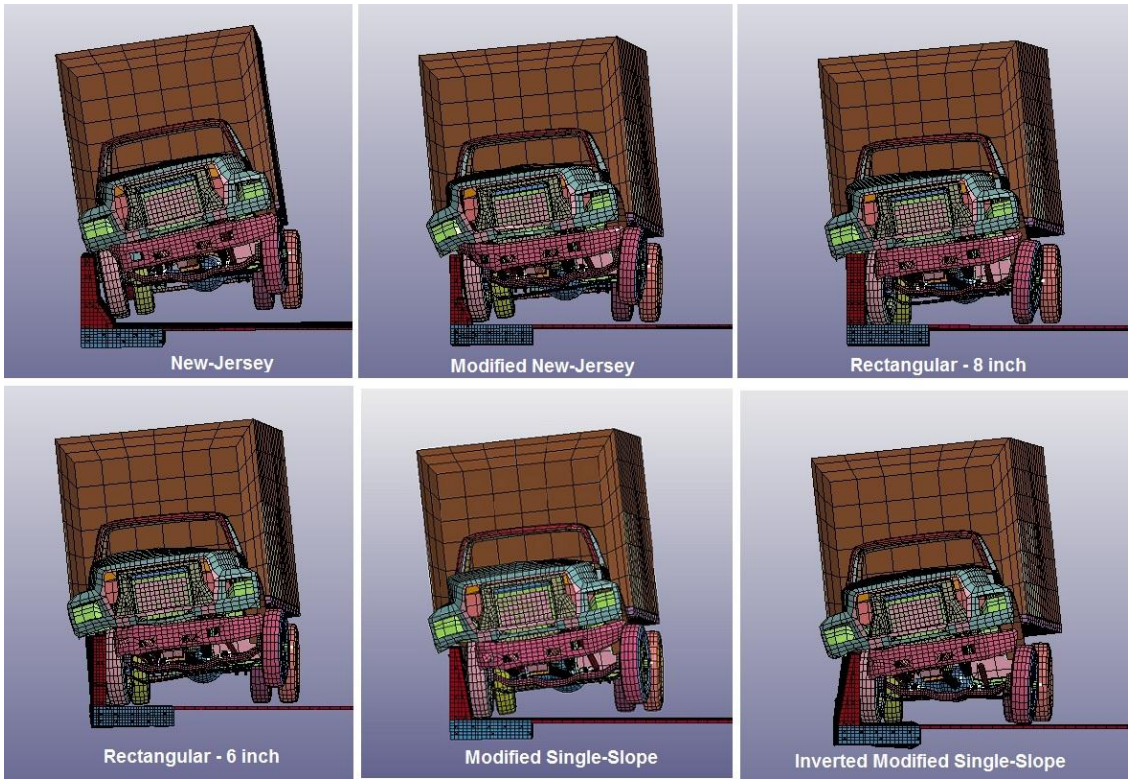

Figure 340: 3d model – second impact

As seen in the above figure, after the second impact, vehicles on the New Jersey geometry simulation completely lifted off the bridge. This observation proves that this geometry produces the highest frequency of vehicle rolling over.

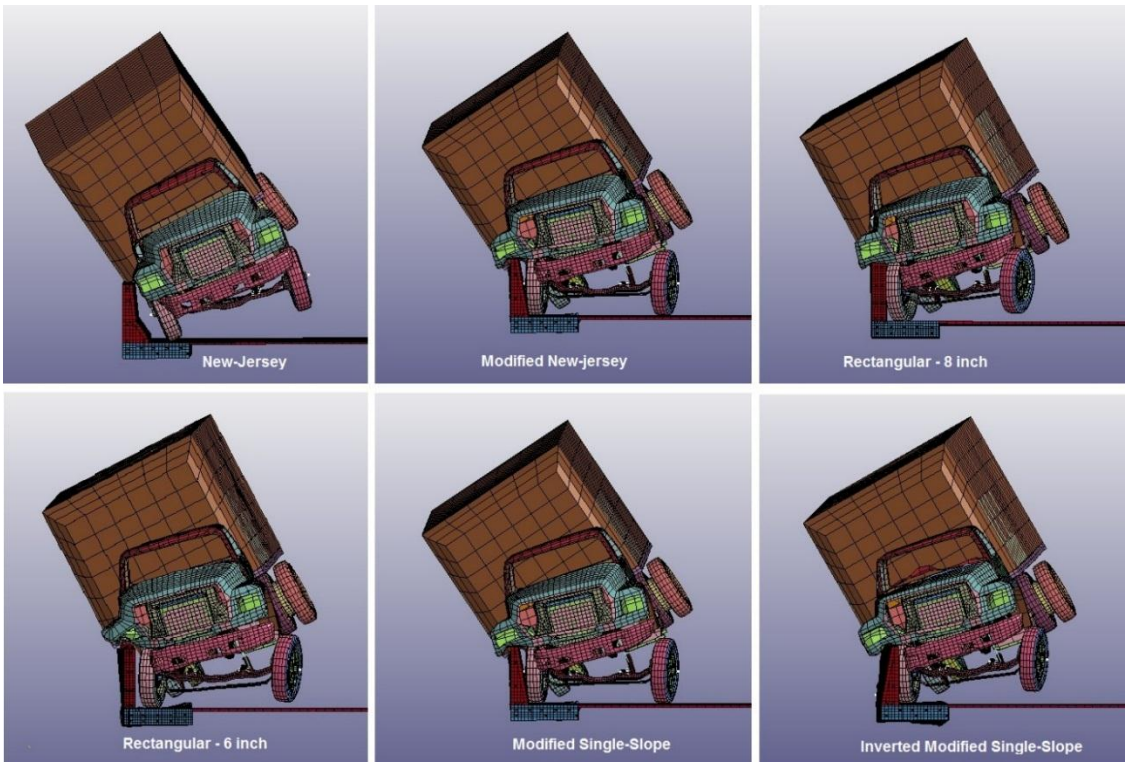

Figure 341: 3d model – second impact + 0.28 sec

As seen with the above figure, after “second impact + 0.28 second”, a vehicle on rectangular – 6 inch geometry simulation experienced some deformation at its right front head light.

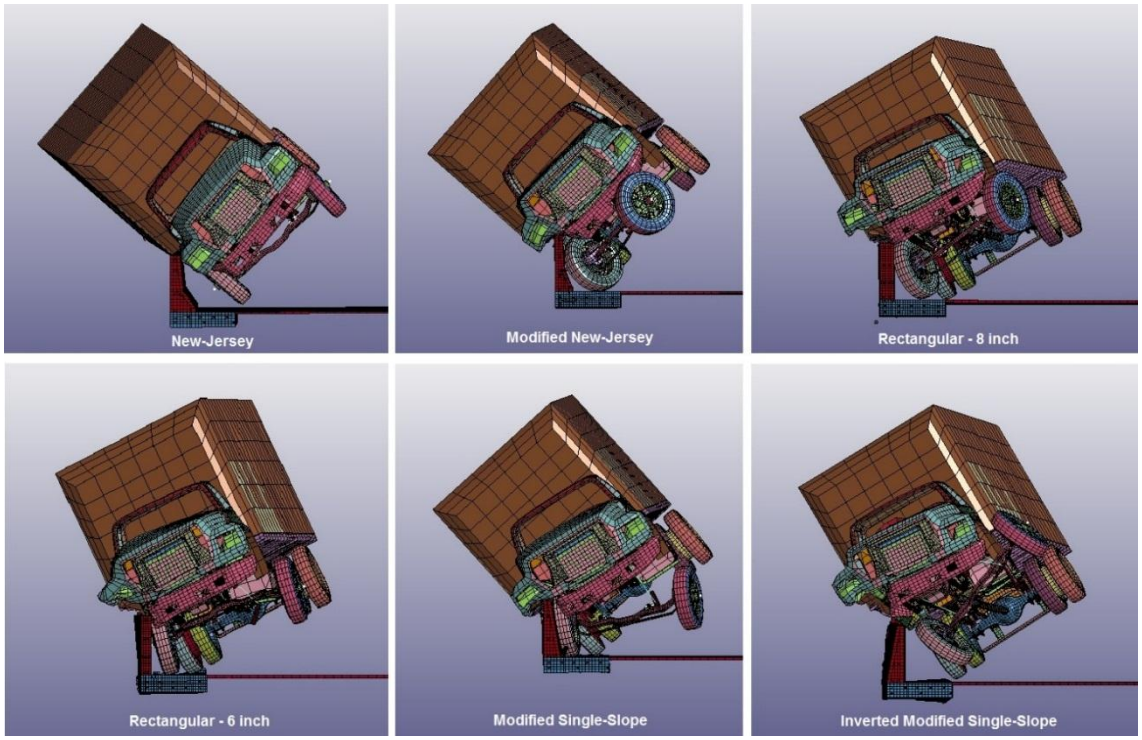

Figure 342: 3d model – second impact + 0.815 sec

As seen from the above figure, after second impact + 0.815 second, all the vehicle's tires on New Jersey barrier geometry lifted off the ground and this geometry had the maximum amount of rolling over. Modified New Jersey geometry had almost the same results but less rolling over than the New Jersey geometry. The rear of the vehicle at "rectangular – 8 inch", "rectangular – 6 inch", and "inverted modified single-slope" was redirected to the traffic lane again. Though unlikely, there may be some slight damage to the traffic lane.

The only geometry that did not produce a great deal of roll over and remained in line with the barrier was the Modified Single-Slope barrier.

8.5 Comparison between Geometries

8.5.1 Static Results

The Rectangular – 6 inch geometry barrier has the thinnest section and therefore it is expected to experience the maximum compressive stress of 15.20 MPa. Reinforcement bars on Modified New Jersey and Rectangular – 6 inch barriers, reached their yield point. Since these results are based on static load, it is expected for these geometries to experience the maximum tensile stress due to having less thickness in comparison to other geometries. Consequently, the compression block of the concrete is smaller and most of the load is carried by the tension block which contains the hairpin dowels that connect the barrier to deck overhang, located at the front face of the barrier.

Moreover, the Rectangular – 6 inch geometry also experienced the maximum deflection at the barrier, a total deflection of 15.9 mm. Similarly, Modified New Jersey barrier had the second greatest deflection since its thickness is less than most of the proposed geometries with the exception of the Rectangular – 6 inch barrier.

On the other hand, the old New Jersey barrier had the minimum stress at the compression side of the barrier due to static load because it has the thickest geometry (6 in at top and 15 inches at bottom), and more concrete was poured to build this barrier compared to the other geometries. Also, the minimum deflection occurred on the Rectangular – 8 inch geometry. This observation is interesting because less concrete was poured for this geometry compared to the New Jersey geometry, but since it had a uniform thickness from top to bottom, it seems reasonable to have minimum deflection in this geometry. Typical New Jersey geometry has a thickness of 6 inches at the top, 8 inches at the middle, and 15 inches at the bottom. Since the load applied is at the top of

the geometry, which varies from 6 to 8 inches for the New Jersey geometry, greater deflection was observed compared to the Rectangular – 8 inch geometry.

8.5.2 Dynamic Results

As the results show, the second impact applied a greater force to the barrier and deck overhang than the first impact. By comparing the geometries in the compression block of the barrier, the maximum stress was experienced by the Rectangular 6 and 8 inches geometries. The author believes that these results can demonstrate the fact of how "the energy absorption results of the truck show that the minimum energy absorbed by a barrier was that of those with the rectangular 6 and 8 inch geometries". It is important to note that, lack of taper in these two geometries caused the vehicle to stay in contact with the bridge deck surface in contrast to other geometries. This fact causes the vehicle to apply a greater force to the barrier compared to the other geometries, which results in greater stress in the compression block of the concrete. Although the truck's response in these geometries acted better in terms of lifting up and rolling over, the damage to deck overhang when having geometries with flat surface at the front side was relatively high in comparison to other geometries. It is therefore more reasonable to install these barriers at structures that do not possess a deck overhang and simulate them in a finite element analysis model to make sure that the thickness is enough and they are able to provide maximum safety.

In addition, reinforcement bars in the tension side of all geometries reached their yield point with the exceptions of the New Jersey and Modified Single Slope barriers. It

is reasonable to say that these geometries had the minimum amount of damage and they are more efficient and optimized compared to other geometries.

Maximum deflection was observed at the Rectangular – 6 inch geometry and it was 39.1 mm (1.54 in). This number is relatively high compared to the other geometries. The author believes that this result is related to the uniform thickness and flat surface of the geometry. The uniform 6 inches thickness is relatively less than all other geometries, and the flat surface of the geometry caused the vehicle to apply more force to the barrier, which translates into more displacement.

On the other hand, the four remaining geometries had almost the same stress at the compression side in the range of 22 to 26 MPa.

Although the New Jersey barrier had a thickness of 15 inches at the bottom, the minimum deflection was observed at the Rectangular – 8 inch geometry. The author believes that this is due to the uniform thickness of this geometry which is 8 inches from top to bottom in contrast to the varying thickness of the New Jersey barrier which displays 6 inches at the top.

By observing the damage to each geometry after the second impact, it is obvious that on the New Jersey geometry, the deck overhang experienced the least damage. This is reasonable since it is assumed that this barrier is overdesigned and therefore able to fare well in high-loading scenarios. The Modified Single Slope geometry showed a higher damage in the deck overhang compared to the New Jersey barrier. This damage was between the top and bottom segment of the barrier in between the two tapered slopes. From this result, the author concludes that the Modified New Jersey barrier does not

display the appropriate geometry to safely withstand the loading scenario. This conclusion is derived from the assumption that if the vehicle speed increases, there might be significant chance that the impact would break the top segment of this geometry and the vehicle would fall off the bridge. Similarly, significant damage was observed in the geometries with flat surface such as Rectangular 6 and 8 inches, and the Inverted Modified Single Slope. The author believes that the reason for this significant damage is due to the flat surface geometry which causes concentrated stress to the deck overhang causing significant damage to it. Therefore, the author concludes that flat surface geometries are not appropriate to be located on deck overhangs.

New Jersey and Modified Single Slope geometry were the only barriers that did not have significant damage to the barrier or the deck overhang.

Observations on vehicle roll over after second impact for all geometries showed that the New Jersey barrier displayed the worst geometry in terms of vehicle safety. Figure 342 shows that the only geometry that caused all the vehicle tires to be lifted up is the New Jersey geometry. For all other geometries, at least one tire remains in contact with the bridge deck after second impact.

Although the Modified New Jersey geometry has a sharper taper at the bottom than the New Jersey barrier, the front tire does not get lifted up as much after the first impact as it does by the New Jersey geometry.

All variables into account, the author concludes that with the exception of the New Jersey geometry, the only geometry that could resist the impact loads and was able

to satisfy all safety criteria, was the Modified Single Slope geometry. Figure 343 is an overview comparison between all geometries.

GEOMETRY	New Jersey	Modified New Jersey	Rectangular – 8"	Rectangular – 6"	Modified Single Slope	Inverted Modified Single Slope
Cross Section Area	307 (in^2)	204.60 (in^2)	272 (in^2)	204 (in^2)	238 (in^2)	238 (in^2)
Barrier Reached Max Compressive Strength	✗	✗	✓	✓	✗	✗
Barrier Reached Max Tensile Strength	✗	✗	✗	✗	✗	✗
Deck Overhang Reached Max Compressive Strength	✗	✗	✗	✗	✗	✗
Deck Overhang Reached Max Tensile Strength	✗	✗	✗	✗	✗	✗
Rebar exceeded yield strength	✗	✓	✓	✓	✗	✓
Minimum Internal Energy Absorbed by All Components (Increasing Order)	(3)	(4)	(1)	(5)	(2)	(6)
Significant Damage to the Barrier	✗	✓	✗	✓	✗	✓
Significant Damage to the Deck Overhang	✗	✗	✓	✓	✗	✓
Remarkable Vehicle Roll-Over / Redirection	✓	✓	✓	✓	✗	✓

Figure 343: Overview Comparison

8.6 Static versus Dynamic Load Comparison

All geometries could resist without any serious damage as seen in Chapter 6, at the 54 kip static load simulation. That load represents Test Level 4 and is used nowadays in order to design barriers located for highway traffic. On the other hand, dynamic simulation had different results. All the barriers had some minor and major damage. At

three of the geometries, some damage was imposed to the deck overhang, and reinforcement bars within all barriers tolerated more stress compare to static load measurements, and deflection was different than for static simulation. Since in static simulation, certain amounts of load are imposed to the barrier within a certain time, all tension blocks, compression blocks, reinforcement bars in tension, and reinforcement bars in compression for the simulation were the same in all geometries, while in dynamic simulation, based on the geometry of the barrier, all of the said criteria were different and unique for each geometry.

It might be possible to design a barrier based on static load and it might be safe in terms of resistance, but since there is no vehicle in this assumption, it cannot provide results for situations such as vehicle roll-over, or vehicle redirection to the traffic lane, or account for the exact damage amounts that are imposed to the vehicle after impact.

Moreover, barriers are designing based on static load assumption, a methodology which is almost forty years old. Research might unearth new calculations and assumptions applicable to barrier design.

Last but not least, although static load might be efficient in order to design structures with dead or live load, this research proved that static load is not suitable for designing the components subjected to impact or explosion.

8.7 Deck Overhang Deflection

As mentioned in Chapter 7, with New Jersey geometry, the deck absorbed almost 50% of the impact energy after second impact of the vehicle. This research proved that although the nature and purpose of deck overhang is not to absorb vehicle impact energy, it is located on a critical spot on bridges, and so there is a significant chance for this component to absorb some of the impact energy. Hence, there might be a significant chance to revise and redesign the barriers located on bridge deck overhangs by considering its energy absorption.

8.8 Most Efficient Geometry

This research tried to cover all of the possible highway barrier surfaces that a vehicle can impact.

As a review, barriers located on highways have three major tasks, (1) to minimize the damage imposed to the vehicle caused by the crash via absorbed energy (2) to keep the vehicle in line and not to redirect it into the traffic flow, and (3) by applying appropriate geometry, to avoid vehicle roll-over.

After considering all of these criteria, "The Modified Single-Slope Geometry" was the only barrier that all components absorbed an acceptable amount of energy caused by vehicle impact, without imposing any serious damage to deck overhang and/or vehicle. Although the barrier itself had some damages after impact, the research was looking for a geometry that could maximize the energy absorption by breaking while still maintaining the barrier's serviceability. In addition to this geometry providing all of these

safety criteria, it had, as well, a cross-sectional area measured at 77.5% of the New Jersey geometry. This means that 22.5% less concrete was poured, as compared to the New Jersey, while still providing more safety features than the New Jersey barrier.

9 SUMMARY AND CONCLUSION

The research first explained the history of the New Jersey barrier and two different methods to design it. One method did not consider the deflection of the deck overhang (Yield Line Analysis), while the other method modified the Yield Line Equation and added the contribution of the deck overhang deflection to the system (Barrier Rail Design Procedure).

After the shortcomings of the aforementioned methods were analyzed, a finite element model simulation was proposed in order to replicate the behavior of the barrier and deck overhang after static or dynamic load.

Consequently, after the finite element model provided an accurate representation of the New Jersey barrier, problems with its geometry and strength parameters were considered. This research proposed five different barrier shapes varying in thickness and geometry.

In order to prove this method can be acceptable and accurate, the results of a real test were compared with a finite element simulation, and the results of the real study (barrier has the same material properties as in this research) were fairly close to reality.

In order to understand the physics of the problem and to demonstrate the improvement over static analysis, LS-DYNA static simulation was performed first. All geometries were compared based on static load using Test Level 4. After the static load simulation, dynamic impact simulation was performed. The research used a Ford F800 (Single Unit Truck), which represents Test Level 4 based on AASHTO manual. By comparing all of the proposed geometries with the New Jersey geometry, in terms of

stress, deflection, deformation, energy absorption, damage to each component, and all safety criteria, this research proposed the Modified Single Slope geometry as the best geometry.

Recommendations for Future Studies:

After this study, the research suggests to perform a real test on Modified Single Slope geometry under Test Level 4 criteria, and compare the results with the proposed method to make sure that the realistic results can match with the results extracted from FE model.

Additionally, the research suggests to increase the length of the barrier and deck overhang from 120 feet to 240 feet in the finite element model, in order to observe the exact behavior of the vehicle roll over and lift up.

Moreover, the next step for this research is to reduce the reinforcement in the aforementioned geometry and observe its behavior to make the geometry more economical.

LIST OF REFERENCES

ACI 318-11. (2011). American Concrete Institute.

Albin, R. (2011). M.A.S.H.: The New Safety Hardware Crash Testing Criteria. *Annual.* Federal Highway Administration.

Badiee, E. (2014). Bridge Rail Design Procedure.

Bala, S., & Day, J. (n.d.). *General Guidelines for Crash Analysis in LS-DYNA.* Livermore Software Technology.

Barker, R. M., & Puckett, J. A. (2013). *Design of Highway Bridges.* JohnWiley & Sons, Inc.

Calloway, B. R. (1993). Yield Line Analysis of an AASHTO New-Jersey Concrete Parapet Wall.

Caltrans Seismic Design Criteria Version 1.7. (2013).

Finite Element Model Archive. (2008). Retrieved from National Crash Analysis Center: http://www.ncac.gwu.edu/vml/models.html

Hirsh, T. J. (1978). *Analytical Evaluation of Texas Bridge Rails to Contain Buses and Trucks.* Texas: Texas Transportation Institute.

Kozel, S. M. (2004). *New Jersey Median Barrier History*. Retrieved from Roads to the Future: http://www.roadstothefuture.com/Jersey_Barrier.html

LRFD Bridge Design Specifications. (2012). *AASHTO* .

LS-DYNA Keyword User's Manual. (2007). Livermore Software Technology Corporation.

Mohan, P., Marzougui, D., & Kan, C.-D. (. (2003). *Validation of a Single Unit Truck Model for Roadside Hardware Impacts.*

Murray, Y. D. (2007). *Users Manual for LS-DYNA Concrete Material Model 159.*

Murray, Y. D., Abu-Odeh, A., & Bligh, R. (2007). Evaluation of LS-DYNA Concrete Material Model 159.

(1997). *NCHRP Synthesis 244.*

PAJAK, M. (2011). the Influence of the Strain Rate on the Strength of Concrete Taking Into Account the Experimental Techniques.

RoadSafe. (2012). Roadside Safety Analysis. *Journal of Transportation*.

Ross, H. E., Sicking, D. L., Zimmer, R. A., & Michie, J. D. (1993). *NCHRP Report 350.*

Sheikh, N. M., Bligh, R. P., & Menges, W. L. (2011). *Determination of Minimum Height and Lateral Design Load for Mash Test Level 4 Bridge Rails.* College Station: Texas Transportation Institute Proving Ground, The Texas A&M University System.